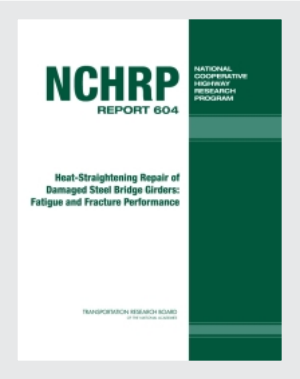

Heat-Straightening Repair of Damaged Steel Bridge Girders: Fatigue and Fracture Performance

DETAILS

129 pages | | PAPERBACK
ISBN 978-0-309-41993-2 | DOI 10.17226/23087

AUTHORS

NATIONAL COOPERATIVE HIGHWAY RESEARCH PROGRAM

NCHRP REPORT 604

Heat-Straightening Repair of Damaged Steel Bridge Girders: Fatigue and Fracture Performance

R.J. Connor
PURDUE UNIVERSITY
West Lafayette, IN

M.J. Urban
HNTB CORPORATION
Philadelphia, PA

E.J. Kaufmann
LEHIGH UNIVERSITY
Bethlehem, PA

Subject Areas
Bridges, Other Structures, and Hydraulics and Hydrology • Maintenance

Research sponsored by the American Association of State Highway and Transportation Officials
in cooperation with the Federal Highway Administration

TRANSPORTATION RESEARCH BOARD

WASHINGTON, D.C.
2008
www.TRB.org

NATIONAL COOPERATIVE HIGHWAY RESEARCH PROGRAM

Systematic, well-designed research provides the most effective approach to the solution of many problems facing highway administrators and engineers. Often, highway problems are of local interest and can best be studied by highway departments individually or in cooperation with their state universities and others. However, the accelerating growth of highway transportation develops increasingly complex problems of wide interest to highway authorities. These problems are best studied through a coordinated program of cooperative research.

In recognition of these needs, the highway administrators of the American Association of State Highway and Transportation Officials initiated in 1962 an objective national highway research program employing modern scientific techniques. This program is supported on a continuing basis by funds from participating member states of the Association and it receives the full cooperation and support of the Federal Highway Administration, United States Department of Transportation.

The Transportation Research Board of the National Academies was requested by the Association to administer the research program because of the Board's recognized objectivity and understanding of modern research practices. The Board is uniquely suited for this purpose as it maintains an extensive committee structure from which authorities on any highway transportation subject may be drawn; it possesses avenues of communications and cooperation with federal, state and local governmental agencies, universities, and industry; its relationship to the National Research Council is an insurance of objectivity; it maintains a full-time research correlation staff of specialists in highway transportation matters to bring the findings of research directly to those who are in a position to use them.

The program is developed on the basis of research needs identified by chief administrators of the highway and transportation departments and by committees of AASHTO. Each year, specific areas of research needs to be included in the program are proposed to the National Research Council and the Board by the American Association of State Highway and Transportation Officials. Research projects to fulfill these needs are defined by the Board, and qualified research agencies are selected from those that have submitted proposals. Administration and surveillance of research contracts are the responsibilities of the National Research Council and the Transportation Research Board.

The needs for highway research are many, and the National Cooperative Highway Research Program can make significant contributions to the solution of highway transportation problems of mutual concern to many responsible groups. The program, however, is intended to complement rather than to substitute for or duplicate other highway research programs.

NCHRP REPORT 604

Project 10-63
ISSN 0077-5614
ISBN: 978-0-309-099370
Library of Congress Control Number 2008928066

COPYRIGHT PERMISSION

NOTICE

The project that is the subject of this report was a part of the National Cooperative Highway Research Program conducted by the Transportation Research Board with the approval of the Governing Board of the National Research Council. Such approval reflects the Governing Board's judgment that the program concerned is of national importance and appropriate with respect to both the purposes and resources of the National Research Council.

The members of the technical committee selected to monitor this project and to review this report were chosen for recognized scholarly competence and with due consideration for the balance of disciplines appropriate to the project. The opinions and conclusions expressed or implied are those of the research agency that performed the research, and, while they have been accepted as appropriate by the technical committee, they are not necessarily those of the Transportation Research Board, the National Research Council, the American Association of State Highway and Transportation Officials, or the Federal Highway Administration, U.S. Department of Transportation.

Each report is reviewed and accepted for publication by the technical committee according to procedures established and monitored by the Transportation Research Board Executive Committee and the Governing Board of the National Research Council.

The Transportation Research Board of the National Academies, the National Research Council, the Federal Highway Administration, the American Association of State Highway and Transportation Officials, and the individual states participating in the National Cooperative Highway Research Program do not endorse products or manufacturers. Trade or manufacturers' names appear herein solely because they are considered essential to the object of this report.

Published reports of the

NATIONAL COOPERATIVE HIGHWAY RESEARCH PROGRAM

are available from:

Transportation Research Board
Business Office
500 Fifth Street, NW
Washington, DC 20001

and can be ordered through the Internet at:

http://www.national-academies.org/trb/bookstore

Printed in the United States of America

THE NATIONAL ACADEMIES

Advisers to the Nation on Science, Engineering, and Medicine

The **National Academy of Sciences** is a private, nonprofit, self-perpetuating society of distinguished scholars engaged in scientific and engineering research, dedicated to the furtherance of science and technology and to their use for the general welfare. On the authority of the charter granted to it by the Congress in 1863, the Academy has a mandate that requires it to advise the federal government on scientific and technical matters. Dr. Ralph J. Cicerone is president of the National Academy of Sciences.

The **National Academy of Engineering** was established in 1964, under the charter of the National Academy of Sciences, as a parallel organization of outstanding engineers. It is autonomous in its administration and in the selection of its members, sharing with the National Academy of Sciences the responsibility for advising the federal government. The National Academy of Engineering also sponsors engineering programs aimed at meeting national needs, encourages education and research, and recognizes the superior achievements of engineers. Dr. Charles M. Vest is president of the National Academy of Engineering.

The **Institute of Medicine** was established in 1970 by the National Academy of Sciences to secure the services of eminent members of appropriate professions in the examination of policy matters pertaining to the health of the public. The Institute acts under the responsibility given to the National Academy of Sciences by its congressional charter to be an adviser to the federal government and, on its own initiative, to identify issues of medical care, research, and education. Dr. Harvey V. Fineberg is president of the Institute of Medicine.

The **National Research Council** was organized by the National Academy of Sciences in 1916 to associate the broad community of science and technology with the Academy's purposes of furthering knowledge and advising the federal government. Functioning in accordance with general policies determined by the Academy, the Council has become the principal operating agency of both the National Academy of Sciences and the National Academy of Engineering in providing services to the government, the public, and the scientific and engineering communities. The Council is administered jointly by both the Academies and the Institute of Medicine. Dr. Ralph J. Cicerone and Dr. Charles M. Vest are chair and vice chair, respectively, of the National Research Council.

The **Transportation Research Board** is one of six major divisions of the National Research Council. The mission of the Transportation Research Board is to provide leadership in transportation innovation and progress through research and information exchange, conducted within a setting that is objective, interdisciplinary, and multimodal. The Board's varied activities annually engage about 7,000 engineers, scientists, and other transportation researchers and practitioners from the public and private sectors and academia, all of whom contribute their expertise in the public interest. The program is supported by state transportation departments, federal agencies including the component administrations of the U.S. Department of Transportation, and other organizations and individuals interested in the development of transportation. **www.TRB.org**

www.national-academies.org

CRP STAFF FOR NCHRP REPORT 604

Christopher W. Jenks, *Director, Cooperative Research Programs*
Crawford F. Jencks, *Deputy Director, Cooperative Research Programs*
Edward T. Harrigan, *Senior Program Officer*
Eileen P. Delaney, *Director of Publications*
Margaret B. Hagood, *Editor*
Andrea Briere, *Editor*

NCHRP PROJECT 10-63 PANEL
Field of Materials and Construction—Area of Specifications, Procedures, and Practices

Harold R. "Skip" Paul, *Louisiana DOTD, Baton Rouge, LA* (Chair)
Scot Becker, *Wisconsin DOT, Madison, WI*
David R. Bruce, *Washington State DOT, Olympia, WA*
Jon J. Edwards, *Springfield, IL*
John P. Weisner, *Maryland State Highway Administration, Greenbelt, MD*
Dingyi Yang, *Texas DOT, Austin, TX*
Ellen Zinni, *New York State DOT, Poughkeepsie, NY*
William Wright, *FHWA Liaison*
Krishna K. Verma, *Other Liaison*
Frederick Hejl, *TRB Liaison*

AUTHOR ACKNOWLEDGMENTS

The research reported herein was performed under NCHRP Project 10-63 by the ATLSS Engineering Research Center at Lehigh University. Robert J. Connor, Assistant Professor at Purdue University and Eric J. Kaufmann, Senior Research Engineer at the ATLSS Center, are the principal investigators. The other author of this report is Michael J. Urban, a bridge design engineer with HNTB Corporation, formerly a Graduate Research Assistant at Lehigh University during the time of the research. Professor Emeritus, Dr. John W. Fisher, of Lehigh University, also provided valuable input throughout the research. The authors appreciate the support of NCHRP, the direction of Edward Harrigan, and the planning, review, and suggestions of the project panel.

FOREWORD

By Edward T. Harrigan
Staff Officer
Transportation Research Board

This report summarizes the results of a project to establish limits, based on fatigue and fracture performance, on the number of damage and repair cycles to which damaged steel bridge girders may be subjected using the heat-straightening procedure. A key product presented here are suggested revisions to the Federal Highway Administration (FHWA) manual of practice for heat straightening. The report will be of particular interest to engineers in state highway agencies and industry responsible for bridge maintenance and repair.

Heat straightening refers to the in-place application of heat and jacking forces to remove bends and distortion in steel bridge girders damaged by the impact of over-height vehicles. The procedure is often described as combining art with engineering, and is principally conducted by specialized firms in the private sector. Since 1999, however, the FHWA has presented workshops intended to acquaint state forces and consultants with the use of heat straightening. The syllabus for this workshop is based on the 1998 report FHWA-IF-99-004, "Heat-Straightening Repairs of Damaged Steel Bridges: A Manual of Practice and Technical Guide," prepared by R. Avent and D. Mukai.

Key questions in heat-straightening technology are the procedure's effect on the fatigue and fracture of repaired steel girders and the degree to which the damage and heat-straightening history of the steel influence that performance. These questions have been prompted by situations in which field-repaired girders subsequently fractured.

Under NCHRP Project 10-63, "Heat-Straightening Repair of Damaged Steel Bridge Girders: Fatigue and Fracture Performance," the ATLSS Engineering Research Center of Lehigh University was assigned the tasks of (1) determining the relative effects of damage and subsequent heat-straightening on the fatigue and fracture performance of steel girders; (2) identifying and quantifying the material and process parameters that may affect the fatigue and fracture performance of heat-straightened steel girders; and (3) establishing guidelines, including limits on initial damage and critical process parameters, to minimize the potential for fracture and fatigue problems in heat-straightened steel girders.

The research team designed and conducted a major program of large-scale laboratory experiments to accomplish these tasks. Multiple steel girders were dynamically damaged using a large-scale, purpose-built drop-weight machine, repaired using the heat-straightening procedure, and fatigue tested. Up to three damage and repair cycles were made at the same position on a girder. Based on the results of this testing program, the report concludes that the number of repairs should be limited to two for subsequent impact damage within the geometric limits of the first impact repair (i.e., the region where the most severe initial damage was focused).

The research also reviewed and developed (as needed) techniques for evaluation, repair, and inspection of damaged steel girders to assist the owner, engineer, and heat-straightening contractor during the repair process. Finally, the research team suggested changes to the FHWA manual of practice that reflect the findings and conclusions of the project.

This report presents the full text of the contractor's final report of the project and four appendices, which present (1) drawings of purpose-built test equipment and specimen gages (Appendix A), (2) fatigue test results (Appendix B), (3) material properties of the damaged and repaired steel girders (Appendix C), and (4) suggested revisions to 1998 report FHWA-IF-99-004, "Heat-Straightening Repairs of Damaged Steel Bridges: A Manual of Practice and Technical Guide," (Appendix D).

CONTENTS

SUMMARY

Heat-Straightening Repair of Damaged Steel Bridge Girders: Fatigue and Fracture Performance

Based on the results of this research, the effect of damage and subsequent heat-straightening repairs on the fatigue and fracture performance of steel girders has been established. Results of the fatigue testing strongly suggest a consistent decrease in base metal fatigue life following the third repair at the same location. As a result, it is recommended to limit the number of heat-straightening repairs at the same location to two. After the third damage and repair (D/R) cycle, the fatigue testing showed a substantial decrease in the fatigue life at some details, along with a moderated decrease in base metal fracture toughness where the impact occurred.

Following the impact, nondestructive testing (NDT) inspection of the damage areas was performed prior to, during, and following the heat-straightening repair to determine acceptable techniques that can prove whether the above recommendation is viable. Magnetic particle and dye penetrant were deemed effective, and, based on the owner's preference, either one can be employed by qualified personnel conducting inspections of initial damage and completed repairs. Whichever NDT method is selected, inspection concurrent with the evaluation and documentation of the impact is necessary to determine whether any cracks caused by the impact will affect repair methods. This inspection includes the area of impact, other areas damaged due to the impact, and any welded or bolted details within the vicinity of the damage. Careful visual inspection should be made following each heating sequence to ensure that no cracking occurred during the heating and cooling process. Any questionable areas should be subsequently NDT inspected and, if needed, repaired before the heat-straightening continues.

Throughout the research program, other particular factors affecting the fracture performance were recognized. One was the treatment of the impact prior to the heat-straightening process. The research also revealed that untreated impact areas can fracture upon a subsequent impact or even during a repair when high restraining forces are applied for the heat-straightening repair. Simply grinding the impact location to remove or smooth any nicks or gouges greatly reduces the risk of a fracture during the repair process. Another aspect involved limiting the restraining force used to remove sweep from a damaged member. Finite element (FE) studies and laboratory testing indicated that the applied jacking forces may produce large tensile stresses adjacent to the localized damage that can lead to hairline fracture/tearing and possibly brittle pop-in fractures. Reducing the horizontal jacking force 1% for each unit of strain ratio, as determined for the localized damage, appears to prevent brittle fractures during the repair process.

During the repair of impacts near transverse stiffeners, localized bending about the flange-stiffener weld occurred. As repairs of these details progressed, cracks were observed forming at this welded connection and subsequently extend into the flange. To avoid this cracking, the whole stiffener or the portion of the stiffener near the flange being repaired should be removed prior to heat-straightening. Upon completion of the repair, the stiffener may be replaced or reattached to the flange if required using a welded or bolted connection. Lastly, unrepaired damage in the vicinity of fatigue prone details may adversely affect the fatigue life of those details.

FE parametric studies of numerous details with localized damage also were conducted. These studies were performed to develop a stress amplification factor (SAF) equation that could be used to predict the increase in service stress (as a ratio of the calculated nominal stress in the damaged condition) due to the residual damage at that location. Although a repaired member may be within specified tolerances of straightness according to the FHWA manual of standard practice (*2*), the presence of residual damage locally increases the in-service stresses in the member. This equation not only is useful for determining the adequacy of a repair but also provides an assessment of the member during the initial evaluation of the damage.

CHAPTER 1

Introduction and Research Approach

1.1 Background

Damage to highway bridge members can occur when overheight vehicles dynamically impact a structure or a vehicle loses control and strikes a member, such as a hanger in a through truss. The damage occurs at very high strain rates and results in significant plastic deformation of the member. Heat-straightening, along with external restraining forces, has proven to be an effective, accurate, and cost-efficient repair technique when applied correctly.

Fortunately, significant research efforts over the past 20 years led to the development of appropriate techniques and methods to return severely damaged members to their original geometries. Key factors such as heating temperature limits, recommended heating patterns for specific types of damage, calculating the degree of damage and strain ratio, and predicting movement during heat-straightening are now better defined. Less certain, however, is the subsequent fatigue and fracture performance of heat-straightened bridge members.

Although heat-straightening of damaged members provides an economical repair method, the influence of this repair method on the fatigue life or fracture toughness had not been fully investigated prior to this study. Obviously, decreased fatigue life or resistance (e.g., reducing the fatigue resistance of a detail from Category B to D due to heat-straightening) may shorten service life or result in costly future repairs. Details not traditionally prone to fatigue cracking, such as full-penetration butt welds, may become fatigue critical details reducing design loads and anticipated structure longevity and require future retrofitting or repairs if cracking is discovered prior to failure. Furthermore, fatigue cracking in materials with reduced toughness can lead to sudden unanticipated failures. Such a failure occurring in a fracture critical member could cause a sudden catastrophic failure.

1.2 Objectives and Scope

For heat-straightening to become a more widely accepted repair technique and used with confidence, the fatigue and fracture performance of repaired members must be determined. As a result, NCHRP Project 10-63 was initiated with these objectives:

- Determine the relative effects of repeated damage and subsequent heat-straightening on the fatigue and fracture performance of steel girders.
- Identify and quantify the material and process parameters that may affect the fatigue and fracture performance of heat-straightened steel girders
- Establish guidelines, including limits on damage, number of D/R cycles, and critical process parameters, to minimize the potential for premature fracture and fatigue problems in heat-straightened steel girders.

1.3 Research Approach

1.3.1 Experiment Design

Prior to the experimental program development, the current state of knowledge about fatigue and fracture performance of heat-straightened steel girders and applicable field inspection procedures was documented through a critical review of existing literature and relevant research. In addition, a questionnaire to identify fatigue and fracture problems that have occurred as a result of heat-straightening, field inspection and NDT techniques, maintenance practices and policies, and relevant case studies was sent to transportation agencies within and outside the United States. Consultants with experience in heat-straightening and inspection also were contacted to establish the current state-of-practice. In addition, an FHWA-sponsored workshop on heat-straightening repair for damaged steel bridges was held at Lehigh University's

ATLSS Center. The survey and literature review yielded information related to the parameters of the heat-straightening repair process that may affect the fatigue and fracture performance of steel girders after a repair. The experimental program was developed to incorporate these findings. The results of the survey and literature review are presented in detail in the Interim Report (*1*) for this project.

1.3.2 Specimen Configuration and Materials

The most significant aspect of this research was the ability to conduct large-scale fatigue tests on damaged and heat-straightened steel girder specimens with welded details. For this research, three different types of beams were used as the test specimens. A reputable fabricator was contracted to build the specimens using normal bridge fabrication techniques, workmanship, and inspection procedures. All welds were fillet welds made using flux core arc welding (FCAW) and conformed to AWS D1.5 specifications. A visual inspection of the specimens also was conducted upon arrival at the laboratory. This was to identify and provide an opportunity to repair any initial flaws that could have been present that could have influenced the results of the research (e.g., a defect that could initiate fracture during the impact).

The first type of beam tested was an 18 ft (5.5 m) rolled beam. Both a W27X129, shown in Figure 1.1, made of ASTM A992/A572 Grade 50 steel and a W30X116, shown in Figure 1.2, made of ASTM A709/A588 Grade 50 steel were used in the testing program. The details included on these specimens were transverse stiffeners welded to the flanges (Category C′) and cover plate terminations (Category E′). The cover plates and stiffeners were fabricated from A588/A709 Grade 50 steel.

The second type of specimen was an 18 ft (5.5 m) plate girder, referred to as Plate Girder A, fabricated from plates of ASTM A709 Grade 36 steel and includes longitudinal web/flange welds (Category B), transverse stiffeners welded to the flanges (Category C′), and flange attachments (Category E). Plate Girder A (type 1) and Plate Girder A (type 2) contained different size flange attachments as shown in Figure 1.3 and Figure 1.4, respectively. The flange attachments and stiffeners were fabricated from A588/A709 Grade 50 steel.

The last type of beam was also an 18 ft (5.5 m) plate girder, identified as Plate Girder B, fabricated from ASTM A709 Grade 50 steel plates, and includes longitudinal web/flange welds (Category B) and transverse stiffeners not welded to the bottom flange (Category C′). This specimen is shown in Figure 1.5. The stiffeners were fabricated from A588/A709 Grade 50 steel.

1.3.3 Detail Categories Investigated

The specimens were designed and proportioned to include multiple detail categories. With proper detailing, each detail category can be subjected to appropriate stress ranges, ensuring

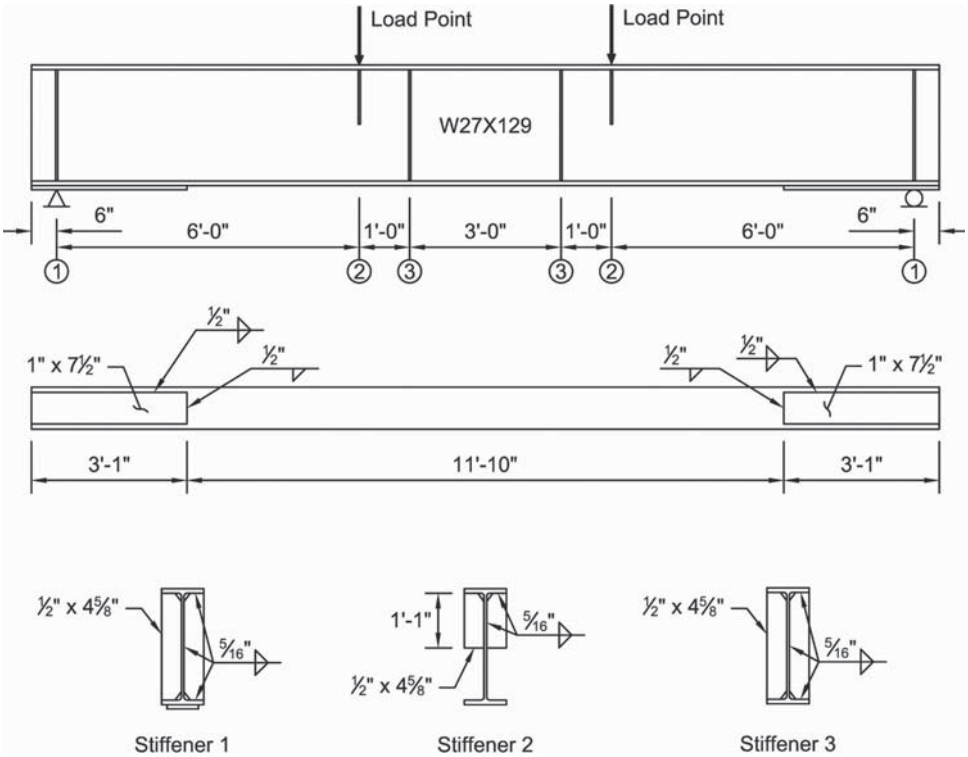

Figure 1.1. W27X129 specimen.

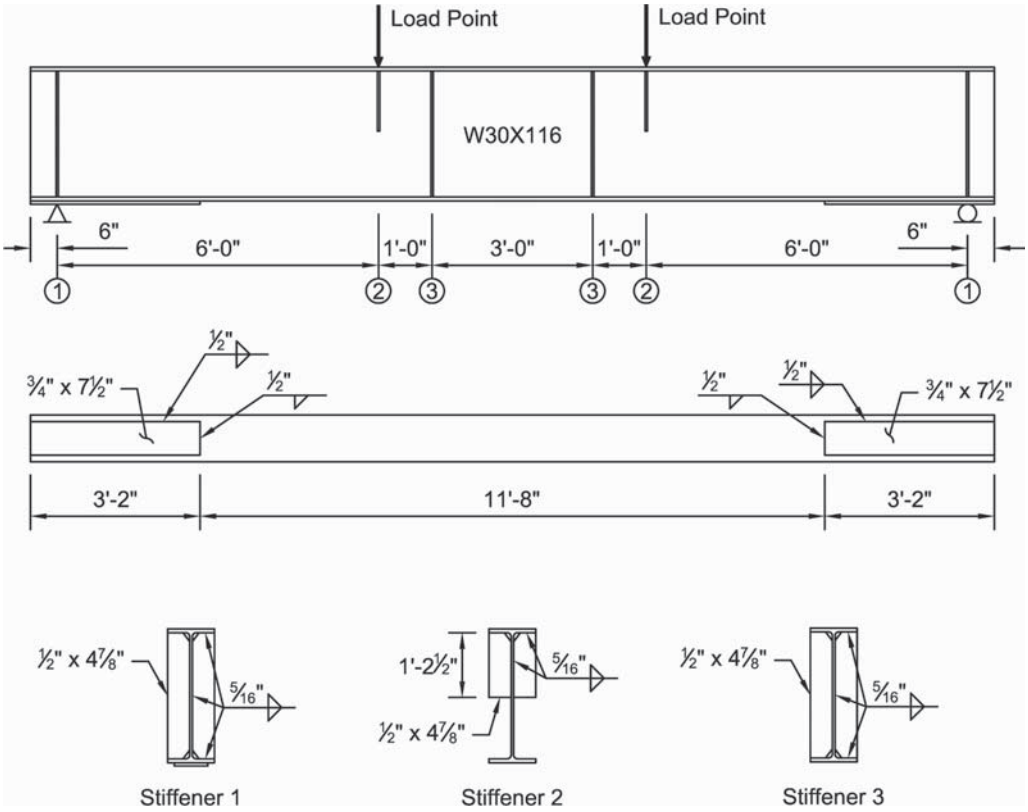

Figure 1.2. W30X116 specimen.

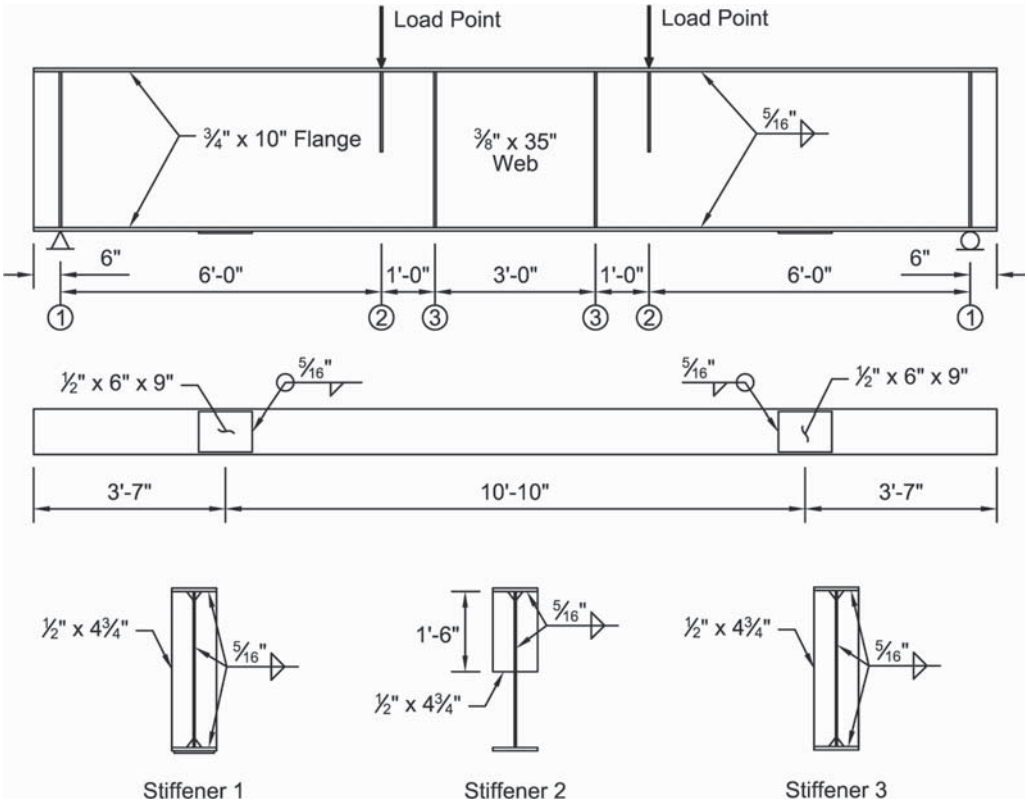

Figure 1.3. Plate Girder A (Type 1) specimen.

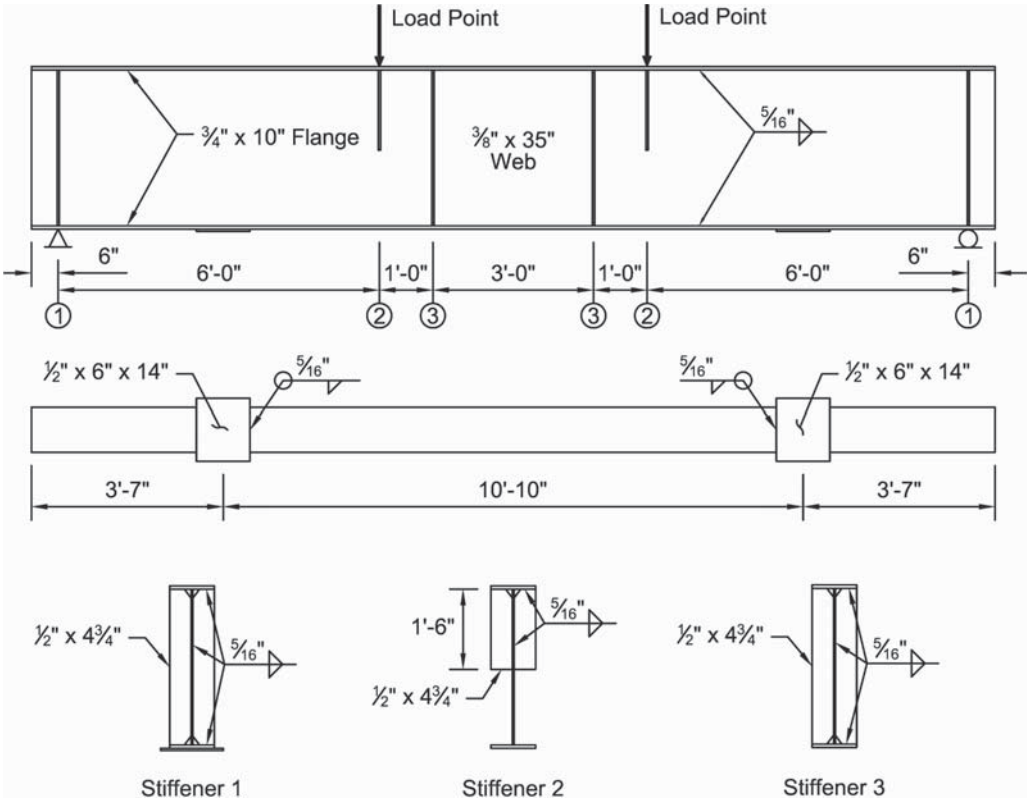

Figure 1.4. Plate Girder A (Type 2) specimen.

accurate results and economy. This is a common approach used to increase the amount of data obtained from each specimen and test program. These specimens all include fatigue testing of base metal (Category A) and the welded plate girders cover longitudinal web-to-flange welds (Category B). Furthermore, even if stress ranges were high enough to cause cracking in base metal, other details such as cover plates or stiffeners, present in welded or rolled beam bridges, would be expected to fail much earlier. Therefore, testing was conducted at much more realistic stress ranges that did not exceed the constant amplitude fatigue limit (CAFL) of Category A and Category B details.

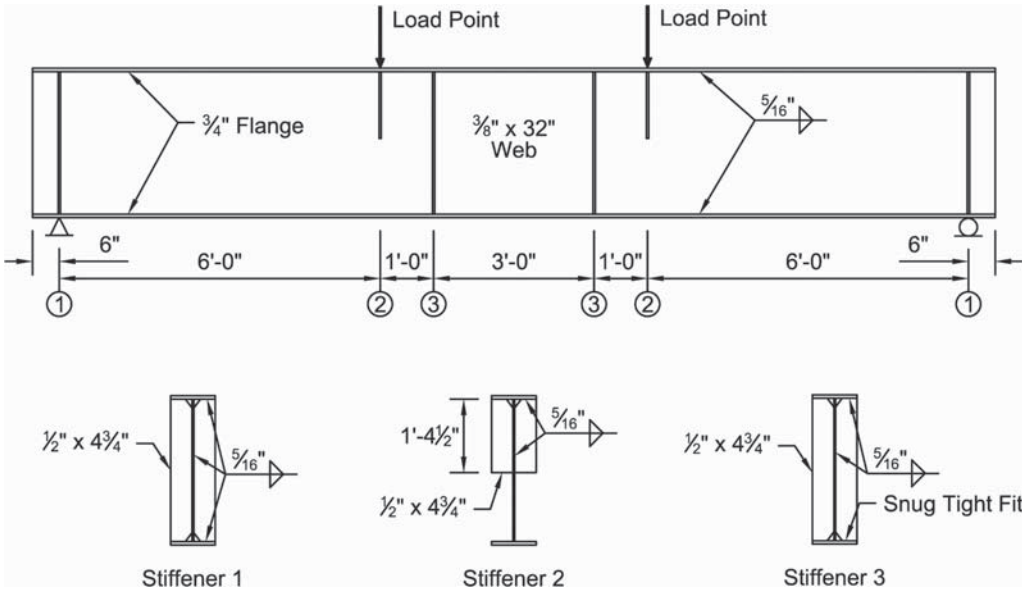

Figure 1.5. Plate Girder B specimen.

Table 1.1. Test matrix.

Specimen Name	Type of Member	Detail Categories	Testing
1D/R-1	W27X129	A/C'/E'	Fatigue test until failure to establish effect of one D/R cycle on fatigue resistance.
1D/R-2	PG-A (Type 1)	A/B/C'/E	
2D/R-1	W30X116	A/C'/E'	Fatigue test until failure to establish effect of two D/R cycles on fatigue resistance.
2D/R-2	PG-A (Type 2)	A/B/C'/E	
2D/R-3	W30X116	A/C'/E'	
2D/R-4	PG-A (Type 2)	A/B/C'/E	
3D/R-1	W30X116	A/C'	Fatigue test until failure to establish effect of three D/R cycles on fatigue resistance.
3D/R-2	PG-B	A/B/C'	

PG – Welded Plate Girder

Transverse stiffeners welded and not welded to flanges are classified as Category C′ details. The CAFL to avoid cracking at such details is 12 ksi (82.7 MPa); the stress range used to test this detail was around 15 ksi (103.4 MPa), a range unlikely in most bridges. When transverse stiffeners are not positively connected to flanges, especially if acting as bracing connections, concentrated out-of-plane deformation may occur within the gap between the stiffener-to-web weld and the flange after an impact. Therefore, these details were considered separately from transverse stiffeners and connection plates welded to the tension flange. In some cases, bracing connection plates not welded to the tension flange have punched through or torn from the web due to an impact.

Cover plate terminations are examples of Category E or E′ details with very low fatigue resistance. The CAFL for Category E′ is only 2.6 ksi (17.9 MPa). Flange attachments with Category E also have a very low CAFL of 4.5 ksi (31.0 MPa). In-service stress ranges in bridges constructed before current fatigue restrictions may exceed these values by a factor of 1.5 to even 2.0. These details were included in the experimental program and tested at a target stress range around 8.0 ksi (55.2 MPa).

1.3.4 Test Matrix

Many bridges damaged by over-height vehicles are periodically struck. In many cases, this is because the bridge was originally built with insufficient under clearance or it is the lowest clearance structure on a route with heavy truck traffic. It is not unreasonable for a given bridge to be damaged and repaired several times. The FHWA manual of standard practice (*2*) currently suggests limiting heat-straightening repairs to the same bridge member to two times regardless of the severity of damage. That manual stated that more than two heat-straightening repairs should not be performed because the remaining ductility may have been exhausted in the member. As a result, fracture of the member could be expected during subsequent straightening or use. However, the conclusion in the FHWA publication was not fully substantiated by large-scale test data.

Therefore, the testing of the specimens included in this research consist of one, two, or three damage and heat-straightening repair cycles. That is, for a specific location near a welded detail, the specimen was damaged and repaired one, two, or three times prior to the fatigue testing. The test matrix outlining these tests is listed in Table 1.1.

Specimens 1D/R-1 and 1D/R-2 were used to study the effect of one D/R cycle on the fatigue and fracture performance of both a rolled beam and a welded plate girder. For two D/R cycles, Specimens 2D/R-1 through 2D/R-4 included rolled beams and welded plate girders. Specimens 3D/R-1 and 3D/R-2—a rolled beam and welded plate girder, respectively—determined the effects three D/R cycles have on fatigue and fracture performance. Each specimen contains multiple detail categories in order maximize the amount of data obtained. The welded details that were fatigue tested on each specimen are listed in Table 1.1 and described in detail in Section 1.3.3. These specimens were fatigue tested until failure or until the test exceeded the mean fatigue resistance of the details.

1.4 Experimental Procedures

1.4.1 Damaging the Specimens

The first part of the testing involved damaging a specimen dynamically near welded details (i.e., cover plate terminations, flange attachments, and transverse stiffeners). Prior to damaging these specimens, an inspection was conducted to ensure any cracking that occurred during the impact was not a result of the fabrication process. To inflict damage to these specimens, a drop-weight machine, similar to those used for drop-weight tear tests but larger in capacity, was used. Detailed drawings of the drop-weight machine are included in Appendix A of this report. The drop-weight machine has a capacity of 200,000 ft-lbs (271,164 J) of energy. The machine is shown in Figure 1.6 and stands approximately 33 ft (10.1 m) high.

The location of the drop-weight machine in the laboratory required a 16 in. (0.4 m) thick post-tensioned, heavily

Figure 1.6. Drop-weight machine.

reinforced concrete pad in order to prevent damage to the lab floor at the ATLSS Center. This also simplified the design by allowing support members to be placed directly on this concrete pad. The two main columns used are 31 ft (9.5 m) W12X190 steel sections secured with 2 in. (51 mm) threaded rod embedded in the concrete pad. As seen in Figure 1.7, the test specimens are supported and secured by rockers welded to the specimen supports (W14X257). The specimen supports are bolted to the main supports (W14X193) that are secured to the concrete pad with concrete anchors. These two supports will raise the specimen enough to prevent the specimen from hitting the concrete pad during the impact.

Along the length of the columns, a Teflon-coated rail separated into two sections was attached. The top portion of the rail is 20 ft (6.1 m) long consisting of a 2 in. (51 mm) wide by 5 in. (127 mm) deep steel bar welded to a series of plates, 10 in. (254 mm) wide by 6 in. (152 mm) high spaced at 1.5 ft (0.5 m), that are bolted along the length of the column. The bottom 8 ft 4.5 in. (2.6 m) of the rail consists of the same 2 in. (51 mm) wide by 5 in. (127 mm) deep steel bar welded to a single plate 10 in. (254 mm) wide by 8 ft 4.5 in. (2.6 m) high by 2 in. (51 mm) thick. This bottom portion is separate from the top to allow for easy and efficient replacement if it were to become damaged during the testing.

The weight dropped on the specimen consisted of a W14X173 steel beam attached to vertical guides that slid along rails. The entire sled that was used for a majority of the specimens weighed 2,945 lbs (1,336 kg); however, additional steel plates were added to increase the weight to 4,600 lbs (2,087 kg) for the W27X129 specimen. The drop-weight machine has a capacity of up to 10,000 lbs (4,536 kg), based on the amount of weight added to the sled. On the underside of the sled is a tup, which applies concentrated impact damage to the specimen. The tup design was based on feedback to the questionnaire that suggested the most common cause of severe impact was large construction equipment, often a backhoe or an excavator, being transported on flatbed trailers. Therefore, the tup was designed to simulate a hydraulic ram on a boom angled at 20°, as illustrated in Figure 1.8.

The tup was fabricated from a 10 in. (254 mm) 4 XX-strong steel hollow pipe bolted onto a solid steel block and angled 20° as shown in Figure 1.9. Calibration specimens were used prior to damaging the actual test specimens to ensure the

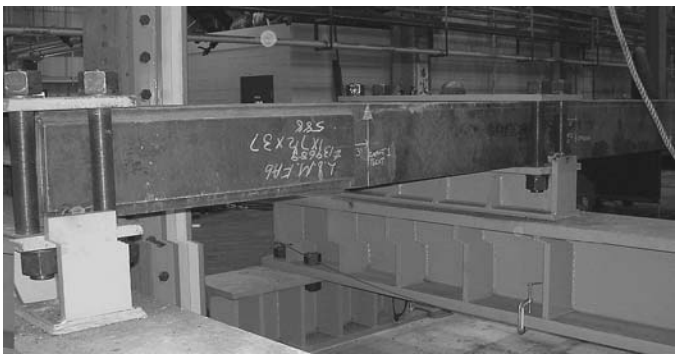

Figure 1.7. Typical setup of a specimen in the drop-weight machine.

Figure 1.8. Illustration of typical impact angle of large equipment.

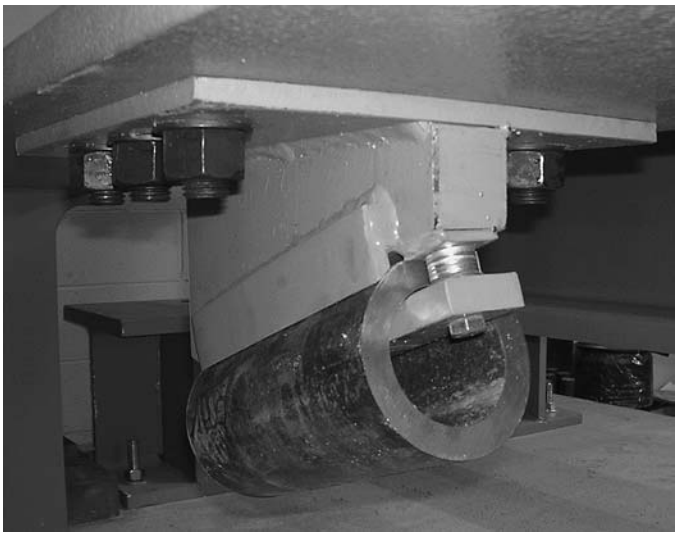

Figure 1.9. Drop-weight machine tup.

impact by the drop-weight machine closely simulated impacts occurring in the field. These calibration beams, which have material thicknesses similar to the test specimens, were used to determine the sled weight and drop height required to achieve the desired strain ratio and degree of damage. This design consistently produced a reasonable replica of "worst case localized damage" suitable for heat-straightening for laboratory testing.

The approach to damaging the specimens was to impact two details (i.e., two impact locations), remove the beam from the drop-weight machine, and repair the damaged areas. In general, the specimens are symmetrical and contain one stiffener and one flange attachment or cover plate detail per half. Following the repair, the beam is repositioned in the drop-weight machine and the other two (undamaged) details on the second half were impacted and subsequently repaired. All four details cannot be impacted in one session since the beam becomes extremely distorted during the first and second impacts; without repairs the beam could not be kept in a stable and safe position within the drop-weight machine for the third and fourth impacts. The procedure to damage and repair in two stages per D/R cycle worked very well for 1D/R and 2D/R specimens, but was not required on specimens 3D/R-1 and 3D/R-2. These 3D/R specimens were used to study the effects of three D/R cycles at only stiffener details and did not include impacts at flange attachments or cover plates.

For the majority of the tests, the impacts were made 5 in. (127 mm) from the flange attachments/cover plates and 6 in. (152 mm) from transverse stiffeners on the specimens. Initially, shorter distances of 3 in. (76 mm) to 5 in. (127 mm) were used, but the localized damage produced by the impact near a stiffener was not as severe as anticipated. Furthermore, although the expected strain ratio was achieved near the flange

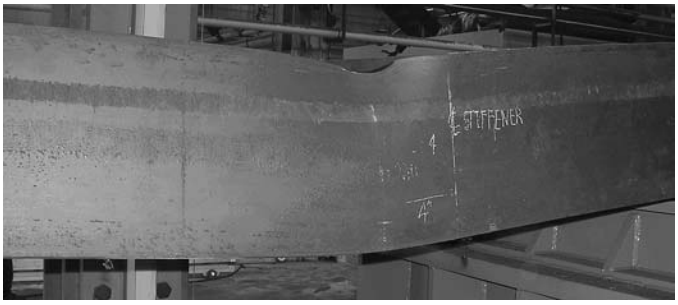

Figure 1.10. Typical global damage from the drop-weight machine impact.

attachments and cover plates with these shorter distances, the weld attaching details to the flange would tear as a result of the impact. Impacts 6 in. (152 mm) from the stiffeners resulted in acceptable strain ratios, and impacts 5 in. (127 mm) from the flange attachments and cover plates did not result in tearing the welds.

The targeted strain caused by these impacts was 100 times the yield strain ($100\epsilon_y$). However, because the method of calculating the strain ratios of the member is approximate and accurately producing this damage on each specimen is difficult, the actual strain ratios were larger or smaller then 100, but within a reasonable amount. Figure 1.10 and Figure 1.11 show typical global and localized damage, respectively, near a stiffener caused by an impact from the drop-weight machine.

The methods used to calculate the degree of damage, ϕ_d, and the strain ratio, μ, in the FHWA manual were incorporated in this program. To calculate the global degree of damage (sweep induced on the bottom flange due to the impact), a taunt line was attached to the specimen on the centerline of the flange

Figure 1.11. Typical local damage from the drop-weight machine impact.

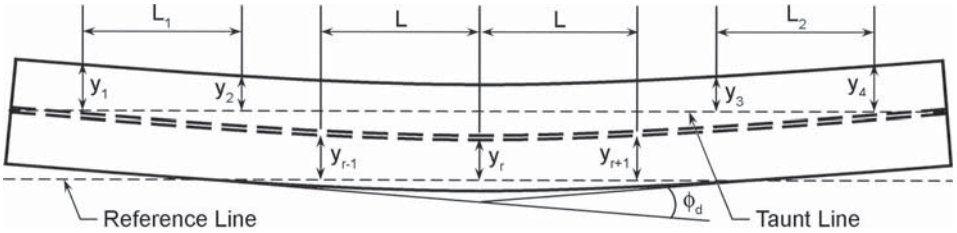

Figure 1.12. Offset measurements to calculate the strain ratio and degree of damage for global damage.

away from the impact as illustrated in Figure 1.12. Measurements y_1 through y_4 and associated lengths L through L_2 were recorded. Note that L_1 and L_2 are arbitrary distances established on a straight portion of the specimen to calculate the slope of each side of the specimen adjacent to the bend. The degree of damage can then be calculated using Equation 1.1.

$$\phi_d = \tan^{-1}\left(\frac{y_1 - y_2}{L_1}\right) + \tan^{-1}\left(\frac{y_4 - y_3}{L_2}\right) \qquad \textit{Equation } 1.1$$

The strain ratio was calculated by taking offset measurements from the web right at the web/flange connection to most accurately represent the curvature of the damage. This was done while the specimen was still lying horizontally in the drop-weight machine. The offsets, y_{r-1}, y_r, and y_{r+1} were measured at a distance, L from each other. The distance, L, must be carefully selected to be within the yield zone of the damage. For these tests, the yield zone was roughly 10 in. (254 mm) long and a distance of 4 in. (102 mm) was used for L. First the radius of curvature was calculated using Equation 1.2.

$$\frac{1}{R} = \frac{y_{r-1} - 2y_r + y_{r+1}}{L^2} \qquad \textit{Equation } 1.2$$

Next, the strain ratio, μ, was calculated using Equation 1.3.

$$\mu = \frac{Ey_{\max}}{RF_y} \qquad \textit{Equation } 1.3$$

where

E = the modulus of elasticity,
F_y = the nominal yield stress,
$y_{\max}$ = the distance from the centroid to the extreme fiber of the element, and
R = the radius of curvature as found using Equation 1.2.

The degree of damage for the typical global damage shown in Figure 1.10 is 8°, with a strain ratio of 126.

For the localized damage, a contour gauge was used to transfer the shape of this damage to a piece of paper where the offsets could easily be measured as illustrated in Figure 1.13. For this type of damage, the degree of damage was not of interest, so only the strain ratio was calculated using Equation 1.2 and Equation 1.3. The strain ratio for the localized damage shown in Figure 1.11 is 79.

Following the impact, thorough grinding of the damaged area ensured that microcracks present in the cold-worked region of the impact would not propagate, generating larger cracks during the heat-straightening process. This is also important to prevent sudden fractures during subsequent impacts, which, through an oversight, occurred on one specimen being damaged at a second location. When the specimen was moved in the drop-weight machine for the second impact within the first half, the previously impacted area at the stiffener detail was directly over a support, placing it in tension during the second impact. This led to a fracture that severed three-quarters of the flange and extended into the web. This

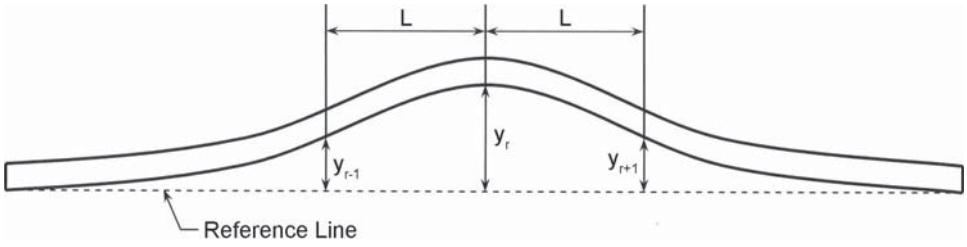

Figure 1.13. Offset measurements to calculate the strain ratio for localized damage.

demonstrated that after an impact, the area must be ground smooth to remove microcracks before a subsequent impact or repair-induced stresses might propagate into larger fractures.

1.4.2 Nondestructive Testing of the Specimens

Recommended NDT methods include, but are not limited to, the following common testing practices: visual (VT), dye penetrant (PT), magnetic particle (MT), and ultrasonic (UT). Although some contacted agencies indicated they do no inspection of impacted members except VT, typically used techniques are considered adequate and were evaluated by the research team. This included VT before an impact along with PT and MT after the impact but before heat-straightening repair, during the repair process, and after the heat-straightening is complete. When repair welds were required on cracked specimens to allow continued testing, an outside contractor used UT. The following sections briefly describe each procedure to better define research team techniques.

1.4.2.1 Visual Inspection

VT inspection is the basic technique used for all welding and damage assessment. It is relatively quick, easy, and requires common equipment, including a camera, flashlight, magnifying glass, mirrors, dial gauges, and measuring equipment. Abundant information should be recorded to completely document the condition to avoid multiple assessment trips to the site. To properly identify problems, the inspector must be familiar with numerous types of deformations, distortions, nicks, cracks and gouges, more serious defects commonly associated with each, anomalies that may preclude certain types of repair, and how each can influence the long-term performance of the member.

1.4.2.2 Dye Penetrant Inspection

PT inspection is useful only to detect discontinuities open to the surface. The surface is cleaned to remove oil, dirt, water, or other contaminants. Then a penetrating liquid dye, either visible or fluorescent, is placed on the surface of the member and enters any discontinuities. After a period of time (up to 30 minutes) based on temperature and crack size, the excess dye not drawn into crack-like openings by capillarity is removed, and the area is allowed to dry. Then a developer is applied with a hygroscopic attraction greater than capillarity, pulling the residual dye from the discontinuities. Figure 1.14 shows PT of the impact zone after the specimen has been damaged. Note the crack circled on the right side of the impact. Penetrant inspection is inexpensive, simple, and easy to learn. However, inspectors need to be properly trained in preparation, dwell time, limitations, and distinguishing between real and false indications.

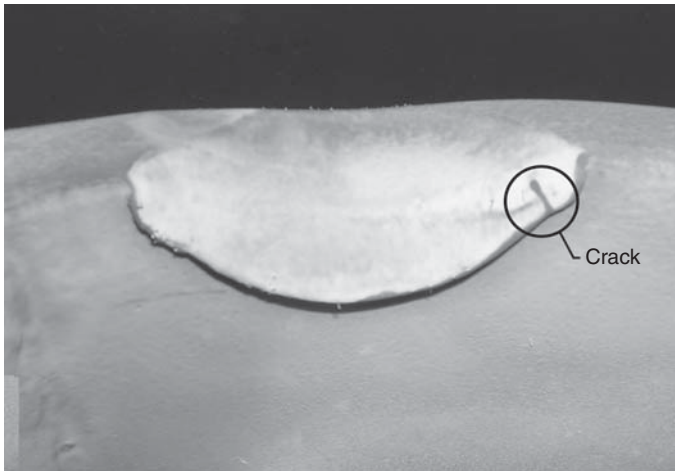

Figure 1.14. Example of dye penetrant inspection.

1.4.2.3 Magnetic Particle Inspection

MT inspection involves the use of magnetic fields to determine whether surface or near-surface cracks exist by indications of disruption of the field by a discontinuity in the member (e.g., a crack). The material can either be magnetized by an electromagnetic yoke (direct magnetization) or by inducing a magnetic field around a current path between prod contacts (indirect magnetization) in the member. Once the field is established, magnetically attracted particles (typically in the form of a colored iron powder) are placed on the inspection surface. Discontinuities are exposed when they are drawn together by the leakage of magnetic flux at a disruption in the magnetic field. The location, shape, and length of a crack or other discontinuity can accurately be determined. Figure 1.15

Figure 1.15. Magnetic particle inspection—placement of the magnetic field.

Figure 1.16. Magnetic particle inspection—application of magnetic particles.

through Figure 1.17 show this process and the required equipment.

With sufficient access, the test can be conducted very quickly, and, compared with other NDT methods, it is relatively cost effective in terms of equipment and preparation. In contrast to PT, MT can reveal shallow cracks below the surface, is very accurate, requires less time, and may be more economical after the equipment is obtained. This procedure is favored by many inspectors for assessing impact damage.

1.4.2.4 Ultrasonic Inspection

UT inspection is another commonly used NDT method. By using high-frequency sound waves, subsurface discontinuities can be detected. As the sound waves travel through the material and are reflected back by anomalies, the presence and location of discontinuities in the member can be determined based on information displayed on a screen. A repair weld at a stiffener due to a crack received UT as shown in Figure 1.18. Advantages in using this type of test are the ability to detect and evaluate small internal discontinuities; accuracy; and real-

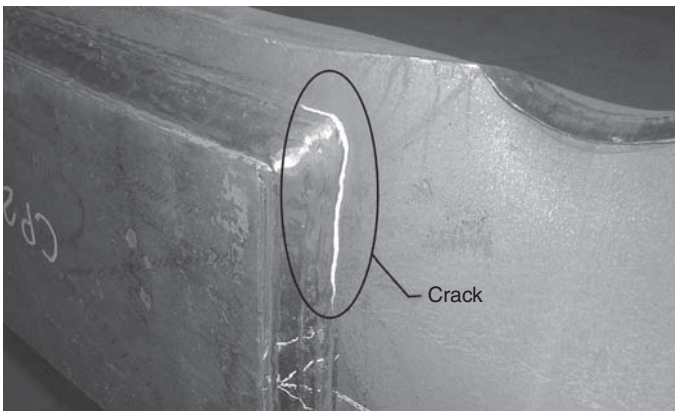

Figure 1.17. Magnetic particle inspection—results.

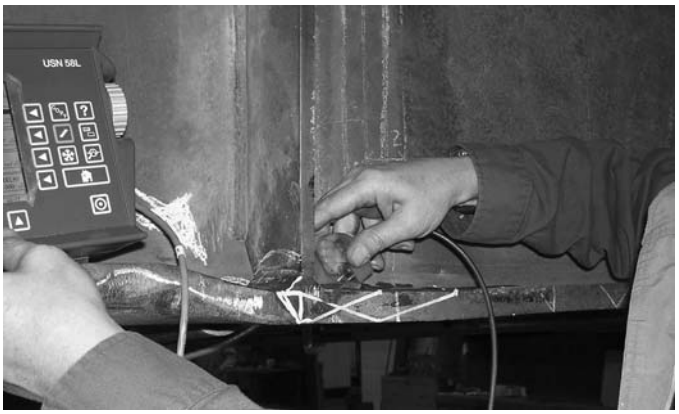

Figure 1.18. Example of ultrasonic inspection.

time and repeatable test results. The primary disadvantage is that highly trained and experienced technicians are needed to operate and accurately interpret this equipment.

1.4.3 Heat-Straightening the Specimens

After the inspection is completed, any flaws caused by the impact have been repaired or removed, and the degree of damage, strain ratio, local damage, and other factors are deemed appropriate for heat-straightening, the specimen was repaired by the current state-of-practice heat-straightening techniques. Members of the FHWA manual project review committee were contracted to train selected individuals on the heat-straightening repair of the specimens used for this research project. The training included a demonstration of a heat-straightening repair of two impacts made on two specimens from the calibration of the drop-weight machine by the contractor. A third impact was repaired under the supervision of the contractor to ensure that the training was adequate and the work was completed properly.

The training closely followed the guidelines listed in the FHWA manual, but other procedures used in the field also were covered by this training and utilized for this research to be consistent with typical field practice. The fixture used for the heat-straightening repairs can secure two specimens simultaneously and is shown in Figure 1.19. A reaction beam, similar in size to the specimens, was welded to heavy W14 sections to raise the specimens off the ground. The reaction beam provided resistance for the jacks when the restraining forces were applied to the specimen.

Heat-straightening is a basic concept that relies on three properties of steel used for bridge construction. First, once steel passes its yield point, further strain causes permanent deformation. Second, the yield point of steel decreases significantly when the temperature is elevated to around 700°F (370°C) to 1300°F (700°C). Third, steel expands when heated and contracts during cooling. This expansion or contraction

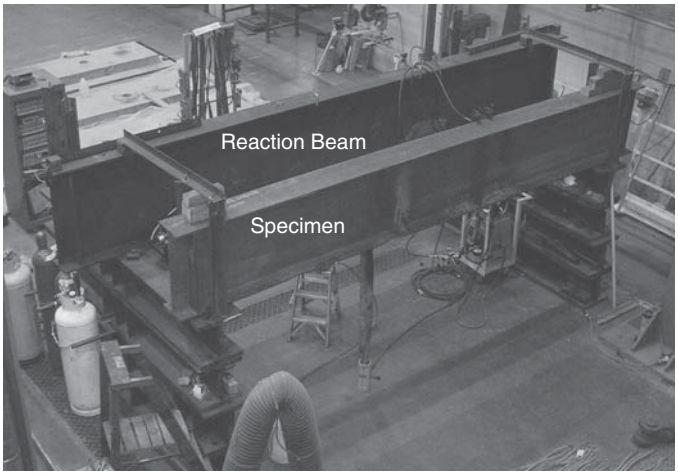

Figure 1.19. Heat-straightening fixture for two specimens.

occurs in all directions if the steel is unrestrained, but a restraint in one direction can increase displacement in the other unrestrained directions. Figure 1.20 illustrates how steel can be permanently deformed using these two properties. Figure 1.20a consists of an undeformed steel bar. This bar then is placed in a clamp that is tightened snugly, and then a zone is heated as shown in Figure 1.20b. During this heating process, the steel only will expand laterally and transversely because of the longitudinal restraint, thus creating restraining forces on the clamp as seen in Figure 1.20c. Also shown is the bulge that occurred due to yielding at an increase in temperature in that heated zone. Once the heat is removed from the area, the bar will contract in three-dimensions causing the bar to shorten and the bulge to shrink as seen in Figure 1.20d. This process can be repeated until the desired length is attained.

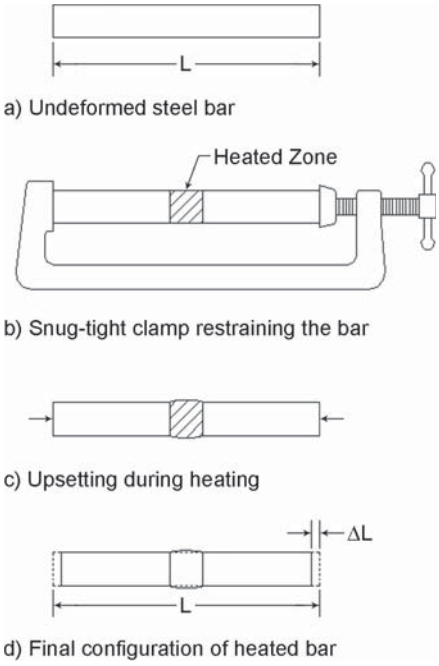

Figure 1.20. Conceptual example of shortening a steel bar.

The same principle can straighten damaged steel bridge girders, but different heating patterns along with restraining forces are used. The most common type of heating pattern for straightening damaged bridge members is called the vee heat, used to remove sweep from the specimen. A vee is drawn in the yield zone of the flange and heating begins at the apex. Once the desired temperature of 1,200°F (650°C) is reached, the torch is advanced in a serpentine motion toward the base of the vee. During heating, as metal expands, a hydraulic jack restrains the flange from moving laterally toward the base of the vee, as shown in Figure 1.21. As the steel cools, the vee will contract, shortening the side of flange elongated by the impact. This process was repeated until sufficient sweep is removed from the specimen to satisfy straightness tolerances. Initially, full-depth vee heats were used, as shown in Figure 1.21, which produces the most movement, however moderate longitudinal shortening of the flange occurred. To prevent this shortening, three-quarter depth vee heats, typical for most applications in practice, were used for the remaining specimens.

Another common heating pattern is a line heat. This is used mostly for weak axis bending of plates and localized damage around the impact zone and web bulges. A line placed on the convex area of the damage, as shown in Figure 1.22, is subjected to bending moments produced by the restraining force. The line is heated in one pass and during the cooling process, the side of plate that was heated will contract, flattening the convex side of the bend. This may need to be repeated until the damage is sufficiently removed. Both line heats and vee heats are used together to restore the original geometry. No accelerated cooling was used for this research,

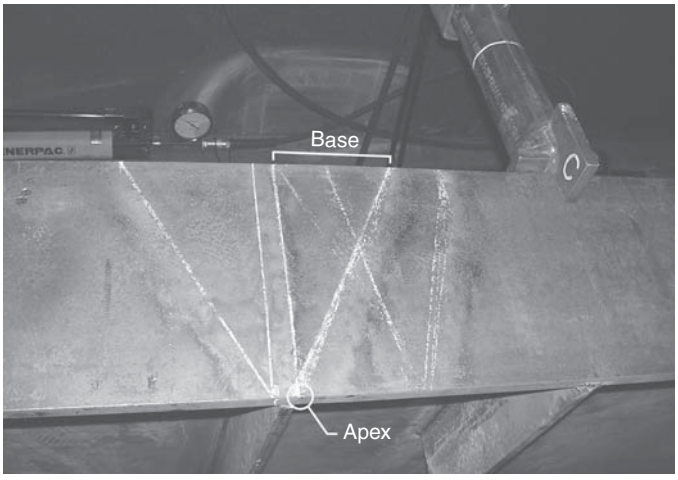

Figure 1.21. Example of a vee heat and restraining force.

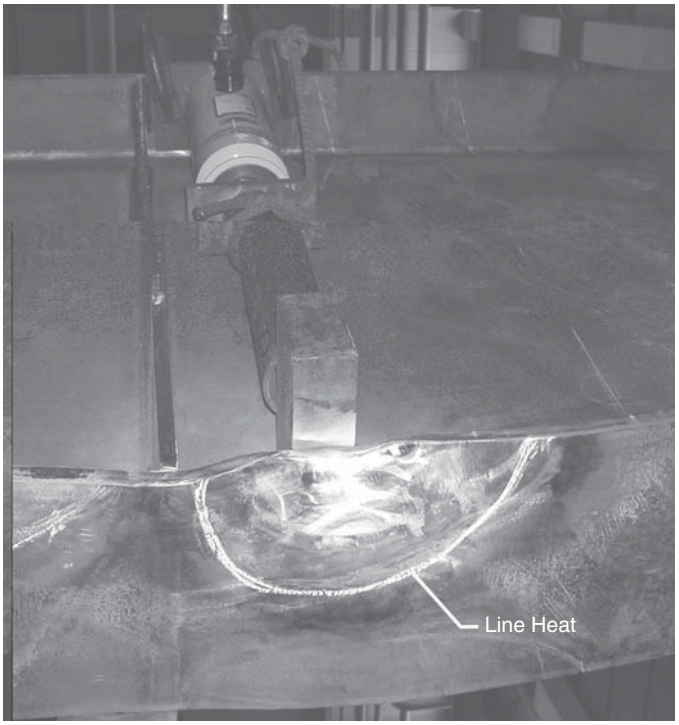

Figure 1.22. Example of a line heat and restraining force.

and subsequent heating cycles began once the steel cooled to 250°F (120°C) or less.

The restraining forces selected for this research project were determined using the simplified estimating methods in the FHWA manual and based on the plastic moment capacity of the member. Because the material's yield strength at 1,200°F (650°C) is approximately 50% of yield at ambient temperature, the moment (M_j) produced in the damaged area by the restraining force must be less then one-half of the calculated plastic moment capacity of the area, M_p, at ambient temperature, as in Equation 1.4:

$$M_j \leq \frac{M_p}{2} \qquad \textit{Equation } 1.4$$

Using the appropriate heat-straightening techniques, the distortion caused by an impact can be successfully corrected. Figure 1.23 shows the damaged specimen after an impact near a flange attachment and the same specimen after a successful heat-straightening repair. Depending on the number of D/R cycles specified in the testing matrix, a welded detail may have been damaged at the same location up to three times, for this research.

1.4.4 Fatigue Testing the Specimens

Upon completion of the heat-straightening process, the specimens were inspected and then fatigue tested. The testing equipment, shown in Figure 1.24, was the same used for previous NCHRP fatigue studies conducted at Lehigh University's Fritz Laboratory. The Amsler system uses two variable-stroke hydraulic pumps, or pulsators, spaced 5 ft (1.5 m) apart, creating four-point bending on the specimen. The pulsators ran at a constant amplitude, based on the configuration of the specimen, at 64 cycles per minute. The constant moment region between the two pulsators contained the transverse stiffeners, which are Category C′ details. The moment gradient regions on both sides of the constant moment region contained the Category E′ cover plate terminations for the rolled beam specimens or the Category E flange attachments for the Plate Girder A specimens.

Figure 1.23. Before and after a heat-straightening repair.

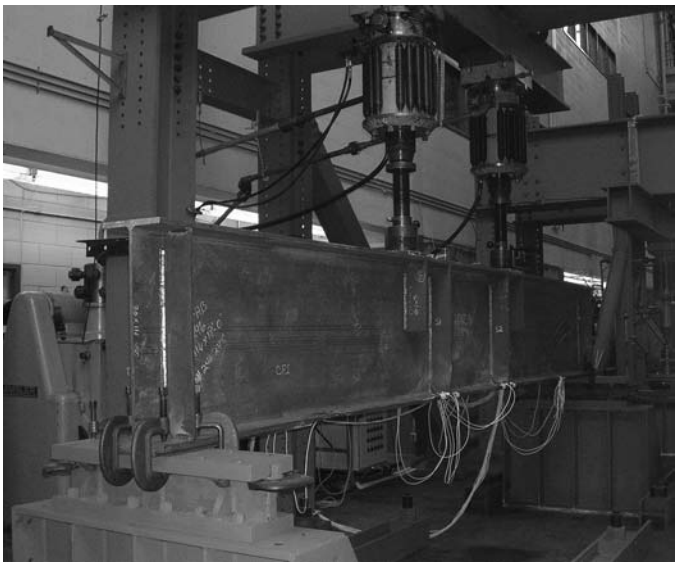

Figure 1.24. Typical fatigue test setup.

The instrumentation included both type CEA-06-250UW-350 bondable and type LWK-06-W250B-350 weldable strain gages manufactured by Measurements Group Inc. These uniaxial gages had an active grid length of 0.25 in. (6 mm), a resistance of 350 ohms, and an excitation voltage of 10 volts. Grinding, fine sanding, and cleaning were required for the preparation of the metal surfaces before the installation of the gages. Figure 1.25 shows both protected and unprotected bondable strain gages placed at a cover plate detail. A Campbell Scientific CR9000 Data Logger used for the collection of the data is a high-speed, multi-channel 16-bit system configured with digital and analog filters to ensure noise-free signals. This logger was connected to Lehigh University's network and the real-time data could be viewed from any computer with the necessary software. A Sony webcam also was connected to the network, providing real-time test video that could be viewed from any web browser.

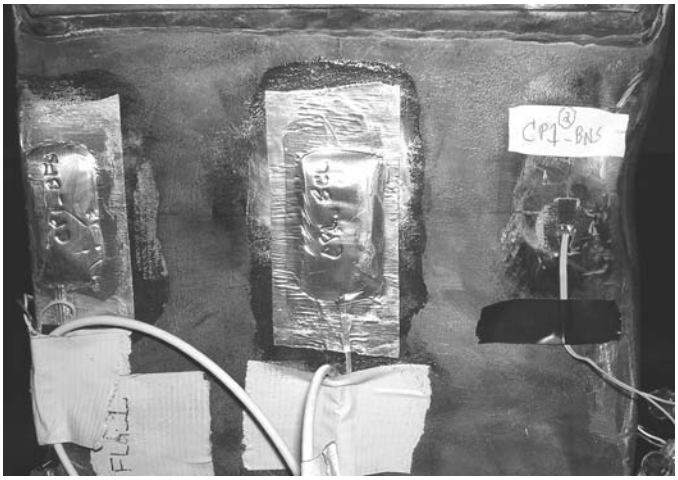

Figure 1.25. Protected and unprotected bondable strain gages at a cover plate detail.

The fatigue testing consisted of two parts. First a static test was conducted on the specimen to ensure instrumentation accurately indicated that the desired stresses were present due to the applied load. The stress was recorded by the logger at a sampling rate of 10 Hz. Following the static test, a dynamic test was conducted with the stress range determined during the static calibration. The dynamic data was recorded by the logger at a sampling rate of 250 Hz. Stress range histograms, periodic stress cycles, and real-time monitoring were available throughout the testing. The stress-range histogram was used to determine the effective stress range for the number of cycles experienced. This data then was compared with the current AASHTO stress cycle curves to determine any effects the heat-straightening had on the fatigue performance of the specimens.

1.4.5 Material Testing of the Specimens

Changes in the material properties of steel—such as toughness, ductility, and the ratio of yield to ultimate tensile strength due to a damage and heat-straightening repair as well as an unrepaired impact—were measured. The material properties for all the specimens were determined at the time of the rolling process as listed in the mill certifications provided by the fabricator. Laboratory Testing Inc. was hired to machine material from the specimens into tensile and Charpy V-notch (CVN) specimens along with conducting a chemical analysis of each of the specimens. These specimens were machined from extra material from each specimen supplied by the fabricator; material from the localized damage region of each of the specimens following the fatigue testing; material from impacts made at the repaired locations following the fatigue testing; and material from impacts made on the compression flange where no previous D/R cycles had been made. These specimens then were tested at the ATLSS Center at Lehigh University. Fractographic analysis also was conducted for all these locations as well.

CHAPTER 2

Findings

2.1 Literature Review

A literature review of all domestic and foreign literature and research pertaining to the current state of knowledge on the fatigue and fracture performance of heat-straightened steel members was conducted. The results were presented in the Interim Report (*1*) for this project. Overall, it has been found that the process associated with heat-straightening repair has been well studied and documented. The outcome of the previous work has resulted in generally acceptable repair techniques currently used in practice today. A compilation of these repair methods are in an FHWA manual of standard practice (*2*), considered as the accepted guideline by agencies across the United States.

The effects on the material properties of bridge steel caused by cold working/forming, hot working/forming, flame straightening (rapid cooling without restraining forces), and heat-straightening (current practice) also is presented in the FHWA manual. This and other earlier studies also reported some general trends about changes in bridge steel properties due to heat-straightening, including a modest increase in the yield and tensile strength, a slight decrease in the modulus of elasticity and hardness, a one-third reduction in ductility, and small changes in the notch toughness. However, the number of D/R cycles was not correlated to material property changes in all tests. For example, tensile properties were evaluated on specimens subjected to multiple (up to eight) D/R cycles, while the notch toughness test was typically conducted on specimens after only one D/R cycle.

Recent research was conducted by Varma and Kowalkowski on the effects of multiple D/R cycles on the structural properties of steel (*3*). Numerous specimens from different grades of steels were tested with varying strain ratios, restraining forces, and numbers of D/R cycles. Tensile properties and fracture toughness were determined at the completion of the testing. The tensile property results were analogous to previous research and the fracture toughness showed slight to moderate decreases. Results were dependent of the severity of damage and the grade of steel. For the most part, the final fracture toughness was at least 50% of the original toughness when observing the recommended temperature and restraint limits for three repairs for ASTM A7 and A36 steel and five repairs for A588 steel. Note that material tests were taken at the base of the vee heats to provide an adequate amount of specimens from heated areas, but earlier research has shown that the greatest reduction in the fracture toughness occurs at the apex of the vee. Although the generalized effects of the heat-straightening process should be represented by that testing, the worst case, in terms of fracture toughness, would require taking CVN test specimens from the apex of the vee heats. Variability in the results also must be taken into consideration during analysis.

Aside from the two preceding studies that focused on material properties, two papers essentially reporting the same findings documented the fatigue performance of heat-shortened eyebars. This was the only research found related to fatigue of heat-shortened bridge material. Two publications (*4, 5*) from 1946 summarized research conducted by Wilbur Wilson on the fatigue strength of eyebars shortened by heating and upsetting. This research was performed on eyebars that stretched due to heavy locomotives traveling at high speeds across pin-connected truss bridges. To correct this elongation, the eyebars were clamped to prevent additional elongation, then heated to a cherry red, 1,600°F–1,800°F (870°C–980°C), causing them to upset. Due to bar size, cutting and bolted splicing was not an option, and welding was not practical, so this was the favored method since 1916.

Wilson conducted fatigue tests at the University of Illinois on shortened and unshortened specimens taken from a bridge to determine the effect on the fatigue and static strength. The tests conducted on the flame-shortened eyebars resulted in failure after 814,200, 941,900 and 956,500 cycles under a stress cycle of 0 to 33.5 ksi (0 to 231.0 MPa), 0 to 33.0 ksi (0 to 227.5 MPa), and 0 to 33.0 ksi (0 to 227.5 MPa), respectively.

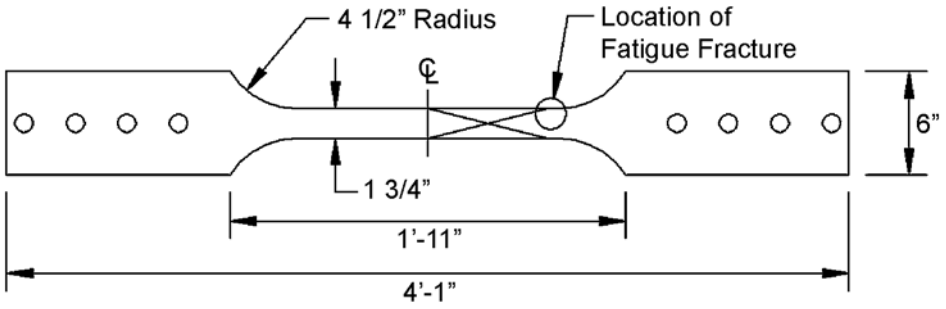

Figure 2.1. Location of fatigue fracture of heat-shortened eyebar.

All failed at the limit of upsetting length, shown in Figure 2.1. It was concluded that there was no effect on the fatigue or static strength. This study, however, did not include any major initial damage (i.e., strains greatly exceeding yield strain) other then minor plastic strains (i.e., strains just exceeding yield strain) caused by dynamic loading and only considered one damage and repair cycle.

2.2 Questionnaire

A two-part questionnaire was sent to 54 departments of transportation, including Washington, D.C., Puerto Rico, and Northern Mariana Islands; seven Canadian provinces' Ministries of Transportation; England's Department of Public Works; and 26 other agencies, including turnpike authorities and bridge commissions. The questionnaire was designed to collect detailed information about previous heat-straightening projects and inspection techniques. A total of 32 responses to the questionnaire were returned, including 25 from state departments of transportation, one from a Canadian province's ministry of transportation, and six from miscellaneous agencies. A detailed summary of the responses to each question in the two-part questionnaire were presented in the Interim Report for this project (*1*).

2.3 Fatigue Performance

The results of the fatigue testing are presented in this section. In addition, findings associated with the repair processes for each specimen also are discussed. Gage plans for each of the specimens are located in Appendix A. Detailed results for each of the fatigue tests are located in Appendix B.

2.3.1 One Damage/Repair Cycle

2.3.1.1 Specimen 1D/R-1

Specimen 1D/R-1 was a W27X129 rolled beam used to investigate the effect one D/R cycle has on the fatigue performance of rolled beams. The fatigue details on this specimen were transverse stiffeners welded to the tension flange (Category C′) and cover plate terminations (Category E′). The summary of the damage imposed on this specimen is listed in Table 2.1. The weight (including the sled of the drop-weight machine) used for the impacts made near Stiffener 1 and Cover Plate 1 was 2,945 lb (1,336 kg) that was dropped 20 ft (6.1 m). For the impacts made at Stiffener 2 and Cover Plate 2 the weight was increased to 4,600 lb (2,087 kg) and dropped 20 ft (6.1 m) in order to reach the desired strain ratio established during the design of the experimental program. No cracks or fractures due to these impacts were found by PT inspection following the impacts.

During the repair process of the impact at Stiffener 2, a crack formed during a cooling cycle at the toe of the weld on the flange as seen in Figure 2.2. This crack extended from the edge of the bottom flange to approximately 1 in. (25 mm) from the web and roughly through three-quarters of the flange thickness. Upon finding this crack, the heating temperatures and restraining forces were closely evaluated to ensure all were within limits. This proved that applicable heat-straightening procedure recommendations in the FHWA manual were being satisfied, so the crack was not the result of procedure errors during the process. The general repair procedures used by the researchers also were consistent with those specified and commonly used in practice today. After examination of the exposed crack surface, the research team was confident that the crack was initiated by the tearing of localized "bunched" flange material at weld toe and not by a brittle fracture caused by overheating. This inelastic compressive bunching of flange material at the flange-stiffener weld was due to the impact bending the top of the flange toward the stiffener. As the steel

Table 2.1. Specimen 1D/R-1 damage summary.

Location	Impact Distance from Detail (in.)	Global Damage		Localized Damage
		Degree of Damage	Strain Ratio	Strain Ratio
Stiffener 1	6	10	57	20
Stiffener 2	5	8	91	80
Cover Plate 1	3	9	34	15
Cover Plate 2	3	12	91	25

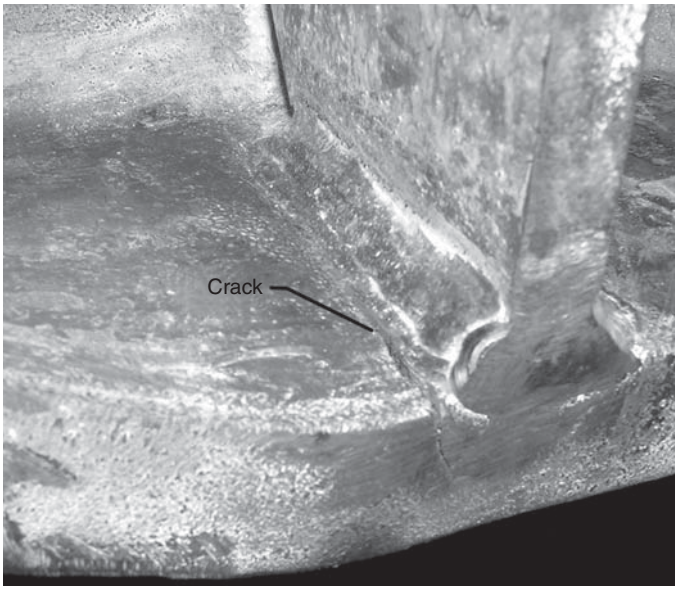

Figure 2.2. Crack at Stiffener 2 on Specimen 1D/R-1.

cooled, the bunched flange material tore away from the flange-stiffener weld, forming the crack.

The heat-straightening was halted and the crack was completely ground out to prevent further propagation. Because of the reduced thickness of the flange, a repair weld (see Figure 2.3) was made prior to finishing the heat-straightening repair to ensure that further damage would not result. After completion of the repair weld, the area was UT inspected by a certified outside contractor and was accepted in accordance to AWS D1.5-2002. This type of cracking, although very minor, also occurred at Stiffener 1, where the localized damage was not as severe.

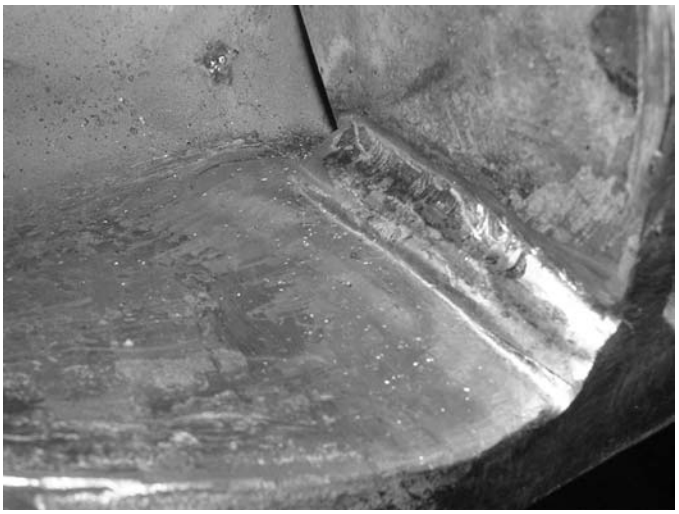

Figure 2.3. Repair weld at Stiffener 2 on Specimen 1D/R-1.

Although the restraining forces were within the limits listed in the FHWA manual, minor hairline fractures, 0.75 in. (17 mm) long and 0.1 in. (3 mm) deep or smaller, formed on the underside of the flange in the repaired localized damage regions of all four impacts on Specimen 1D/R-1. The FHWA manual indicated that this type of cracking is a common occurrence and may be a result of over jacking. These hairline fractures were ground out and the area was inspected using PT to ensure the cracks were removed. In addition, minor cracking developed in the weld toe on the flange at the cover plate corner closest to the impact on both cover plate details. These cracks also were ground out and inspected using PT.

During the heat-straightening process, clamps were used to ensure stability of the beam in the fixture so it could not roll over as the repair progressed. Due to the lack of dead load restricting the upward movement and the restraint of the clamps, the beam developed camber, resulting in minor localized bending of the bottom flange in addition to that caused by the impact, as shown in Figure 2.4. Full-depth vee heats on the flange to remove the sweep from the damage caused member shortening, also contributing to the camber. No further repairs were made, and this bending was considered to be damage that was not fully repaired. The repaired damage was within the tolerance limits listed in the FHWA manual. As verified through FE analysis and instrumentation installed on the specimen, this global camber had no effect on the fatigue stress range at the details of interest. To mitigate this problem on subsequent repairs, new supports were made to allow the specimen to be free to move, yet remain stable in the heat-straightening fixture.

After repairs were complete, the specimen was cyclically loaded at a constant amplitude for 2.242 million cycles. The test ended when a crack formed at Stiffener 2, severing 90% of the flange and extending up 6 in. (152 mm) into the web. The failure occurred at roughly 183,233 cycles past the mean value of fatigue life at a stress range of 16.3 ksi (112.4 MPa). This data point, shown as a solid diamond in Figure 2.5, along with the remaining data that did not crack are presented on a

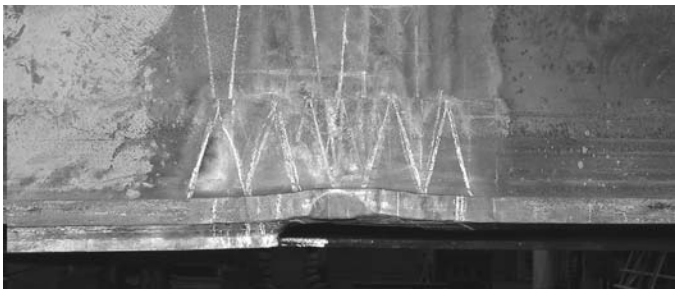

Figure 2.4. Induced camber due to heat straightening on Specimen 1D/R-1.

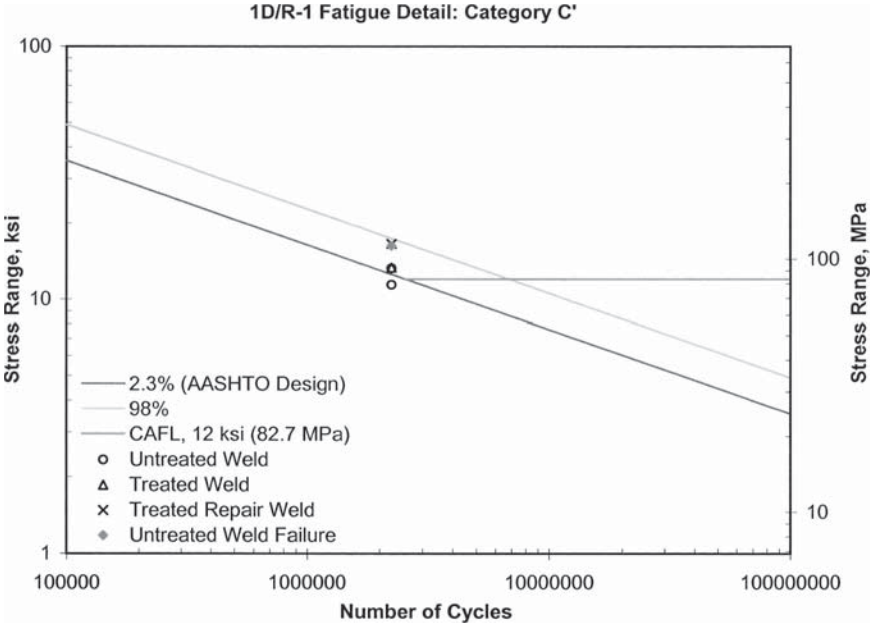

Figure 2.5. Specimen 1D/R-2 fatigue test results—Category C′.

stress-cycle (SN) curve for the particular detail category along with the CAFL, the 2.3% probability of failure AASHTO design curve, and the 98% probability of failure curve. Note that because of the cracking that occurred on the specimen prior to fatigue testing, some of the data include "treated" weld toes. (In this case, treated means the welds were either ground to remove small cracks at the weld toe or repaired.) The tabulated results of the fatigue tests can be found in Appendix B. Similarly, the data, none of which represent a failure, for the Category E′ details is shown in Figure 2.6.

2.3.1.2 Specimen 1D/R-2

Specimen 1D/R-2 was a welded plate girder specimen (Plate Girder A, Type 1) used to investigate the effect one D/R cycle has on the fatigue performance of welded plate girders.

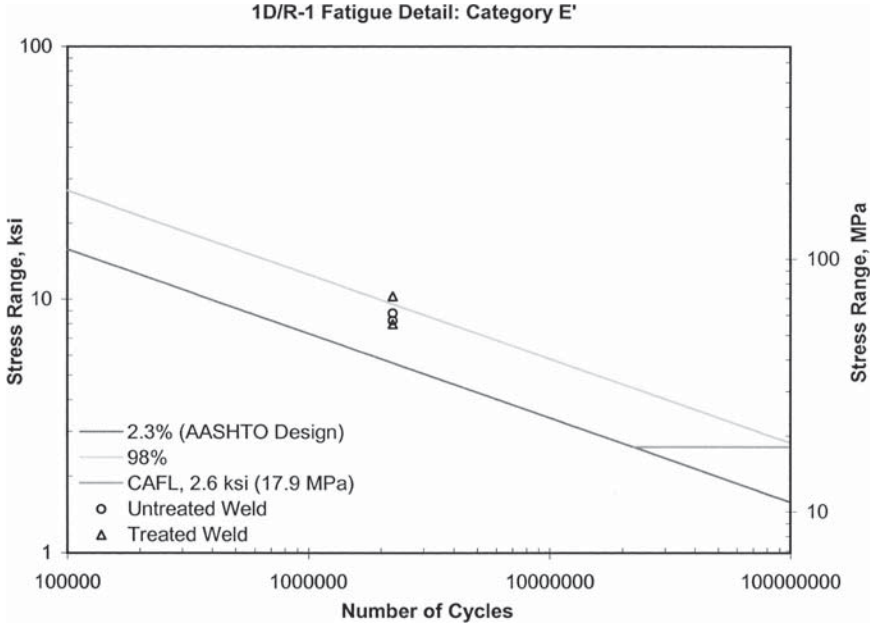

Figure 2.6. Specimen 1D/R-1 fatigue test results—Category E′.

The fatigue details included transverse stiffeners welded to the tension flange (Category C′) and flange attachments (Category E). The summary of the damage imposed on this specimen is listed in Table 2.2. Using PT immediately following the impacts, no cracks or fractures were found.

During the repair process, cracking occurred at the weld toes on the flange at both stiffener details that were closest to the impact point. The cause of these cracks was similar to those that occurred on specimen 1D/R-1, however not as severe. These shallow cracks were ground smooth, which did not require a repair weld, and inspected using PT.

Minor hairline cracks were observed on the underside of the repaired flange in the localized damage region, similar to those seen on specimen 1D/R-1. These cracks, occurring at all four impact locations, were removed by grinding and inspected using PT. In addition, minor cracking developed in the weld toe on the flange at the corner of each flange attachment closest to the impact point. This was removed by grinding and inspected using PT. No repair welds were required for either of these minor cracks.

Prior to the fatigue testing, a static load is applied to the specimen to ensure all instrumentation was operating properly. During this static calibration, it was found that the stresses near the points of impact on the underside of the bottom flange near the flange attachments were much higher than anticipated and did not agree well with elementary (Mc/I) beam theory. Although the damage was repaired consistently with the recommended procedures and tolerance included in the FHWA manual, these permit some level of residual geometric damage to remain. Additional instrumentation was added and an FE model, which included the geometry of one of the damaged details, was built to investigate the cause for the discrepancy. The increase in stress was determined to be due to the effects of residual geometric damage that remained in the flange. As tensile stresses are applied to the locally curved portion of the flange, secondary bending stresses are produced as the flange tends to straighten. Since these are (local) bending stresses, they are additive on one side of the flange but are subtractive on the opposite surface, an issue described in more detail in Section 2.6 Residual Damage Evaluation.

The distribution of measured stresses in the beam is presented in Figure 2.7. Also shown in parenthesis are the theoretical stresses for the same loading. As can be seen, the stresses at the flange attachments are as much as 1.8 times greater than predicted by traditional beam theory. This presented a problem for the fatigue testing since the beam was proportioned so the flange attachment and stiffener details would theoretically last for approximately the same number of cycles. Due to the elevated stresses observed at the flange attachments, cracking was expected between 300,000 and 500,000 cycles but cracking at the stiffeners would not be expected until 1.3 to 1.5 million cycles. Furthermore, an objective of the research was to conduct the testing at nominal stress ranges that were not significantly greater than the CAFL of the given detail. If tests were run at a load producing sufficient stress ranges at the stiffeners, about 15 ksi (103.4 MPa), the applied stress range at the flange attachments would approach twice the target value. Hence, the details would likely crack well before the stiffeners even if the heat-straightening had no effect on toughness or ductility.

To compensate for the increase in stress at the flange attachments, a decision was made to divide the test into two separate phases, evaluating each of the details separately. The first fatigue test was used to test the flange attachments, Category E, at a stress range of 9 ksi (62.1 MPa). The stress range produced at the stiffeners, Category C′, was only 10.5 ksi (72.4 MPa), which is below the CAFL of 12 ksi (82.7 MPa) for these details. At this stress range, the C′ details are considered to have infinite fatigue life and the cycles applied during the first half of the test should not produce any fatigue damage. This first test ran for 2.822 million cycles. At the end of the test, there was a noticeable crack, roughly 5 in. (127 mm) long, along the toe of the weld on flange attachment Detail 1. However this was not considered failure by traditional testing criteria developed in early fatigue testing conducted by Fisher, et al. (*6*). Failure is defined as a through thickness (of the flange) fracture that has severed about 75% of the flange area or has resulted in excessive deflection. There was also a small crack at the toe of the weld on flange attachment Detail 2 but again, nothing that constituted failure since the test exceeded the lower bound design curve. Nevertheless, these cracks would likely grow very quickly from this point forward. The data are shown in Figure 2.8.

The second fatigue test of Specimen 1D/R-2 for the Category C′ details ran for 2.233 million cycles. It should be noted

Table 2.2. Specimen 1D/R-2 damage summary.

Location	Impact Distance from Detail (in.)	Global Damage		Localized Damage
		Degree of Damage	Strain Ratio	Strain Ratio
Stiffener 1	4	8	126	79
Stiffener 2	6	7	110	76
Flange Attachment 1	3	10	110	47
Flange Attachment 2	3	11	110	42

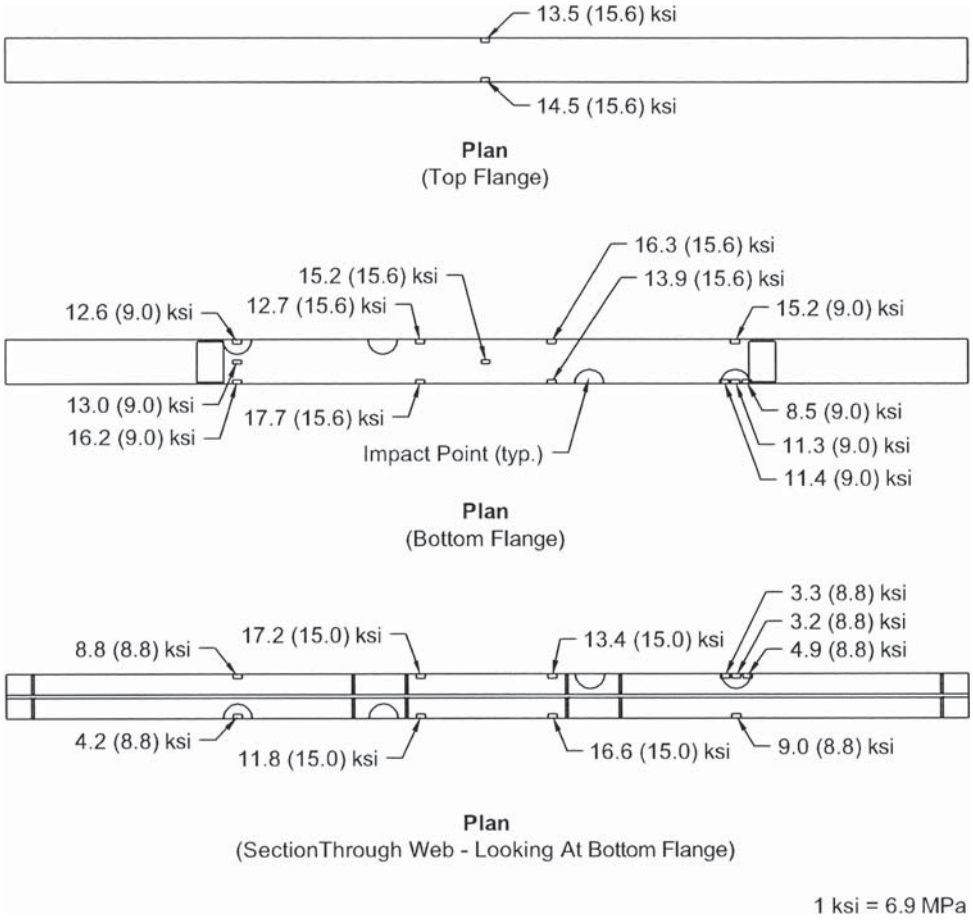

Figure 2.7. Stresses at detail locations under static load, Specimen 1D/R-2.

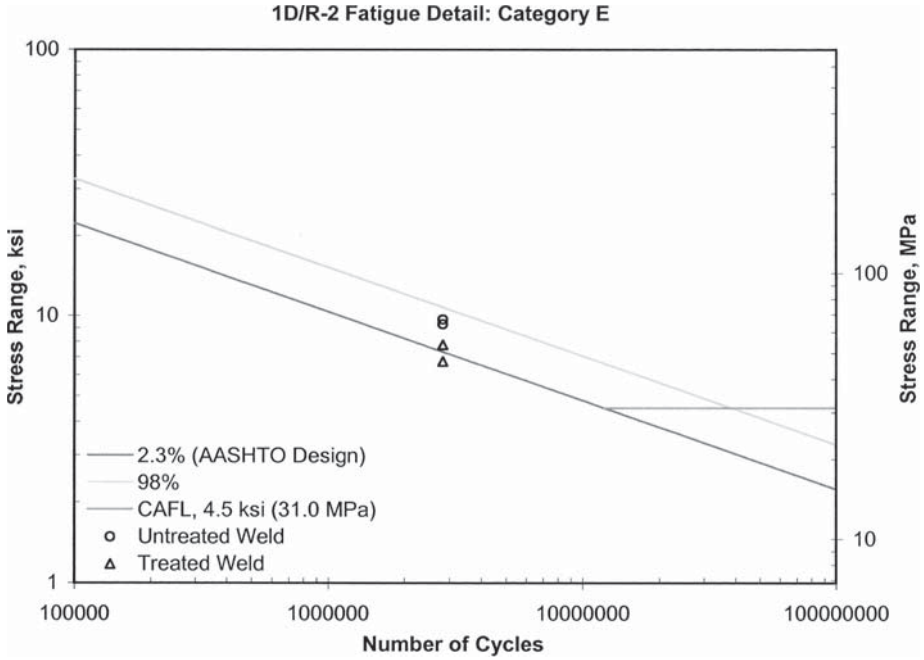

Figure 2.8. Specimen 1D/R-2 fatigue test results—Category E.

that a crack formed at the toe of the weld at Stiffener 1 at a stress range of 14.8 ksi. This extended through the thickness of the flange but only severed about 15% of the flange area and was not considered a failure based on the criteria cited. Data are shown in Figure 2.9. The tabulated results for both fatigue tests can be found in Appendix B.

After the fatigue testing was complete for Specimen 1D/R-2, it was placed back into the drop-weight machine at the two detail locations that did not have any signs of fatigue damage. Although not part of the original test plan, this was done to investigate whether there was any degradation in the resistance of the beam to a secondary impact and whether any micro-defects that may have initiated during the fatigue test, but not detectable with MT and PT, would affect the results. In the presence of such small flaws, potentially reduced toughness due to the first D/R cycle and the high strain rate, the potential for brittle fractures would be expected to increase. Two details were impacted at room temperature and neither failed in brittle fracture, showing that for this specimen and test conditions, the details could tolerate a subsequent severe impact.

2.3.2 Two Damage/Repair Cycles

The results of the fatigue tests for Specimens 1D/R-1 and 1D/R-2 demonstrate that data fall within the normal scatter for the given details, and it was concluded that there is no effect on fatigue life when subjected to a single D/R cycle. The second series of specimens (2D/R-1 through 2D/R-4) were subjected to two D/R cycles followed by a fatigue test. Since the first series tests demonstrated that fatigue resistance remained acceptable after 1 D/R cycle, the research team and project panel agreed there was no need to fatigue test between D/R cycles. This was further justified by impacting fatigue tested girder 1D/R-2 at two locations after fatigue testing without fracture or any unusual damage.

2.3.2.1 Specimen 2D/R-1

Specimen 2D/R-1 was a W30X116 rolled beam used to investigate the effect two D/R cycles has on the fatigue performance of rolled beams. This size beam was used in place of the W27X129 rolled beam to easily produce the desired impact damage on the specimen without having to change the weight of the sled on the drop-weight machine. The fatigue details on this specimen were transverse stiffeners welded to the tension flange (Category C′) and cover plate terminations (Category E′). The summary of the damage imposed on this specimen is listed in Table 2.3.

For the first two impacts, Cover Plate 1 and Stiffener 1 were struck, first impacting adjacent to Stiffener 1, then moving the specimen in the drop-weight machine for a second impact adjacent to Cover Plate 1. However, in this position, Stiffener 1 was located directly over the support. Statically, there is no significant stress at this location in the flange; however, the impact abruptly raised the cantilevered portion of the beam off the support and its mass resulted in substantial tensile stresses at Stiffener 1. Immediately after the impact, a brittle fracture occurred at the impact at the Stiffener 1 impact location subsequently severing three-quarters of the flange and extending into the web shown in Figure 2.10. This same behavior was ob-

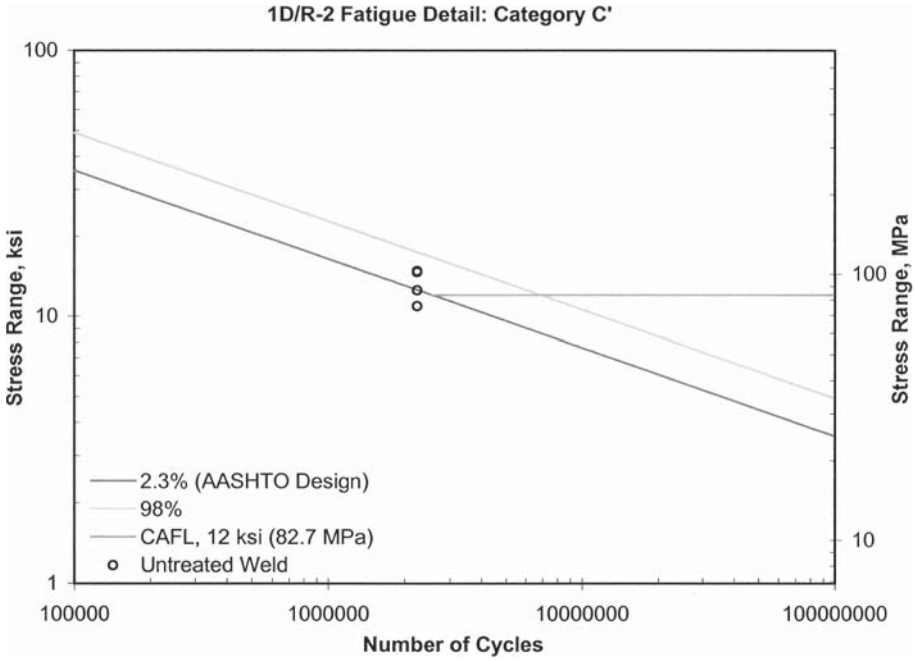

Figure 2.9. Specimen 1D/R-2 fatigue test results—Category C′.

Table 2.3. Specimen 2D/R-1 damage summary.

Location	Impact Distance from Detail (in.)	Global Damage		Localized Damage
		Degree of Damage	Strain Ratio	Strain Ratio
Damage Cycle 1				
Stiffener 1	6	*	*	59
Stiffener 2	6	6	59	20
Cover Plate 1	3	18	167	71
Cover Plate 2	4	10	107	25
Damage Cycle 2				
Stiffener 1	6	6	95	59
Stiffener 2	6	4	95	63
Cover Plate 1	4	12	119	95
Cover Plate 2	4	9	119	87

* – Unable to determine due to cracking caused by impact.

served in one of the dummy full-scale specimens impacted during the calibration tests of the drop-weight machine. However, at that time, the observed fracture was thought to be an anomaly and that the fracture toughness of the dummy beam from laboratory stock was not known. After discussion with department of transportation (DOT) engineers from Pennsylvania, Illinois, and Indiana, similar behavior has been observed in the field on bridges that have been hit multiple times. Specifically, during a later impact, brittle fractures initiated out of the location where the girder was struck previously, even if this location was several feet away.

Examination of this region demonstrated that there is a relatively thin layer of cold-worked material that has very low fracture toughness. In addition, there are multiple small cracks in this low-toughness material due to the extreme strains and rolling of the material at the exact point of the impact. The brittle fractures observed in the lab initiated at one of these discontinuities. Additionally under the high strain rates produced during the impact, the dynamic fracture toughness (K_{ID}) of the material would control the potential for fracture, and it will be lower than the static fracture toughness (K_{IC}).

The fracture was repaired in conjunction with heat-straightening. A hole was drilled in the flange and in the web to prevent further propagation of the crack and the specimen heat-straightened. Upon completion of the straightening, a complete joint penetration (CJP) groove weld was made and inspected using UT. This area was successfully damaged and repaired a second time. In order to prevent similar fracture on other specimens, a simple procedure was developed. After each impact and inspection, the area is ground smooth to remove any micro-cracks that were induced during the impact.

In addition to the fracture that occurred at Stiffener 1, a crack initiated at the corner of the cover plate, shown in Figure 2.11, during this same impact at the cover plate detail. This crack was ground out and inspected using both PT and MT methods. Since the removal of the crack required a significant gouge in the flange, a repair weld was required. This was made after the heat-straightening was completed.

In order to prevent cracking that formed at flange-stiffener welds during the heat-straightening repair of Specimens 1D/R-1 and 1D/R-2, the weld toe was treated by using a 0.25 in. (6 mm) tree-radius end rotary file. This was performed after the impact and prior to beginning the heat-straightening repair. For the first D/R cycle, this prevented any cracking or tearing at this weld toe. However during the second repair cycle, minor cracking still formed at these treated areas. Upon discovery, these cracks were ground out and inspected using both PT and MT methods. Minor hairline fractures also formed on the underside of the flange in the localized damage region and were subsequently ground out and inspected.

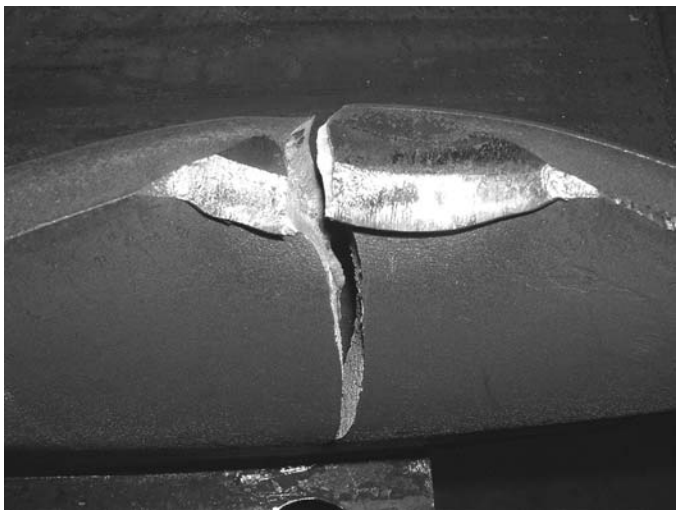

Figure 2.10. Crack at Stiffener 1 due to subsequent impact at Cover Plate 1, Specimen 2D/R-1.

Figure 2.11. Tear at Cover Plate 1, Specimen 2D/R-1.

When the second heat-straightening repair of the impact near Cover Plate 1 was 25% complete, a brittle pop-in fracture occurred on the underside of the flange in the middle of the impact region. This was approximately 3 in. (76 mm) away from Cover Plate 1 and occurred as heat was being applied to the steel at the beginning of a heating sequence. The fracture occurred during the repair process when the steel was approximately 100°F to 150°F (38°C to 66°C) and expected to be on the upper shelf for toughness. This crack extended 2 in. (51 mm) in from the edge of the flange and was roughly 75% of the flange thickness. A hole was drilled to prevent further propagation of the crack and the flange was successfully heat-straightened. Following the heat-straightening repair, a CJP groove weld repair was made and inspected using the UT method.

As a result of this pop-in fracture and the hairline fractures on this specimen, an evaluation of the restraining forces was made prior to completing the repair. Instrumentation of a localized damage area and an FE analysis of Specimen 2D/R-2 that also experienced similar fractures were conducted to determine the cause of this cracking. The hairline fractures found on the underside of the localized damage were determined to be due to unanticipated high tensile stresses in the localized damage area caused by the horizontal restraining forces used in removing the induced sweep from the specimen. These high tensile forces also were present at the welds on the stiffeners, flange attachments, and cover plates. As a result, the horizontal restraining force was reduced, based on the geometry of the localized damage. Following this evaluation, no hairline fractures occurred on the remaining specimens. However, the tearing of the stiffener-to-flange weld toe still occurred. This evaluation is discussed in more detail in Section 2.5 Restraining Force Evaluation.

The fatigue testing of this specimen ended prematurely due to a crack that formed at the repair weld near Stiffener 1 severing 100% of the flange. This occurred after 1.542 million cycles. Note that this crack was not at the weld toe of the stiffener, the fatigue detail that was a focus of the test. In order to test the other details, the lower portions of Stiffener 1 on both sides of the web were removed and splice plates were attached to continue fatigue testing. This procedure is often used in fatigue testing. Once the beam was repaired, the testing resumed. Testing was terminated after a total of 2.644 million cycles were applied and transverse Stiffener 2 failed due to a crack severing 100% of the flange and extending up three-quarters of the web. This occurred at a stress range of 11.3 ksi (77.9 MPa), below the CAFL of this detail, but considered to be within normal scatter of the available database for this detail. This, along with the other Category C′ data, are shown on the SN curve in Figure 2.12. Figure 2.13 presents the results for the Category E′ details that were tested.

2.3.2.2 Specimen 2D/R-2

Specimen 2D/R-2 was a welded plate girder specimen (Plate Girder A, Type 2) used to investigate the effect of two D/R cycles on the fatigue performance of welded plate girders. The fatigue details on this specimen were transverse stiffeners welded to the tension flange (Category C′) and flange attachments (Category E). For this specimen, wider flange attachments were

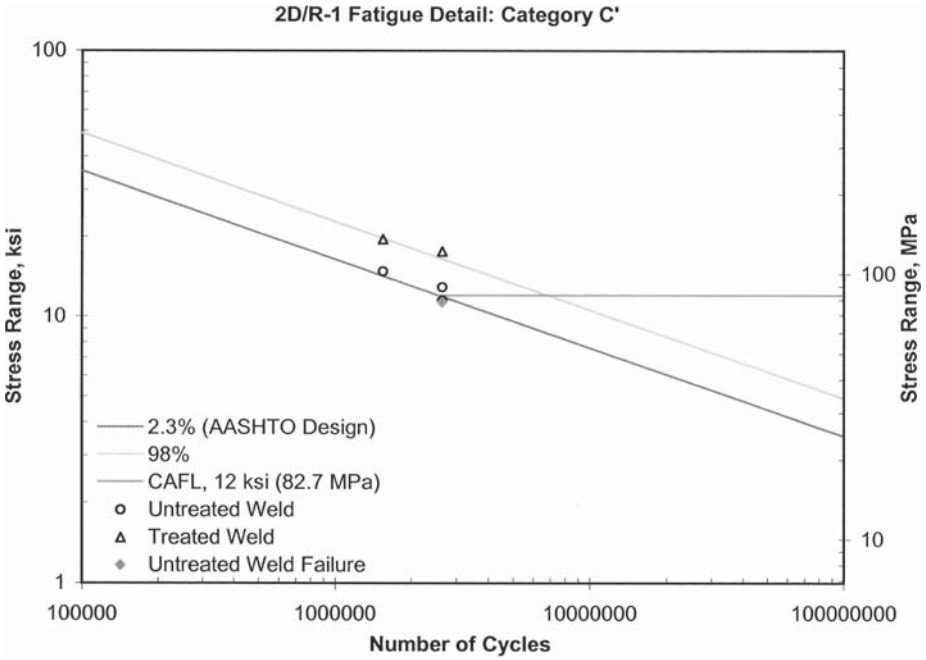

Figure 2.12. Specimen 2D/R-1 fatigue test results—Category C′.

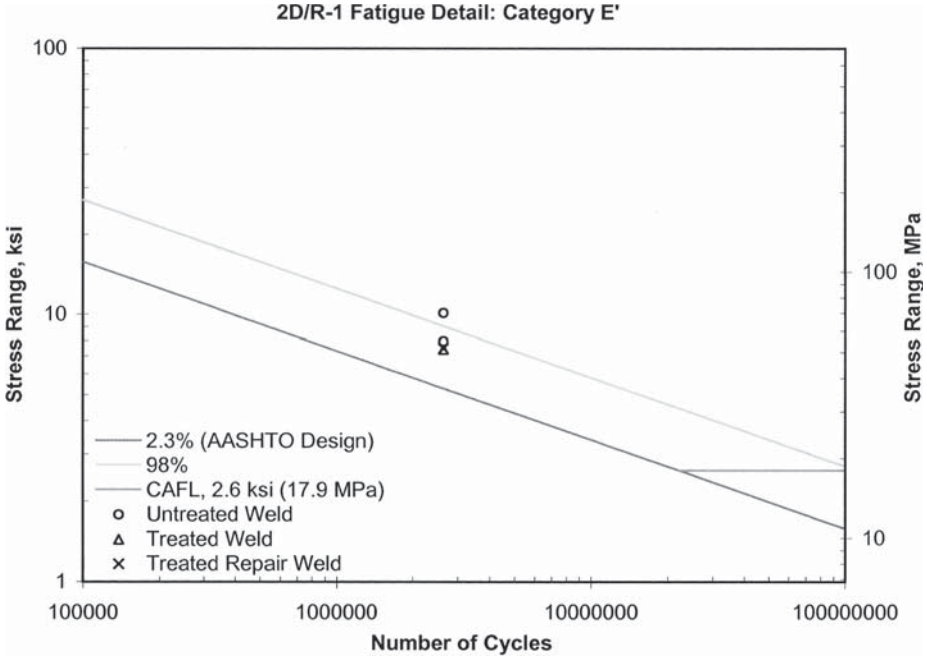

Figure 2.13. Specimen 2D/R-1 fatigue test results—Category E′.

fabricated to ensure a Category E detail. The summary of the damage imposed on this specimen is listed in Table 2.4.

In order to prevent cracking that formed at flange-stiffener welds during previous heat-straightening repairs, the weld toe was treated by using a 0.25 in. (6 mm) tree-radius end rotary file. This was done after the impact and prior to beginning the heat-straightening repair. For the first repair cycle, this prevented any cracking from occurring. However, during the second repair cycle, minor cracking still formed at these treated areas, which also occurred on Specimen 2D/R-1. Upon discovery, these cracks were ground out and inspected using both PT and MT.

Minor hairline fractures also occurred on the underside of the flange in the localized damage region. In addition, minor cracking developed at the flange weld toe on the corner of the flange attachment closest to the impact point on both flange attachment details. Upon discovery, these were ground out and inspected using both PT and MT methods. After 80% of the second repair at Flange Attachment 2, a 2.5 in. (64 mm) crack was discovered at the weld toe of the flange attachment in the center of the flange that required a repair weld. It was decided to remove the entire original weld to ensure a proper repair and to avoid uncertainties during the fatigue testing. A repair weld was made across the width of the flange, ground smooth, and inspected by an outside contractor using UT inspection.

During the repair process, a brittle fracture occurred at the localized damage adjacent to the stiffener during the preloading of the restraining forces (i.e., no heat had been applied).

Table 2.4. Specimen 2D/R-2 damage summary.

Location	Impact Distance from Detail (in.)	Global Damage		Localized Damage
		Degree of Damage	Strain Ratio	Strain Ratio
Damage Cycle 1				
Stiffener 1	6	11	110	82
Stiffener 2	6	10	47	19
Flange Attachment 1	4	7	94	85
Flange Attachment 2	4	6	126	90
Damage Cycle 2				
Stiffener 1	6	11	142	86
Stiffener 2	6	11	157	57
Flange Attachment 1	4	8	142	99
Flange Attachment 2	4	7	142	80

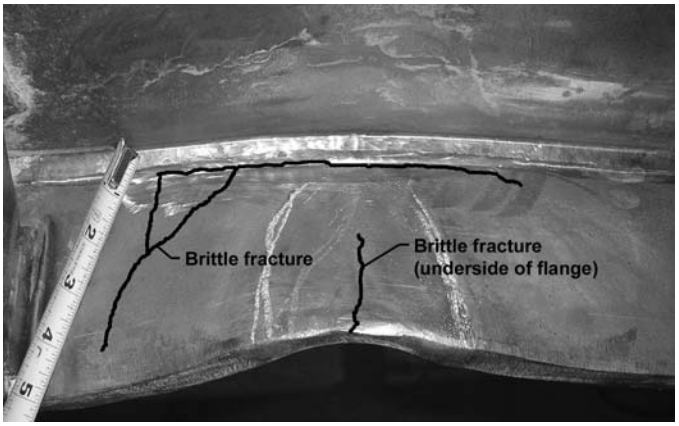

Figure 2.14. Brittle fracture near Stiffener 1, Specimen 2D/R-2.

Figure 2.14 shows fractures that consisted of a crack on the underside of the flange at the center of the localized damage as well as on the top of the flange around the localized damage perimeter. Holes were drilled to prevent further propagation of the cracks and the area was successfully heat-straightened. A 5 in. (127 mm) by 10 in. (254 mm) portion of the flange was removed and extra plate material that was supplied by the fabricator was used to replace this area with a welded repair, as shown in Figure 2.15. Although this repair would not be recommended in the field, the original remaining stiffener welds still provided data for this detail.

As a result of this brittle fracture (the crack that formed at the flange attachments and the hairline fractures on this specimen), an evaluation of the restraining forces was made prior to completing the repair. Instrumentation of a localized damage area and an FE analysis of this specimen were conducted to determine the cause of the cracking. It was determined that the hairline fractures discovered on Specimens 1D/R-1, 1D/R-2, and 2D/R-1 were due to unanticipated high tensile stresses in the area of the localized damage caused by the horizontal restraining forces used to remove the induced sweep from the specimen.

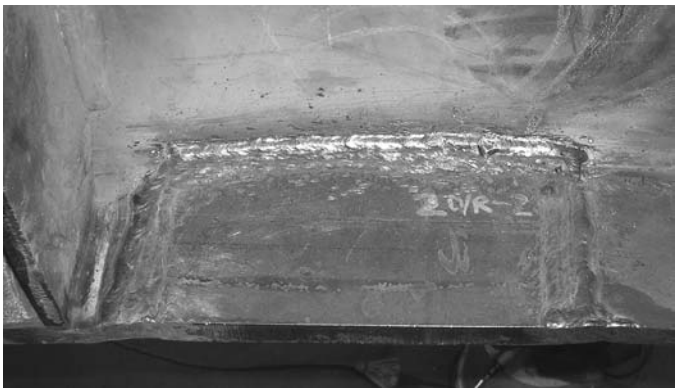

Figure 2.15. Repair of brittle fracture near Stiffener 1, Specimen 2D/R-2.

The fatigue test ran for 4.049 million cycles and was terminated due to a crack at a repair weld made near Stiffener 1 that severed 100% of the flange and extended up 12 in. (305 mm) into the web. This failure was not at a detail that was being investigated, and because the testing of the details was roughly at or past the mean fatigue life, the testing was stopped. The results of the Category C′ details are shown in Figure 2.16. In addition, the results of the Category E details are shown in Figure 2.17.

2.3.2.3 Specimen 2D/R-3

Specimen 2D/R-3 was a W30X116 rolled beam also used to investigate the effect two D/R cycles has on the fatigue performance of rolled beams. The fatigue details on this specimen were transverse stiffeners welded to the tension flange (Category C′) and cover plate terminations (Category E′). The summary of the damage imposed on this specimen is listed in Table 2.5. The first impact made at both cover plate details resulted in slight tearing of the corner of the weld at the cover plate. This area was ground down to remove the tear and inspected using both PT and MT methods prior to beginning the heat-straightening repair.

To prevent cracking that had formed at flange-stiffener welds during previous heat-straightening repairs, the weld toe was treated by using a 0.25 in. (6 mm) tree-radius end rotary file. This was done after the impact prior to beginning the heat-straightening repair. However during the first repair cycle, minor cracking still formed at these treated areas even with the reduction in the horizontal restraining force. Upon discovery, these cracks were ground out and inspected using both PT and MT methods.

The fatigue testing was terminated after a total of 2.241 million. No failures were experienced on this specimen and the testing was stopped just past the mean life before cracking was observed, ensuring material was available from the critical locations for subsequent impacts and material property testing. Results of the testing are shown in Figure 2.18 and Figure 2.19 for the Category C′ and Category E′ details, respectively.

Specimen 2D/R-4 was a welded plate girder specimen (Plate Girder A, Type 2) also used to investigate the effect two D/R cycles has on the fatigue performance of welded plate girders. The fatigue details on this specimen were transverse stiffeners welded to the tension flange (Category C′) and flange attachments (Category E). The summary of the damage imposed on this specimen is listed in Table 2.6. Minor tearing occurred during the first impact at the corners of both flange attachments. This required a 2 in. (51 mm) repair weld at the corner of Flange Attachment 1 that was inspected by an outside con-

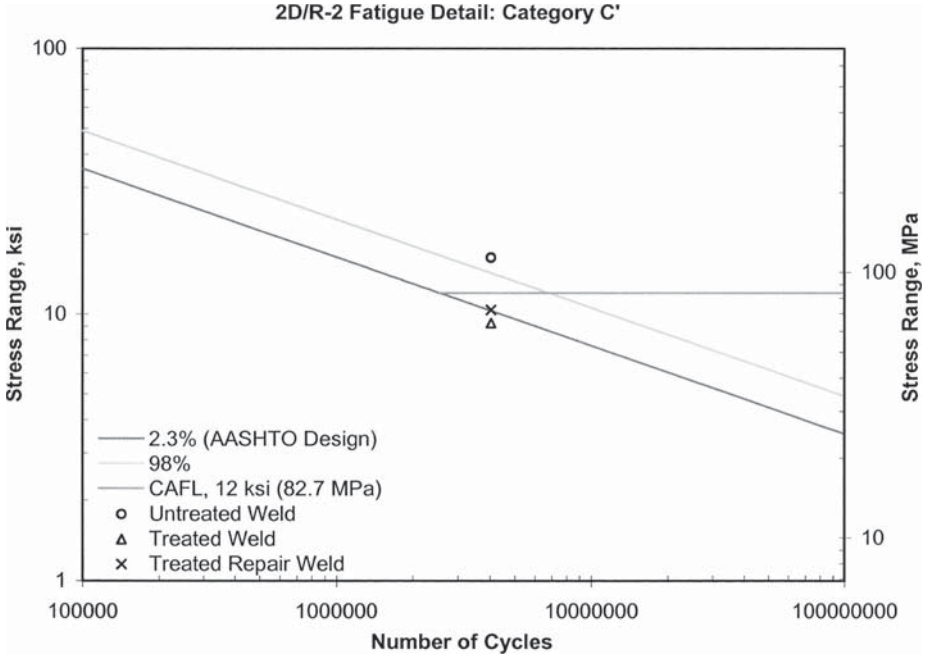

Figure 2.16. Specimen 2D/R-2 fatigue test results—Category C'.

tractor using UT to ensure no discontinuities were present. At Flange Attachment 2, only grinding was required followed by inspection using both PT and MT methods.

2.3.2.4 Specimen 2D/R-4

Specimen 2D/R-4 had to be fatigue tested in two separate tests, similar to the process used for Specimen 1D/R-2. The greater-than-expected stress range measured at the flange attachments would likely result in fatigue failure before data could be obtained at the more fatigue–resistant transverse stiffeners. Testing was divided into two separate fatigue test phases so each details were tested separately. The first fatigue test was used to evaluate the performance of the flange attachments (i.e., Category E details) at a stress range of 8.5 ksi (58.6 MPa). Under this load, the stress range produced at the

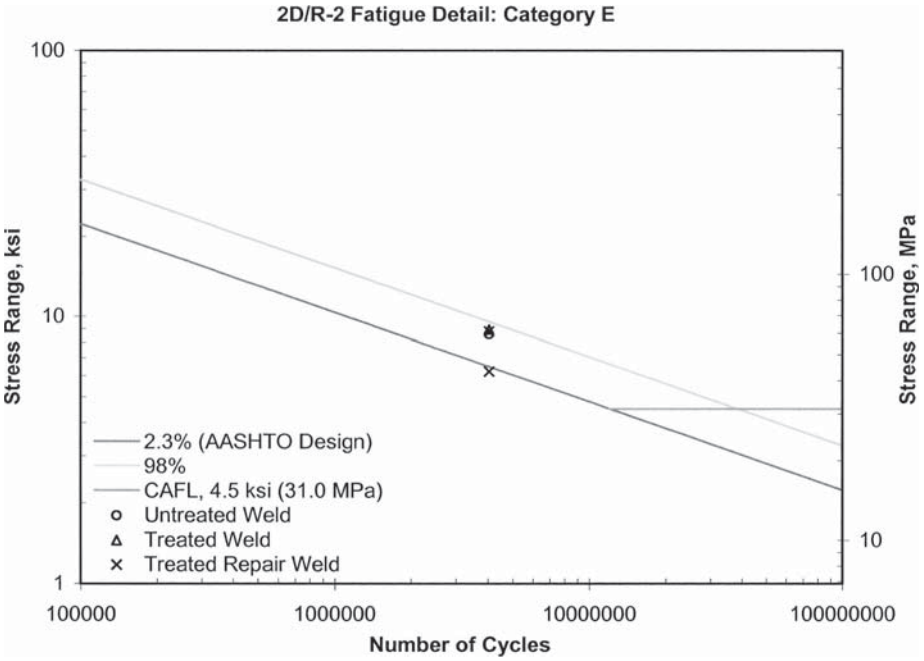

Figure 2.17. Specimen 2D/R-2 fatigue test results—Category E.

Table 2.5. Specimen 2D/R-3 damage summary.

Location	Impact Distance from Detail (in.)	Global Damage		Localized Damage
		Degree of Damage	Strain Ratio	Strain Ratio
Damage Cycle 1				
Stiffener 1	6	4	48	36
Stiffener 2	6	4	48	48
Cover Plate 1	4	8	83	44
Cover Plate 2	5	7	59	36
Damage Cycle 2				
Stiffener 1	6	4	59	52
Stiffener 2	6	3	71	48
Cover Plate 1	5	9	131	61
Cover Plate 2	5	8	83	59

stiffeners (Category C′) was only 10 ksi (68.9 MPa), below the CAFL of 12 ksi (82.7 MPa) for these details. At this stress range, the C′ details are considered to have infinite fatigue life so the cycles applied during the first half of the test should not produce significant fatigue damage. The test ran for 3.037 million cycles, which is 470,000 cycles over the mean value for fatigue life for the E details. These results are shown in Figure 2.20

The second fatigue test, for the Category C′ details, was run at a stress range of 18 ksi (124.1 MPa) and 14 ksi (96.5 MPa) at Stiffeners 1 and 2, respectively. Because of the increased stress range at the flange attachment details (i.e., the E details) and the potential for fatigue cracking, doubler plates were attached to the flange using wrench clamps to prevent these details from cracking during the second test. The addition of the doubler plates prevents or postpones fatigue cracking at the cover plates so that useful data can be gathered from the transverse stiffeners. This approach, successfully used for Specimen 1D/R-2, prevented fatigue cracking at the E details. The test was terminated when the C′ details were cycled well past the predicted mean fatigue strength. These results are shown in Figure 2.21. No failures were experienced on this specimen; testing was stopped roughly past the mean life but before and cracking was observed, ensuring material was available from the critical locations for subsequent impacts and material property testing.

2.3.3 Three Damage/Repair Cycles

Results of the fatigue tests for specimens 2D/R-1 through 2D/R-4 show that data fall within the normal scatter for the given details. It was concluded there was no noticeable effect on fatigue life of these specimens when subjected to two D/R cycles.

Based on the above, a third series of specimens (3D/R-1 and 3D/R-2) were subjected to three D/R cycles followed by a fatigue test to examine whether there was a reduction in fatigue strength with three D/R cycles. For these tests, only transverse stiffeners were tested. This included a portion of the stiffener removed prior to the heat-straightening repair on the rolled beam and stiffeners not welded to the tension flange on the plate girder.

2.3.3.1 Specimen 3D/R-1

Specimen 3D/R-1 was a W30X116 rolled beam used to investigate the effect of three D/R cycles on the fatigue per-

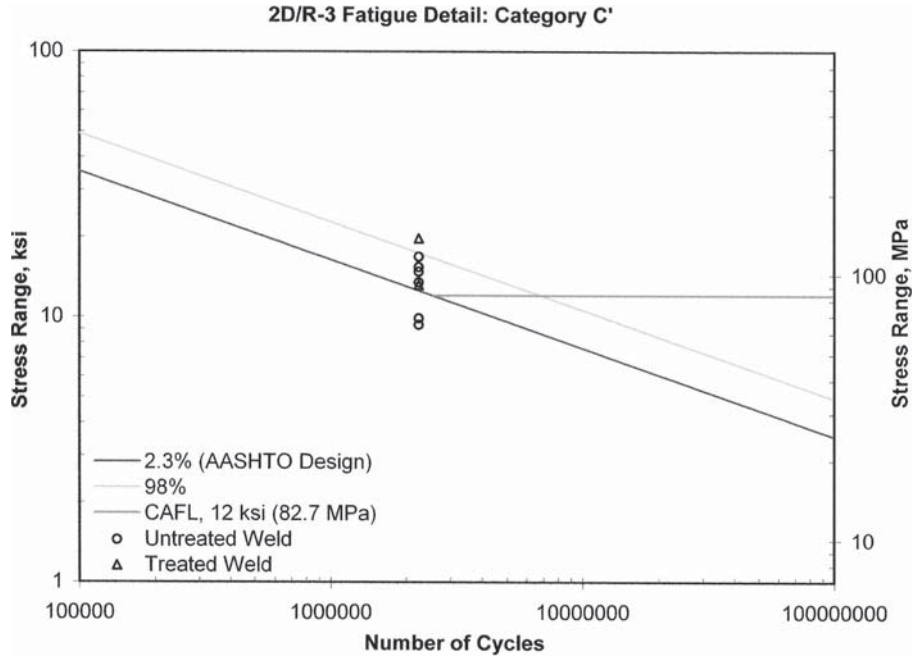

Figure 2.18. Specimen 2D/R-3 fatigue test results—Category C′.

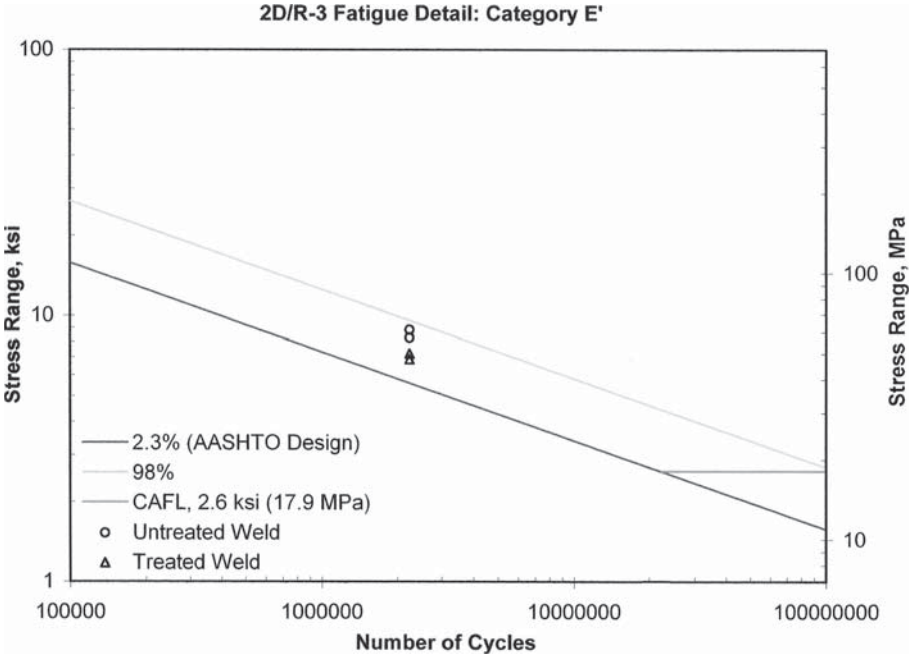

Figure 2.19. Specimen 2D/R-3 fatigue test results—Category E′.

formance of rolled beams. The fatigue details on this specimen were transverse stiffeners welded to the tension flange (Category C′). However, the test regime included removing a portion of the stiffener following each impact, completing the heat-straightening repair and replacing the removed portion of the stiffener with a welded replacement. This process was repeated three times with the portion being removed each D/R cycle. The summary of the damage imposed on this specimen is listed in Table 2.7.

The Category C′ detail on this specimen was a transverse stiffener welded to the tension flange. As a result of the tearing at the weld toe that occurred on previous specimens, a repair procedure that would reduce the possibility of potential tearing or cracking during the heat-straightening repair at this detail was developed. This procedure involved removing a 6 in. (152 mm) portion of the stiffener by flame cutting 0.125 in. (3 mm) above the fillet welds. The flange was protected by a plate to prevent damage to the adjacent base metal. The remaining fillet weld and stiffener were then ground smooth and flush with surrounding surfaces and parallel to the direction of applied stress. A sanding disc was used for final finishing to avoid deep grinding marks in the flange. The area was then inspected using MT. Figure 2.22 and Figure 2.23 show the portion of the stiffener that was removed before and after the heat-straightening repair, respectively. The replacement stiffener then was fit and welded with the same size fillets used in the fabrication and grove welds at the stiffener-to-stiffener connection. The completed repair is shown in Figure 2.24. This repair procedure was repeated after every impact at both stiffener details.

Table 2.6. Specimen 2D/R-4 damage summary.

Location	Impact Distance from Detail (in.)	Global Damage		Localized Damage
		Degree of Damage	Strain Ratio	Strain Ratio
Damage Cycle 1				
Stiffener 1	6	10	94	63
Stiffener 2	6	8	126	71
Flange Attachment 1	4	8	110	52
Flange Attachment 2	5	6	94	66
Damage Cycle 2				
Stiffener 1	6	9	142	99
Stiffener 2	6	9	126	66
Flange Attachment 1	5	7	126	94
Flange Attachment 2	5	6	205	90

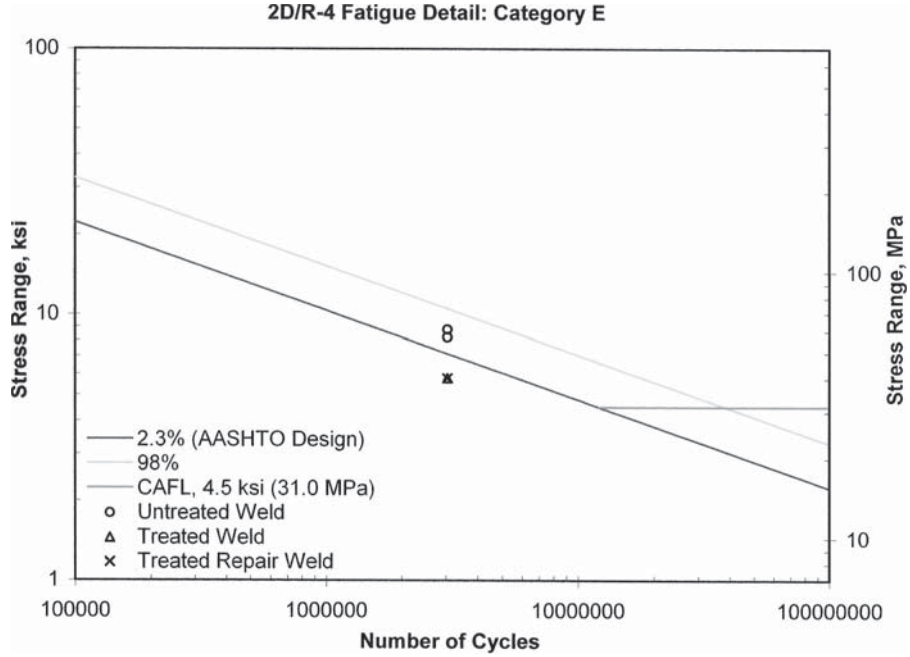

Figure 2.20. Specimen 2D/R-4 fatigue test results—Category E.

The fatigue testing ran for 689,500 cycles until a crack formed at the flange weld toe adjacent to the impact point at Stiffener 2. The crack severed 90% of the flange and extended half way up the web. The low number of cycles would have terminated testing of Stiffener 1, so splice plates were added to complete the testing, similar to previous specimens that also formed cracks. The test ran for an additional 2.793 million cycles for a total of 3.429 million cycles at Stiffener 1 without the formation of a crack. These results are shown in Figure 2.25.

2.3.3.2 Specimen 3D/R-2

Specimen 3D/R-2 was a welded plate girder specimen (Plate Girder B) used to investigate the effect three D/R cycles has on the fatigue performance of welded plate girders. The

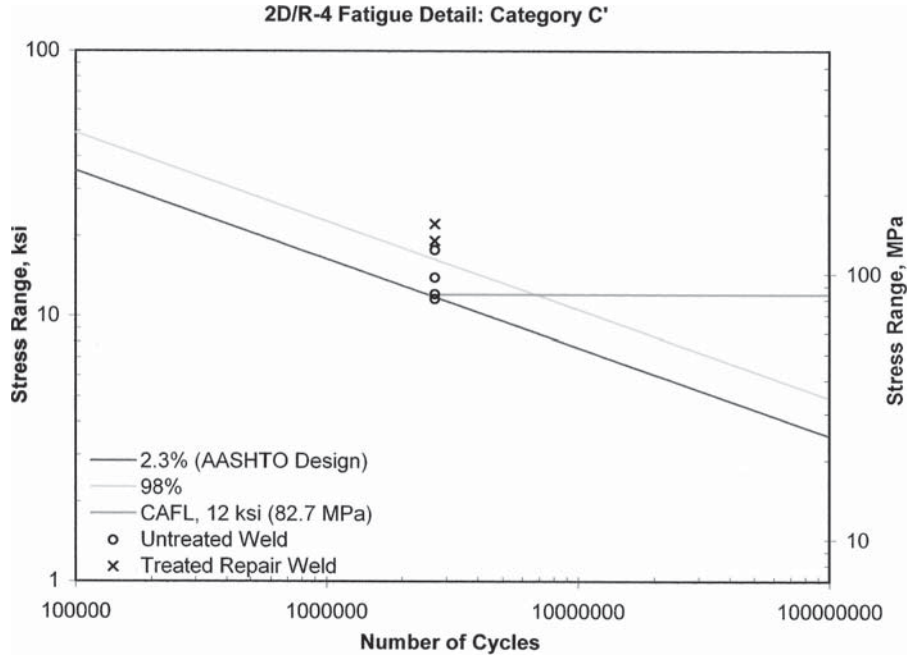

Figure 2.21. Specimen 2D/R-4 fatigue test results—Category C′.

Table 2.7. Specimen 3D/R-1 damage summary.

Location	Impact Distance from Detail (in.)	Global Damage		Localized Damage
		Degree of Damage	Strain Ratio	Strain Ratio
Damage Cycle 1				
Stiffener 1	6	4	71	63
Stiffener 2	6	6	48	48
Damage Cycle 2				
Stiffener 1	6	6	167	75
Stiffener 2	6	7	95	63
Damage Cycle 3				
Stiffener 1	6	7	131	113
Stiffener 2	6	7	95	70

fatigue detail on this specimen was transverse stiffeners not welded to the tension flange (Category C′). The summary of the damage imposed on this specimen is listed in Table 2.8.

The fatigue test ran for 222,400 cycles and was terminated due to a crack that initiated in the flange at the impact point *near* Stiffener 2 (i.e., not at the weld toe). Although this location was not instrumented and the exact stress range is not known, the nominal stress range at this location was 19.6 ksi (135.1 MPa). As discussed with Specimen 1D/R-2, the presence of the residual damage caused an increase in the stress at this location, so the stress on the underside of the flange (concave side of the residual damage) at this location was higher then the nominal stress. (Reasons for this will be discussed further in Section 2.6 Residual Damage Evaluation.)

Because the testing fell considerably short of the targeted number of cycles, the crack was spliced using doubler plates, and the test was restarted. Unfortunately, the redistribution of stress to these doubler plates reduced the stress range at the Stiffener 2 details near the crack too much to adequately test these details. Therefore, these details were no longer considered in the testing. After an additional 72,200 cycles were applied, another crack formed in base metal at the Impact 1 location, similar to the Impact 2 location. With this crack, the beam could no longer be fatigue tested since the stress range at the weld toe of Impact 1 location would be significantly altered if splice plates were added. These Category C′ details could not be fully evaluated due to the cracking of the base metal at the points of impact.

2.4 Material Properties

Following the completion of the fatigue tests, the impact areas on the flange were removed and sectioned into both CVN and tensile specimens, as shown in Figure 2.26. Tests

Figure 2.22. Portion of stiffener removed prior to heat-straightening repair.

Figure 2.23. Completed heat-straightening repair at stiffener detail.

Figure 2.24. Portion of stiffener replaced using a welded repair following the heat-straightening repair.

were conducted in accordance with ASTM A370, E8 (Tensile), and E23 (CVN). A majority of the CVN specimens were taken from areas to the left of the impact (looking down at the inside face) where the flange experienced severe straining during the impact, and line heats were used to remove the localized damage during heat-straightening. The other three CVN specimen locations (denoted with an asterisk in Figure 2.26) were centered on the impact point for Specimens 2D/R-3 and 2D/R-4. These tests were compared with the material properties of the original material supplied by the fabricator, and the results are summarized in the following sections, along with tabulated comprehensive results listed in Appendix C.

2.4.1 Fracture Toughness

The fracture toughness of the damaged and repaired material was determined using CVN specimens machined from the impact areas following the fatigue testing of the specimens. The specimens were tested in accordance with ASTM E23 specifications. All of the CVN specimens that were machined from the impact locations (three CVN specimens per impact location) were tested at a temperature of 40° F (4°C). There was considerable scatter in the data obtained in the "nonvirgin" specimens. However, substantial scatter can be expected in base metal that has not been subjected to any damage or repair cycles—something to keep in mind for the following discussions.

Due to the variability in the data collected here and in previous research conducted on the fracture toughness of heat-straightened members, a distinct change in fracture toughness has not been established. It has been reported in previous research, as discussed in Section 2.1 Literature Review, slight to moderate decreases have occurred. Although the FHWA manual suggests a small change in fracture toughness can be expected, recent research has reported as much as a 50% decrease (*3*). For comparative purposes, the fracture toughness requirement as listed in AASHTO of 15 ft-lbs (20 J) at 40°F (4°C) for redundant bridges in temperature Zone 2 was used as a baseline for the data. Tabulated comprehensive results are listed in Appendix C.

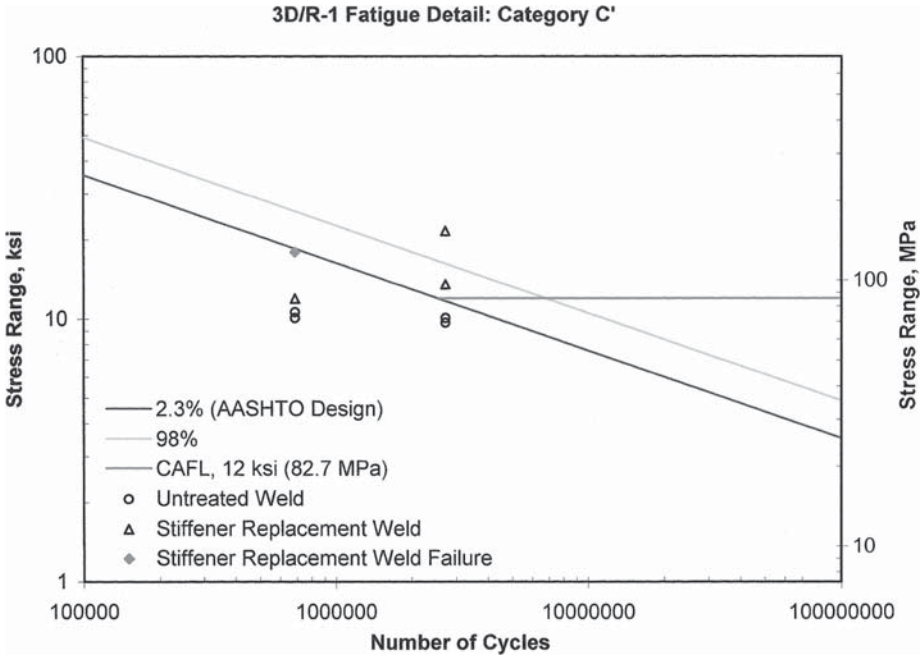

Figure 2.25. Specimen 3D/R-1 fatigue test results—Category C'.

Table 2.8. Specimen 3D/R-2 damage summary.

Location	Impact Distance from Detail (in.)	Global Damage		Localized Damage
		Degree of Damage	Strain Ratio	Strain Ratio
Damage Cycle 1				
Stiffener 1	6	9	79	60
Stiffener 2	6	10	91	41
Damage Cycle 2				
Stiffener 1	6	9	113	54
Stiffener 2	6	8	91	37
Damage Cycle 3				
Stiffener 1	6	9	147	65
Stiffener 2	6	8	147	60

2.4.1.1 One Damage/Repair Cycle

The fracture toughness testing for one D/R cycle on specimens 1D/R-1 and 1D/R-2 showed a decrease of approximately 64% from undamaged material with an average fracture toughness of 33 ft-lbs (45 J). This is well above the percentage decrease cited in previous research. However it is important to note that the average toughness still exceeded the AASHTO requirement for Zone 2 nonfracture critical members, with the exception of one specimen. Interestingly, one of the three CVN specimens from the original *undamaged* material also failed to meet the minimum toughness requirement. (Upon investigating the cause for this, the research team discovered that the fabricator had provided material that was slightly out of specification, as compared with what was ordered. After review of the material more closely, it was concluded that this deficiency was not significant enough to compromise the validity of the results obtained in the full-scale fatigue testing.)

Other specimens tested consisted of flange material that was damaged but not heat-straightened and material that was subjected to 1D/R cycle and then damaged a second time, but not repaired. Results show that a significant reduction in fracture toughness occurs after an impact. However the fracture toughness appears to increase somewhat after the material has been repaired. In all sets of data, there were unacceptably low toughness values measured after the impacts, but the trend indicates an improvement in toughness, although not guaranteed or significant, may be realized by the heat-straightening process. This should be considered in particular when an owner decides not to make any repairs to a damaged section of girder since choosing not to make a repair will likely mean leaving material with reduced toughness in place. It should be noted that this reduction may not be enough, however, to place the material out of specification.

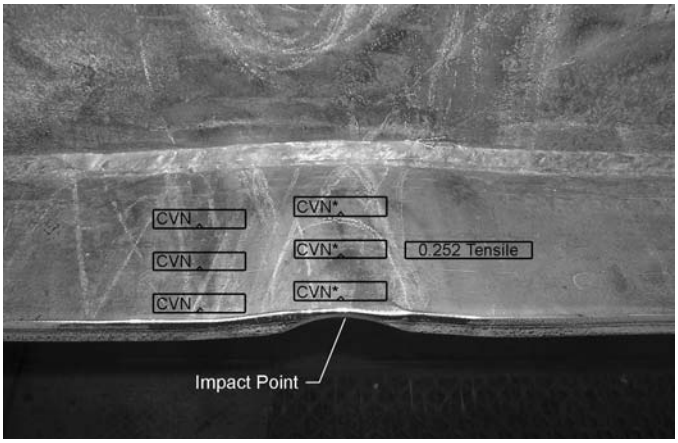

Figure 2.26. Location of CVN and tensile specimens taken from an impact location.

2.4.1.2 Two Damage/Repair Cycles

Fracture toughness tests for material subjected to two D/R cycles were reduced an average of 37% as compared with the original material for three of the four girders (2D/R-1, 2D/R-3, and 2D/R-4). Of those three girders, one impact area on specimen 2D/R-1 demonstrated a 9% increase following the repairs. The average toughness of all tests on these three girders was above the minimum AASHTO requirement, although a few individual CVN specimens taken from Girders 2D/R-3 and 2D/R-4 were below the specification. [For example, for 2D/R-4, the CVN toughness was as low as 11 ft-lbs (15 J).] All of the impact areas tested on the fourth girder (2D/R-2) demonstrated an average increase in the fracture toughness of 88%. Tests conducted on material removed from the center of the impact location showed a slightly lower average increase in fracture toughness of 34%. For the most part, both locations yielded similar results.

One location on Girder 2D/R-3 that was subject to two D/R cycles was then damaged a third time near Stiffener 1 following the fatigue testing. The specimen was not repaired at this third impact location, and material was removed there to

obtain CVN data. The results showed a 28% decrease in the fracture toughness compared to the original undamaged material, but were still about 30% higher than the average of six tests on material obtained near Cover Plate 2, only subjected to two D/R cycles. Although reasons for this are not entirely clear, they further reinforce the considerable variability expected in CVN data obtained for girders subjected to multiple D/R cycles.

2.4.1.3 Three Damage/Repair Cycles

The results of the CVN testing for three D/R cycles yielded a decrease of approximately 59% and 42% for 3D/R-1 and 3D/R-2, respectively. In fact, of the four locations subjected to 3D/R cycles where CVN data were obtained, all locations exhibited individual data (i.e., one CVN specimen) that were less than the required AASHTO limit of 15 ft-lbs (20 J) at 40°F (4°C) for Zone 2 nonfracture critical members. Interestingly, one CVN specimen yielded data as high as 146 ft-lb (198 J), higher than observed in the undamaged condition, again highlighting variability in the data.

2.4.2 Tensile Properties

Tensile specimens also were machined from several of the impacts from the specimens, as seen in Figure 2.26. These tensile specimens were used to determine the yield strength, tensile strength, and ductility (determined by percent elongation) after the heat-straightening repairs and compared to testing conducted on the original material. This testing was conducted in accordance with ASTM E8 specifications. The results of these tests are summarized herein along with comprehensive tabulated results listed in Appendix C. For comparison, the FHWA manual indicates an increase in yield and tensile strength of 20% and 10%, along with a decrease in ductility of 30% after a heat-straightening repair.

2.4.2.1 One Damage/Repair Cycle

Two specimens were taken from material that underwent one D/R cycle. The results demonstrated an increase in the yield stress from 7% to 20%, an increase in the tensile strength from 1% to 14%, and a decrease in the ductility of approximately 30% to 38% from that of the original material. Compared to what is listed in the FHWA manual, results are within reasonable agreement. Furthermore, the scatter in the data is not surprising due to the fact that only a limited number of specimens could be extracted from each damaged girder.

As discussed, an additional impact (i.e., damage) was made near a partial depth stiffener on 1D/R-2, which was not repaired. This was done in attempt to isolate the effect an impact alone has on the material properties. The results were an increase in the yield and tensile strength of 40% and 17%, respectively along with the loss in ductility of 38% to that of the virgin material. The results are not entirely unexpected: the effect of the damage alone, in the absence of a repair, would be expected to primarily contribute to the increase in yield strength and loss of ductility. The effect the heat-straightening process on the material has a tendency to lower (restore) the yield strength and improve the ductility evidenced by the results, as it is in effect a heat treatment process. Similar findings and conclusions have been observed by Varma and Kowalkowski (*3*).

A second impact that was not repaired was made on 1D/R-2 at a location previously subjected to 1 D/R cycle to investigate the effect an unrepaired second impact has on the tensile strength. Results indicated an increase in the yield strength of about 55% compared to the virgin material and about a 20% increase to the yield strength in material subjected to one D/R cycle. Interestingly the ductility and tensile strength remained essentially the same after the subsequent impact; however, without a significant amount of data a distinct conclusion cannot be made.

2.4.2.2 Two Damage/Repair Cycles

Ten tensile specimens were taken from four of the girders that were damaged and repaired two times (two D/R cycles). The results of these tests yielded an increase in the yield stress of 8% to 15% along with an increase in the tensile strength of 1% to 8%. The average decrease in ductility of all these tensile specimens was approximately 16% compared to the original material. The increase in the yield and tensile strengths as well as the ductility all are very similar to what is described in the FHWA manual.

A third impact was made at one of the previously repaired impacts (two complete D/R cycles) to investigate the effect an unrepaired third impact has on the material properties. The results of the tensile testing indicated an increase in the yield strength of 4.5% compared to data obtained from specimens from this girder (i.e., 2D/R-3) subjected to two D/R cycles. The ductility after this third impact decreased by roughly 14% below that observed for the undamaged condition and was about 5% below that observed after two D/R cycles for this specimen.

2.4.2.3 Three Damage/Repair Cycles

Four specimens were taken from the two girders that were damaged and repaired three times (three D/R cycles). The results of these tests provided an increase in the yield stress of 8% to 30% for girders 3D/R-1 and 3D/R-3, respectively. An increase in the tensile strength of about 6% also was observed for these two girders. The decrease in ductility of these tensile specimens was more substantial and was approximately 21%

to that of the original material. The increase in the yield and tensile strengths are slightly more than the increase listed in the FHWA manual. Likewise, the decrease in the ductility was slightly more than what is listed.

2.4.3 Chemical Composition

The chemical composition of the steel was determined at the time of the rolling process and again by an outside contractor from a portion of the specimen following the completion of the fatigue testing. All specimens met the requirements listed in ASTM specifications for the applicable types of steel. The tabulated results of these analyses are located in Appendix C.

2.4.4 Microstructure Inspection

The microstructure at several impact locations along with corresponding material from the specimen prior to the D/R cycles was investigated. The samples used were taken from the CVN specimens following the impact testing. Two pieces from each impact location on each specimen were investigated and compared to the original material to establish if any changes in the microstructure due to the D/R cycle could be observed. Selected photographs of the microstructure from various specimens are included in Appendix C.

2.4.4.1 One Damage/Repair Cycle

Following one D/R cycle, the microstructure of the steel was compared to the original undamaged condition at several locations. With the exception of one specimen, there were no adverse changes in the microstructure compared to that of the original material. After closer examination of the exception, the change in the microstructure was determined to be due to overheating, and the microstructure was altered only on one face of the material sample. This suggests the overheating was concentrated on one side of the flange and did not occur through the thickness.

For Specimen 1D/R-2, flange material that underwent an impact alone (1D/0R), one D/R cycle (1D/1R) and a subsequent impact without a repair (2D/1R) was compared. The microstructure of these specimens were comparable and did not indicate a significant change (see Figure C-2).

2.4.4.2 Two Damage/Repair Cycles

Following two D/R cycles, samples were removed from repaired specimens, and the microstructure examined. This investigation also revealed only one instance of overheating of the material. Again the overheating was concentrated on only one side of the flange, which indicates that the overheating was not through the thickness of the flange.

2.4.4.3 Three Damage/Repair Cycles

Following three D/R cycles, samples were removed from repaired specimens, and the microstructure examined. The examination revealed no evidence suggesting any significant changes in the microstructure.

2.5 Restraining Force Evaluation

During the heat-straightening repairs for the experimental program, hairline fractures appeared on the underside of the flange in the localized damage region. In addition, two brittle pop-in fractures occurred in Specimens 2D/R-1 and 2D/R-2. One brittle fracture occurred when heat was applied without significant restraining force. The other occurred before heating while the restraining force was being applied to the specimen. This second brittle fracture occurred at the localized damage adjacent to the stiffener as shown in Figure 2.14 and did not initiate at the weld toe. The FHWA manual cites that hairline fractures may occur during the heat-straightening repair and are believed to be caused by excessive restraining forces, repetitive repair, or further growth of microcracks initiated during the impact. The FHWA manual states that the primary cause of such cracking would be excessive restraining force and that the material should not be heat-straightened more than two times, apparently because of decreases in toughness.

As discussed, procedures developed as a result of this research demonstrated that prior to repair, two steps must be taken to help ensure success. First, the area must be ground smooth to minimize the stress concentration at the weld toe by improving the geometry at this location. Second, the location must be thoroughly inspected using the PT and MT methods to ensure that no surface cracks are present at the impact area. Although the above procedures improved the likelihood of a successful repair, a few fractures and/or tears were still observed during the first and second D/R cycle.

Because of these problems, the repair process was closely evaluated with particular attention given to the restraining forces applied. The temperature of the heated steel was continuously monitored to make certain the material properties would not be adversely affected by overheating the steel. The heating temperature was kept under 1200°F (650°C) for both Grade 36 and Grade 50 steels. The hydraulic jacks used to apply the restraining forces were recalibrated and equipped with pressure gauges to ensure the desired forces were being applied. The jacking moment (M_J) produced by the restraining forces, determined by the calculation procedures listed in the FHWA manual, was never greater then 65% of the plastic moment, M_P.

The repair procedures followed by the researchers were consistent with the currently accepted state of practice in the field. Nevertheless, finding the cause of the observed cracks

remained. The limits on the restraining forces recommended by the FHWA manual (i.e., a percentage of M_P of the weak axis) were questioned. For example, the cross-section used to calculate M_{PWeak} is based on the undamaged geometry. However, in reality the damage in the girder, primarily the local damage in the lower flange, substantially changes the cross-sectional geometry and hence the actual moment that corresponds to the plastic moment at the damaged section. The damage also results in a drastic reduction in lateral stiffness. As a result, loads that would produce a moment equal to 50% of M_{PWeak} in the undamaged girder would produce much greater local stress in the damaged cross-section. As stated, this suggested possible deficiencies in the procedures to calculate the restraining forces.

To verify the above statements and establish that there was no unusual degradation of the material properties due to the damage and repair process, CVN and tensile specimens were machined from a portion of the specimen containing the cracks that had been removed. The results of these tests indicated the following:

- The yield strength of the original material averaged 52.8 ksi (50.6 ksi and 54.9 ksi) [364 MPa (349 MPa and 379 MPa)] compared to 61.9 ksi (62.0 ksi and 61.8 ksi) [427 MPa (427 MPa and 426 MPa)] from the material that had contained the brittle fracture.
- The tensile strength of the original material averaged 76.6 ksi (76.6 ksi and 76.5 ksi) [528 MPa (528 MPa and 527 MPa)] compared to 84.9 ksi (84.8 ksi and 84.9 ksi) [585 MPa (585 MPa and 585 MPa)] from the material that had contained the brittle fracture.
- The fracture toughness of the original material at 40°F (4°C) averaged 31 ft-lbs (28 ft-lbs, 30 ft-lbs, and 35 ft-lbs) [42 J (38 J, 41 J, and 47 J)]. The fracture toughness of the material at 40°F (4°C) after the brittle fracture occurred averaged 52 ft-lbs (48 ft-lbs, 53 ft-lbs, and 54 ft-lbs) [71 J (65 J, 72 J, and 73 J)].
- The percent elongation for the original material averaged 34.2% (34.0%, 33.3%, and 35.2%) compared to 20.0% (25.1% and 14.8%) from the material that had contained the brittle fracture.

Results show there was a 17% increase in the yield strength along with an 11% increase in the tensile strength. Interestingly, there was a 40% increase in the fracture toughness. The ductility of the material was, however, reduced by 42%. The above data supports the initial assumption that the fractures were not due to material degradation and reinforce the notion that local stress from jacking led to the fracture. Specimens could not be extracted from the exact locations where the fractures occurred for obvious reasons, but properties obtained are believed to represent the material at these locations.

Based on the material property testing and the repair procedures that followed, further investigation of the restraining forces was conducted to determine what restraining forces can actually be applied without causing such fractures. These fractures occurred within the localized damage region, so instrumentation and FE modeling were used to determine the actual stresses located around the impact zone since traditional "hand methods" can't be used with confidence.

2.5.1 Laboratory Instrumentation of Localized Damage

To verify the actual stresses on the specimen due to the applied restraining forces, a specimen was instrumented after the impact and prior to beginning heat-straightening. This was a Plate Girder A (Type 2) specimen, fabricated of Grade 36 steel plate, and previously damaged and repaired in the same location. The localized damage near a welded transverse stiffener is shown in Figure 2.27, the flange has a thickness of 0.75 in. (19 mm) and a width of 10 in. (254 mm), and the impact produced a localized bulge with a strain ratio (μ) of 66.

For this instrumentation, bondable uniaxial strain gages were used: type CEA-06-250UW-350 produced by Measurements Group Inc. with an active grid length of 0.25 in. (6 mm), a resistance of 350 ohms, and used an excitation voltage of 10 volts. The sampling rate of 25 Hz was used for this specific testing. Grinding, fine sanding, and cleaning were needed for the preparation of the metal surfaces before the installation of the gages. A Campbell Scientific CR9000 Data Logger was used to collect the data. This logger is a high-speed, multi-channel 16-bit system configured with digital and analog filters to ensure noise-free signals. Real-time data were viewed by connecting a logger to a laptop computer. The placement of the gages on the top and bottom surface of the flange around the localized impact is shown in Figure 2.28 and Figure 2.29, re-

Figure 2.27. Localized damage at a transverse stiffener detail.

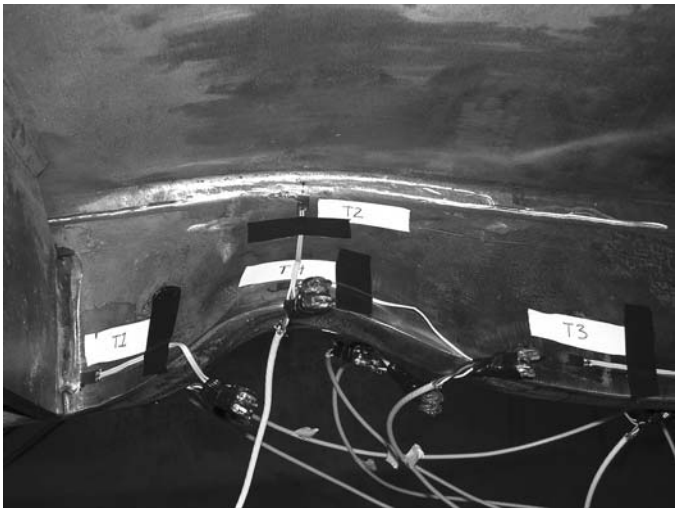

Figure 2.28. Strain gage layout (top surface of flange).

spectively. Each gage is labeled T1 through T4 for the gages on the topside of the flange and B1 through B4 for the gages on the underside of the flange, as referenced in this section.

The setup of the vertical and horizontal hydraulic jacks is shown in Figure 2.30 and Figure 2.31, respectively. Current recommended limits on restraining forces are such that the moment produced by the restraining force is no more then 50% of the plastic moment capacity, M_P, of that member. This was calculated as bending the strong axis of the flange over the length of the supported specimen. However, current field practices use as much as 65% of the plastic moment capacity. To be consistent with field practice, laboratory procedures were conducted such that the restraining force produced a moment that was 65% of the plastic moment capacity of the member.

First, the vertical load used during the repair process up to this testing was incrementally increased to a maximum of

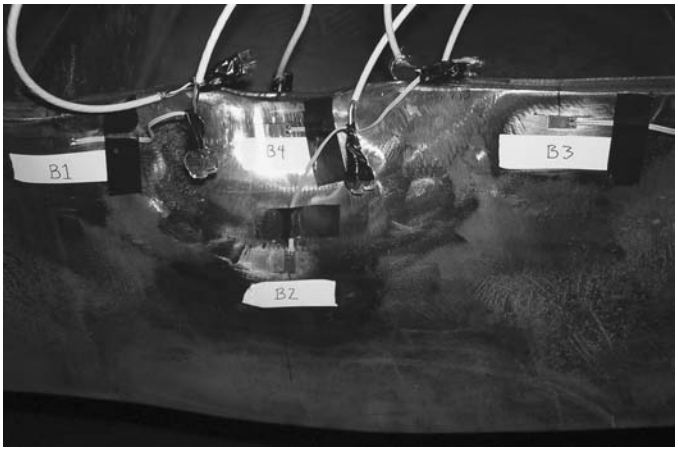

Figure 2.29. Strain gage layout (looking up at the bottom surface of flange).

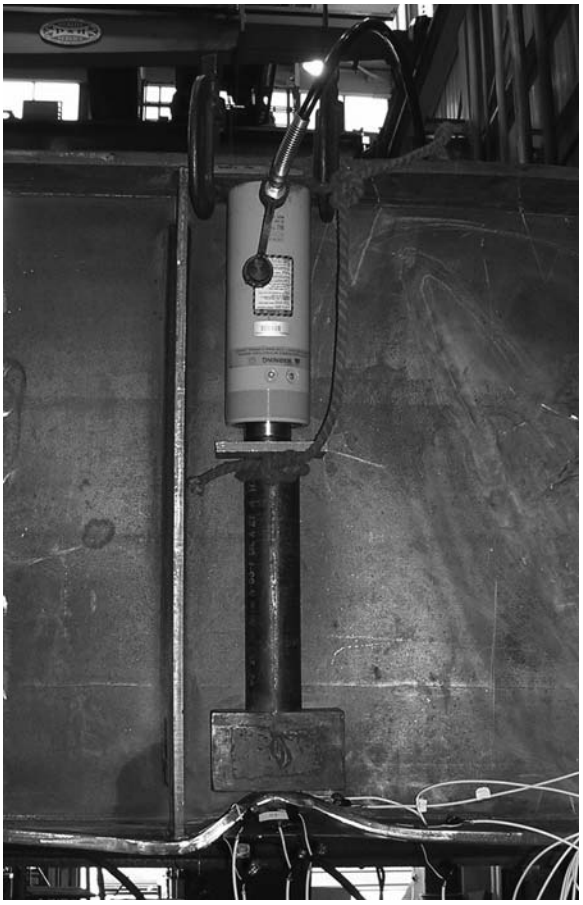

Figure 2.30. Vertical restraining force.

10.5 tons (3005 kN), and stress was recorded at each gage location for the increments. A maximum tensile stress of 12.6 ksi (86.9 MPa), 35% of the nominal yield stress, was measured on the underside of the flange at strain gage B4 with the 10.5 ton (3005 kN) load. Note that the instrumentation could not measure locked-in stresses, such as residual stresses present in the

Figure 2.31. Horizontal restraining force.

member from the fabrication process, the previous damage and repair, or the impact that caused the localized damage.

Next, the horizontal load was applied separately in several increments while stresses were recorded at each increment. Surprisingly, at a restraining force of only 3 tons (859 kN), a stress of about 19.6 ksi (135.1 MPa) was measured at the weld toe of the stiffener (strain gage T1) and 18.2 ksi (125.5 MPa) on the underside of the flange (strain gage B4). This was a little more than 50% of the nominal yield stress for these two locations, but the load was only 60% of that previously applied during the repair process. The horizontal load of 5 tons (1431 kN), which was applied during the previous repairs, was found acceptable by the methods provided in the FHWA manual. Obviously, this load would have produced local stresses approaching the nominal yield point at these two locations. Although the vertical restraining force was initially thought to have been the primary factor contributing to the hairline fractures, the data showed that the horizontal restraining force produced levels of stress high enough to produce cracking.

Finally the combination of both the horizontal and vertical jacking load was applied. Since the horizontal load was determined to be more critical of the two, the vertical jack first applied 10.5 tons (3005 kN) to the specimen. Next, the horizontal load was applied in increments until nominal yield was reached in tension. At a horizontal restraining force of 3.2 tons (916 kN), a stress of 36 ksi (248 MPa) occurred on the underside of the flange at the center of the localized damage (strain gage B4). Fifty percent of the nominal yield stress was reached with only 2 tons (572 kN) on the horizontal jack and 10.5 tons (3005 kN) on the vertical jack. A stress of 18.3 ksi (126 MPa) was recorded at the same location (Strain Gage B4) with this loading.

Clearly, the existing methodologies for estimating the appropriate restraining forces do not take into account the localized damaged geometry and can lead to very high local stresses near this damaged area. Hence restraining forces can contribute to the hairline cracks and premature fracture of a member during the heat-straightening repair. This factor has probably contributed to several unexplained fractures that occurred during repairs in the field, as reported in the surveys (*1*).

2.5.2 Finite Element Modeling

To further examine the effects localized damage has on the stresses in the member under applied restraining forces, FE modeling of the specimens was completed. The FE results were calibrated using the strain measurements made on the repaired specimens. The modeling resulted in the development of two FE models based on the geometry of the Plate Girder A (Type 2) specimen. One model was an undamaged specimen and used to verify the applicability of methods presented in the FHWA manual for determining the restraining forces in the experimental program. The second compared the results from the laboratory instrumentation and included the geometry of the damage in the specimen. This model was used to attempt to establish a better method to determine the appropriate restraining forces to apply to the specimen.

The software packages used for the modeling were FEMAP v8.3 and ABAQUS 6.4-1. FEMAP was used for the pre- and post-processing while ABAQUS was used as the FE solver. The type of elements used for this analysis consisted of ABAQUS S4 shell elements for the majority of the specimen and S8R shell elements for the area containing the localized damage. The S4 shell element is a 4-node linear doubly-curved general-purpose shell element while the S8R element is an 8-node quadratic doubly-curved shell element with reduced integration. Simple three-point bending models were created to verify the accuracy of these elements for this application and were in agreement with elementary beam theory.

2.5.2.1 Undamaged Finite Element Model

As stated above, the magnitude of the restraining force used during the experimental program (up to this phase of the research) was intended to produce bending equivalent to 65% of the plastic moment capacity of the member. This was determined by the methods listed in the FHWA manual. Based on the calculations, a 5 ton (1431 kN) horizontal load was applied to the FE model, containing no localized damage, as shown in Figure 2.32. Results of this analysis predicted a stress of 33 ksi (227.5 MPa) on the flange opposite to where the load was applied. Similarly, a load of 4 tons (1145 kN), producing a moment 50% of the plastic moment capacity of the member, was applied to the same model resulting in a predicted stress of 27 ksi (186.2 MPa) at the same location. This analysis concluded that for both load cases, the stress due to the loading in the specimen would not reach the nominal yield stress for this specimen of 36 ksi (248.2 MPa). From these results, it was concluded that cracking should have not occurred due to the magnitude of loading and hence a another factor must have contributed to an unforeseen amplification in the stresses, subsequently causing the hairline fractures experienced in the laboratory.

2.5.2.2 Finite Element Model Containing Localized Damage

The second model created, shown in Figure 2.33, included the localized damage present on the laboratory specimen selected for instrumentation. A close-up view of this localized damage is shown in Figure 2.34. Note this model did not include the sweep present in the laboratory specimen. To verify the applicability of this exclusion, a comparison of two

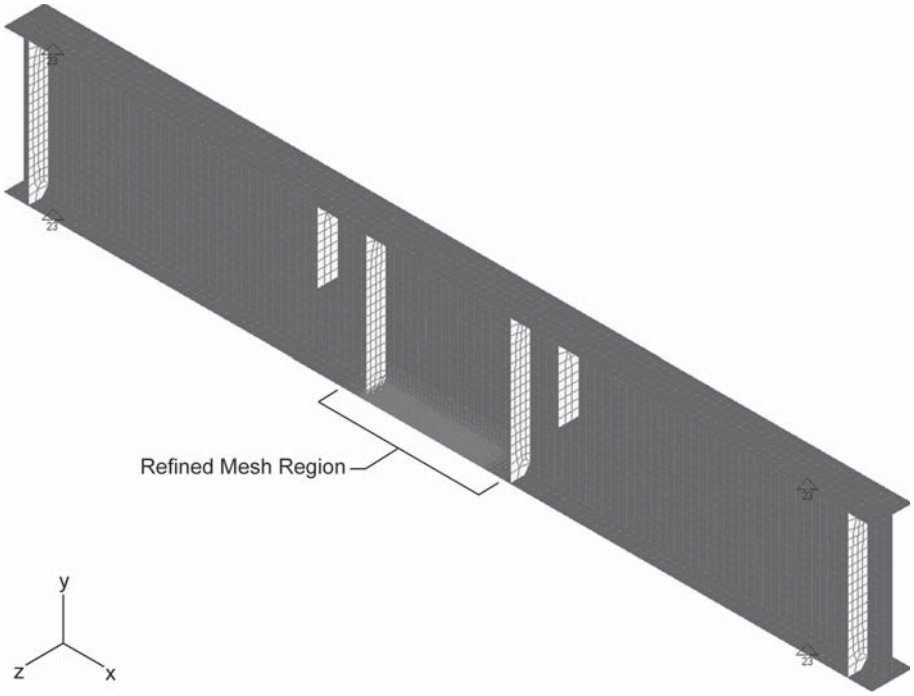

Figure 2.32. Undamaged finite element model.

model specimens, one straight and the other with the bottom flange plate bent about its strong axis (i.e., weak axis for the beam) simulating sweep in the bottom flange, were created, but these models did not contain localized damage. A load was applied at the midpoint bend in the bottom flange plate, simulating the horizontal restraining force, for the model containing sweep and at the same location for the model that did not have any sweep. The maximum tensile stress for both cases was on the opposite side of the flange where the load was applied and there was only a 6% increase for the model containing sweep. Therefore, in order to simplify the FE models, sweep was ignored for this analysis.

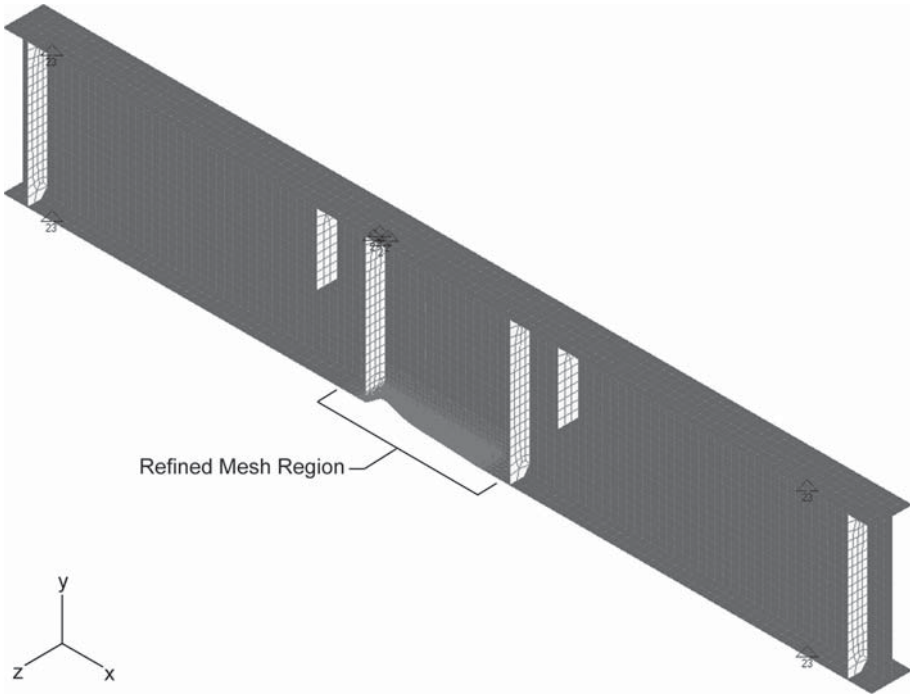

Figure 2.33. Finite element model containing localized damage.

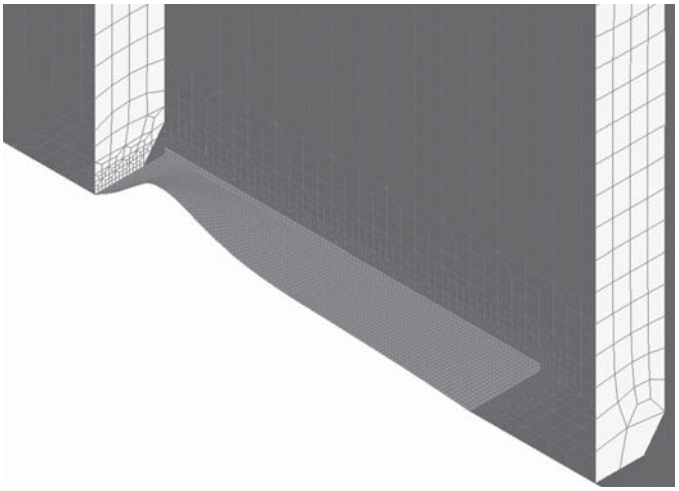

Figure 2.34. Close up view of localized damage.

To determine the magnitude of stress attributed to each restraining force, the analysis was run with each load applied separately, similar to the laboratory testing. First, only the horizontal restraining force of 3 tons (859 kN) was applied to the model to match the actual specimen. Stresses from the laboratory instrumentation were compared with the analysis at two locations of concern: the weld toe (Strain Gage T1) of the stiffener and the underside of the flange at the center of the localized damage (Strain Gage B4). The calculated stresses at both locations on the model were 27 ksi (186.2 MPa), 50% greater than measured by the instrumentation. The remaining locations for which laboratory instrumentation was available had a similar increase in tension or decrease at areas of compression. The cause for the discrepancy is partially attributed to the steep strain gradients in this region under this loading and to the boundary conditions in the model that assumed frictionless pin/rollers while the actual laboratory conditions suggest a partially restrained connection due to friction between the specimen and its support on the heat-straightening fixture.

Next the vertical restraining force of 10.5 ton (3005 kN) was applied in the model. The analysis of this loading resulted in a stress of 13.6 ksi (93.8 MPa) on the underside of the flange at the localized damage location, roughly 8% greater than what was recorded by the instrumentation. High stresses also were calculated at the weld toe of the longitudinal web-to-flange weld directly behind the localized damage (Strain Gage T2 as seen in Figure 2.28). Although the instrumentation only indicated a stress of 6.9 ksi (47.6 MPa), the FE modeling yielded a stress of 16.1 ksi (111.0 MPa) at the same location. This is a location where very localized stress concentrations are present. The gages measure an average strain over a length of 0.25 in. (for these gages), so they are not capable of measuring the actual peak stress in regions of very high strain gradient.

The preceding material demonstrates that under the combined vertical and horizontal loading, local stresses will approach or exceed the yield stress of the material and place excessive strain demands on material in the damaged condition as restraining forces are applied prior to heating. Hence, the fractures observed in the laboratory and reported in several field repairs are not entirely unexpected.

To determine the magnitude of horizontal and vertical restraining forces that could be applied without causing excessive strains, various combinations of restraining force were applied in the model. The research team determined that the vertical restraining force would be held constant and the horizontal force varied. After several trials with the vertical force kept "high" so the local flange damage could be removed, the following combination was selected: a 10.5 ton (3005 kN) vertical restraining force was applied while varying the horizontal restraining force for each analysis to determine a force that could be applied while remaining within acceptable strain limits. A horizontal force of 2 tons (572 kN), concurrent with the vertical restraining force of 10.5 ton (3005 kN), was found to produce acceptable stress levels at the localized damage. For example, this load combination produced a stress of 18.4 ksi (126.9 MPa) on the concave underside at the center of the localized damage. At the stiffener weld toe on the flange, a stress of 17.8 ksi (122.7 MPa) was calculated. This combination of restraining forces was selected to repair this specimen and prevent the potential of fracture.

2.6 Residual Damage Evaluation

Prior to beginning the fatigue testing, researchers discovered that measured stresses within areas where some geometric damage remained after heat straightening were different than predicted by simple beam theory. Prior to fatigue testing, a static calibration test was performed by applying load in defined steps and recording data at all gages. Although the results indicated the response of the specimen was linearly elastic, the measured strains did not agree well with calculated elementary ($\sigma = Mc/I$) beam theory. Following the completion of the heat-straightening repair, the areas where small residual geometric damage remained were not thought to be of sufficient magnitude to significantly alter the stress distribution in the flange. The research team consulted a well-known heat-strengthener along with the FHWA manual prior to beginning the fatigue testing to verify that the beam was sufficiently straightened. Although "as repaired" geometry satisfied specified tolerances listed in the publications, the opinion of one with direct experience was solicited to establish if the remaining damage on the test girder would typically be permitted to remain in the field. The individual felt that based upon the severity of damage imposed on the beam, it was adequately repaired and most owners would not spend

the extra money required to get the localized damage area "perfect." Note that less damage is removed during later heating cycles. For example, if 80% of the damage can be removed in a certain number of heat cycles, removing the last 20% may take three times that number. Most owners find it too costly to have the damage area returned to as-built condition and are satisfied if most damage is corrected and the overall geometry, such as the sweep in the girder, is removed. Owners also realize impacted members are often hit again.

A review of the data clearly showed that remaining geometric damage (i.e., local flange bends not removed during straightening) altered the stress adjacent to the gages, sometimes substantially. Since the bottom flange was in tension, the folds or distortions were stretched as the tensile forces in the flange tried to flatten them. This produced local bending stresses in the flange that were either additive or subtractive to the flange's design tensile stress. A FE model that incorporated the residual damage was built for the instrumented girder. Stresses obtained from the model were in excellent agreement with the measured results. This is an important observation as in-service local stresses at fatigue sensitive details may be much higher than calculated using traditional methods. The FHWA manual does not address this issue and unconservatively estimates the remaining fatigue life in some repaired girders. Although not part of the original scope of work, this effect was further investigated through FE parametric studies.

2.6.1 Finite Element Studies

In order to characterize the effects of residual damage on localized bending, FE models were created. As before, the software used for this research was FEMAP v8.3 and ABAQUS 6.4-1. The type of elements used throughout this research was ABAQUS S4 shell elements, S8R shell elements, and C3D20 solid elements. The S4 shell element is a 4-node linear doubly curved general-purpose shell element while the S8R element is an 8-node quadratic doubly curved shell element with reduced integration. The C3D20 element is a 20-node quadratic brick (solid) element. Simple three-point bending models were created to verify the accuracy of these elements for this application and were found to be in agreement with elementary beam theory and laboratory data.

The parametric study was separated into two parts. First, several shell element models were created of the Plate Girder A (Type 1) specimen, consisting of one variation of residual damage geometry at the midpoint of the beam on the bottom flange. For each selected geometry of localized damage, a single model was created that contained only that damage geometry. This damage was not near any welded details or connections. Different flange thicknesses and widths were modeled separately as well. Taken together, this portion of the study determined how the damage geometry, flange thickness, and the flange width influence local stress distribution.

The second part focused on building solid FE models containing "damage not fully repaired" near two details similar to those on the laboratory specimen. This remaining damage was within the tolerance limits listed in the FHWA manual. The purpose for these models was to gain additional insight into the behavior observed in the laboratory. These models also established the influence of residual damage on the fatigue performance of selected welded details. Although shell elements can accurately model the influence of residual damage on the basic section, solid models are required near details, such as cover plates and stiffeners, since the actual geometry (e.g., component thickness and damage) must be considered.

2.6.2 Shell Element Models

The shell element models, based upon the same dimensions of Plate Girder A (Type 1) specimen, were 18 ft (5.5 m) long and 35 in. (889 mm) deep with 0.75 in. (19 mm) thick by 10 in. (254 mm) wide top and bottom flanges. [The beam modeled was simply supported at the bottom flange and had two 75 kip (10734 kN) point loads placed 2.5 ft (0.8 m) from the midpoint of the beam creating four point bending.] The loading and boundary conditions were chosen to simulate the type of setup used for the fatigue testing. The dimensioning and detailing of the beam are shown in Figure 2.35.

For these models, the majority of the beam was modeled using S4 shell elements while S8 shell elements were used in the area where the damage was located. The typical beam model

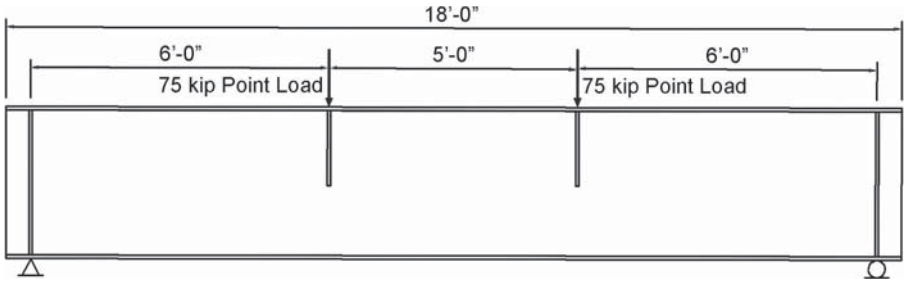

Figure 2.35. Plate girder dimensioning.

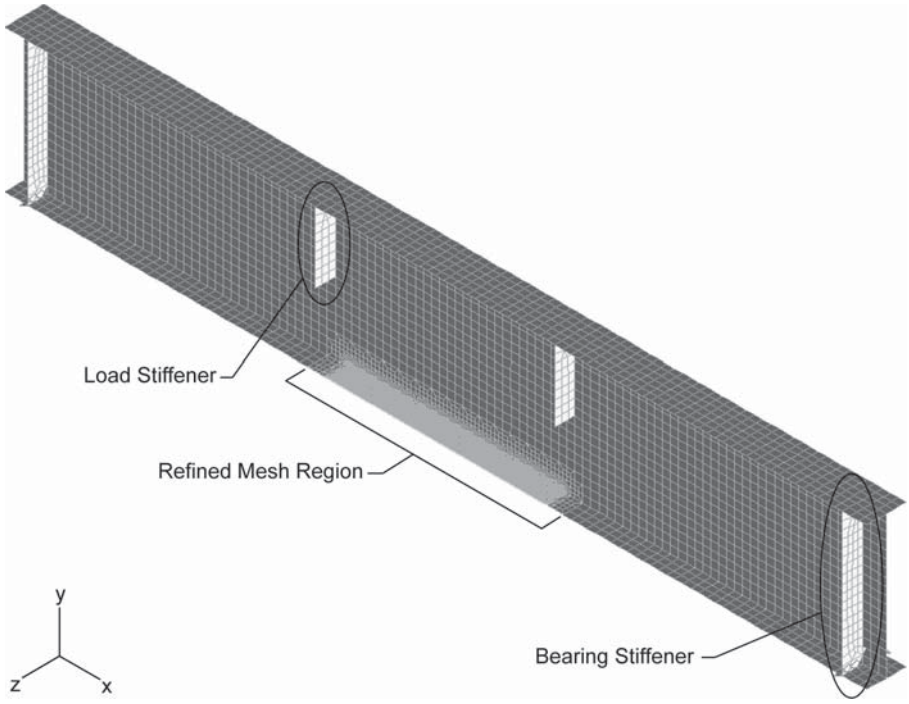

Figure 2.36. Typical shell element model.

and a blown-up detail of the refined mesh are shown in Figure 2.36 and Figure 2.37, respectively. The typical mesh size for the S4 elements were 2 in. (51 mm) square. The refined mesh area was placed at the midpoint of the beam and is 5 ft (1.5 m) long. This mesh contains S8 shell elements 0.25 in. (6 mm) square and are shown in Figure 2.37. Elements of both types were used to transition between the two mesh types.

2.6.2.1 Control Model

A control model of the basic, undamaged, shell element model was analyzed. The analysis is presented as a contour plot of the normal stresses in the *x*-direction (along the length of the beam) on the bottom surface of the shell element as shown in Figure 2.38. The contour plot contains the maximum calculated tension stress and the maximum calculated compression stress. The average stress, obtained by averaging points along the tension region at the bottom of the beam and across the width of the flange between the two load points (constant moment region), was roughly 15.4 ksi (106.2 MPa). Also note the moment gradient, as the stress contours change in color from either load point to the support.

Results of this simple analysis were compared to that of elementary beam theory ($\sigma = Mc/I$) to verify the accuracy of the model. Stress in the constant moment region was calculated to be 15.5 ksi (106.9 MPa), which, when compared to the stress obtained from the FE model, is essentially identical. Stresses along the moment gradient also were compared between the FE model and beam theory and were found to be in excellent agreement.

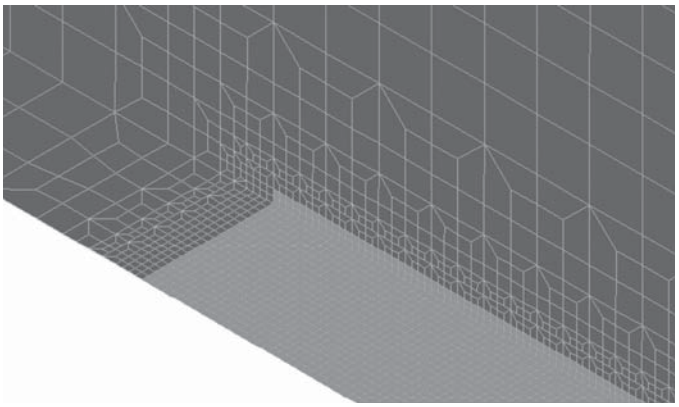

Figure 2.37. Detail of refined mesh.

2.6.2.2 Damaged Models

Using the control model, various levels of damage were placed within the refined mesh region by mapping the mesh to distorted (damaged) surfaces. These geometries consisted of multiple heights of damage as well as multiple lengths of damage. It was found that typical localized damage observed during laboratory-induced impacts that had been heat-straightened would have a minimum length-to-height ratio of about four. That is, for a given height, *H,* of damage, the length, *L,* was no less than four times the height of the respective damage. This is depicted in Figure 2.39.

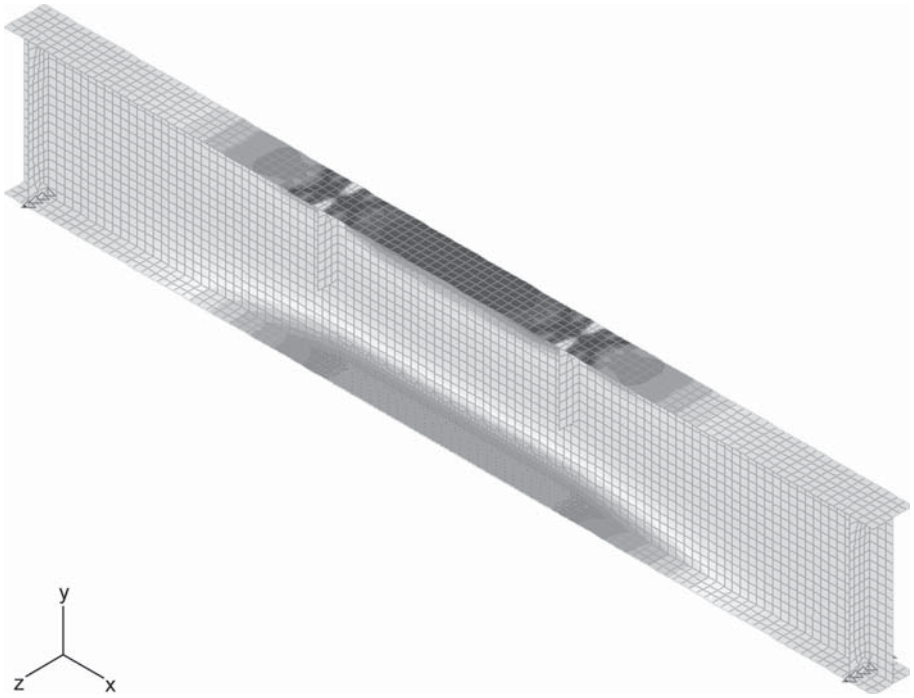

Figure 2.38. Control results of four-point bending analysis.

Note that the minimum *L*/*H* ratio of four becomes impractical as the flange thickness increases. Based on laboratory studies, a minimum limit was placed on the *L*/*H* ratio as being greater than or equal to 5.25 times the flange thickness. This was determined by evaluating the proportions of various damage geometries and flange thicknesses. Once the *L*/*H* ratio for a specific flange thickness seemed unrealistic, a limiting value was identified. For example, a practical *L*/*H* ratio for a flange having a thickness of 1.25 in. (32 mm) would be approximately 6.5, which for a damage height of 0.25 in. (6 mm) would require a length at least 1.625 in. (41 mm) to be considered realistic. Since the damage geometry is for the edge of the flange, flange width will not affect the practicality of this characterization for reasonable flange widths.

A matrix was created based on the *L*/*H* ratio characterization, which determined the various types of damage geometries to consider. The damage that was modeled in this research ranged from damage currently within accepted tolerance for a completed repair for a given flange width to damage beyond those limits. The team chose to model damage that ranged in height from 0.125 in. (3 mm) to 0.75 in. (19 mm), in 0.125 in. (3 mm) increments, and 1 in. Lengths chosen were

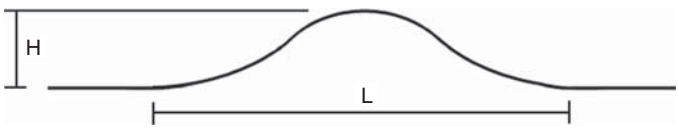

Figure 2.39. Typical damage geometry (L/H = 4).

based on the *L*/*H* ratios of 4, 6, 8, 10, 12, 24, and 48. Note that the flange thickness for this specimen was 0.75 in. (19 mm), thus a minimum *L*/*H* of four would be practical.

To model the damage, a spline curve was created in FEMAP using points that approximated the geometry of the actual damage. A surface was created using the spline to represent the edge of the damaged flange. To ensure the FE mesh was consistent between each of the models (which would have different damage geometries), the mesh shown in Figure 2.37 was projected onto the newly created damaged surface. This allowed for the stresses obtained from each model to be compared consistently. If each surface was uniquely meshed automatically, element shapes were produced that were not desirable, such as triangular elements or shapes that were severely skewed. Also, using different meshes for each model could lead to inconsistencies in determining the highest stress among models and would result in an inaccurate trend between the models based on the different levels of geometry. Figure 2.40 shows both (a) an actual impact from a specimen and (b) a FE model of the impact. Note that this portion of the study does not include welded details in the model and that the thickness of the shell elements is shown for illustrative purposes only.

The bottom normal stress in the *x*-direction (along the length of the beam), as determined in the control model (see Figure 2.38), was used to compare the different models. Figure 2.41 shows the stress contour of the underside of the bottom flange for localized damage that was 0.75 in. (19 mm) high over a length of 6 in. (152 mm) (*L*/*H* ratio of 8) for one

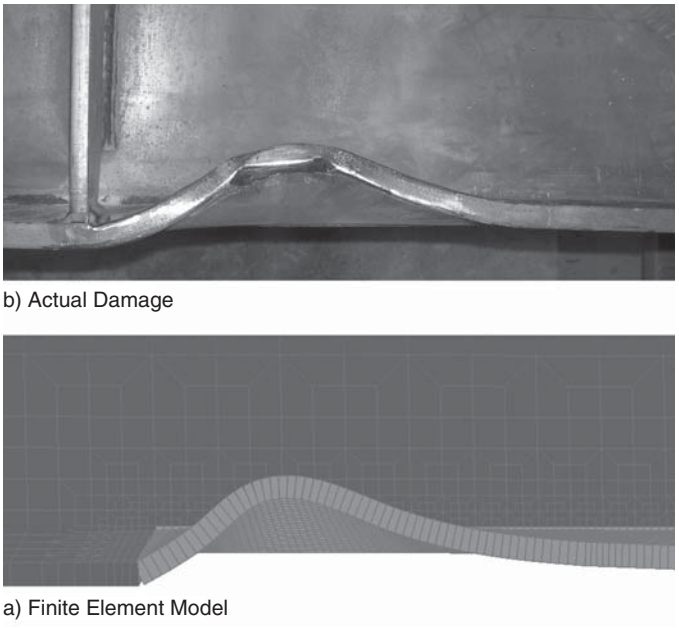

Figure 2.40. Comparison of modeled damage to a typical localized impact.

of the models and can be considered typical. As seen in the figure, large tensile stresses are present on the concave side of the localized damage. This is the area on the residual damage (for all geometries) that experiences the most tensile stress. The increase in stress is limited to that of the damaged area and the opposite side of the flange where the edge of the flange experiences some minor compression.

The models were examined and the maximum stress in the localized damage region was recorded. The location of the maximum stress varied a small amount along the width of the flange. As the height of damage increased, the maximum moved in toward the web. For smaller damage heights the recorded maximum was 0.25 in. (6 mm) in from the edge. For larger damage heights, the maximum was located up to 0.75 in. (19 mm) in from the edge. However the stresses across the width of the flange in the control model were all relatively uniform, [within 0.01 ksi (68.9 Pa) across the width of the flange]. Using this undamaged stress, a stress amplification factor (SAF) was calculated by taking the maximum stress for a given model that included the residual damage and dividing by the stress in the same location determined from the control model. Figure 2.42 is a plot of the each height of damage with the SAF on the ordinate (linear) and the length of damage on the abscissa (logarithmic).

It can be seen in Figure 2.42 that for all damage heights, SAF will decrease nonlinearly and all will eventually approach 1.0 as the length of damage increases (i.e., as the geometry approaches the undamaged condition). Also, the overall generalized slope of the curves increase as the height of the damage increases. For a larger height of damage, as the *L/H* ratio increases, the SAF will decrease more rapidly compared to that of smaller damage heights. Further analysis of the trends for these curves will be discussed in the next section.

To fully characterize the effect of residual damage, different flange thicknesses as well as flange widths also were modeled. Through the process of damaging and heat-straightening several specimens, it has been found that for severe localized impacts there will be a decrease in the flange width as well as thinning of the flange in the immediate vicinity of the impact. This is due in part to the impact as well as grinding the damaged area to remove any microcracking or irregularities after the impact has occurred. This is done to prevent any cracking during the heat-straightening process. As discussed, during the heat-straightening repair, small cracks had formed and were ground out to prevent further propagation. This process also has caused further thinning of the flange. Once the heat-straightening is completed, the area is again ground smooth to reduce any distortions left after the repair has been made.

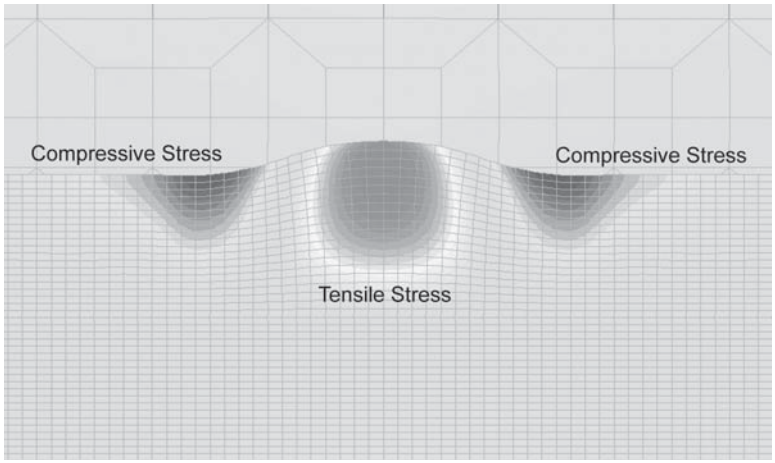

Figure 2.41. Stress contour of localized damage.

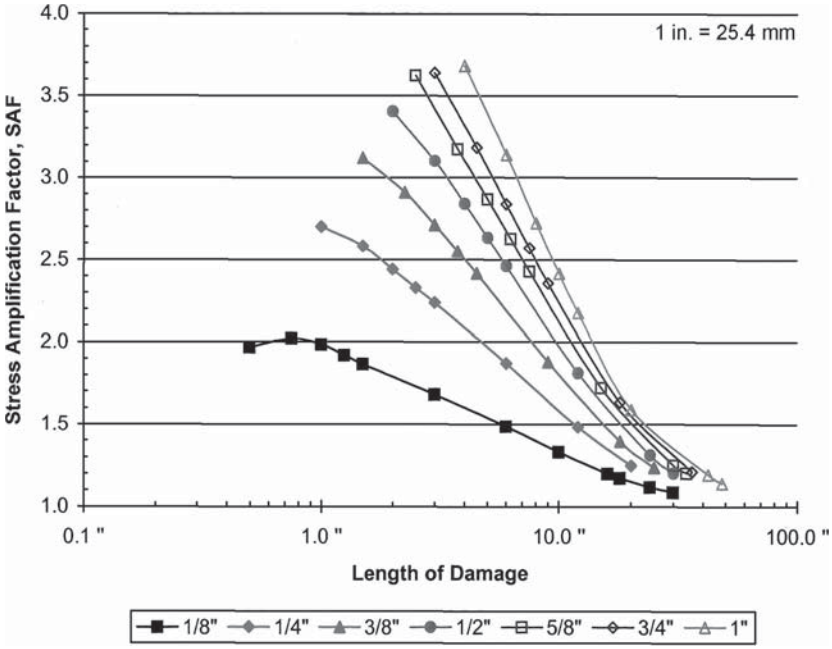

Figure 2.42. Stress amplification factor plot for various heights of damage.

(Note that if the engineer feels that this reduction does not warrant a repair weld or the addition of splice plates to increase the cross section, the area will remain as is.) In Figure 2.43, one of the repaired impacts where this has occurred is shown. It should be noted that this thinning only occurs at the edge of the flange and extends inward about one-eight to one-quarter of the flange width. As shown in Figure 2.43, the geometry only resulted in a reduction of less than 5% of the cross-sectional area.

To understand the influence of nominal flange thickness on SAF, models of varying flange thickness for several of the damage geometries were created. Two curves from Figure 2.42, each representing a specific height of damage, were selected.

Figure 2.43. Detail of repaired localized damage showing thinning of the flange.

For each of these curves, three additional curves were created that represented the different flange thicknesses for the same geometry of damage. The selected heights of residual damage were 0.5 in. (13 mm) and 0.75 in. (19 mm) along with the lengths of damage selected for the previous models. The additional flange thicknesses used for these models were 1 in. (25 mm) and 1.25 in. (32 mm). Since flange thickness less than 0.75 in. (19 mm) is not very common on a highway bridge girder, it was decided not to consider thinner flanges. The results of this analysis are shown in Figure 2.44 on a semi-log plot.

As shown in Figure 2.44, increasing flange thickness reduces SAF. This is due to the increase in stiffness with thicker flanges, which in turn reduces the amount of secondary bending experienced at the residual damage location. Note that two additional curves, representing 1 in. (25 mm) and 1.25 in. (32 mm) flange thicknesses, contain less data than the original curve because the minimum L/H ratio was raised when thicker flanges were modeled. The graph also demonstrates that at a given length of damage, the rate of SAF reduction varies for each curve. Based on this, as the height of damage increases, SAF will not reduce proportionally to flange thickness increases. Section 2.6.2.3 will describe the relationship of these curves and how the general trend can be applied for similar damage geometry.

The same procedure for analyzing the influence of flange thickness also was used for different flange widths. The same two curves, with damage heights of 0.5 in. (13 mm) and 0.75 in. (19 mm), were used for this analysis. For each original curve

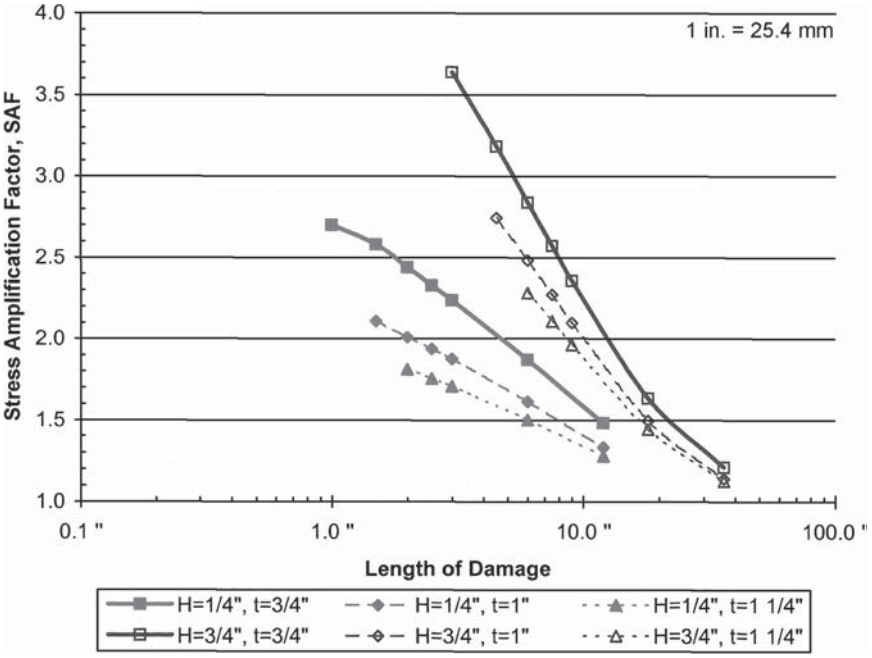

Figure 2.44. Stress amplification factor plot for various flange thicknesses.

using a 10 in. (254 mm) flange width, three more curves were created, representing different flange widths with the same geometry of damage. The additional flange widths used for these models were 14 in. (356 mm), 18 in. (457 mm), and 22 in. (559 mm). The results of the analysis are shown in Figure 2.45 on a semi-log plot.

Figure 2.45 shows that SAF increases with increasing flange widths due to the stiffness of the flange. For a large flange width, the localized bending caused by the residual damage located at the edge of the flange will behave similarly to residual damage in a "free" plate, increasing SAF. For wider flanges, the stiffening influence of the web decreases, thereby increas-

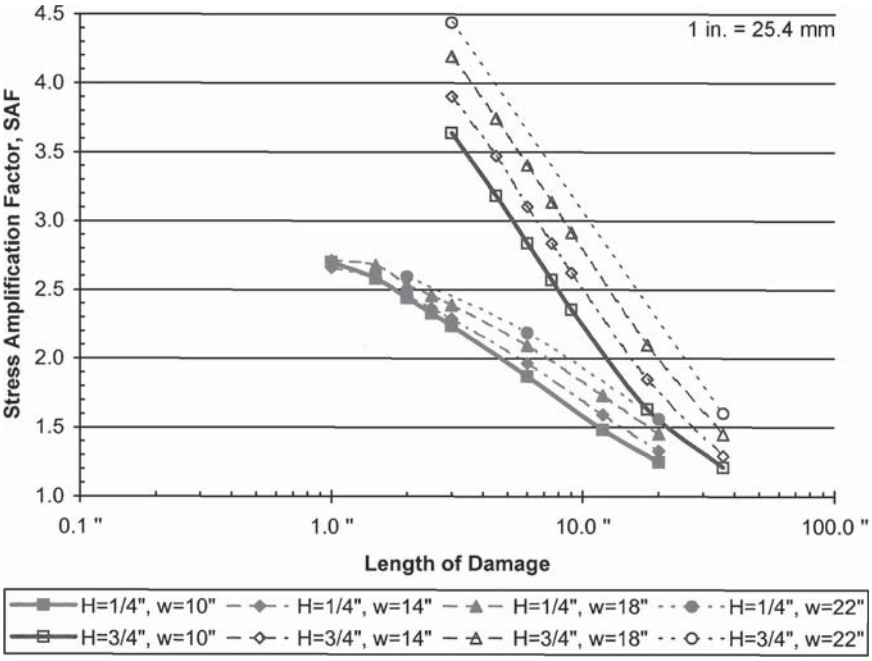

Figure 2.45. Stress amplification factor plot for various flange widths.

ing SAF. With the exception of the 0.25 in. (6 mm) height of damage when the length of damage is less than 4 in. (102 mm), the effect on SAF due to flange width is essentially independent of the length of damage, resulting in corresponding increases. The trend observed for lower lengths of damage [less than 4 in. (102 mm) for a 0.25 in. (6 mm) height of damage] may show that a small amount of damage will not change the SAF, regardless of flange width. Although this geometry of damage has been modeled, it was not typical of experiences during laboratory tests (discussed further in Section 2.6.2.3). However, with a 0.25 in. (6 mm) height of damage, once the length of damage exceeds 4 in. (102 mm), there will be a constant increase in SAF for all flange widths. The increase, although constant, will still vary based on height of damage. As the height of damage increases, the increase in the SAF also will be greater. Preliminary data for greater heights of damage, not shown in Figure 2.45, also agree with the constant increase of the SAF for a given height of damage, regardless of the length of damage, as well as the varying increase in SAF with height of damage.

This pilot study resulted in a general understanding of how damage geometry, flange thickness, and flange width affect stress at the damage location. Based on the analysis, for a given *L*/*H* ratio, the residual damage amplifies the normal bending stresses (i.e., Mc/I) compared to an undamaged condition. For thicker flanges, the increase is not as great compared to the same geometry of damage on a thinner flange. If the flange thickness was reduced (e.g., due to grinding), stress at that location would still be elevated. For larger flange widths, when the flange width was varied, the SAF increased independently of the length of damage for the same amount of damage [with the exception to short lengths of damage with a 0.25 in. (6 mm) height]. Using data obtained in the parametric study, an equation was developed that can predict the SAF based on the height of damage, length of damage, flange thickness, and flange width. The development of this equation is presented in the following section.

2.6.2.3 Trend Analysis

Using results gathered from the FE parametric studies, the influence of residual damage on local stress was determined as a function of flange thickness, flange width, height of residual damage, and length of residual damage. Considering only the flange thickness and flange width used in modeling the specimen, trend lines were developed for each height of damage curve, shown in Figure 2.46. The data obtained from the FE analysis are shown as individual data points, and the solid line is the calculated trend line.

Using a logarithmic trend line, a general equation can be derived based on the two variables, height of damage and length of damage. For a given height and length of damage for the Plate Girder A specimen, the SAF can be determined. Equation 1.4 was developed by modifying the logarithmic trend lines produced in Microsoft Excel for each curve to improve accuracy in the equation, where SAF is the stress amplification factor for a

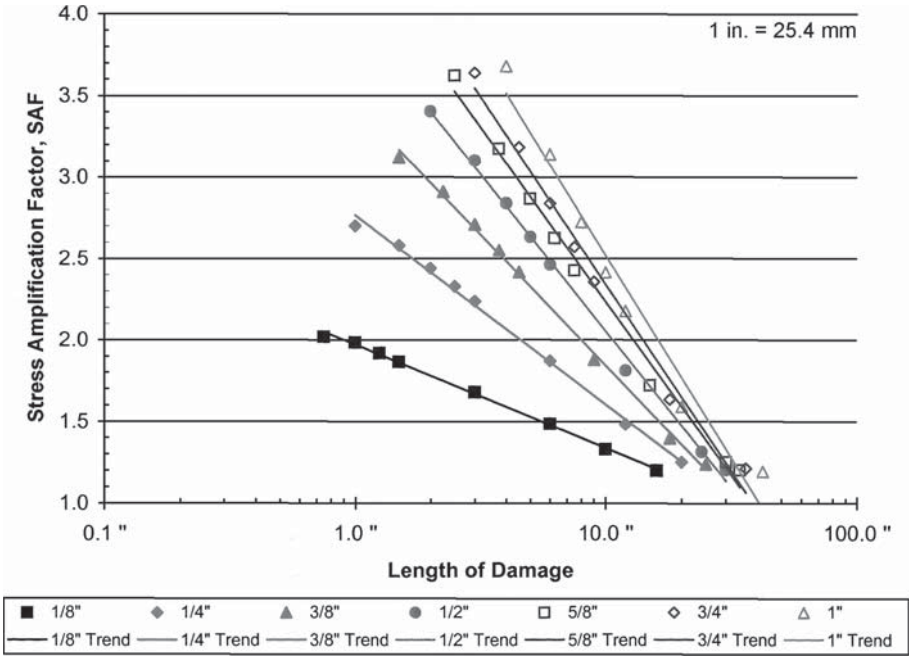

Figure 2.46. Stress amplification factor trend plot for various heights of damage.

given height (in inches) of the residual damage, *H,* and the length (in inches) of the residual damage, *L.* Next, a trend line using data from all curves to produce a final equation for all heights of damage was developed. Equation 1.4 was verified with numerous models confirming that the equation accurately predicts SAF. The estimates from Equation 1.4 are within 3% to 5% of the value obtained with the FE modeling for nearly all cases within reasonable limits of *residual* damage.

$$\mathrm{SAF} = \left(\frac{1.45\ln(H)+3.8}{-\ln(40H^{0.43})} \right) \ln(L) + 1.45\ln(H)+5 \qquad \textit{Equation } 2.1$$

A comparison of results from the FE modeling to results computed using Equation 1.4 is shown in Figure 2.47. Data show results of the modeling and the solid line represents the results using Equation 1.4 for each height of damage. The results from the equation produced values roughly 5% higher for the 0.25 in. (6 mm) and 0.375 in. (10 mm) curves. This overestimation also was present for greater lengths and large heights of damage. Most of the residual damage observed had been localized and the lengths of damage were usually limited to no more than 24 in. (610 mm). However, where the damage under consideration exists prior to a heat-straightening repair, the length of damage would usually be longer (assuming no sweep is present in the beam). Considering typical conditions and small percentage fluctuations, results from the equation are considered acceptable.

Next, a third variable, flange thickness, was added to the equation. Based on data obtained, the effect of the SAF is dependent on the height of damage and the length of damage. Equation 1.4 was modified to include the effect of flange thickness on the SAF. The same procedure in determining Equation 1.4 also was incorporated in determining Equation 2.2, where SAF is the stress amplification factor for a given height (in inches) of the residual damage, *H,* the length (in inches) of the residual damage, *L,* and the flange thickness, t_f (in inches).

$$\mathrm{SAF} = \left(\frac{(1.35\ln(H)+4.25)t_f^{-0.6}-1.2}{-\ln(40H^{0.43})} \right) \ln(L) + (1.35\ln(H)+4.25)t_f^{-0.6} \qquad \textit{Equation } 2.2$$

Based on FE modeling, this refined equation was tested to verify its accuracy. The comparison of equation results to modeled results are shown in Figure 2.48. The data points are the results of the FE modeling and each line represents the equation for each flange thickness and height of damage. This equation produced results that were reasonably accurate, mostly 3% to 5% higher than that of the results from the FE modeling, within the accuracy limits of defining residual damage.

Because the effect of flange width on SAF is independent of the length of damage (with the exception of the limited regions as discussed in Section 2.6.2.2), a width-effect term can be added to Equation 2.2. This term was determined by taking the average of the increase in SAF per a given width of flange. Because this increase varies for each height of damage,

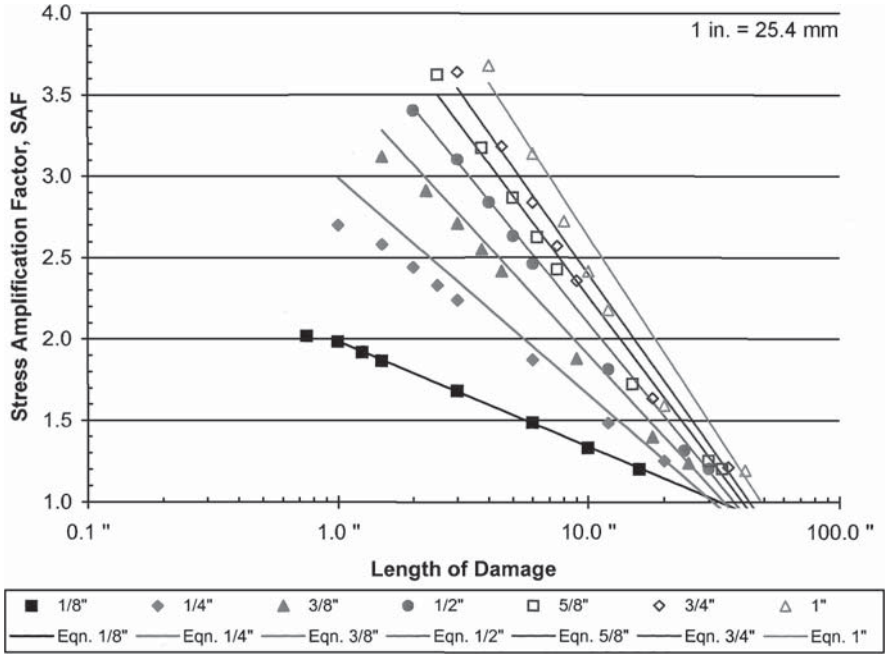

Figure 2.47. Comparison of SAF Equation 1.4 to finite element modeling data.

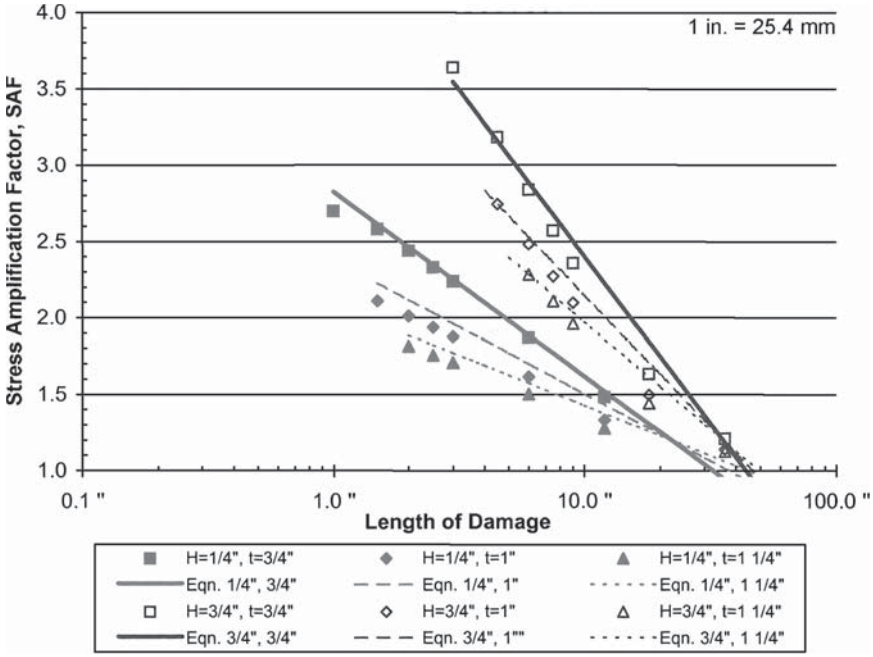

Figure 2.48. Comparison of SAF Equation 2.2 to finite element modeling data.

a trend was developed to include this as well. Equation 2.3 includes all four variables and can be used to predict SAF for a given height (in inches) of the residual damage, *H,* the length (in inches) of the residual damage, *L,* flange thickness, t_f (in inches), and flange width, b_f (in inches).

$$\mathrm{SAF} = \left(\frac{\left(1.35\ln\left(H\right)+4.25\right)t_f^{-0.6} - 1.2}{-\ln\left(40H^{0.43}\right)} \right)\ln\left(L\right) + \left(1.35\ln\left(H\right)+4.25\right)t_f^{-0.6} + 0.1H\left(b_f - 10\right) \qquad \textit{Equation } 2.3$$

This final equation was compared to the modeled data shown in Figure 2.49. Again the individual data are the results of the FE models, and the lines are the results of the equation for a given flange width and height of damage. The general trend of the solid lines remains the same as the previous equation, while the broken lines include the effect of flange width. As seen for the previous two equations, the results are conservative at large heights and lengths of damage as well as small heights and lengths of damage. As stated earlier, most residual damage will not approach these overly conservative regions. Although the final form of the equation appears quite complex, with a PC, spreadsheet, or handheld PDA, the calculation takes little time. The greatest effort is related to obtaining the geometric input (damage, flange size, etc.). As stated earlier, this portion of the research was beyond the original project's scope, but in the opinion of the research team too important to leave unexplored. Nevertheless, the above issue and procedure should be studied further and refined in the future.

Five locations of residual damage were instrumented on the heat-straightened specimens used for the verification of the SAF equation. Four of the five residual damage locations were located in the vicinity of either transverse stiffeners or cover plate terminations. The amplification in stress was determined from the instrumentation and was compared to results of the SAF equation. For cases where the residual damage is located within the area of welded details, the equation predicted the stress amplification, on average, within 25% of instrument readings. This included an exact prediction and estimates above and below the stress amplification determined from the instrumentation. For the case of residual damage not in the vicinity of welded details, the equation over-predicted the stress amplification in the base metal condition by 11%.

One of the five instrumented locations had a flange thickness of 0.75 in. (19 mm) and width of 10 in. (254 mm), and measured residual damage height of 0.25 in. (6 mm) and length of 5 in. (127 mm) as shown in Figure 2.50. The stress amplification determined from the instrumentation yielded roughly 1.8 [refer to Figure 2.7, measured stress of 16.2 ksi (111.7 MPa) at a location where the theoretical stress would be 9 ksi (62.1 MPa)] while the result from the FE model also was approximately 1.8. Using the member and residual damage geometry, the SAF equation generated a result of 2.0. These values are considered comparable, and the residual damage was within the general trend of the curves. It did not

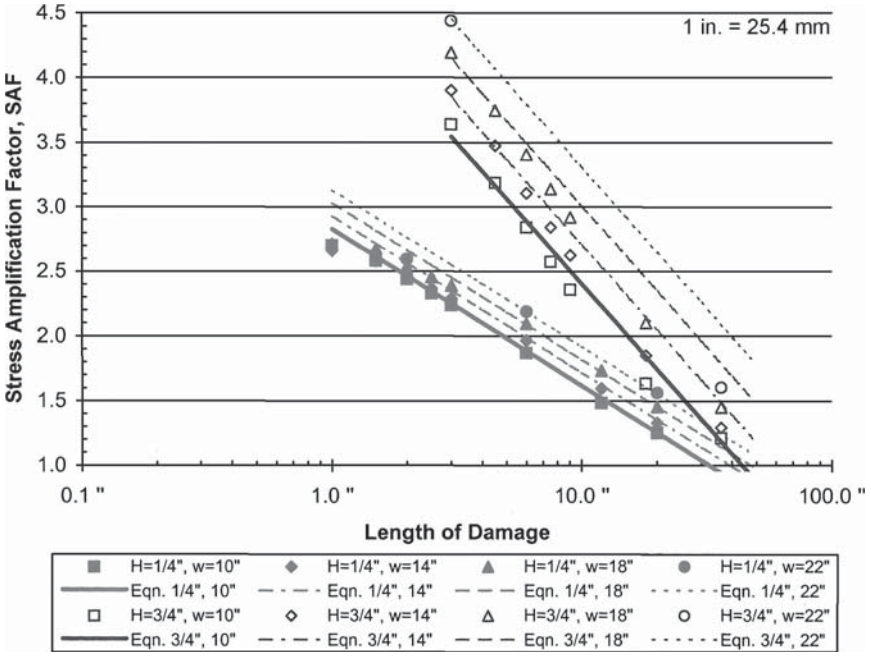

Figure 2.49. Comparison of SAF Equation 2.3 to finite element modeling data.

fall near any areas where the SAF equation would produce overly conservative estimates.

2.6.3 Solid Element Models

The second part of the modeling analysis consists of creating the same specimen using 20-node solid elements. The purpose of this analysis was to verify results of the shell element models and the SAF equation when the damage is located near welded details (flange attachments and stiffeners). In order to accurately model these details, the types of elements selected were necessary to achieve adequate results at weld details, such as cover plates and stiffener details. The solid model is shown in Figure 2.51.

For this FE analysis, four models were created. The first model, shown in Figure 2.51, was the control model for the analysis. This model contained both types of details for which the subsequent models will contain residual damage near. The flange attachment and stiffener details are shown in Figure 2.52 and Figure 2.53, respectively.

Figure 2.50. Residual damage on Specimen 1D/R-2.

The other three models were identical to the control model except that residual damage was modeled either near the flange attachment or the stiffener. The first of these models contained residual damage near the flange attachment that had the convex side of the residual damage facing up, as shown in Figure 2.54. The next was similar to the first, except that the convex side of the residual damage was facing down, as shown in Figure 2.55. The third model contained residual damage near the stiffener, as shown in Figure 2.56. The damage modeled for all locations was 0.25 in. (6 mm) high and 4.5 in. (114 mm) long. This geometry of damage is within tolerances listed in the FHWA manual. According to this publication, the presence of this residual damage would be acceptable in the member after a heat-straightening repair. Note that using Equation 2.3 to determine the SAF for this level of geometry yields a value of 2.0. For Figure 2.54, Figure 2.55, and Figure 2.56, the residual damage is shown on the models.

The residual damage at the flange attachment for the second model was oriented differently than what was previously modeled with the shell elements. For this case, the convex side was now on the underside of the bottom flange. The primary loading of the member would cause the localized residual damage to flatten, producing a tensile stress on the concave side of the damage. However, the convex side (the top side of the bottom flange for the shell element models) would be

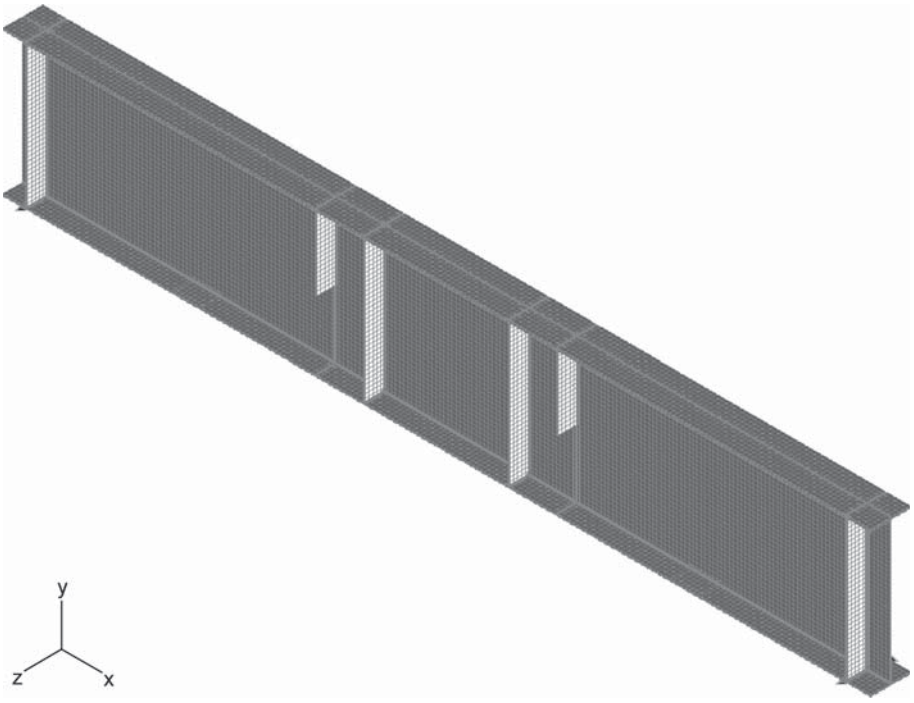

Figure 2.51. Typical solid element model.

subjected to secondary compressive stresses. The locations where the member begins to flatten will experience secondary tensile stresses on the top side of the flange and secondary compressive stresses on the underside of the flange. Thus, if the residual damage was modeled as previously, then the weld toe would experience compressive secondary stresses subtractive from the primary tensile bending stresses. This would result in an apparent improvement in the fatigue performance of this detail and not relevant for this research. However, when the convex side of the residual damage is on the same flange face where the flange attachment is welded (see Figure 2.55), depending on how close the residual damage is to the weld toe, tensile stress increases at that weld toe. This may or may not be the maximum tensile stress experienced on the entire area. The SAF equation was developed on the basis of the maximum stress over the entire area of residual damage since no specific details were considered. However, in the presence of welded details, it is the amplification in stress at the weld toe that is of interest.

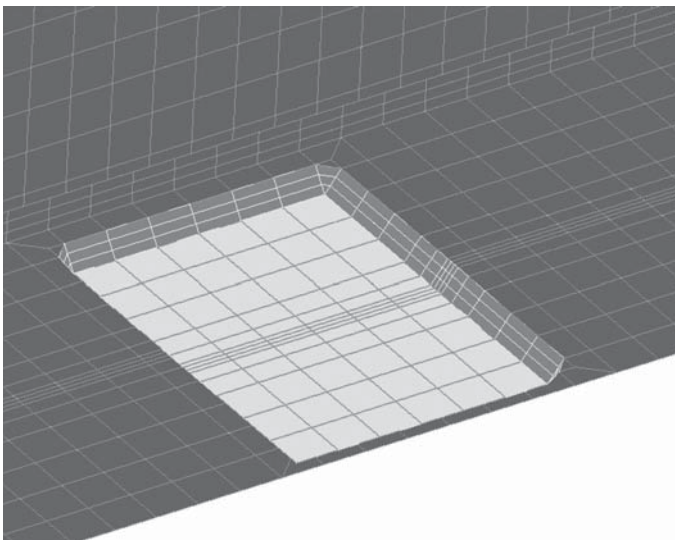

Figure 2.52. Flange attachment detail on solid model.

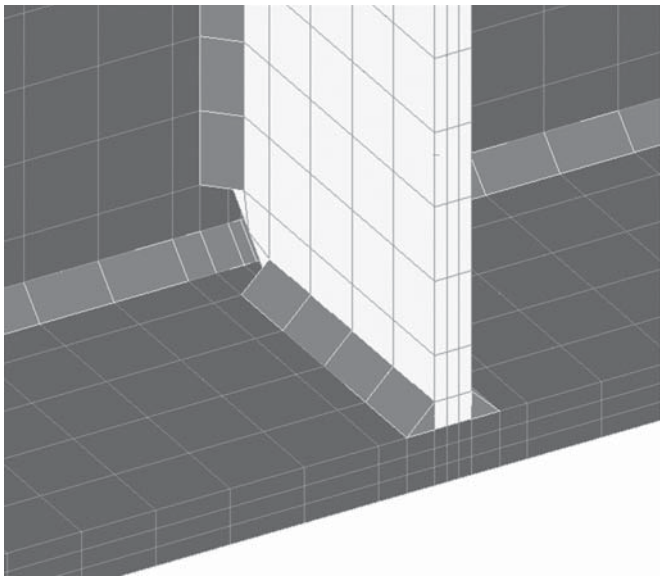

Figure 2.53. Stiffener detail on solid model.

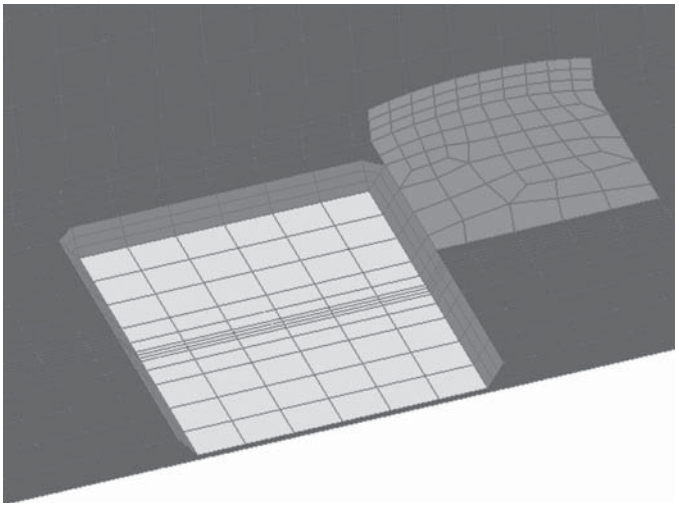

Figure 2.54. Residual damage near flange attachment (convex side up).

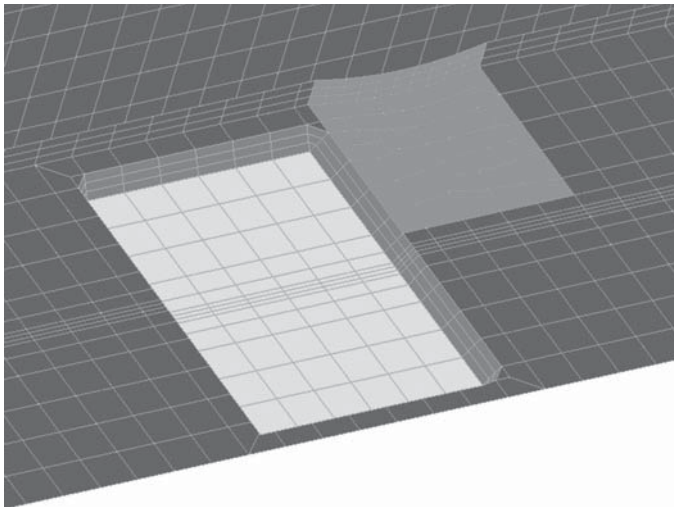

Figure 2.55. Residual damage near flange attachment (convex side down).

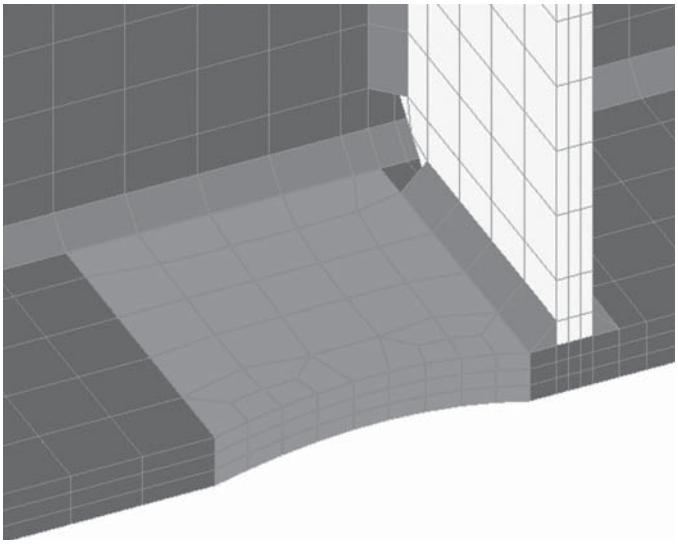

Figure 2.56. Residual damage near stiffener.

Residual damage orientation was not part of the original test matrix in the development of the SAF equation, so how orientation of residual damage will affect SAF is not covered. However, modeling the residual damage was necessary to compare how close the SAF equation was to results obtained from FEM (finite element model) methods. Based on the questionnaire, either orientation is found in the field so modeling both is appropriate.

After the models were analyzed, the first step in determining SAF was to locate the area of largest stress on both models containing residual damage and at the same location on the control model. The stiffener was in the constant moment region; due to normal loading, the stress in this region should be relatively constant. However, because of the presence of the stiffener weld, stress would not be the same at that location. The flange attachment detail was located in the moment gradient, so to accurately determine SAF, the location where the stress was obtained on the residual damage model would need to be consistent with the control model. Figure 2.57 and Figure 2.58 present the results of the analysis as stress contour plots for the flange attachment details with the convex side of the residual damage facing up and down, respectively.

As shown in Figure 2.57, stress at the concave side of the residual damage was 19.1 ksi (131.7 MPa) while at this same location on the control model, it was 11.5 ksi (79.3 MPa); thus SAF is equal to 1.7. The stress at the corner of the weld toe also was compared to the control model and was reduced 40% from 14.8 ksi (102.0 MPa) to 5.6 ksi (38.6 MPa). Stresses along the length of the weld toe on the opposite side of the flange also were compared and found to have a negligible change. When comparing these results (maximum of 1.7) to the SAF equation (2.0), the SAF equation over-predicted the SAF by about 20%. This verified that if the residual damage is oriented in this direction, the SAF equation will over-predict the modeled results. Next, these results were compared to the model containing the residual damage with the convex side facing down. This would determine if Equation 2.3 over-predicted SAF for residual damage near flange attachment details.

Figure 2.58 shows that the maximum stress occurs along the weld toe with a maximum of 36.6 ksi (252.3 MPa) at 2 in. (51 mm) from the edge of the flange attachment. Considering the moment gradient, stress on the control model at this same location was 15.2 ksi (104.8 MPa), resulting in a SAF of 2.4. Stresses at two other locations were not as significant, but did yield a SAF of 1.9 for both locations. From the results of the flange attachment analysis, the orientation of the residual damage does determine the stress present at the flange attach-

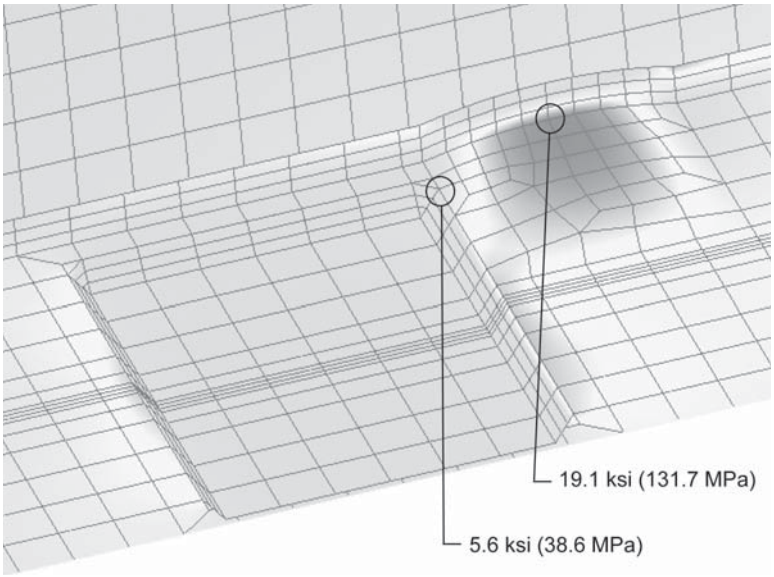

Figure 2.57. Stress contour of residual damage near flange attachment (convex side up).

ment weld toe. As stated earlier, a significant comparison cannot be made between these results and Equation 2.3 because the orientation of the residual damage was not investigated. However, the equation does provide a reasonable estimate of SAF for these two specific cases.

Figure 2.59 shows the three locations that were investigated for the stiffener detail. The first was at the edge of the underside of the bottom flange, where the largest stress was 29.7 ksi (204.8 MPa). At the same location on the control model, the stress was 15.4 ksi (106.2 MPa), resulting in a SAF of 1.9. At the second location, 27.8 ksi (191.7 MPa) was present at the weld toe while stress from the control model at that location was 14.0 ksi (96.5 MPa), resulting in a SAF of 2.0. The last location was at the point where the residual damage begins to flatten. This had a stress of 24.9 ksi (171.7 MPa) on the damaged model and 15.3 ksi (105.5 MPa) on the control model, resulting in a SAF of 1.6. As described earlier, the largest stress taken from the shell models was located on the concave side of the residual damage. However, because of the presence of the stiffener, the larger SAF was located at the weld toe. In

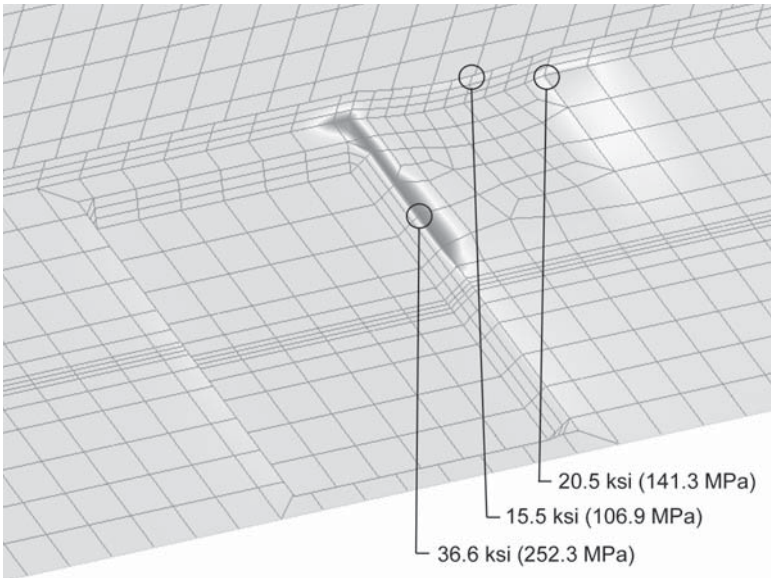

Figure 2.58. Stress contour of residual damage near flange attachment (convex side down).

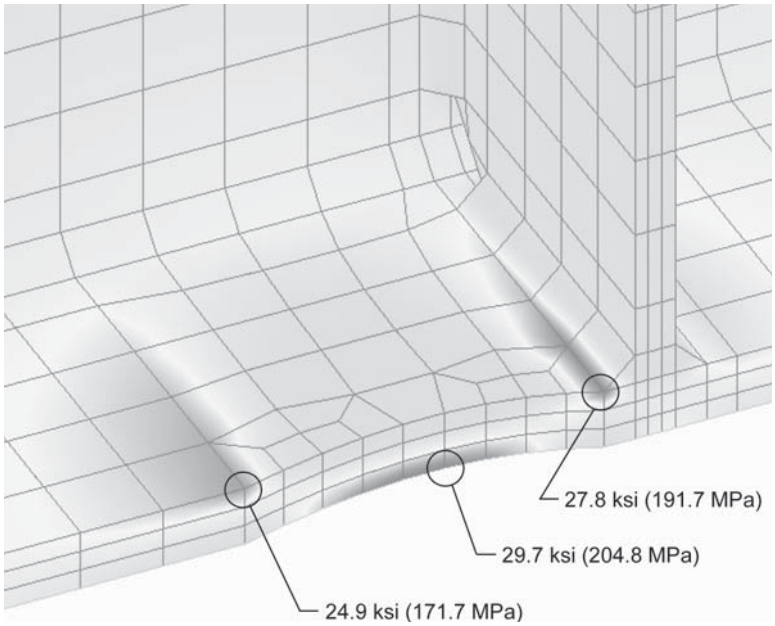

Figure 2.59. Stress contour of residual damage near stiffener.

comparison, both are relatively the same, so SAF due to this residual damage would be roughly 2.0. These values now can be compared to the SAF calculated by Equation 2.3, which yielded a value of 2.0, essentially the same. Thus for this specific case, the SAF equation does give accurate SAF predictions for the transverse stiffener welded to the bottom flange.

The FE modeling results for the residual damage and welded details using solid elements were similar to the results from the SAF equation for these specific models. Although results were similar for these particular cases, the equation cannot be assumed to accurately predict SAF for all levels of residual damage geometry and member geometry without further analysis. Likewise, a reasonable SAF could be obtained from the equation with different orientations of residual damage, as modeled near the flange attachments, but the accuracy of the SAF equation may vary for different relative geometries of the residual damage and the member. This modeling suggests that based upon future analysis of these variables, the SAF equation can be calibrated as necessary to account for these factors.

CHAPTER 3

Interpretation, Appraisal, and Applications

3.1 Fatigue and Fracture Performance

3.1.1 Recommended Number of Repairs

The fatigue and material property tests for each D/R cycle were evaluated to determine the number of times a member can be safely repaired at the same location. After the third D/R cycle, the results of fatigue testing showed substantial decreases in the base metal fatigue life where the impact occurred. Before fatigue testing, this area was inspected using both PT and MT methods concluding that no surface cracks were present. Along with the decreasing base metal fatigue life, the fracture toughness also decreased more than 50% in some cases, with individual tests falling below AASHTO requirements. Although a decrease in toughness was typical as the number of D/R cycles increases, considerable scatter in the CVN data precluded a definitive conclusion, correlating the effect of heat-straightening and a percent reduction per D/R cycle. Therefore, the number of repairs should be limited to two when subsequent impact damage falls within the limits of the first impact repair. This is the same limit on the number of repairs specified in the FHWA manual of standard practice that was based on previous research.

There are a few important points to note regarding this recommendation. First, recognize that this recommendation is based on the observed behavior immediately adjacent to welded stiffener and cover plate connections, making it conservative for base metal without such details. Second, the impacts applied during the research were very severe and focused. If impact locations are separated by at least 12 in. (305 mm), increasing the number of times a member may be repaired beyond two could be justified. Third, to adhere to this limitation, an owner must maintain detailed records of previous impacts and repairs, documenting the degree of damage, calculated strain ratio, location and extent of repairs for each impact. This documentation permits the decision to repair a location that was previously heat-straightened to be based on sound data.

3.1.2 NDT Inspection

During the laboratory testing, MT, PT, and UT inspection methods were evaluated during the repair process. Both MT and PT were used following the impact, during the repair process, and following the completed repair. These methods were deemed adequate by the researchers and either can be used, based on the agency's preference. Regardless of the method, having qualified, experienced personnel conduct the inspection is very important. NDT inspection should be done during the initial damage evaluation and documentation to determine if the impact caused any cracks. Include the area of the impact, any other areas collaterally damaged, and any welded or bolted details in the vicinity of the damaged members. Careful visual inspection should follow each heating sequence to ensure that no cracks initiated during the application of the restraining forces and/or the heating and cooling process. Any questionable areas or indications should be subsequently inspected by PT, MT, and/or UT. Upon completion of the heat-straightening repair, inspection of areas examined prior to the repair should be reexamined. Repair welds must conform to the agency's repair procedures with at least MT of fillet welds and/or UT of complete penetration welds after completing the repair.

3.1.3 Treatment of an Impact Area Prior to Heat-Straightening

During a subsequent impact at a different location on Specimen 1D/R-2, a previous impact location not treated (i.e., ground smooth) fractured. This same phenomenon has been observed on bridges that have been hit multiple times. To avoid similar failures during the laboratory testing, a simple protocol was developed using common hand tools. This procedure should be performed immediately following the assessment and documentation of field impacts.

First the impact area should be ground to bright metal, removing any abrupt irregularities and surface defects. Using a sanding disc or similar tool, smooth the area and slightly

round all edges. Finishing should be parallel to the direction of the primary stresses in the member, ensuring that transverse, nicks, gouges, or grind marks are removed. If the impact is close to a weld detail, the weld toes also should be smoothed with a die grinder (radius to be determined at time of repair), eliminating any microcracks introduced at the weld toe during the impact. Using a sanding disc or similar tool, smooth the weld face. Finish grinding of weld face and toes also should be parallel to the primary design stress, ensuring that transverse grind marks are removed. Thoroughly inspect the area, including any weld toes in the vicinity of the impact, using MT or PT as appropriate.

3.1.4 Restraining Force Evaluation

Based on results of experimental and analytical studies on restraining forces, at the beginning of the repair process when localized damage has the most severe geometry, stresses around the impact produced by the horizontal restraining force can be significantly greater than calculated using a simple "My/I" approach. As a result, local stresses immediately adjacent to the impact may be grossly under-predicted, leading to hairline fractures or even brittle pop-in fractures. However, after a review of the fractures surface characteristics, material tests, strain measurements, and FE analyses, the research team does not believe that the fractures are simply the result of over-jacking. The primary evidence supporting this conclusion includes:

1. No fractures occurred during the first repair cycle, even though the same restraining forces were applied during the second repair, when fracture occurred.
2. Results of material testing verified that the steel had CVN values satisfying the applicable AASHTO specification. There was significant scatter in the CVN data and the *exact* locations of the most significant localized straining where the cracking occurred could not be directly tested.
3. Since the same procedures are used in field practice, fractures would be much more common than are reported, especially since typical control of restraining forces is much less stringent.

Based on the preceding material, the observed fractures were believed to result from two factors: the effect of jacking the damaged geometry and associated over-stressing at the most severe damage location, and, more importantly, the effect of the subsequent impacts (second and later) in the same location. A subsequent impact at exactly the same location and cumulative degradation in material properties can lead to fractures observed during this research. Although jacking of the severely distorted cross-section contributed to the observed fractures, it was not the sole cause. The likelihood of a fracture increased when using the levels of restraining forces suggested in the FHWA manual.

Beams seldom fracture in the field when repaired multiple times because in service, extreme local damage applied in the laboratory and impacting the exact same location more than once are uncommon. Although impacts may appear to be at the same location, the most extreme local damage during the subsequent impact is probably not confined to the same 1 to 2 in. (25 to 51 mm) region as the earlier impact. For this reason, limiting heat-straightening to only one repair would be unreasonably restrictive.

The FHWA manual states there is no direct "quantitative" method for determining the "correct" restraining forces to be used on the member due to the complexity of the structure. The current guidelines are intended more for general cases, are likely acceptable with common levels of localized damage and global damage, such as sweep, is distributed over a few feet. The increase in stress due to severe localized damage documented by instrumentation and FE analysis in this study are not properly accounted for in the current FHWA method. For routine damage or when a quick decision is needed, FE analysis or strain gaging are not practical. A simple procedure to safely estimate the appropriate restraining force is needed. A method to account for the effects of localized damage in girders struck one or more times was developed during this project. This method should reduce the potential for fractures caused by inaccuracy in predicting stresses in the damaged girders due to the restraining forces and the degradation in material properties at localized damage. Since improving material properties is not practical, one must ensure the stresses produced by restraining forces are within acceptable limits substantially reducing the chance of a brittle fracture. The proposed method follows current methods in determining the restraining forces, with only basic modifications.

One approach is simply eliminating the horizontal restraining force when localized damage is present. This may prevent fractures, while maintaining the level of vertical restraining force suggested in the FHWA manual, but will unreasonably lengthen the repair time, essentially making some repairs impractical. For obvious reasons, this strategy is deemed unreasonable.

Short of conducting 3-D FE models for each damage scenario, there is no analytical solution to determine the appropriate horizontal restraining force that accounts for the localized damage. During laboratory repairs, methods to establish repair procedures ensuring a successful repair were developed. This entailed varying restraining forces, measuring strains, and closely inspecting the specimen for any signs of distress during the repairs. After conducting several repairs and through trial and error, a simple, yet effective approach was developed. The authors acknowledge that the method was not subjected to a formal analytical validation process, such as rigorous FEM parametric studies. Nevertheless, the consistent success of laboratory repairs with the method outlined below suggests it is a reasonable approach.

3.1.4.1 Procedures in Determining the Restraining Force

First, the strain ratio of the localized damage must be determined using procedures currently in the FHWA manual. Next, a horizontal restraining force is calculated using the procedures in the FHWA manual. As stated, use of those restraining forces would produce very high local stresses in the region of severe local damage, so the force must be reduced to avoid a potential fracture. As discussed, reducing the horizontal restraining force by 1% for each unit of strain ratio seemed to bring the initial restraining force to an acceptable level and prevent brittle fracture. For example, if a localized bulge in the flange has a calculated strain ratio of 50, the horizontal restraining force per the FHWA manual should be reduced by 50%. As localized damage is repaired and its strain ratio is reduced, the horizontal restraining force can be increased accordingly. Engineering judgment must be applied to ensure the acceptable level is not exceeded, potentially causing a fracture.

A horizontal restraining force as described will allow for reasonable repair time as well as minimizing the potential of brittle fracture. The number of heating cycles and resulting repair time will increase somewhat from what the FHWA manual would predict, but avoiding brittle fracture justifies the change. These guidelines were implemented during the later repairs conducted in this research with no hairline cracks or brittle fractures occurring during the straightening.

3.1.5 Repair of Transverse Stiffeners

During the repair process of the first two specimens, cracks formed during cooling at the flange weld toe of the transverse stiffener details. After examination of the exposed crack surface, the crack was attributed to the tearing of localized "bunched" material at the weld toe and not to a brittle fracture caused by over-heating or over-jacking. This bunching of material at the flange-stiffener weld was caused by bending the flange about the weld adjacent to the impact. As the steel cooled and contracted, the bunched material tore away from the flange-stiffener weld, causing the crack to form through ductile tearing. Based upon attempts to mitigate cracking by grinding the weld toe prior to the heat-straightening repair, a recommended procedure that reduces the possibility of potential tearing or cracking during the heat-straightening repair was developed.

As discussed in Section 2.3.3, a portion of the stiffener should be removed by first cutting about 0.125 in. (3 mm) above the stiffener/flange fillet weld. Regardless of the method used to make this cut, care must be taken to avoid nicks or gouges in the flange and web. If thermal cutting is used, the web and flange must be protected. The height of stiffener removed is based on available access near the localized damage and any deformation in the stiffener. Incorrect location of the cut can result in undesirable distortion of the member, lengthening the time of repair. The fillet weld and stiffener remaining on the flange after the cut should then be ground parallel to the direction of applied stress flush with the surrounding base metal. Significant grind marks should be removed using a sanding disc. The area then should be inspected (e.g., MT), and then normal heat-straightening repairs can be conducted to remove damage caused by the impact. Upon completion of the repair, the portion of the stiffener that was removed can be replaced using a welded or bolted repair as determined by the agency. If the plate served only as a transverse stiffener (i.e., no diaphragms or cross-frames were attached), there may be no need to replace the removed portion of the stiffener.

3.1.6 Residual Damage Evaluation

Prior to beginning the fatigue testing, the measured stresses within areas where some residual geometric damage remained after heat straightening were found to be significantly different than predicted by simple beam theory. As a result, prior to fatigue testing, a static calibration test was performed by applying load in defined steps and recording strain gage data. Although the results indicated the response of the specimen was linear elastic, the measured strains did not agree with calculated elementary ($\sigma = Mc/I$) beam theory. After completion of the heat-straightening repair, areas with small residual geometric damage were not thought to be of sufficient magnitude to significantly alter the stress field in the flange. After review of the data, the remaining geometric damage (i.e., local flange bends not removed during straightening) clearly altered stress adjacent to the gages, in some cases, substantially. Since the bottom flange was in tension, the folds or distortions were stretched as the tensile forces in the flange attempted to flatten them. This produced local bending stress in the flange either additive or subtractive to the nominal tensile stress from external fatigue loads. A FE model incorporating the residual damage was built for the instrumented girder, and the stresses from the model showed excellent agreement with the gage results. This is important because in-service local stresses at fatigue sensitive details may be much higher than calculated using traditional calculations. The FHWA manual of standard practice does not address this issue and, therefore, unconservative estimates of remaining fatigue life in repaired girders can result. Although not part of the original scope of work, this effect was further investigated through FE parametric studies.

Using results of the parametric study, recommended procedures for defining damage geometry as well as SAF have been compiled and are described in the following section. Although the level of residual damage cannot be predicted exactly prior to a repair, some amount of residual damage should be expected to remain. During the initial inspection following an impact, carefully document the damaged loca-

tion, including any welded or other details in the vicinity of the impact and where heat-straightening will occur. In addition, any evidence of previous impact damage or repairs including heat-straightening, welded, or reinforcing also should be documented and verified prior to planning heat-straightening. Based on the design of the member, the engineer should determine an allowable increase in stress at those detail locations after the repair so an acceptable final SAF can be established.

This information must be presented to potential contractors performing the repair. If a severe impact is located at or very near a welded detail (excluding a web-to-flange weld, see Section 3.1.5), this must be considered by the owner and the heat-straightening contractor during the bid stage. A successful repair, which would entail more stringent tolerance limits due to the proximity of the welded detail, may lead to a longer repair time and increase the cost. If the owner feels that this increase in time and cost of repair is unacceptable, other means of repair (including replacement of the damaged area) should be considered. Based on the results of the FE modeling, residual damage greater than the tolerances listed in the FHWA manual may be acceptable without adversely affecting the integrity of the entire member. However, the owner may require adherence to the current FHWA tolerances based on aesthetic considerations.

3.1.6.1 Procedures in Determining the Stress Amplification Factor

In order to accurately determine whether a heat-straightening repair is adequate, with residual damage within the FHWA manual tolerances, the geometry of the remaining damage must be determined. These measurements can be made using simple and inexpensive tools including a ruler or combination square, string, and tape or clamps along with the following procedures:

1. Using a taut line, either taped or clamped to underside edge of the bottom flange beyond the damage, pinpoint the highest deviation in the flange (see Figure 3.1).

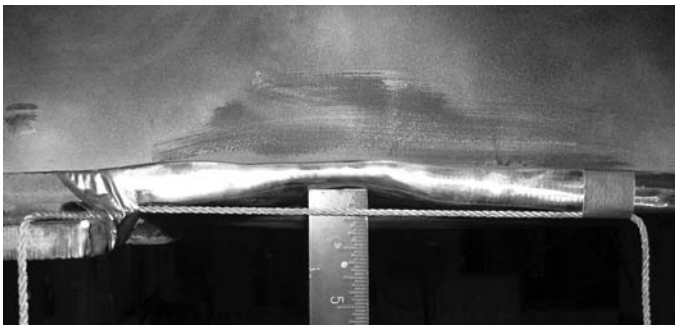

Figure 3.1. Example of measuring H.

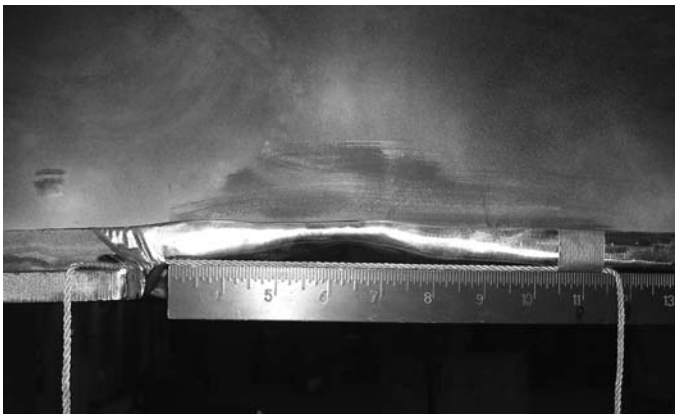

Figure 3.2. Example of measuring L.

2. Measure from the taut line to the highest point of the deviation as shown in Figure 3.1 and record as the height of damage, *H*. Likewise record the length of the flange that is not touching the taut line and record as the length of damage, *L*, as seen in Figure 3.2. The values for these dimensions shown in the figures are 0.25 in. (6 mm) for *H* and 5 in. (127 mm) for *L*. (Note that although both U.S. Customary and Metric units are given, the SAF equation is only valid when using U.S. Customary units.)
3. Record the flange width and thickness at the maximum height of damage. As described in Section 2.6.2.2, it may be possible to observe a thinning of the flange that may occur due to upsetting of the material (see Figure 3.1 and Figure 3.2), which may increase the apparent SAF. To account for such thinning, the reduced thickness can be used as the flange thickness in determining the SAF. In most circumstances, this would be overly conservative and an average thickness, based on engineering judgment, should be used. For the case shown, thinning caused a reduction in the flange thickness from 0.75 in. (19 mm) to 0.5 (13 mm). Because the extreme thinning was only at the edge of the flange and tapered to the center under the web, a flange thickness of 0.7 in. (18 mm) was used for the calculation. There was no noticeable decrease in flange width, so the original width of 10 in. (254 mm) was used.
4. Calculate SAF using Equation 2.3 with the measurements from the previous steps to determine the increase in stress at that location.

The SAF for this residual damage and member geometry was calculated to be 2.04. If this is greater than the SAF permitted by the engineer for the location, then further repair is required. Note that after multiple cycles of heat-straightening, less damage is removed per cycle. If the damage cannot be repaired to acceptable limits, other means, such as removing the damaged area or live-load testing, should be considered.

CHAPTER 4

Conclusions and Suggested Research

4.1 Fatigue and Fracture Performance

Fatigue testing of several common fatigue details has been conducted on steel girders subjected to up to three D/R cycles. In general, the D/R cycles did not have appreciable effects on the fatigue life of the girders at stiffeners and cover plates when the weld toes were subjected to grinding, rewelding, or other repairs during the process that effectively "reset the clock" on the detail's fatigue life. These repairs essentially removed defects present at the weld toe introduced during fabrication, the damage cycle, or the repair cycle. For fatigue cracking that initiates at surface defects, the number of D/R cycles does not seem to influence fatigue life as long as no weld toe or base metal defects are introduced.

However, two fatigue cracks appeared prematurely in base metal that was subjected to three D/R cycles. These were examined, and no conclusive evidence was found that suggested an obvious surface defect was present. Closer examination of the actual fracture surface indicated that a flaw may have been present within the thickness of the flange that propagated in fatigue and lead to the observed fracture. Since such defects cannot be detected by traditional surface NDT techniques, such as MT or PT, the failures are cause for some concern. For this reason, the number of D/R cycles should be limited to two for the fatigue limit state when subsequent impacts are within 12 in. (305 mm) of the previous impact.

As discussed, there was significant scatter in the CVN data obtained from specimens subjected to damage, damage and repair, and only repair. Hence, it is not prudent to predict a percent increase or decrease in measured CVN energy absorption per D/R cycle. In general, there appears to be a decrease in CVN energy values in specimens subjected to multiple D/R cycles.

The above statements must not be taken out of context. The data obtained, in terms of fatigue resistance and CVN data, were from specimens where the damage was extremely severe and repeated in exactly the same location. This is highly unlikely for in-service bridges. A girder may be hit multiple times in the same general location, but that is less severe than that applied in this study. The recommendations are believed to be conservative for most in-service applications. An owner should take this into account when deciding whether to permit a repair after a third impact to ensure both economy and longevity.

Lastly, it is noted that at the point of impact, there is a relatively thin layer of cold-worked material with very low fracture toughness. In addition, there are multiple small cracks in this low-toughness material due to extreme strains and rolling or bunching of the material at the exact point of the impact. Brittle fractures were observed in the lab and in the field that initiated at one of these discontinuities. To prevent similar fracture on other specimens, a simple procedure was developed. After each impact and inspection, the area is ground smooth to remove any micro-cracks induced during the impact. This procedure could be considered a minimum level of repair to remove nicks, gouges, and the cold-worked regions susceptible to brittle fracture during subsequent impacts.

4.2 Restraining Force Evaluation

Based on results of the experimental and analytical studies on restraining forces, at the beginning of the repair process when localized damage has the most severe geometry, localized stresses around the impact produced by the horizontal jacking force can be significantly greater than calculated using simple Mc/I approach. As a result, local stresses in the member immediately adjacent to the impact can potentially be grossly under-predicted, leading to hairline fractures or even brittle pop-in fractures. However, after a review of fractures surfaces, material tests, strain measurements, and results of FE analysis, fractures are not simply the result of over-jacking.

To overcome this problem, a simple yet effective approach was developed. The method requires the strain ratio at localized damage and the horizontal restraining force be calculated using procedures in the FHWA manual. These restraining forces must be reduced to avoid potential fracture because they produce very high local stresses in the region of severe

local damage. Reducing the horizontal jacking force by 1% for every one unit of strain ratio seems to reduce the initial jack force to acceptable levels, thereby preventing brittle fracture. As localized damage is repaired and the strain ratio of localized damage is reduced, the horizontal restraining force can be increased accordingly. These guidelines were implemented during the later repairs conducted in this research, and no other hairline cracks or brittle fractures occurred. The method still provides for a reasonable repair time while minimizing the potential of brittle fracture.

4.3 Residual Damage Evaluation

Based on FE modeling, an equation that determines the increase in stress at residual damage in base metal (without the presence of sweep) of I-shaped beams was developed. This equation can guide engineers as well as heat-straightening contractors on the required flatness of the flange after heat-straightening. Although this research was not intended to predict SAF for large localized gouges, initial studies modeling substantial flange damage were verified with the SAF equation. A majority of the results over-predicted the SAF, especially around large lengths of damage, but the equation could quickly provide a preliminary analysis of the damaged member.

Although little laboratory test data is available to confirm the modeling, one case was used to verify the modeling as well as the SAF equation, and the SAF equation reasonably predicted this increase in stress with slight error. This error was conservative and usually less than 5%, so for the typical residual damage in a member, the SAF equation will yield a reasonable result. During the modeling of welded details, orientation of residual damage at welded details was found to affect SAF.

This research could be applied in practice to increase the confidence and accuracy of the inspector, engineer, and the heat-straightening contractor. Based on initial literature review, what was previously reported did not specifically address the issue of potential fatigue caused by residual damage in any listed tolerances. This research concluded that although a distinct tolerance cannot always be given, setting limits based on allowable SAF is reasonable. This process will better ensure that residual damage will not unacceptably increase fatigue stress and result in a fatigue failure.

4.4 Suggested Research

The following topics are recommended for further study:

- Research has shown that residual damage has a great influence on the local stresses adjacent to repaired details. This effect was studied in base metal away from welded attachments for various flange geometries and accounted for by SAF as part of another study (*7*). However, in that work the influence of sweep and the amplification of stress at details such as cover plates and stiffeners were not fully examined.
- A more important finding is related to bridges that are impacted, but not repaired. With sufficient study, an approach likely can be refined as part of a decision tool for owners to determine if repairs are needed. The effects of residual damage are a major outcome of this research, but one that was not initially included in the original scope. Hence, it was not fully studied due to budget constraints, but the research team feels it is an important area to continue to study. Some of the repaired specimens possess various levels of residual damage and will be available after this project is completed for further instrumenting and testing. Additional data is needed for accurate calibration of FE models to fully develop SAF. Damaging and fatigue testing additional specimens not repaired would better verify the method and conclusions.
- Using the FHWA manual methods to calculate stresses and the appropriate restraining forces in damaged girders can result in actual stresses much higher than anticipated. In some cases, this resulted in cracking in test specimens. The research demonstrated that reductions in jacking force of about 50% often are required to keep local stresses at acceptable levels where damage is severe. However, this estimate is based on limited data obtained by strain gaging and limited FE analysis and may be over-conservative in some cases while under-conservative in others. Although this research suggests the prescribed reduction will yield reasonable results, refinement of this estimate is needed.
- Material testing of base metal, damaged material, and repaired material will continue. However, considerable testing could be performed on the remaining material from this project, especially related to CVN to obtain a statistically significant amount of data. In addition, since most bridges that are struck are older and made from A7 or similar steels, data from these materials would be desirable. Obtaining such material from decommissioned bridges and subsequently damaging and repairing the girders would be an efficient source of material for testing.
- The testing has shown that grinding of the weld toe to remove microcracks and other discontinuities is essential to ensure a successful repair at these details. However, other details, such as complete joint penetration splices without a geometric weld toe, would be worthwhile to damage and repair to ensure the recommended procedures developed are applicable.

References

1. Connor, R. J., Kaufmann, E. J., and Urban, M. J. *NCHRP Project 10-63 Interim Report: Heat-Straightening Repair of Damaged Steel Bridge Girders: Fatigue and Fracture Performance.* National Cooperative Highway Research Program, Washington, D.C., 2004.
2. Avent, R. R., and Mukai, D. J. *Heat-Straightening Repairs of Damaged Steel Bridges.* FHWA Report IF-99-004, FHWA, U.S. Department of Transportation, Washington, D.C., October 1998.
3. Varma, A. H., and Kowalkowski K. J. *Effects of Multiple Damage-Heat Straightening Repairs on the Structural Properties of Bridge Steels.* MDOT Report RC-1456, Michigan Department of Transportation, 2004.
4. "The Shortening of Eyebars to Equalize the Stress." *Bulletin,* Vol. 48 No. 460, American Railway Engineering Association, Chicago, IL, 1946, pp. 1–18.
5. Wilson, W. M. "Fatigue Strength of Weldments Used to Reinforce and Repair Steel Bridge Members." *Bulletin,* Vol. 48 No. 460, American Railway Engineering Association, Chicago, IL, 1946, pp. 19–33.
6. Fisher, J. W., Frank, K. H., Hirt, M. A., and McNamee, B. M. "Effects of Weldments on the Fatigue Strength of Steel Beams." *NCHRP Report 102,* HRB, National Research Council, Washington, D.C., 1970.
7. Urban, M. J. *Effects of Residual Damage on the Fatigue Performance of Steel Bridge Girders.* Masters thesis, Lehigh University, Bethlehem, PA, 2005.

APPENDIX A

Drawings

A.1 Drop-Weight Machine

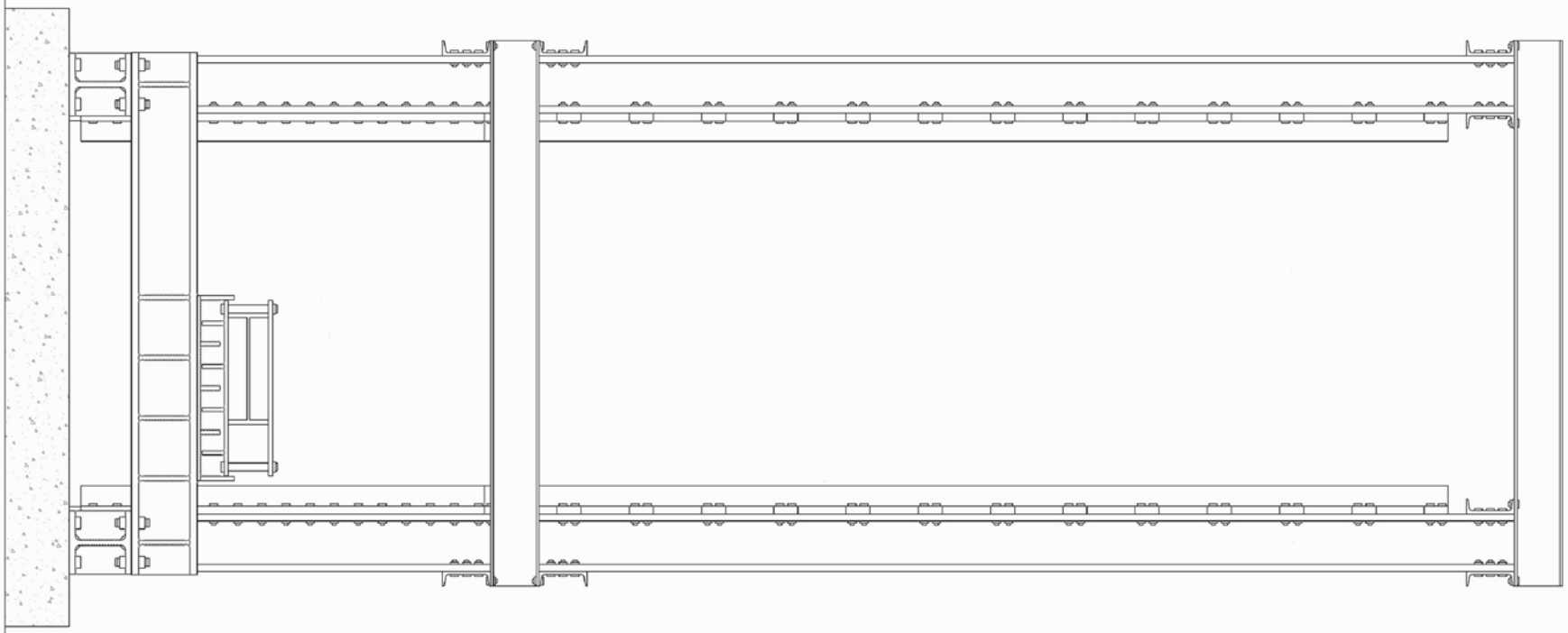

REV	DATE	DESCRIPTION	BY

ADVANCED TECHNOLOGY FOR LARGE STRUCTURAL SYSTEMS
117 ATLSS Drive
Lehigh University
Bethlehem, PA 18015
610-758-3500 FAX 610-758-5553

PROJECT: NCHRP 10-63	DESIGNED BY: MJU	SCALE: NOT TO SCALE
	DRAWN BY: MJU	PROJECT NO.: -
DRAWING TITLE: FULL VIEW	CHECKED BY: RJC	SHEET NO.: 1 OF 17
	DATE: 2/23/04	

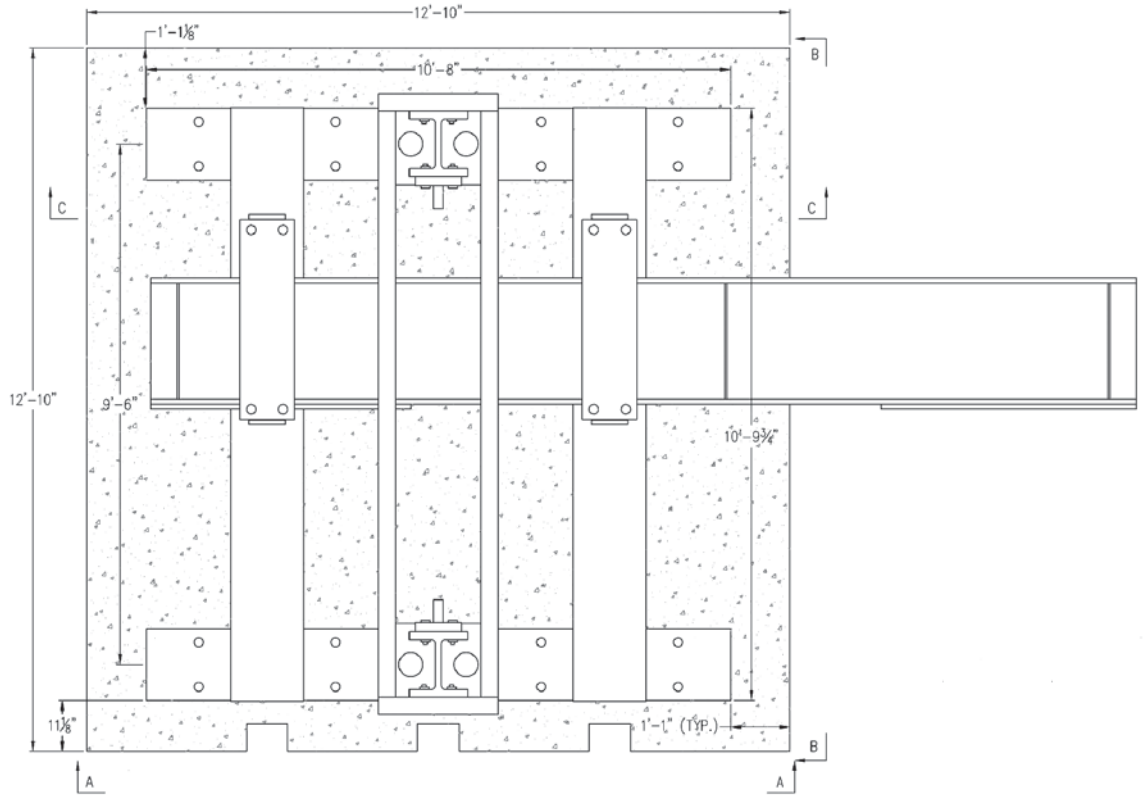

PLAN

REV	DATE	DESCRIPTION	BY

ADVANCED TECHNOLOGY FOR LARGE STRUCTURAL SYSTEMS
117 ATLSS Drive
Lehigh University
Bethlehem, PA 18015
610-758-3500 FAX 610-758-5553

PROJECT: NCHRP 10-63

DRAWING TITLE: DROP-WEIGHT MACHINE - PLAN

DESIGNED BY:	MJU
DRAWN BY:	MJU
CHECKED BY:	RJC
DATE:	2/23/04

SCALE: NOT TO SCALE
PROJECT NO.: -
SHEET NO.: 2 OF 17

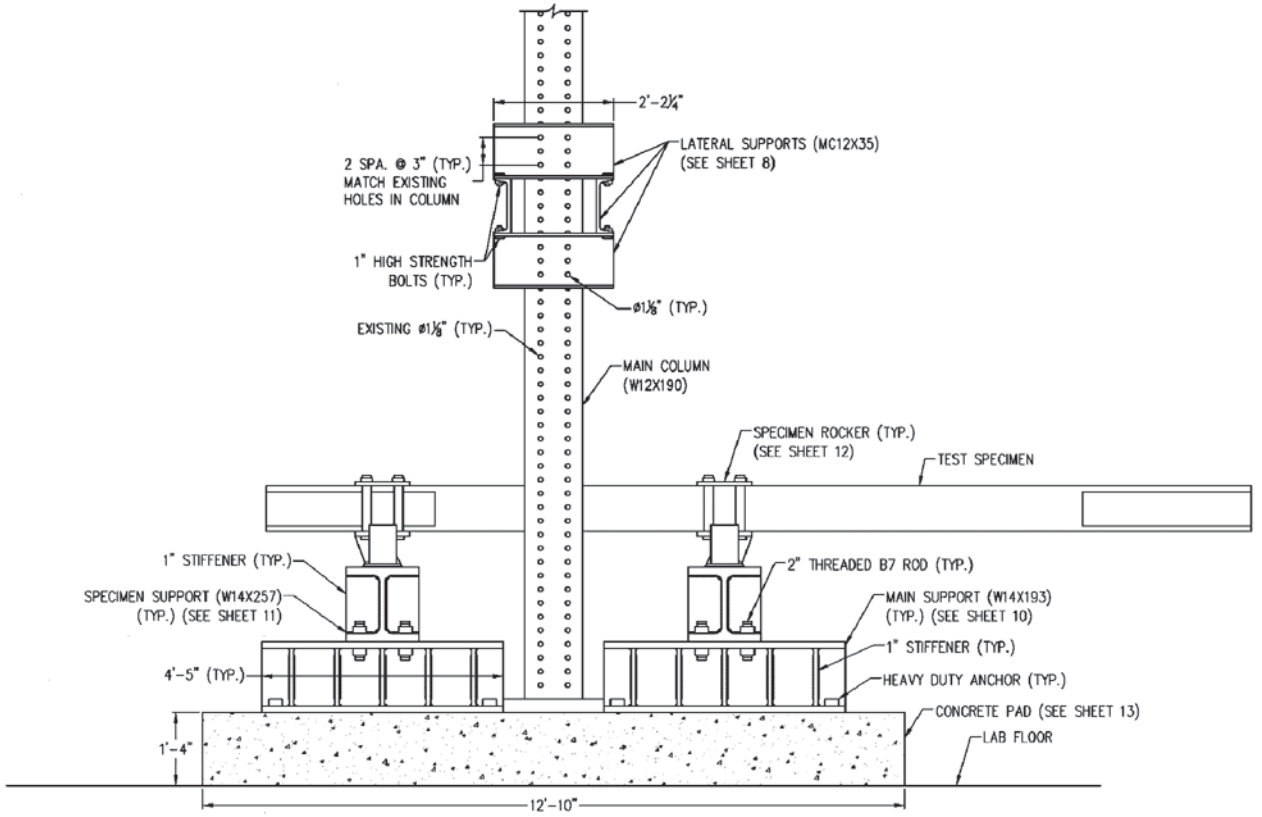

VIEW A-A

REV	DATE	DESCRIPTION	BY

ADVANCED TECHNOLOGY FOR LARGE STRUCTURAL SYSTEMS
117 ATLSS Drive
Lehigh University
Bethlehem, PA 18015
610-758-3500 FAX 610-758-5553

PROJECT: NCHRP 10-63

DRAWING TITLE: DROP-WEIGHT MACHINE - VIEW A-A

DESIGNED BY:	MJU	SCALE:	NOT TO SCALE
DRAWN BY:	MJU	PROJECT NO.:	-
CHECKED BY:	RJC	SHEET NO.:	3 OF 17
DATE:	2/23/04		

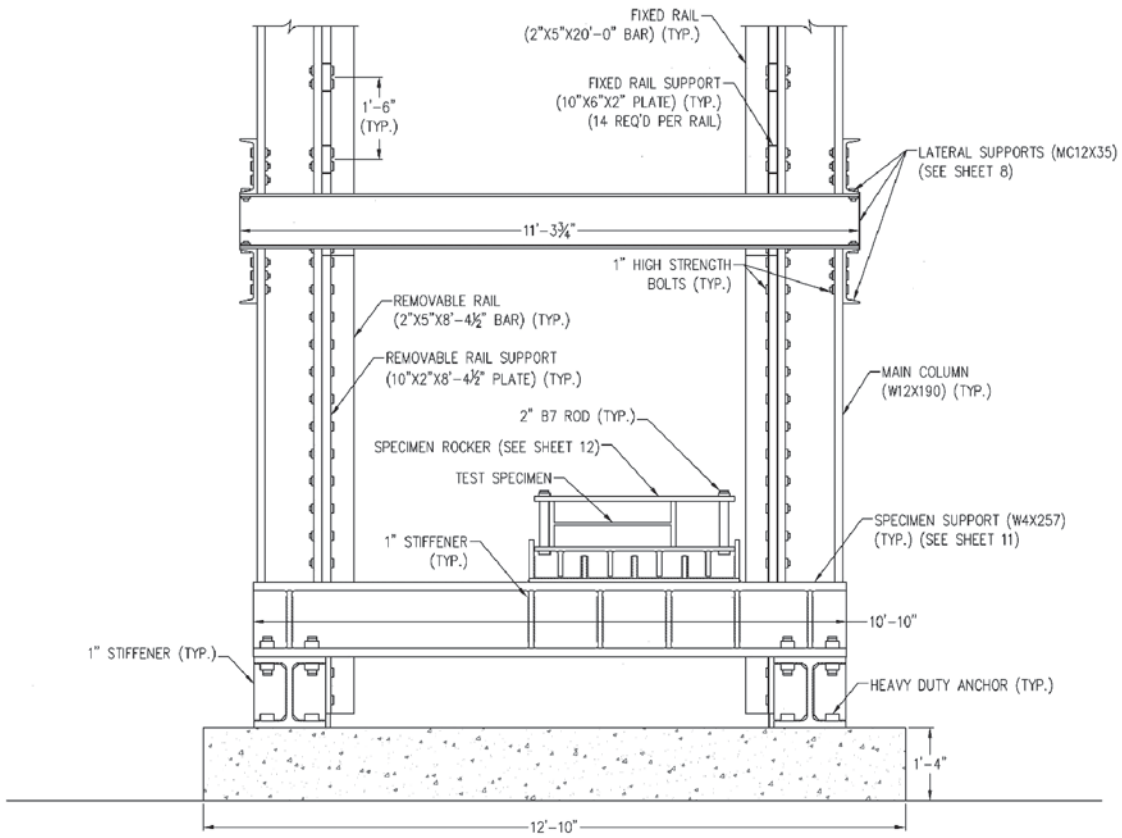

VIEW B–B

REV	DATE	DESCRIPTION	BY

ADVANCED TECHNOLOGY FOR
LARGE STRUCTURAL SYSTEMS
117 ATLSS Drive
Lehigh University
Bethlehem, PA 18015
610-758-3500 FAX 610-758-5553

PROJECT: NCHRP 10-63

DRAWING TITLE: DROP-WEIGTH MACHINE - VIEW B-B

DESIGNED BY:	MJU
DRAWN BY:	MJU
CHECKED BY:	RJC
DATE:	2/23/04

SCALE: NOT TO SCALE
PROJECT NO.: -
SHEET NO.: 4 OF 17

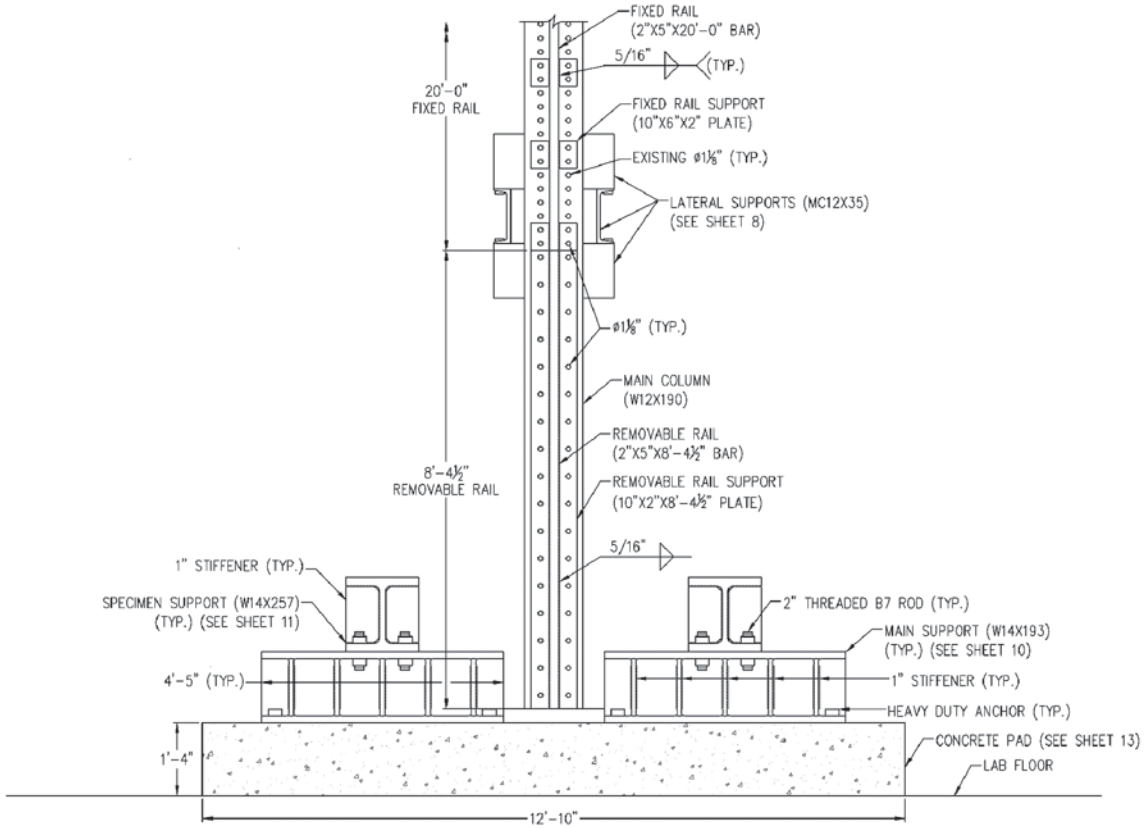

ELEVATION C-C

REV	DATE	DESCRIPTION	BY

ADVANCED TECHNOLOGY FOR LARGE STRUCTURAL SYSTEMS
117 ATLSS Drive
Lehigh University
Bethlehem, PA 18015
610-758-3500 FAX 610-758-5553

PROJECT: NCHRP 10-63

DRAWING TITLE: DROP-WEIGHT MACHINE - ELEVATION C-C

DESIGNED BY:	MJU	SCALE:	NOT TO SCALE
DRAWN BY:	MJU	PROJECT NO.:	-
CHECKED BY:	RJC	SHEET NO.:	5 OF 17
DATE:	2/23/04		

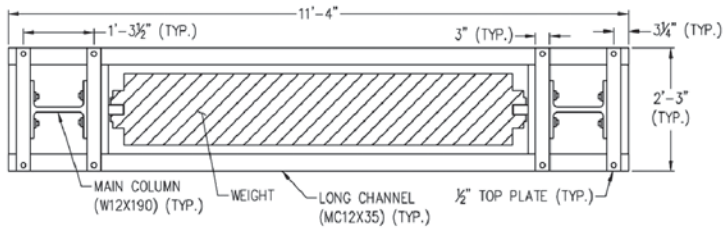

PLAN

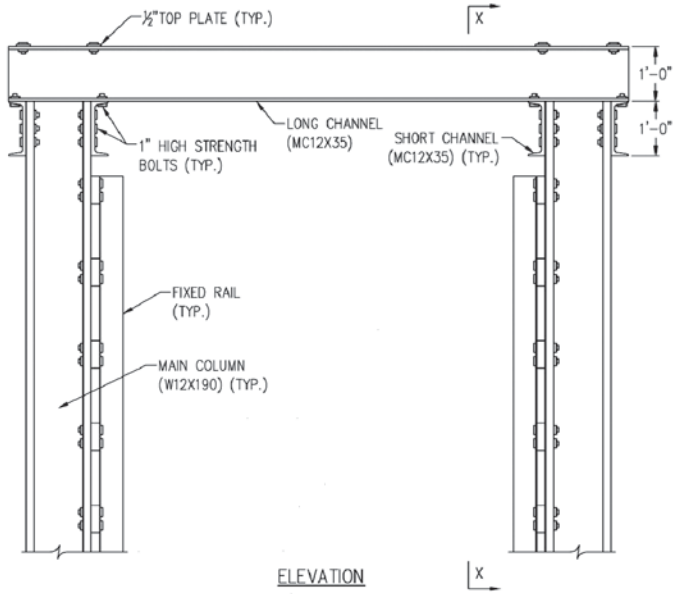

ELEVATION

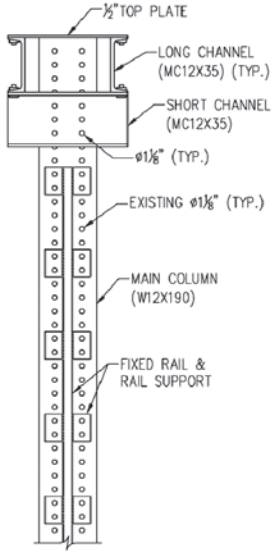

ELEVATION X–X

REV	DATE	DESCRIPTION	BY

ADVANCED TECHNOLOGY FOR LARGE STRUCTURAL SYSTEMS
117 ATLSS Drive
Lehigh University
Bethlehem, PA 18015
610-758-3500 FAX 610-758-5553

PROJECT: NCHRP 10-63

DRAWING TITLE: DROP-WEIGHT MACHINE - TOP SUPPORTS

DESIGNED BY:	MJU
DRAWN BY:	MJU
CHECKED BY:	RJC
DATE:	2/23/04

SCALE: NOT TO SCALE
PROJECT NO.: -
SHEET NO.: 6 OF 17

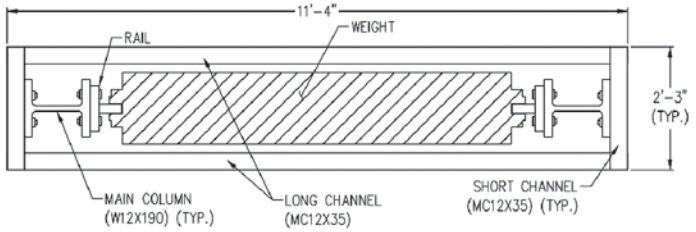

PLAN

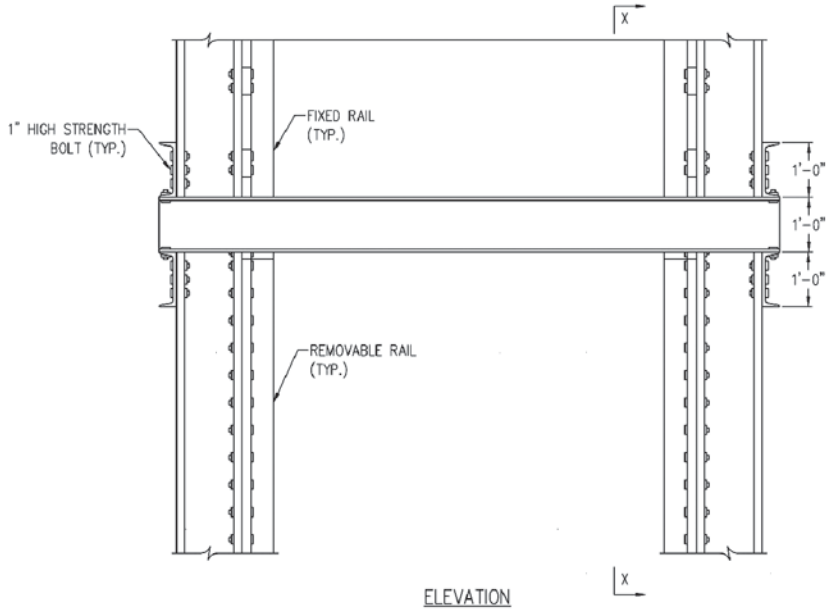

ELEVATION

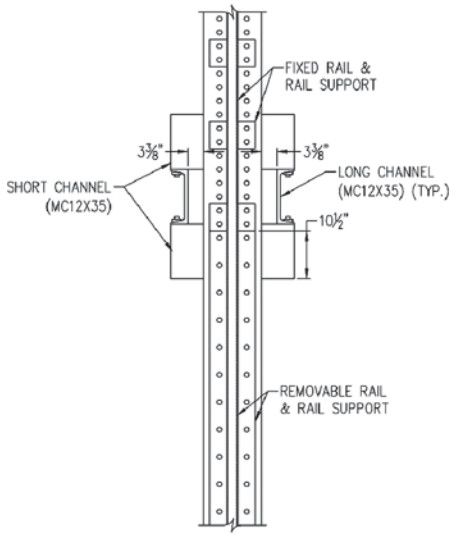

ELEVATION X–X

REV	DATE	DESCRIPTION	BY

ADVANCED TECHNOLOGY FOR LARGE STRUCTURAL SYSTEMS
117 ATLSS Drive
Lehigh University
Bethlehem, PA 18015
610-758-3500 FAX 610-758-5553

PROJECT: NCHRP 10-63

DRAWING TITLE: DROP-WEIGHT MACHINE - MIDDLE SUPPORTS

DESIGNED BY:	MJU
DRAWN BY:	MJU
CHECKED BY:	RJC
DATE:	2/23/04

SCALE: NOT TO SCALE
PROJECT NO.: -
SHEET NO.: 7 OF 17

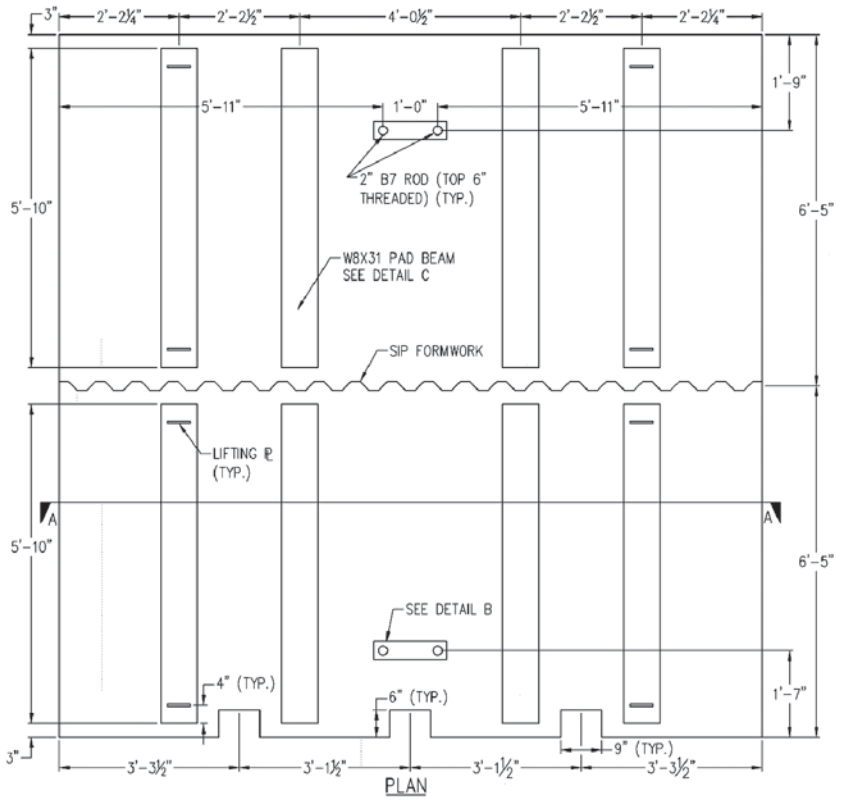

PLAN

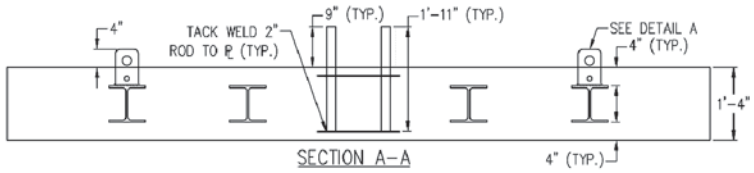

SECTION A–A

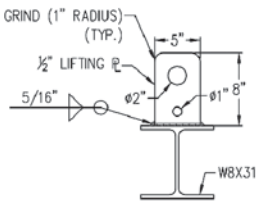

DETAIL A
(8 LIFTING ℄ REQ'D)

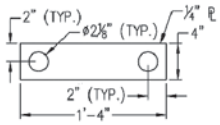

DETAIL B
(4 REQ'D)

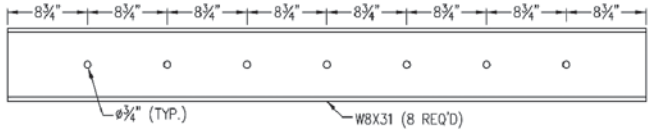

DETAIL C
(8 REQ'D)

REV	DATE	DESCRIPTION	BY

ADVANCED TECHNOLOGY FOR LARGE STRUCTURAL SYSTEMS
117 ATLSS Drive
Lehigh University
Bethlehem, PA 18015
610-758-3500 FAX 610-758-5553

PROJECT:	NCHRP 10-63	DESIGNED BY: MJU	SCALE: NOT TO SCALE
		DRAWN BY: MJU	PROJECT NO.: -
DRAWING TITLE:	CONCRETE PAD - DETAILS	CHECKED BY: RJC	SHEET NO.: 8 OF 17
		DATE: 2/23/04	

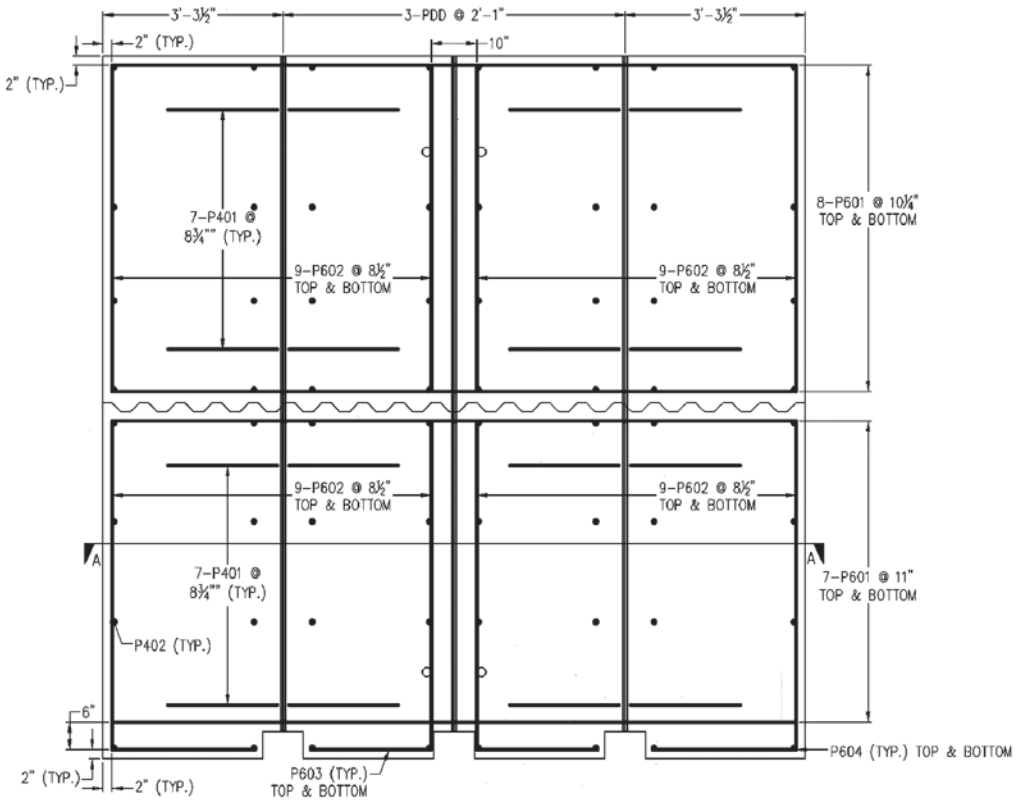

PLAN

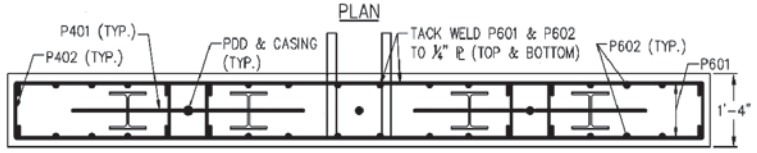

SECTION A-A

BAR SCHEDULE								
MARK	SIZE	NO REQ	LENGTH	TYPE	DIMENSIONS			REMARKS
					A	B	J	
P401	4	56	2'-0"	STR				
P402	4	64	2'-0"	1	2½"	12"	4"	
P601	6	30	12'-6"	STR				
P602	6	72	6'-0"	STR				
P603	6	4	2'-2½"	STR				
P604	6	4	2'-7"	STR				

① 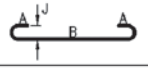

POST-TENSIONING SCHEDULE					
MARK	SIZE	NO REQ	LENGTH	TYPE	REMARKS
PDD	1"	3	14'-0"	STR	POST-TENSION TO 85 KIPS

REV	DATE	DESCRIPTION	BY

ADVANCED TECHNOLOGY FOR LARGE STRUCTURAL SYSTEMS
117 ATLSS Drive
Lehigh University
Bethlehem, PA 18015
610-758-3500 FAX 610-758-5553

PROJECT: NCHRP 10-63

DRAWING TITLE: CONCRETE PAD - REINFORCEMENT

DESIGNED BY:	MJU	SCALE:	NOT TO SCALE
DRAWN BY:	MJU	PROJECT NO.:	-
CHECKED BY:	RJC	SHEET NO.:	9 OF 17
DATE:	2/23/04		

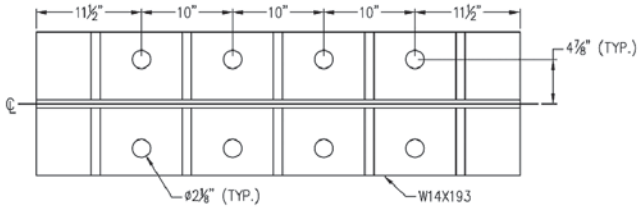

PLAN TOP FLANGE

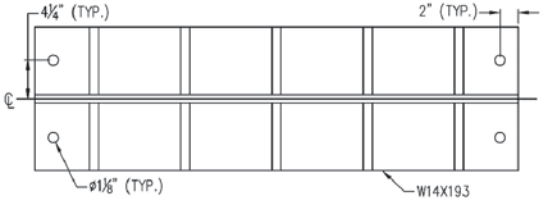

SECTION B–B

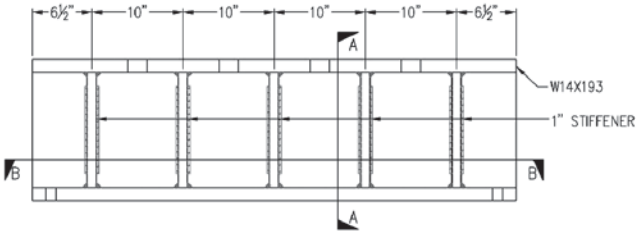

ELEVATION

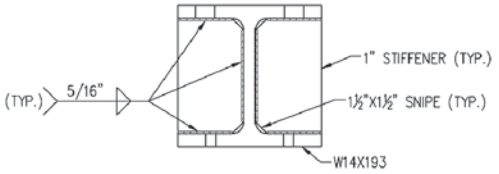

SECTION A–A

NOTES:
1. FOUR (4) MAIN SUPPPORTS REQUIRED.
2. 28'–0" W14X193 TO BE SUPPLIED BY LEHIGH UNIVERSITY.
3. COST ESTIMATE SHALL INCLUDE DELIVERY OF W14X193 FROM LEHIGH UNIVERSITY.
4. STIFFENERS SHALL BE OF GRADE 50 STEEL.

REV	DATE	DESCRIPTION	BY

ATLSS
ADVANCED TECHNOLOGY FOR LARGE STRUCTURAL SYSTEMS
117 ATLSS Drive
Lehigh University
Bethlehem, PA 18015
610-758-3500 FAX 610-758-5553

PROJECT: NCHRP 10-63

DRAWING TITLE: MAIN SUPPORTS - DETAILS

DESIGNED BY:	MJU
DRAWN BY:	MJU
CHECKED BY:	RJC
DATE:	2/23/04

SCALE: NOT TO SCALE
PROJECT NO.: -
SHEET NO.: 10 OF 17

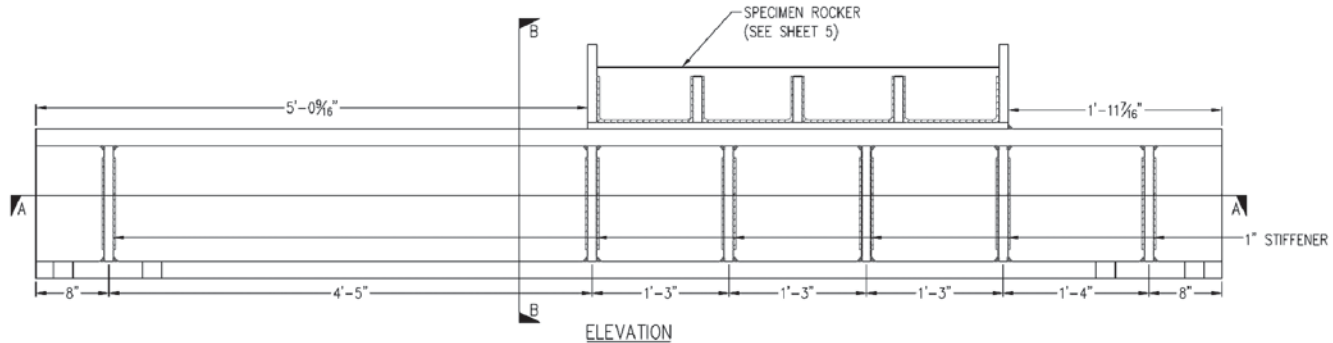

ELEVATION

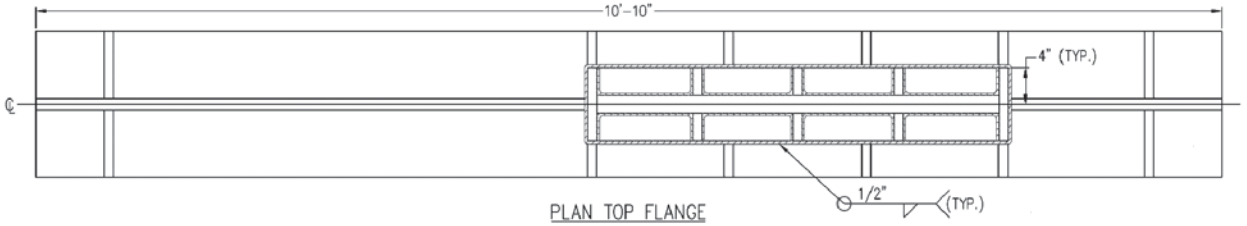

PLAN TOP FLANGE

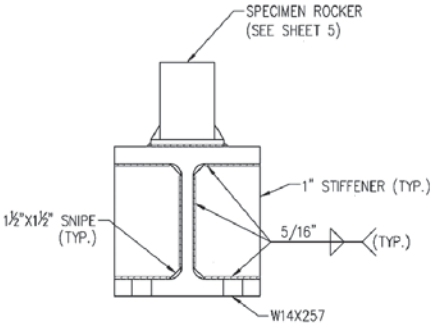

SECTION B–B

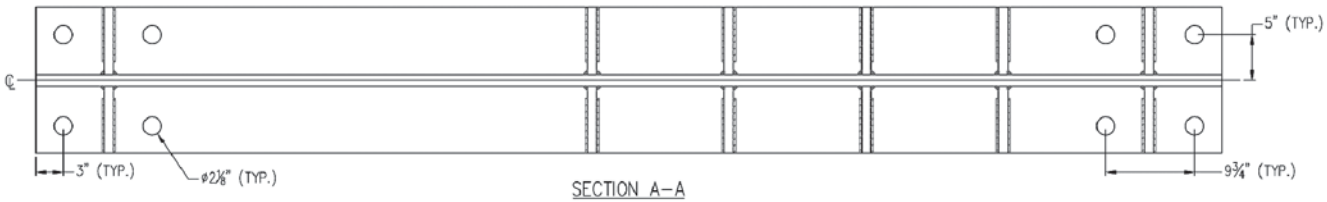

SECTION A–A

NOTES:
1. TWO (2) SPECIMEN SUPPPORTS REQUIRED
2. 1 – 15'–3" AND 1 – 11'–5" W14X257 TO BE SUPPLIED BY LEHIGH UNIVERSITY.
3. COST ESTIMATE SHALL INCLUDE DELIVERY OF W14X257 FROM LEHIGH UNIVERSITY.
4. STIFFENERS SHALL BE OF GRADE 50 STEEL.

REV	DATE	DESCRIPTION	BY

ADVANCED TECHNOLOGY FOR LARGE STRUCTURAL SYSTEMS
117 ATLSS Drive
Lehigh University
Bethlehem, PA 18015
610-758-3500 FAX 610-758-5553

PROJECT: NCHRP 10-63	DESIGNED BY: MJU	SCALE: NOT TO SCALE
	DRAWN BY: MJU	PROJECT NO.: -
DRAWING TITLE: SPECIMEN SUPPORTS - DETAILS	CHECKED BY: RJC	SHEET NO.: 11 OF 17
	DATE: 2/23/04	

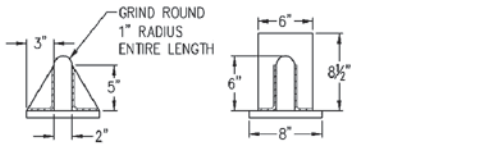

SECTION A–A SECTION B–B

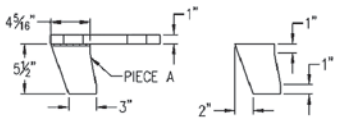

SECTION C–C DETAIL PIECE A

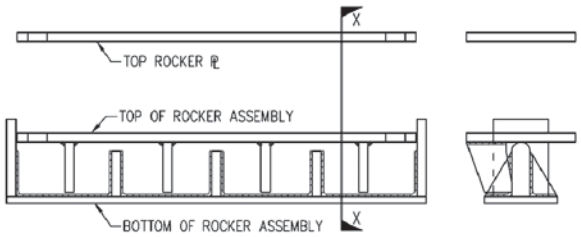

ELEVATION SECTION X–X

SPECIMEN ROCKER ASSEMBLY
(FOR INFORMATION ONLY)

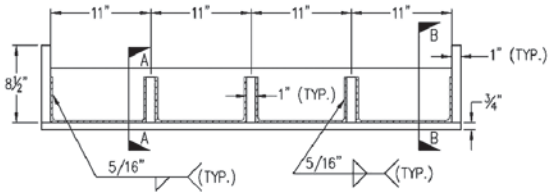

ELEVATION

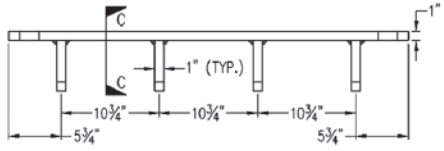

ELEVATION

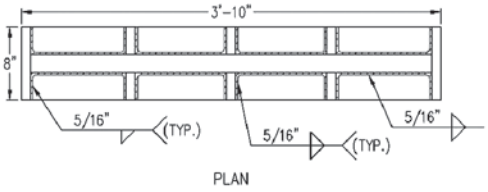

PLAN

BOTTOM OF ROCKER ASSEMBLY

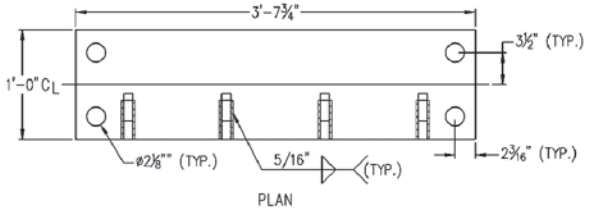

PLAN

TOP OF ROCKER ASSEMBLY

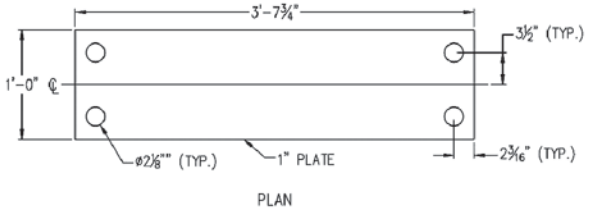

PLAN

TOP ROCKER PLATE

NOTES:
1. TWO (2) SPECIMEN ROCKERS REQUIRED
2. SPECIMEN ROCKERS SHALL BE MADE OF GRADE 50 STEEL.

REV	DATE	DESCRIPTION	BY

ATLSS
ADVANCED TECHNOLOGY FOR LARGE STRUCTURAL SYSTEMS
117 ATLSS Drive
Lehigh University
Bethlehem, PA 18015
610-758-3500 FAX 610-758-5553

PROJECT: NCHRP 10-63

DRAWING TITLE: SPECIMEN ROCKERS - DETAILS

DESIGNED BY:	MJU	SCALE:	NOT TO SCALE
DRAWN BY:	MJU	PROJECT NO.:	-
CHECKED BY:	RJC	SHEET NO.:	12 OF 17
DATE:	2/23/04		

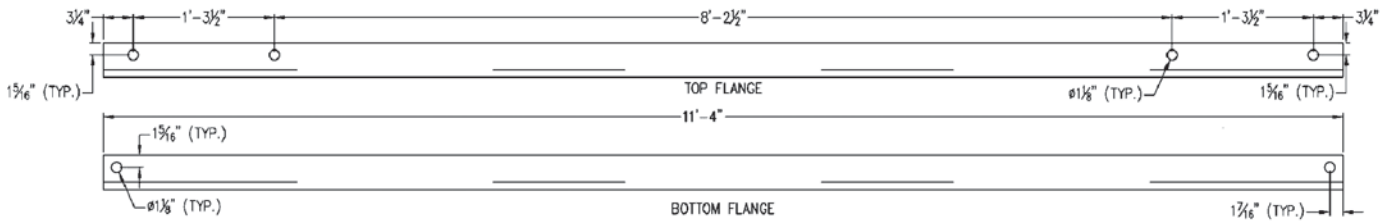

LONG CHANNEL (MC12X35)
(TYP. BOTH FLANGES) – (TWO REQUIRED)

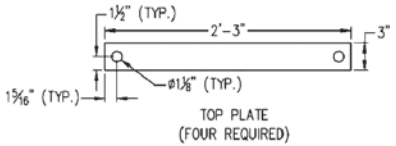

TOP PLATE
(FOUR REQUIRED)

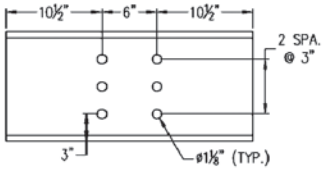

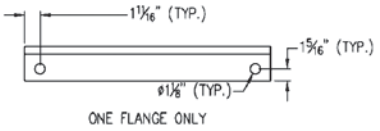

ONE FLANGE ONLY

SHORT CHANNEL (MC12X35)
(FOUR REQUIRED)

TOP SUPPORTS DETAILS

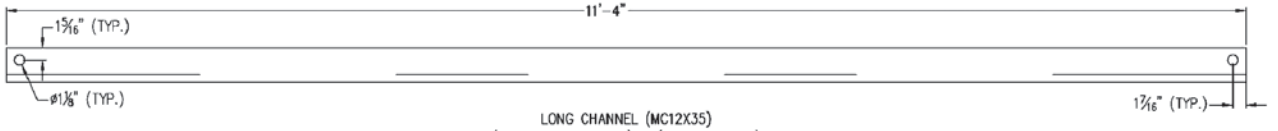

LONG CHANNEL (MC12X35)
(TYP. BOTH FLANGES) – (TWO REQUIRED)

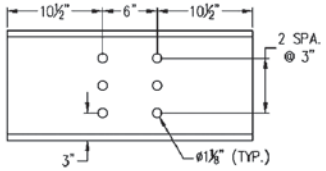

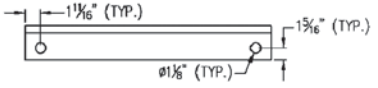

ONE FLANGE ONLY

SHORT CHANNEL (MC12X35)
(FOUR REQUIRED)

MIDDLE SUPPORT DETAILS

NOTES:
1. CHANNELS SHALL BE MADE OF GRADE 50 STEEL.

REV	DATE	DESCRIPTION	BY

ADVANCED TECHNOLOGY FOR LARGE STRUCTURAL SYSTEMS
117 ATLSS Drive
Lehigh University
Bethlehem, PA 18015
610-758-3500 FAX 610-758-5553

PROJECT: NCHRP 10-63

DRAWING TITLE: TOP & MIDDLE LATERAL SUPPORTS - DETAILS

DESIGNED BY:	MJU	SCALE:	NOT TO SCALE
DRAWN BY:	MJU	PROJECT NO.:	-
CHECKED BY:	RJC	SHEET NO.:	13 OF 17
DATE:	2/23/04		

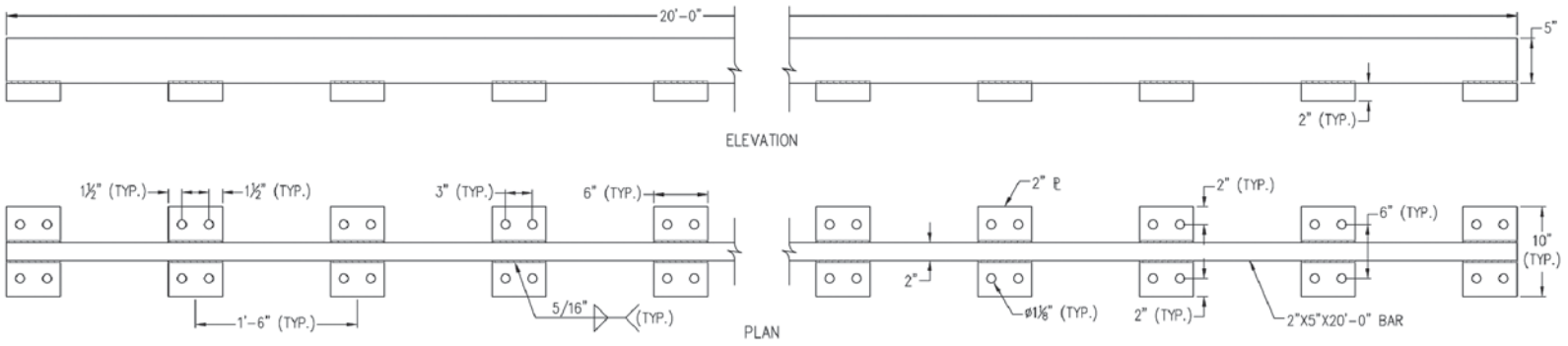

FIXED RAIL
(TWO REQUIRED)

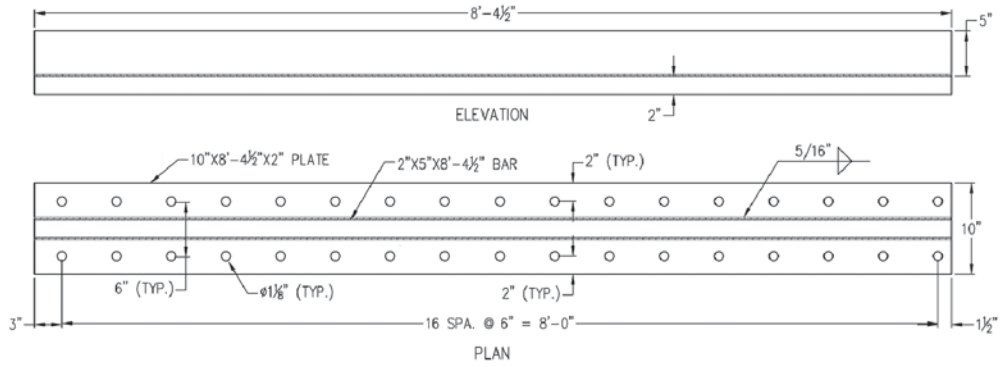

REMOVABLE RAIL
(TWO REQUIRED)

NOTES:
1. RAILS SHALL BE MADE OF GRADE 50 STEEL.
2. CAMBER AND SWEEP SHALL BE EQUAL TO OR LESS THAN ⅛" OVER ENTIRE LENGTH.

REV	DATE	DESCRIPTION	BY

ATLSS
ADVANCED TECHNOLOGY FOR LARGE STRUCTURAL SYSTEMS
117 ATLSS Drive
Lehigh University
Bethlehem, PA 18015
610-758-3500 FAX 610-758-5553

PROJECT:	NCHRP 10-63	DESIGNED BY: MJU	SCALE: NOT TO SCALE
		DRAWN BY: MJU	PROJECT NO.: -
DRAWING TITLE:	RAIL - DETAILS	CHECKED BY: RJC	SHEET NO.: 14 OF 17
		DATE: 2/23/04	

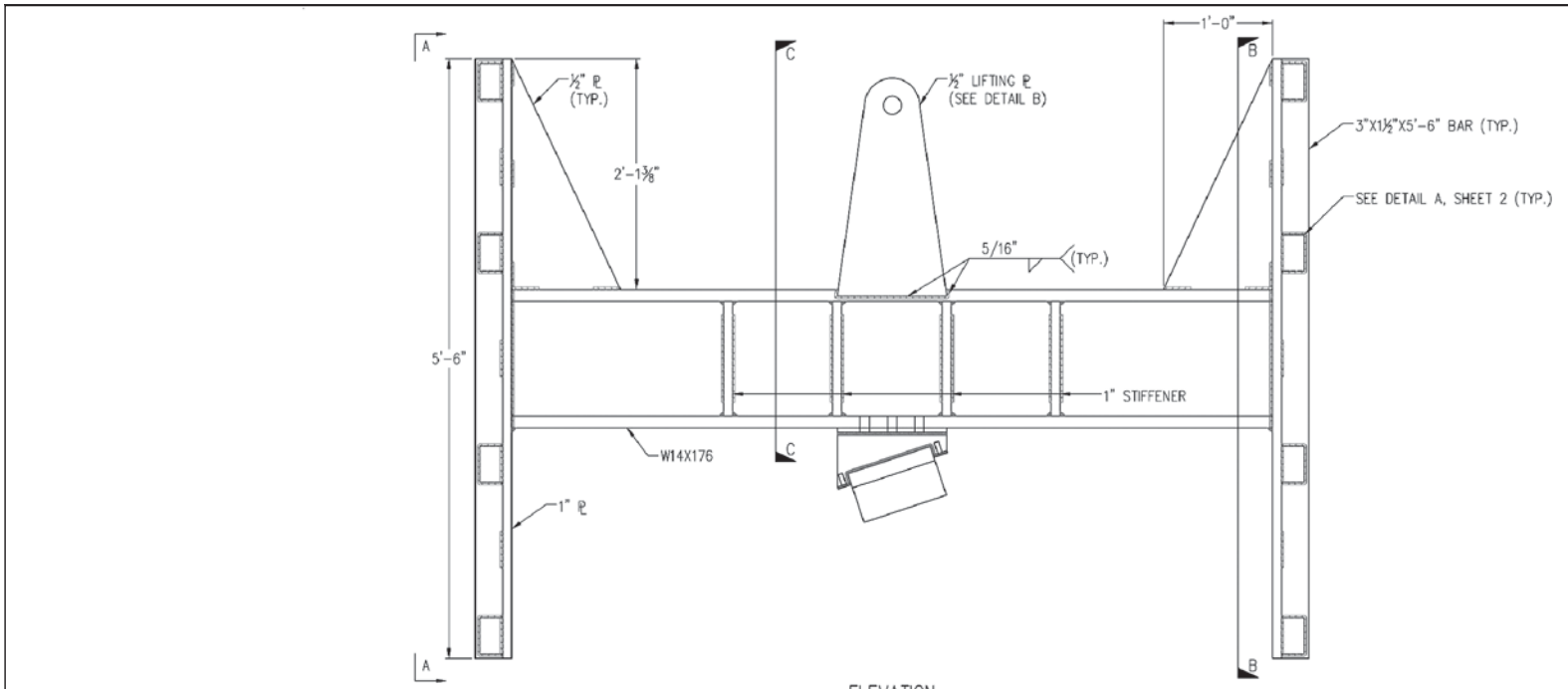

ELEVATION

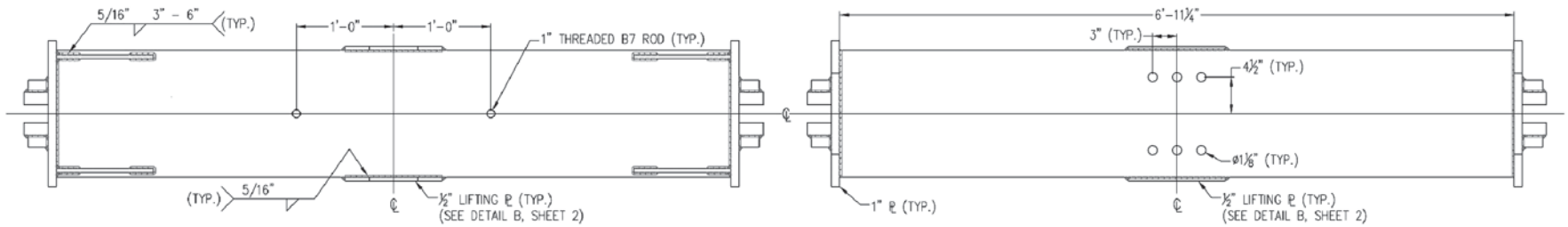

TOP VIEW

BOTTOM VIEW

REV	DATE	DESCRIPTION	BY

ADVANCED TECHNOLOGY FOR LARGE STRUCTURAL SYSTEMS
117 ATLSS Drive
Lehigh University
Bethlehem, PA 18015
610-758-3500 FAX 610-758-5553

PROJECT:	NCHRP 10-63	DESIGNED BY: MJU	SCALE: NOT TO SCALE
		DRAWN BY: MJU	PROJECT NO.: -
DRAWING TITLE:	WEIGHT - DETAILS 1	CHECKED BY: RJC	SHEET NO.: 15 OF 17
		DATE: 2/23/04	

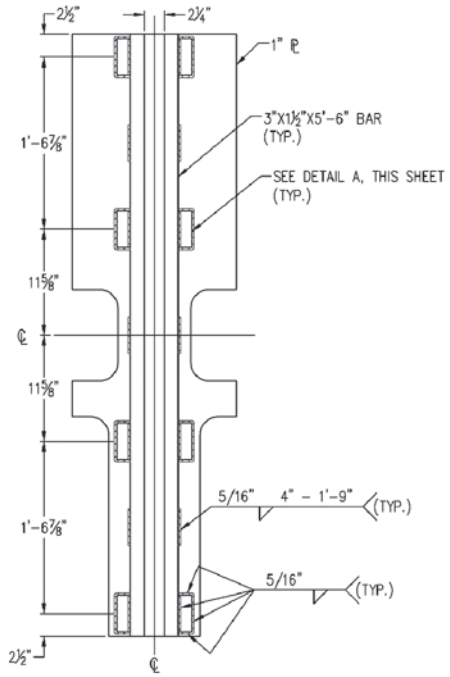

ELEVATION A–A

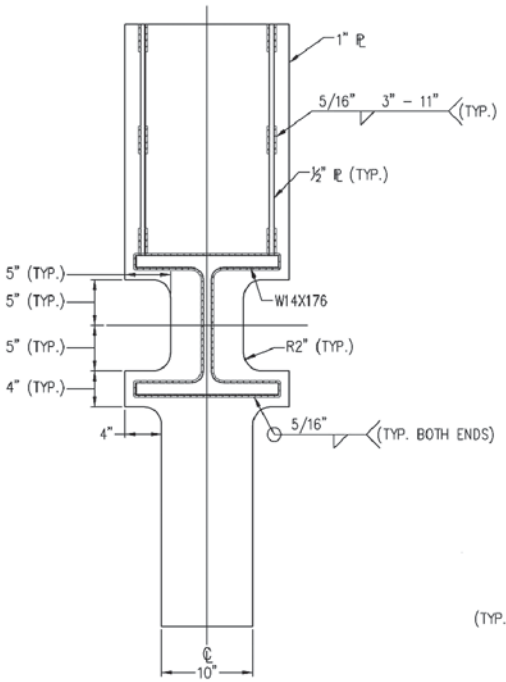

SECTION B–B

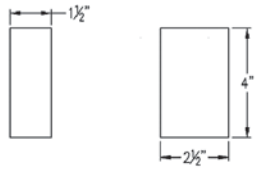

DETAIL A

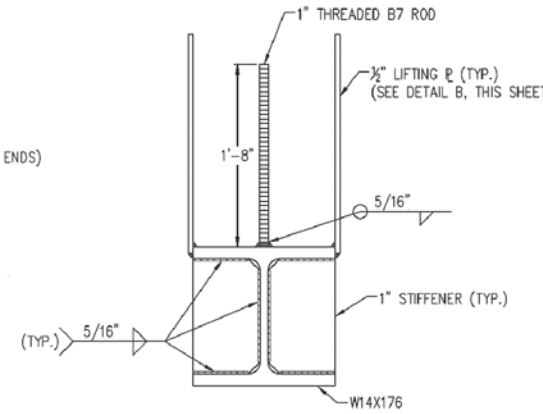

SECTION C–C

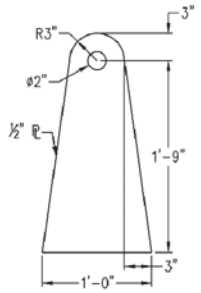

DETAIL B

NOTES:
1. ONE (1) WEIGHT REQUIRED
2. 19'-6" W14X176 TO BE SUPPLIED BY LEHIGH UNIVERSITY.
3. COST ESTIMATE SHALL INCLUDE DELIVERY OF W14X176 FROM LEHIGH UNIVERSITY.
4. PLATES, STIFFENERS AND BARS SHALL BE OF GRADE 50 STEEL.

REV	DATE	DESCRIPTION	BY

ATLSS
ADVANCED TECHNOLOGY FOR LARGE STRUCTURAL SYSTEMS
117 ATLSS Drive
Lehigh University
Bethlehem, PA 18015
610-758-3500 FAX 610-758-5553

PROJECT: NCHRP 10-63

DRAWING TITLE: WEIGHT - DETAILS 2

DESIGNED BY:	MJU	SCALE:	NOT TO SCALE
DRAWN BY:	MJU	PROJECT NO.:	-
CHECKED BY:	RJC	SHEET NO.:	16 OF 17
DATE:	2/23/04		

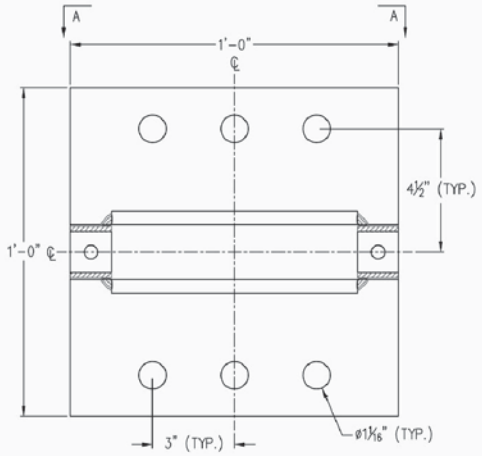

PLAN

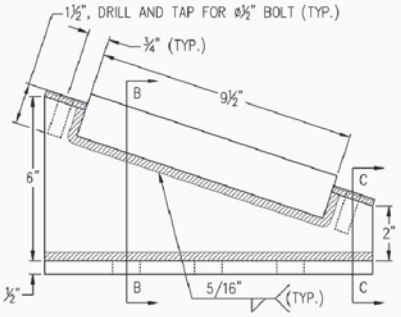

VIEW A–A

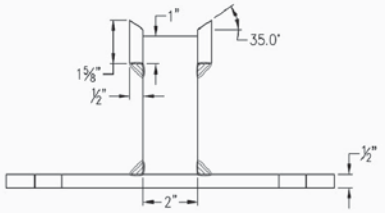

SECTION B–B

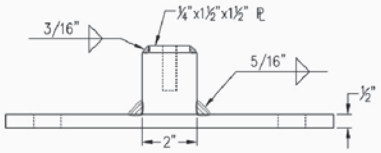

SECTION C–C

REV	DATE	DESCRIPTION	BY

ADVANCED TECHNOLOGY FOR LARGE STRUCTURAL SYSTEMS
117 ATLSS Drive
Lehigh University
Bethlehem, PA 18015
610-758-3500 FAX 610-758-5553

PROJECT:	NCHRP 10-63	DESIGNED BY: MJU	SCALE: NOT TO SCALE
		DRAWN BY: MJU	PROJECT NO.: -
DRAWING TITLE:	TUP - DETAILS	CHECKED BY: RJC	SHEET NO.: 17 OF 17
		DATE: 5/12/04	

A.2 Specimen Gage Plans

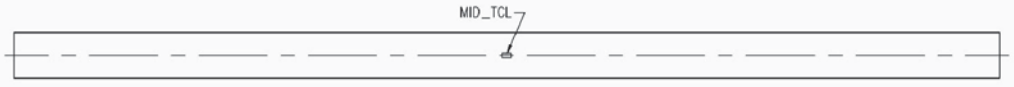

PLAN
(TOP FLANGE)
1/2" = 1'-0"

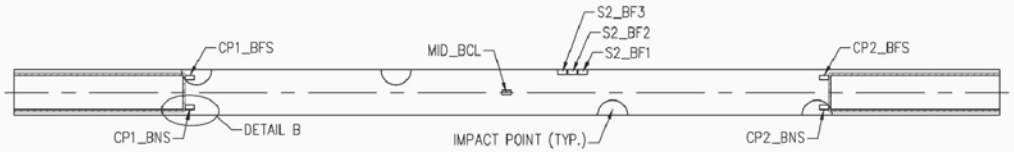

PLAN
(BOTTOM FLANGE)
1/2" = 1'-0"

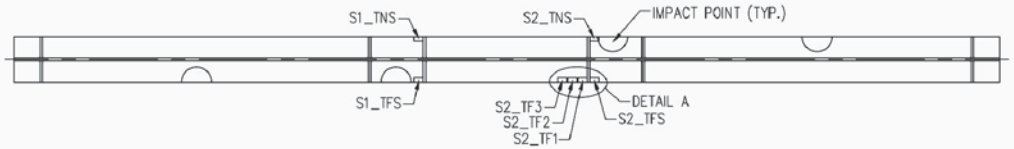

PLAN
(SECTION THROUGH WEB – LOOKING AT BOTTOM FLANGE)
1/2" = 1'-0"

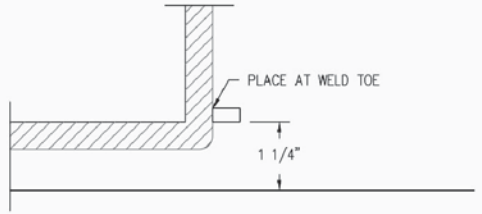

DETAIL A
6" = 1'-0"

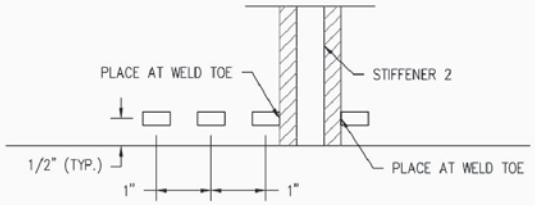

DETAIL B
6" = 1'-0"

NOTES:
1. STRAIN GAGE: CEA-06-250UW-350

REV	DATE	DESCRIPTION	BY

ADVANCED TECHNOLOGY FOR LARGE STRUCTURAL SYSTEMS
117 ATLSS Drive
Lehigh University
Bethlehem, PA 18015
610-758-3500 FAX 610-758-5553

PROJECT: NCHRP 10-63

DRAWING TITLE: SPECIMEN 1D/R-1 - GAGE PLAN

DESIGNED BY:	MJU	SCALE:	AS SHOWN
DRAWN BY:	MJU	PROJECT NO.:	540438
CHECKED BY:	RJC	SHEET NO.:	1 OF 1
DATE:	1/7/05		

PLAN
(TOP FLANGE)

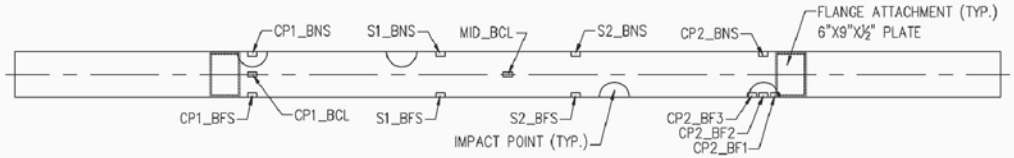

PLAN
(BOTTOM FLANGE)

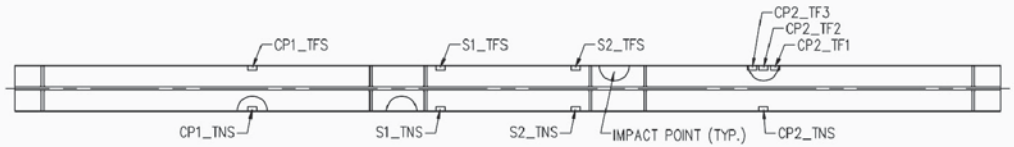

PLAN
(SECTION THROUGH WEB – LOOKING AT BOTTOM FLANGE)

NOTES:
1. STRAIN GAGE: CEA-06-250UW-350

REV	DATE	DESCRIPTION	BY

ATLSS
ADVANCED TECHNOLOGY FOR LARGE STRUCTURAL SYSTEMS
117 ATLSS Drive
Lehigh University
Bethlehem, PA 18015
610-758-3500 FAX 610-758-5553

PROJECT: NCHRP 10-63

DRAWING TITLE: SPECIMEN 1D/R-2 - GAGE PLAN

DESIGNED BY:	MJU
DRAWN BY:	MJU
CHECKED BY:	RJC
DATE:	12/3/04
SCALE:	½" = 1'-0"
PROJECT NO.:	540438
SHEET NO.:	1 OF 1

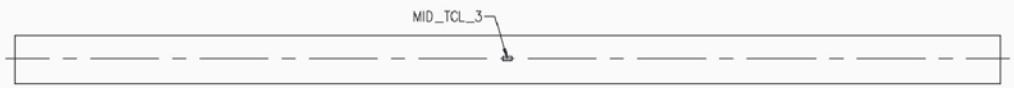

PLAN
(TOP FLANGE)
1/2" = 1'-0"

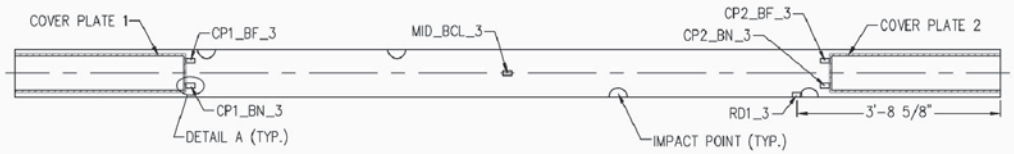

PLAN
(BOTTOM FLANGE)
1/2" = 1'-0"

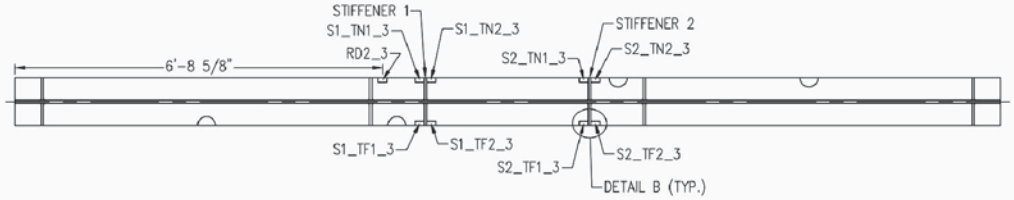

PLAN
(SECTION THROUGH WEB - LOOKING AT BOTTOM FLANGE)
1/2" = 1'-0"

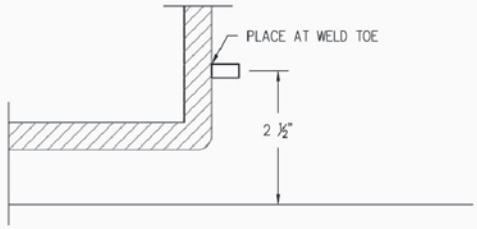

DETAIL A
6" = 1'-0"

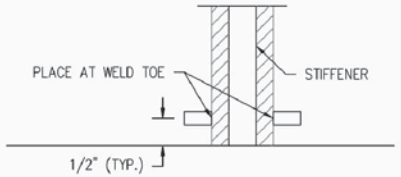

DETAIL B
6" = 1'-0"

REV	DATE	DESCRIPTION	BY

ADVANCED TECHNOLOGY FOR LARGE STRUCTURAL SYSTEMS
117 ATLSS Drive
Lehigh University
Bethlehem, PA 18015
610-758-3500 FAX 610-758-5553

PROJECT: NCHRP 10-63

DRAWING TITLE: SPECIMEN 2D/R-1 - GAGE PLAN

DESIGNED BY:	MJU	SCALE:	AS SHOWN
DRAWN BY:	MJU	PROJECT NO.:	540438
CHECKED BY:	RJC	SHEET NO.:	1 OF 1
DATE:	6/20/05		

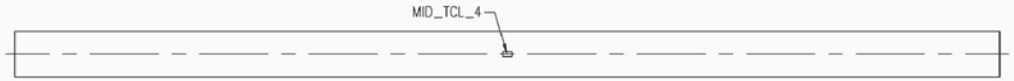

PLAN
(TOP FLANGE)
1/2" = 1'-0"

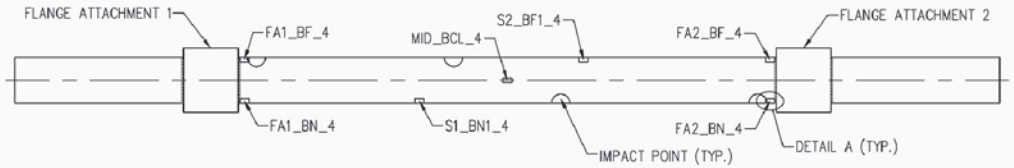

PLAN
(BOTTOM FLANGE)
1/2" = 1'-0"

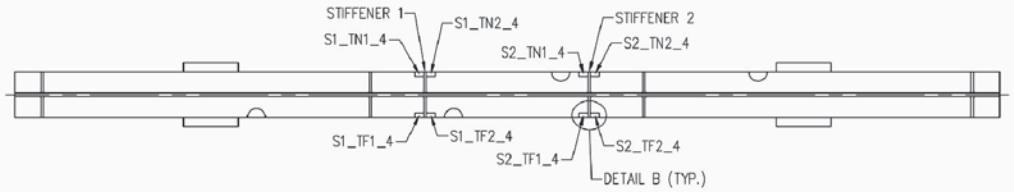

PLAN
(SECTION THROUGH WEB – LOOKING AT BOTTOM FLANGE)
1/2" = 1'-0"

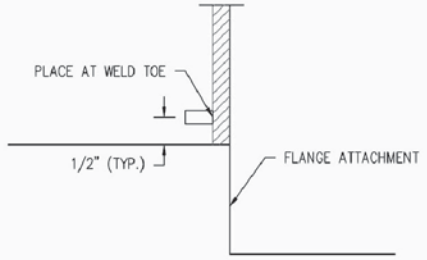

DETAIL A
6" = 1'-0"

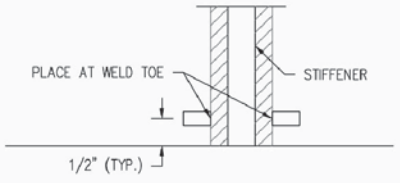

DETAIL B
6" = 1'-0"

REV	DATE	DESCRIPTION	BY

ADVANCED TECHNOLOGY FOR LARGE STRUCTURAL SYSTEMS
117 ATLSS Drive
Lehigh University
Bethlehem, PA 18015
610-758-3500 FAX 610-758-5553

PROJECT: NCHRP 10-63

DRAWING TITLE: SPECIMEN 2D/R-2 - GAGE PLAN

DESIGNED BY:	MJU
DRAWN BY:	MJU
CHECKED BY:	RJC
DATE:	6/8/05
SCALE:	AS SHOWN
PROJECT NO.:	540438
SHEET NO.:	1 OF 1

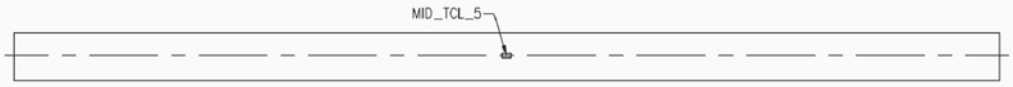

PLAN
(TOP FLANGE)
1/2" = 1'-0"

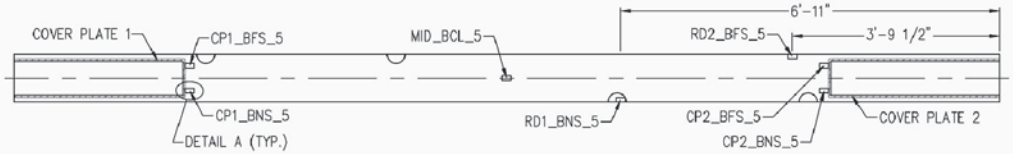

PLAN
(BOTTOM FLANGE)
1/2" = 1'-0"

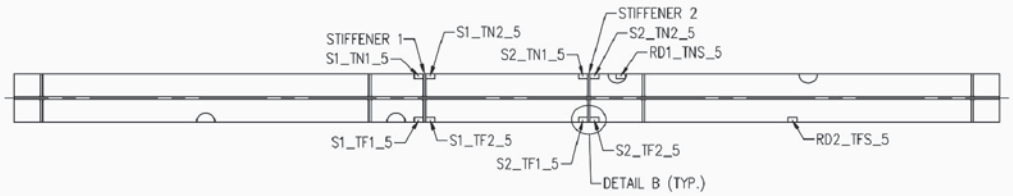

PLAN
(SECTION THROUGH WEB – LOOKING AT BOTTOM FLANGE)
1/2" = 1'-0"

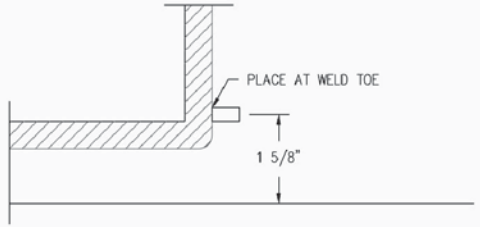

DETAIL A
6" = 1'-0"

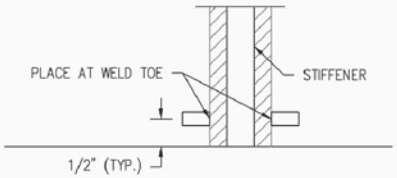

DETAIL B
6" = 1'-0"

REV	DATE	DESCRIPTION	BY

ATLSS
ADVANCED TECHNOLOGY FOR LARGE STRUCTURAL SYSTEMS
117 ATLSS Drive
Lehigh University
Bethlehem, PA 18015
610-758-3500 FAX 610-758-5553

PROJECT: NCHRP 10-63

DRAWING TITLE: SPECIMEN 2D/R-3 - GAGE PLAN

DESIGNED BY:	MJU
DRAWN BY:	MJU
CHECKED BY:	RJC
DATE:	10/13/05
SCALE:	AS SHOWN
PROJECT NO.:	540438
SHEET NO.:	1 OF 1

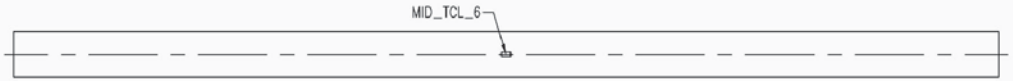

PLAN
(TOP FLANGE)

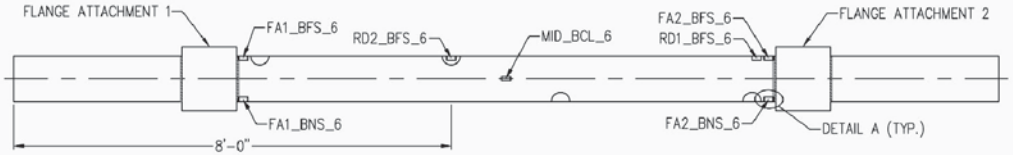

PLAN
(BOTTOM FLANGE)
1/2" = 1'-0"

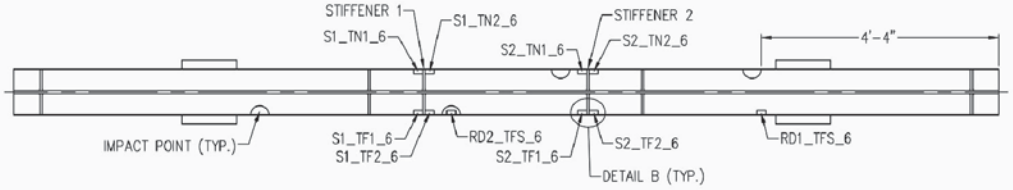

PLAN
(SECTION THROUGH WEB – LOOKING AT BOTTOM FLANGE)
1/2" = 1'-0"

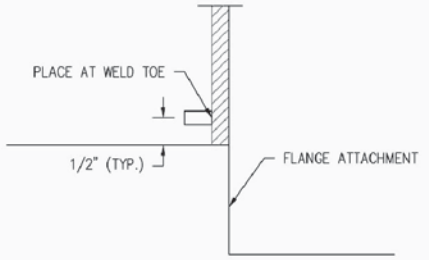

DETAIL A
6" = 1'-0"

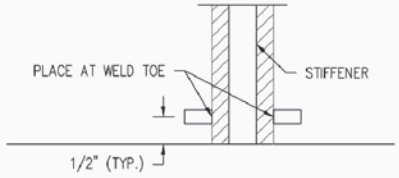

DETAIL B
6" = 1'-0"

REV	DATE	DESCRIPTION	BY

ADVANCED TECHNOLOGY FOR LARGE STRUCTURAL SYSTEMS
117 ATLSS Drive
Lehigh University
Bethlehem, PA 18015
610-758-3500 FAX 610-758-5553

PROJECT: NCHRP 10-63

DRAWING TITLE: SPECIMEN 2D/R-4 - GAGE PLAN

DESIGNED BY:	MJU
DRAWN BY:	MJU
CHECKED BY:	RJC
DATE:	11/18/05
SCALE:	AS SHOWN
PROJECT NO.:	540438
SHEET NO.:	1 OF 1

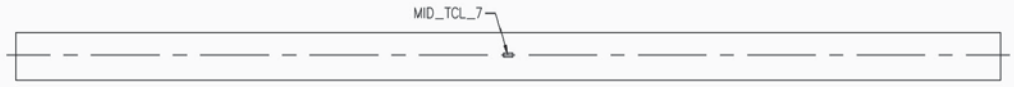

PLAN
(TOP FLANGE)
1/2" = 1'-0"

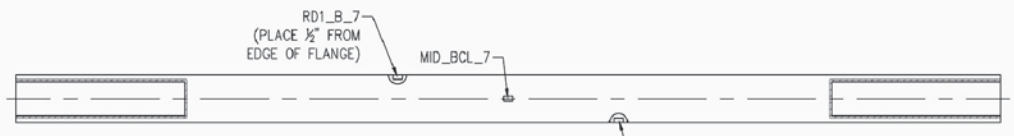

PLAN
(BOTTOM FLANGE)
1/2" = 1'-0"

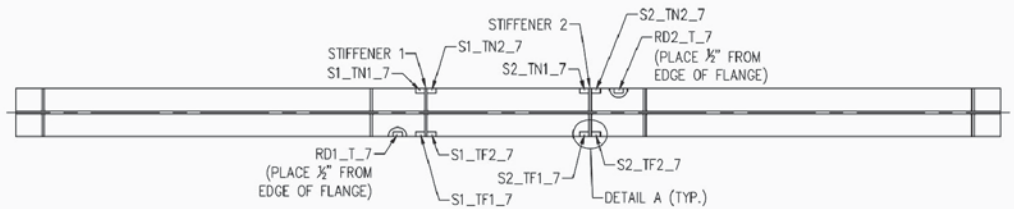

PLAN
(SECTION THROUGH WEB – LOOKING AT BOTTOM FLANGE)
1/2" = 1'-0"

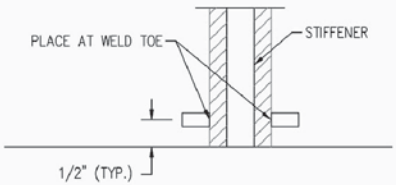

DETAIL A
6" = 1'-0"

NOTES:
1. STRAIN GAGE: CEA-06-250UW-350

REV	DATE	DESCRIPTION	BY

ADVANCED TECHNOLOGY FOR LARGE STRUCTURAL SYSTEMS
117 ATLSS Drive
Lehigh University
Bethlehem, PA 18015
610-758-3500 FAX 610-758-5553

PROJECT: NCHRP 10-63	DESIGNED BY: MJU	SCALE: AS SHOWN
	DRAWN BY: MJU	PROJECT NO.: 540438
DRAWING TITLE: SPECIMEN 3D/R-1 - GAGE PLAN	CHECKED BY: RJC	SHEET NO.: 1 OF 1
	DATE: 4/26/06	

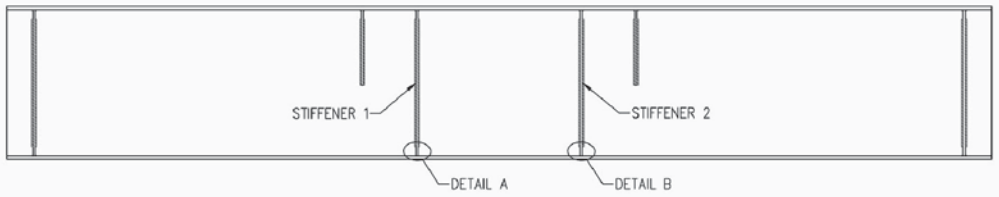

ELEVATION
(SCALE: 1/2" = 1'-0")

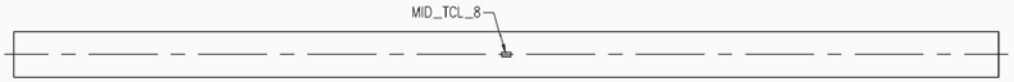

PLAN
(TOP FLANGE)
(SCALE: 1/2" = 1'-0")

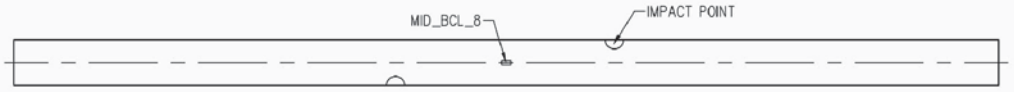

PLAN
(BOTTOM FLANGE)
(SCALE: 1/2" = 1'-0")

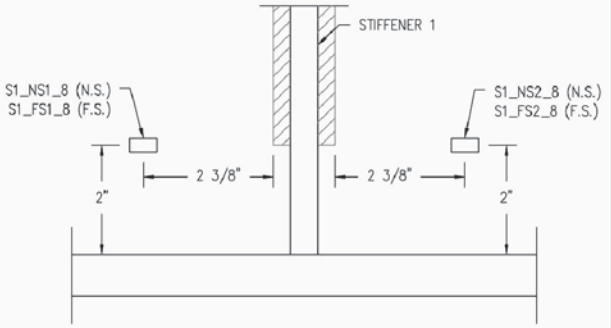

DETAIL A
6" = 1'-0"

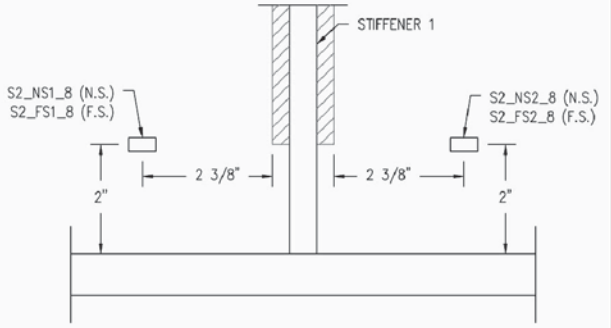

DETAIL B
6" = 1'-0"

NOTES:
1. STRAIN GAGE: CEA-06-250UW-350

REV	DATE	DESCRIPTION	BY

ADVANCED TECHNOLOGY FOR LARGE STRUCTURAL SYSTEMS
117 ATLSS Drive
Lehigh University
Bethlehem, PA 18015
610-758-3500 FAX 610-758-5553

PROJECT: NCHRP 10-63

DRAWING TITLE: SPECIMEN 3D/R-2 - GAGE PLAN

DESIGNED BY:	MJU
DRAWN BY:	MJU
CHECKED BY:	RJC
DATE:	3/17/06
SCALE:	AS SHOWN
PROJECT NO.:	540438
SHEET NO.:	1 OF 1

APPENDIX B

Fatigue Test Results

B.1 One Damage/Repair Cycle

Table B-1. One damage/repair fatigue test results.

Specimen	Detail	Stress Range	Cycles	Result	Notes
1D/R-1	Transverse Stiffener 1	16.26	2242433	Failure	Impact side of stiffener, opposite side web. Crack - 90% of flange and 6" into web.
		13.33	2242433	Runout	Impact. Weld toe ground smooth slightly ~ 1/16".
	Transverse Stiffener 2	16.57	2242433	Runout	Impact. Repair weld ground smooth.
		11.40	2242433	Runout	Impact side of stiffener, opposite side of web.
		13.25	2242433	Runout	Impact opposite side stiffener, opposite side web.
	Cover Plate Termination 1	8.79	2242433	Runout	Impact opposite side.
		7.98	2242433	Runout	Impact side. Corner ground smooth.
	Cover Plate Termination 2	8.23	2242433	Runout	Impact opposite side.
		10.27	2242433	Runout	Impact side. Corner ground smooth.
1D/R-2	Transverse Stiffener 1	14.79	2232500	Runout	Impact opposite side of stiffener, opposite side of web. Full depth crack, 3/4" into width of flange but not failure.
		10.89	2232500	Runout	Impact opposite side stiffener.
	Transverse Stiffener 2	12.50	2232500	Runout	Impact opposite side stiffener.
		14.62	2232500	Runout	Impact opposite side of stiffener, opposite side of web.
	Flange Attachment 1	7.78	2822400	Runout	Impact side. Corner ground smooth. Crack noticeable but not failure.
		9.67	2822400	Runout	Impact opposite side. Crack noticeable but not failure.
	Flange Attachment 2	9.29	2822400	Runout	Impact opposite side.
		6.74	2822400	Runout	Impact side. Corner ground smooth.

B.2 Two Damage/Repair Cycles

Table B-2. Two damage/repair fatigue test results.

Specimen	Detail	Stress Range	Cycles	Result	Notes
2D/R-1	Cover Plate Termination 1	7.48	2644380	Runout	Impact point. Repair weld ground smooth.
		10.12	2644380	Runout	Impact opposite side.
	Cover Plate Termination 2	7.93	2644380	Runout	Impact opposite side.
		7.41	2644380	Runout	Impact point. Corner ground smooth ~1/8".
	Transverse Stiffener 1	19.55	1542392	Runout	Impact point. Weld toe ground smooth slightly ~ 1/16". Stiffener cutout for splice plates.
		14.76	1542392	Runout	Impact opposite side of stiffener. Stiffener cutout for splice plates.
		10.42	1542392	Runout	Impact opposite side of web. Stiffener cutout for splice plates. Data not used.
		11.75	1542392	Runout	Impact opposite side of stiffener, opposite side of web. Stiffener cutout for splice plates. Data not used.
	Transverse Stiffener 2	11.28	2644380	Failure	Impact opposite side of web.
		12.88	2644380	Runout	Impact opposite side of stiffener.
		17.57	2644380	Runout	Impact point. Weld toe ground smooth slightly ~ 1/8".
		11.45	2644380	Runout	Impact opposite side of stiffener, opposite side of web.
2D/R-2	Flange Attachment 1	8.56	4049450	Runout	Impact point. Corner ground smooth ~1/8".
		8.91	4049450	Runout	Impact opposite side.
	Flange Attachment 2	6.22	4049450	Runout	Impact opposite side. Repair weld ground smooth.
		8.77	4049450	Runout	Impact point. Repair weld ground smooth.
	Transverse Stiffener 1	16.26	4049450	Runout	Impact opposite side of stiffener.
		2.77	4049450	Runout	Impact opposite side of stiffener, opposite side of web. Data not used.
		1.11	4049450	Runout	Impact opposite side of web. Data not used.
		9.25	4049450	Runout	Impact point. Weld toe ground smooth ~1/4".
	Transverse Stiffener 2	10.35	4049450	Runout	Impact point. Repair weld ground smooth.
		16.37	4049450	Runout	Impact opposite side of stiffener.
		5.35	4049450	Runout	Impact opposite side of web. Data not used.
		5.45	4049450	Runout	Impact opposite side of stiffener, opposite side of web. Data not used.
2D/R-3	Cover Plate Termination 1	7.22	2240832	Runout	Impact point. Corner ground smooth.
		8.84	2240832	Runout	Impact opposite side.
	Cover Plate Termination 2	8.27	2240832	Runout	Impact opposite side.
		6.87	2240832	Runout	Impact point. Corner ground smooth.
	Transverse Stiffener 1	15.39	2240832	Runout	Impact opposite side of web.
		13.46	2240832	Runout	Impact opposite side of stiffener, opposite side of web.
		13.18	2240832	Runout	Impact point. Weld toe ground smooth ~1/16".
		14.78	2240832	Runout	Impact opposite side of stiffener.
	Transverse Stiffener 2	16.85	2240832	Runout	Impact opposite side of stiffener.
		19.74	2240832	Runout	Impact point. Weld toe ground smooth ~1/8".
		9.86	2240832	Runout	Impact opposite side of stiffener, opposite side of web.
		9.34	2240832	Runout	Impact opposite side of web.

Table B-2. (Continued)

Specimen	Detail	Stress Range	Cycles	Result	Notes
2D/R-4	Flange Attachment 1	8.78	3036500	Runout	Impact opposite side.
		5.78	3036500	Runout	Impact point. Repair weld ground smooth.
	Flange Attachment 2	8.23	3036500	Runout	Impact opposite side.
		5.78	3036500	Runout	Impact point. Corner ground smooth ~1/8".
	Transverse Stiffener 1	17.74	2702700	Runout	Impact opposite side of stiffener.
		22.26	2702700	Runout	Impact point. Repair weld ground smooth. Stress estimated from static data.
		6.72	2702700	Runout	Impact opposite side of stiffener, opposite side of web. Stress estimated from static data. Data not used.
		1.82	2702700	Runout	Impact opposite side of web. Stress estimated from static data. Data not used.
	Transverse Stiffener 2	13.95	2702700	Runout	Impact opposite side of stiffener, opposite side of web.
		19.24	2702700	Runout	Impact point. Repair weld ground smooth. Stress estimated from static data.
		12.09	2702700	Runout	Impact opposite side of stiffener. Stress estimated from static data.
		11.57	2702700	Runout	Impact opposite side of web. Stress estimated from static data.

B.3 Three Damage/Repair Cycles

Table B-3. Three damage/repair cycles.

Specimen	Detail	Stress Range	Cycles	Result	Notes
3D/R-1	Transverse Stiffener 1	21.66	3428600	Runout	Impact point. Replaced stiffener weld.
		13.56	3428600	Runout	Impact opposite side of stiffener. Replaced stiffener weld.
		9.68	3428600	Runout	Impact opposite side of web.
		10.08	3428600	Runout	Impact opposite side of stiffener, opposite side of web.
	Transverse Stiffener 2	10.09	689500	Runout	Impact opposite side of stiffener, opposite side of web.
		10.62	689500	Runout	Impact opposite side of web.
		11.97	689500	Runout	Impact opposite side of stiffener. Replaced stiffener weld.
		18.02	689500	Failure	Impact point. Replaced stiffener weld.
3D/R-2	Transverse Stiffener 1	14.11	294600	Runout	Impact point.
		15.68	294600	Runout	Impact opposite side of web.
		15.32	294600	Runout	Impact opposite side of stiffener.
		17.44	294600	Runout	Impact opposite side of stiffener, opposite side of web.
	Transverse Stiffener 2	18.25	222400	Runout	Impact opposite side of stiffener, opposite side of web.
		13.20	222400	Runout	Impact opposite side of stiffener.
		15.85	222400	Runout	Impact opposite side of web.
		15.32	222400	Runout	Impact point.

APPENDIX C

Material Properties

This appendix contains the tabulated comprehensive results of the material testing that was described in Section 2.4.

C.1 Fracture Toughness

The results to the notch toughness testing as conducted using standard size CVN specimens for several of the impacts from each of the specimens are listed in this section. These tests were conducted in accordance with ASTM E23 specifications. Listed in each of the tables are the locations where three CVN specimens were taken from and the corresponding strain ratio for the localized impact at those locations. For two and three D/R cycles, the strain ratio for each impact is listed separately and denoted with a numeral subscript for that impact number.

C.1.1 One Damage/Repair Cycle

The results of the fracture toughness for specimen 1D/R-1 are listed in Table C-1. Charpy V-notch specimens R4 through R6 were taken from extra flange material prior to the damage and repair process (0D/0R) and specimens 1D1 through 1D3 were taken from flange material at the impact area (strain ratio of the localized damage listed) following the repair (1D/1R).

The results of the fracture toughness results for specimen 1D/R-2 are listed in Table C-2. Charpy V-notch specimens F4 through F6 were taken from extra flange material prior to the damage/repair process. Specimens 2D1 through 2D3 were taken from flange material that was damaged but *not* heat-straightened. Specimens 2D4 through 2D6 were taken from flange material that was damaged, repaired, and damaged a second time but *not* repaired. Specimens 2D10 through 2D12 were taken from flange material that underwent one damage/repair cycle.

C.1.2 Two Damage/Repair Cycles

The results of the fracture toughness tests conducted on details on specimen 2D/R-1 are listed in Table C-3. The Charpy V-notch specimens 3F4 through 3F6 were taken from extra flange material prior to the damage/repair process and specimens 3D1 through 3D12 were taken from flange material at impact areas following the two D/R cycles.

The results of the fracture toughness tests conducted on details on specimen 2D/R-1 are listed in Table C-4. Charpy V-notch specimens 4F4 through 4F6 were taken from extra flange material prior to the damage/repair process, and specimens 4D4 through 4D12 were taken from flange material at impact areas following the two D/R cycles.

The results of the fracture toughness tests conducted on specimen 2D/R-3 are listed in Table C-5. The Charpy V-notch specimens 5F4 through 5F6 were taken from extra flange material prior to the damage/repair process, and specimens 5D7 through 5D12 were taken from flange material at impact areas following the two D/R cycles. In addition, specimens 5D1 through 5D6 were taken from flange material at the impact following a third impact (no repair). In addition to the location on the impact where the specimens were machined from were three specimens (5D4 through 5D6 and 5D10 through 5D12) taken from the center of the localized impact. The purpose for these specimens was to investigate additional area around the localized impact to determine the location of the most significant decrease in fracture toughness.

The results of the fracture toughness tests conducted on specimen 2D/R-4 are listed in Table C-6. The Charpy V-notch specimens 6F4 through 6F6 were taken from extra flange material prior to the damage/repair process, and specimens 6D1 through 6D12 were taken from flange material at impact areas following the two D/R cycles. In addition to the location on the impact where the specimens were machined from were three specimens (6D4 through 6D6 and 6D10 through 6D12) taken from the center of the localized impact.

C.1.3 Three Damage/Repair Cycles

The results of the fracture toughness tests conducted on specimen 3D/R-1 are listed in Table C-7. Note that this spec-

Table C-1. Notch toughness test results, specimen 1D/R-1.

Location (Strain Ratio)	Specimen Number	Test Temp. °F (°C)	Energy Absorbed ft-lb (J)	Average Energy ft-lb (J)	Condition
Original	R4	40 (4)	9 (12)	46 (62)	0D/0R
	R5		68 (92)		
	R6		61 (83)		
Cover Plate 2 (μ_L = 80)	1D1	40 (4)	44 (60)	24 (33)	1D/1R
	1D2		12 (16)		
	1D3		15 (20)		

Table C-2. Notch toughness test results, specimen 1D/R-2.

Location (Strain Ratio)	Specimen Number	Test Temp. °F (°C)	Energy Absorbed ft-lb (J)	Average Energy ft-lb (J)	Condition
Original	F4	40 (4)	114 (155)	197 (267)	0D/0R
	F5		238 (323)		
	F6		238 (323)		
Partial Stiffener 1 (Unknown)	2D1	40 (4)	7 (9)	20 (7)	1D/0R
	2D2		16 (22)		
	2D3		37 (50)		
Stiffener 2 (μ_L = 76)	2D4	40 (4)	5 (7)	15 (20)	1D/1R, 2D
	2D5		11 (15)		
	2D6		28 (38)		
Flange Attachment 1 (μ_L = 47)	2D10	40 (4)	56 (76)	41 (56)	1D/1R
	2D11		11 (15)		
	2D12		56 (76)		

Table C-3. Notch toughness test results, specimen 2D/R-1.

Location (Strain Ratio)	Specimen Number	Test Temp. °F (°C)	Energy Absorbed ft-lb (J)	Average Energy ft-lb (J)	Condition
Original	3F4	40 (4)	114 (155)	117 (159)	0D/0R
	3F5		133 (80)		
	3F6		103 (140)		
Stiffener 1 ($\mu_L = 59_1$ & 59_2)	3D1	40 (4)	99 (134)	95 (129)	2D/2R
	3D2		75 (102)		
	3D3		111 (150)		
Stiffener 2 ($\mu_L = 20_1$ & 63_2)	3D4	40 (4)	148 (201)	128 (174)	2D/2R
	3D5		84 (114)		
	3D6		152 (206)		
Cover Plate 1 ($\mu_L = 99_1$ & 95_2)	3D7	40 (4)	88 (119)	63 (85)	2D/2R
	3D8		56 (76)		
	3D9		45 (61)		
Cover Plate 2 ($\mu_L = 66_1$ & 87_2)	3D10	40 (4)	126 (171)	91 (123)	2D/2R
	3D11		100 (136)		
	3D12		47 (64)		

Table C-4. Notch toughness test results, specimen 2D/R-2.

Location (Strain Ratio)	Specimen Number	Test Temp. °F (°C)	Energy Absorbed ft-lb (J)	Average Energy ft-lb (J)	Condition
Original	4F4	40 (4)	30 (41)	31 (42)	0D/0R
	4F5		35 (47)		
	4F6		28 (38)		
Stiffener 2 ($\mu_L = 22_1$ & 66_2)	4D4	40 (4)	86 (117)	74 (100)	2D/2R
	4D5		84 (114)		
	4D6		53 (72)		
Flange Attachment 1 ($\mu_L = 99_1$ & 116_2)	4D7	40 (4)	11 (15)	46 (62)	2D/2R
	4D8		30 (41)		
	4D9		97 (132)		
Cover Plate 1 ($\mu_L = 105_1$ & 94_2)	4D10	40 (4)	66 (89)	55 (75)	2D/2R
	4D11		57 (77)		
	4D12		43 (58)		

Table C-5. Notch toughness test results, specimen 2D/R-3.

Location (Strain Ratio)	Specimen Number	Test Temp. °F (°C)	Energy Absorbed ft-lb (J)	Average Energy ft-lb (J)	Condition
Original	5F4	40 (4)	98 (133)	87 (118)	0D/0R
	5F5		87 (118)		
	5F6		75 (102)		
Stiffener 1 ($\mu_L = 36_1$ & 52_2)	5D1	40 (4)	113 (153)	59 (80)	2D/2R, 3D
	5D2		53 (72)		
	5D3		12 (16)		
Stiffener 1 -Center ($\mu_L = 36_1$ & 52_2)	5D4	40 (4)	99 (134)	67 (91)	2D/2R, 3D
	5D5		36 (49)		
	5D6		67 (90)		
Cover Plate 2 ($\mu_L = 36_1$ & 59_2)	5D7	40 (4)	105 (142)	56 (76)	2D/2R
	5D8		46 (62)		
	5D9		17 (23)		
Cover Plate 2 - Center ($\mu_L = 36_1$ & 59_2)	5D10	40 (4)	37 (50)	34 (46)	2D/2R
	5D11		52 (71)		
	5D12		12 (16)		

Table C-6. Notch toughness test results, specimen 2D/R-4.

Location (Strain Ratio)	Specimen Number	Test Temp. °F (°C)	Energy Absorbed ft-lb (J)	Average Energy ft-lb (J)	Condition
Original	6F4	40 (4)	50 (68)	50 (68)	0D/0R
	6F5		63 (85)		
	6F6		36 (49)		
Stiffener 1 ($\mu_L = 63_1$ & 99_2)	6D1	40 (4)	33 (45)	26 (35)	2D/2R
	6D2		28 (38)		
	6D3		17 (23)		
Stiffener 1 – Center ($\mu_L = 63_1$ & 99_2)	6D4	40 (4)	64 (87)	43 (58)	2D/2R
	6D5		43 (58)		
	6D6		22 (30)		
Stiffener 2 ($\mu_L = 71_1$ & 66_2)	6D7	40 (4)	11 (15)	25 (34)	2D/2R
	6D8		23 (31)		
	6D9		42 (57)		
Stiffener 2 – Center ($\mu_L = 71_1$ & 66_2)	6D10	40 (4)	38 (52)	36 (49)	2D/2R
	6D11		46 (62)		
	6D12		24 (33)		

Table C-7. Notch toughness test results, specimen 3D/R-1.

Location (Strain Ratio)	Specimen Number	Test Temp. °F (°C)	Energy Absorbed ft-lb (J)	Average Energy ft-lb (J)	Condition
Original Same as 2D/R-2	3F4	40 (4)	114 (115)	117 (159)	0D/0R
	3F5		133 (180)		
	3F6		103 (140)		
Stiffener 1 (μ_L = 63_1, 75_2 & 113_3)	7D1	40 (4)	90 (122)	61 (83)	3D/3R
	7D2		78 (106)		
	7D3		15 (20)		
Stiffener 2 (μ_L = 48_1, 63_2 & 70_3)	7D4	40 (4)	146 (198)	55 (75)	3D/3R
	7D5		11 (15)		
	7D6		8 (11)		

imen was fabricated from the same rolled beam as was specimen 2D/R-2. Therefore the results from the original flange material that was used for specimen 2D/R-2 was used (specimens 3F4 through 3F6) for comparison to the CVN specimens taken from specimen 3D/R-1. Specimens 7D1 through 7D6 were taken from flange material at the two impact areas following three D/R cycles.

The results of the fracture toughness tests conducted on specimen 3D/R-2 are listed in Table C-8. The CVN specimens 8F4 through 8F6 were taken from extra flange material prior to the damage/repair process, and specimens 7D1 through 7D6 were taken from flange material at the two impact areas following three D/R cycles.

C.2 Tensile Properties

Tabulated results to the tensile testing are listed in the following sections. These tensile specimens were used to determine the yield strength, tensile strength, and ductility (measured as the elongation over a gage length expressed as a percentage) before and after the heat-straightening repairs. This testing was conducted in accordance with ASTM E8 specifications. A summary of the results can be found in Section 2.4.2.

C.2.1 One Damage/Repair Cycle

Tensile specimens RF1, RF2, and RF4 were taken from virgin flange material supplied by the fabricator. Tensile specimen 1DT1 was flange material taken from the localized damage that had a strain ratio, μ, of 80, near cover plate 2 as listed in Table C-9.

Tensile tests on flange material before and after one D/R cycle on specimen 1D/R-2 were conducted. The results to these tests are listed in Table C-10. Tensile specimens PF1 through PF3 were taken from extra flange material supplied by the fabricator. Tensile specimen 2DT1 was taken from flange material that was damaged but not heat-straightened. Tensile specimen 2DT2 was taken from flange material that was damaged, repaired, and damaged a second time but not repaired a second time. Tensile specimen 2DT4 was taken from flange material that underwent one D/R cycle.

C.2.2 Two Damage/Repair Cycles

Tensile specimens 3FT1 through 3FT4 were taken from virgin flange material supplied by the fabricator. Tensile specimens 3DT1 through 3DT4 were taken from flange material from the area of the localized impact that experienced the

Table C-8. Notch toughness test results, specimen 3D/R-2.

Location (Strain Ratio)	Specimen Number	Test Temp. °F (°C)	Energy Absorbed ft-lb (J)	Average Energy ft-lb (J)	Condition
Original	8F4	40 (4)	41 (56)	51 (69)	0D/0R
	8F5		48 (65)		
	8F6		65 (88)		
Stiffener 1 (μ_L = 60_1, 54_2 & 65_3)	8D1	40 (4)	18 (24)	16 (22)	3D/3R
	8D2		11 (15)		
	8D3		19 (26)		
Stiffener 2 (μ_L = 41_1, 37_2 & 60_3)	8D4	40 (4)	22 (30)	27 (37)	3D/3R
	8D5		14 (19)		
	8D6		44 (60)		

Table C-9. Tensile test results, specimen 1D/R-1.

Location (Strain Ratio)	Specimen Name	Yield Strength ksi (MPa)	Tensile Strength ksi (MPa)	Total Elongation %	Reduction of Area %	Condition
Original	RF1	52.3 (360.6)	76.2 (525.4)	30.1%	66.4%	0D/0R
Original	RF2	52.0 (358.5)	76.1 (524.7)	31.0%	66.2%	0D/0R
Original	RF4	53.5 (368.9)	76.4 (526.8)	30.8%	67.1%	0D/0R
Cover Plate 2 (μ_L = 80)	1DT1	57.3 (395.1)	76.7 (528.8)	22.3%	68.5%	1D/1R

largest amount of straining after two D/R cycles at all four details that were investigated. The results to these tests for specimen 2D/R-1 are listed in Table C-11.

The results to the tensile tests for specimen 2D/R-2 are listed in Table C-12. Tensile specimens 4FT1 and 4FT3 were taken from extra flange material supplied by the fabricator. Tensile specimens 4DT3 through 4DT5 were taken from flange material from the area of the localized impact that experienced the largest amount of straining after two D/R cycles near three of the details being tested.

For specimen 2D/R-3, tensile specimens 5FT1 through 5FT4 were taken from virgin flange material supplied by the fabricator. Tensile specimen 5DT1 was taken from flange material that was damaged and repaired two times and then was damaged a third time without a subsequent repair. Tensile specimen 3DT4 was taken from flange material from the area of the localized impact after two D/R cycles. The results to these tests are listed in Table C-13.

The results to tensile tests for specimen 2D/R-4 are listed in Table C-14. Tensile specimens 6FT1 through 6FT3 were taken from virgin flange material supplied by the fabricator. Tensile specimens 6DT1 and 6DT2 were taken from flange material that was damaged and repaired two times by both of the stiffeners.

C.2.3 Three Damage/Repair Cycles

The results to tensile tests for specimen 3D/R-1 are listed in Table C-15. This specimen came from the same rolling process as specimen 2D/R-1; therefore, the original tensile properties (tensile specimens 3DT1 through 3DT4) are the same as listed for specimen 2D/R-1. Tensile specimens 7DT1 and 7DT2 were taken from flange material that was damaged and repaired three times near the transverse stiffener details.

Tensile specimens 8FT1 through 8FT3 were taken from virgin flange material of specimen 3D/R-2 that was supplied by the fabricator. Tensile specimens 8DT1 and 8DT2 were taken from flange material that was damaged and repaired three times by both of the stiffeners. The results to these tensile tests are listed in Table C-16.

Table C-10. Tensile test results, specimen 1D/R-2.

Location (Strain Ratio)	Specimen Name	Yield Strength ksi (MPa)	Tensile Strength ksi (MPa)	Total Elongation %	Reduction of Area %	Condition
Original	RF1	41.0 (282.7)	67.1 (462.6)	42.2%	63.4%	0D/0R
Original	RF2	42.4 (292.3)	67.2 (463.3)	39.9%	64.2%	0D/0R
Original	RF4	41.3 (284.8)	67.2 (463.3)	41.4%	63.2%	0D/0R
Partial Stiffener 1 (Unknown)	2DT1	58.3 (402.0)	78.8 (543.3)	25.4%	70.8%	1D/0R
Stiffener 2 (μL = 76)	2DT2	64.4 (444.0)	77.8 (536.4)	22.4%	67.9%	1D/1R, 1D
Flange Attachment 1 (μ_L = 47)	2DT4	53.9 (371.6)	76.6 (528.1)	25.8%	64.2%	1D/1R

Table C-11. Tensile test results, specimen 2D/R-1.

Location (Strain Ratio)	Specimen Name	Yield Strength ksi (MPa)	Tensile Strength ksi (MPa)	Total Elongation %	Reduction of Area %	Condition
Original	3FT1	55.7 (384.0)	78.8 (543.3)	31.1%	75.4%	0D/0R
Original	3FT2	55.8 (384.7)	78.8 (543.3)	30.2%	77.5%	0D/0R
Original	3FT3	56.9 (392.3)	78.2 (539.2)	29.9%	76.5%	0D/0R
Original	3FT4	54.1 (373.0)	75.4 (519.9)	30.6%	77.6%	0D/0R
Stiffener 1 ($\mu_L = 59_1$ & 59_2)	3DT1	52.2 (359.9)	69.7 (481.3)	27.6%	75.4%	2D/2R
Stiffener 2 ($\mu_L = 20_1$ & 63_2)	3DT2	65.6 (452.3)	83.2 (573.6)	27.7%	72.3%	2D/2R
Cover Plate 1 ($\mu_L = 99_1$ & 95_2)	3DT3	62.8 (433.0)	79.5 (548.1)	27.4%	76.0%	2D/2R
Cover Plate 2 ($\mu_L = 66_1$ & 87_2)	3DT4	63.6 (438.5)	81.6 (562.6)	28.7%	76.0%	2D/2R

Table C-12. Tensile test results, specimen 2D/R-2.

Location (Strain Ratio)	Specimen Name	Yield Strength ksi (MPa)	Tensile Strength ksi (MPa)	Total Elongation %	Reduction of Area %	Condition
Original	4FT1	50.6 (348.9)	76.6 (528.1)	34.0%	52.9%	0D/0R
Original	4FT3	54.9 (378.5)	76.5 (527.4)	35.2%	53.4%	0D/0R
Stiffener 2 ($\mu_L = 22_1$ & 66_2)	4DT3	53.1 (366.1)	77.8 (536.4)	31.8%	67.2%	2D/2R
Flange Attachment 1 ($\mu_L = 99_1$ & 116_2)	4DT4	65.3 (450.2)	89.5 (617.1)	28.5%	60.1%	2D/2R
Flange Attachment 2 ($\mu_L = 105_1$ & 94_2)	4DT5	53.3 (367.5)	81.8 (564.0)	24.8%	63.0%	2D/2R

Table C-13. Tensile test results, specimen 2D/R-3.

Location (Strain Ratio)	Specimen Name	Yield Strength ksi (MPa)	Tensile Strength ksi (MPa)	Total Elongation %	Reduction of Area %	Condition
Original	5FT1	56.1 (386.8)	76.8 (529.5)	30.4%	76.0%	0D/0R
Original	5FT2	57.9 (399.2)	79.2 (546.1)	29.9%	75.9%	0D/0R
Original	5FT3	59.1 (407.5)	79.5 (548.1)	29.5%	75.7%	0D/0R
Original	5FT4	59.5 (410.2)	79.5 (548.1)	30.1%	76.4%	0D/0R
Stiffener 1 ($\mu_L = 36_1$ & 52_2)	5DT1	60.6 (417.8)	83.5 (575.7)	25.8%	77.2%	2D/2R, 3D
Cover Plate 2 ($\mu_L = 36_1$ & 59_2)	5DT2	65.6 (452.3)	80.8 (557.1)	27.4%	76.2%	2D/2R

Table C-14. Tensile test results, specimen 2D/R-4.

Location (Strain Ratio)	Specimen Name	Yield Strength ksi (MPa)	Tensile Strength ksi (MPa)	Total Elongation %	Reduction of Area %	Condition
Original	6FT1	59.2 (408.2)	86.3 (595.0)	34.8%	58.6%	0D/0R
Original	6FT2	59.8 (412.3)	86.1 (593.6)	34.8%	59.5%	0D/0R
Original	6FT3	61.9 (426.8)	88.1 (607.4)	35.2%	58.2%	0D/0R
Stiffener 1 ($\mu_L = 63_1$ & 99_2)	6DT1	64.7 (446.1)	88.5 (610.2)	25.8%	68.2%	2D/2R
Stiffener 2 ($\mu_L = 71_1$ & 66_2)	6DT2	69.5 (479.2)	91.5 (630.9)	24.5%	69.3%	2D/2R

C.3 Chemical Composition

The chemical composition of each of the specimens, as determined by a heat analysis and a product analysis, was confirmed with the ASTM requirements for the type of steel used as described in Section 1.3.2. The heat analysis was provided by the fabricator on the mill certifications when the specimens had arrived. The product analysis was conducted by an outside contractor after the testing of the specimens had been completed. Table C-17 lists the results for the two specimens that were used to investigate one D/R cycle. Specimen 1D/R-1 met the requirements for both A992 and A572 grade 50 steel. Likewise, specimen 1D/R-2 met the requirements for A709 grade 36 steel.

The specimens used to investigate two damage repair cycles are listed in Table C-18. The heat and product analysis for specimens 2D/R-1 and 2D/R-3, both fabricated from A709 and A 588 grade 50 steel, were satisfied in accordance with ASTM specifications. For specimens 2D/R-2 and 2D/R-4, there was a significant dissimilarity in the heat and product analyses. This may be due to incorrect mill certifications supplied by the fabricator. The product analysis did confirm that the requirements for A709 grade 36 steel were met for these specimens.

Table C-19 lists the results for the two specimens used to investigate three D/R cycles. The requirements for A709 and A588 grade 50 steel were satisfied for specimen 3D/R-1. Although there was some variation in the results of the heat and product analyses for specimen 3D/R-2, both met the requirements for A709 grade 50 steel.

C.4 Microstructure Inspection

The microstructure of several of the impacts along with corresponding material from the specimen prior to any D/R cycles was investigated. The inspection was conducted on the CVN specimens after the testing.

Table C-15. Tensile test results, specimen 3D/R-1.

Location (Strain Ratio)	Specimen Name	Yield Strength ksi (MPa)	Tensile Strength ksi (MPa)	Total Elongation %	Reduction of Area %	Condition
Original	3FT1	55.7 (384.0)	78.8 (543.3)	31.1%	75.4%	0D/0R
Original	3FT2	55.8 (384.7)	78.8 (543.3)	30.2%	77.5%	0D/0R
Original	3FT3	56.9 (392.3)	78.2 (539.2)	29.9%	76.5%	0D/0R
Original	3FT4	54.1 (373.0)	75.4 (519.9)	30.6%	77.6%	0D/0R
Stiffener 1 ($\mu_L = 63_1$, 75_2 & 113_3)	7DT1	66.4 (457.8)	82.9 (571.6)	27.0%	58.2%	3D/3R
Stiffener 2 ($\mu_L = 48_1$, 63_2 & 70_3)	7DT2	66.5 (458.5)	82.4 (568.1)	26.1%	70.0%	3D/3R

Table C-16. Tensile test results, specimen 3D/R-2.

Location (Strain Ratio)	Specimen Name	Yield Strength ksi (MPa)	Tensile Strength ksi (MPa)	Total Elongation %	Reduction of Area %	Condition
Original	8FT1	61.9 (426.8)	88.2 (608.1)	35.9%	61.5%	0D/0R
Original	8FT2	64.4 (444.0)	90.5 (624.0)	36.6%	64.2%	0D/0R
Original	8FT3	61.9 (426.8)	89.3 (615.7)	36.8%	62.2%	0D/0R
Stiffener 1 ($\mu_L = 60_1, 54_2$ & 65_3)	8DT1	68.4 (471.6)	97.8 (674.3)	24.8%	61.1%	3D/3R
Stiffener 2 ($\mu_L = 41_1, 37_2$ & 60_3)	8DT2	65.8 (453.7)	90.6 (624.7)	26.4%	65.1%	3D/3R

Table C-17. Chemical composition, one D/R cycle specimens.

	1D/R-1			1D/R-2	
	Product	**Heat**		**Product**	**Heat**
Al	0.006%	0.002%		0.019%	-
C	0.110%	0.090%		0.120%	0.140%
Cb	-	-		-	0.001%
Cr	0.059%	0.080%		0.045%	0.040%
Cu	0.270%	0.310%		0.190%	0.210%
Mn	1.110%	1.100%		0.820%	0.810%
Mo	0.031%	0.015%		0.033%	0.020%
N	-	-		-	-
Nb	0.028%	0.022%		0.009%	-
Ni	0.078%	0.100%		0.083%	0.090%
P	0.008%	0.007%		0.008%	0.009%
Pb	-	-		-	-
S	0.035%	0.039%		0.002%	0.005%
Si	0.200%	0.230%		0.250%	0.250%
Sn	-	0.019%		-	0.012%
Ti	-	-		-	-
V	0.001%	0.002%		0.003%	0.001%

Table C-18. Chemical composition, two D/R cycles specimens.

	2D/R-1			2D/R-2			2D/R-3			2D/R-4	
	Product	**Heat**		**Product**	**Heat**		**Product**	**Heat**		**Product**	**Heat**
Al	0.001%	-		0.020%	0.042%		0.002%	-		0.027%	0.004%
C	0.100%	0.070%		0.130%	0.130%		0.110%	0.080%		0.180%	0.160%
Cb	-	0.002%		-	-		-	0.001%		-	0.006%
Cr	0.430%	0.430%		0.540%	0.040%		0.120%	0.120%		0.530%	0.100%
Cu	0.300%	0.320%		0.350%	0.020%		0.280%	0.280%		0.290%	0.250%
Mn	1.260%	1.270%		0.940%	1.160%		1.290%	1.310%		1.040%	0.910%
Mo	0.070%	0.020%		0.070%	0.004%		0.082%	0.030%		0.070%	0.020%
N	0.003%	-		0.003%	0.004%		0.005%	-		0.002%	0.000%
Nb	0.002%	-		0.002%	-		0.002%	-		0.002%	-
Ni	0.260%	0.280%		0.160%	0.010%		0.120%	0.120%		0.230%	0.070%
P	0.012%	0.017%		0.012%	0.016%		0.010%	0.012%		0.008%	0.020%
Pb	0.003%	-		0.002%	-		0.003%	-		-	-
S	0.020%	0.025%		0.016%	0.012%		0.016%	0.017%		0.008%	0.018%
Si	0.280%	0.280%		0.140%	0.210%		0.250%	0.230%		0.340%	0.210%
Sn	-	0.010%		-	0.005%		-	0.010%		-	0.011%
Ti	-	-		-	0.001%		-	-		-	0.000%
V	0.032%	0.030%		0.037%	0.001%		0.042%	0.040%		0.035%	0.006%

Table C-19. Chemical composition, three D/R cycles specimens.

	3D/R-1			3D/R-2	
	Product	Heat		Product	Heat
Al	0.001%	-		0.001%	0.004%
C	0.100%	0.070%		0.190%	0.160%
Cb	-	0.002%		-	0.006%
Cr	0.430%	0.430%		0.180%	0.100%
Cu	0.300%	0.320%		0.270%	0.250%
Mn	1.260%	1.270%		1.190%	0.910%
Mo	0.070%	0.020%		0.080%	0.020%
N	0.003%	-		0.003%	0.000%
Nb	0.002%	-		0.002%	-
Ni	0.260%	0.280%		0.090%	0.070%
P	0.012%	0.017%		0.016%	0.020%
Pb	0.003%	-		-	-
S	0.020%	0.025%		0.023%	0.018%
Si	0.280%	0.280%		0.280%	0.210%
Sn	-	0.010%		-	0.011%
Ti	-	-		-	0.000%
V	0.032%	0.030%		0.033%	0.006%

C.4.1 One Damage/Repair Cycle

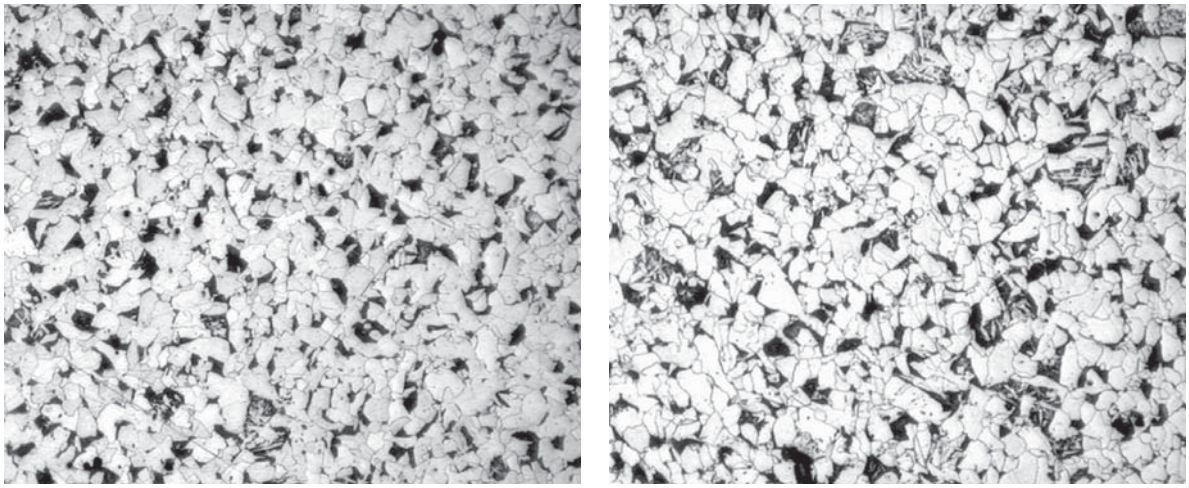

a) Original material (1000X) b) One D/R cycle (1000X)

Figure C-1. Microstructure before and after one D/R cycle, specimen 1D/R-1.

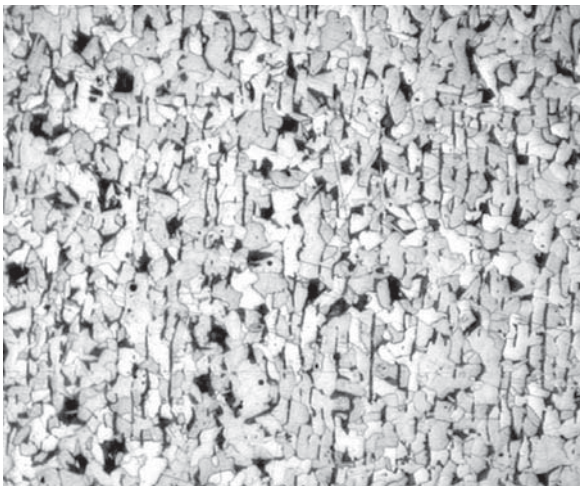

a) Original material (1000X)

b) 1D/0R (1000X)

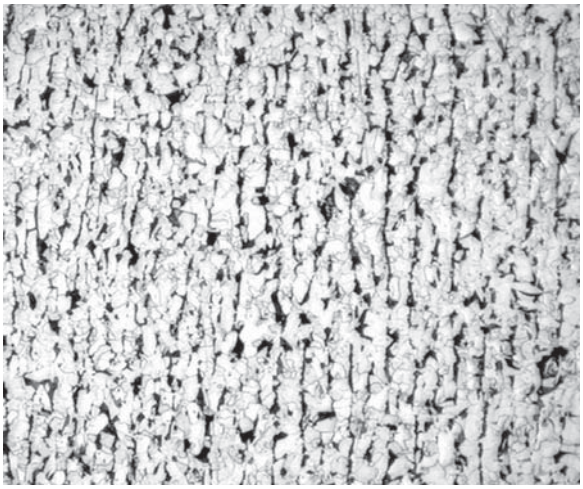

c) 1D/1R (1000X)

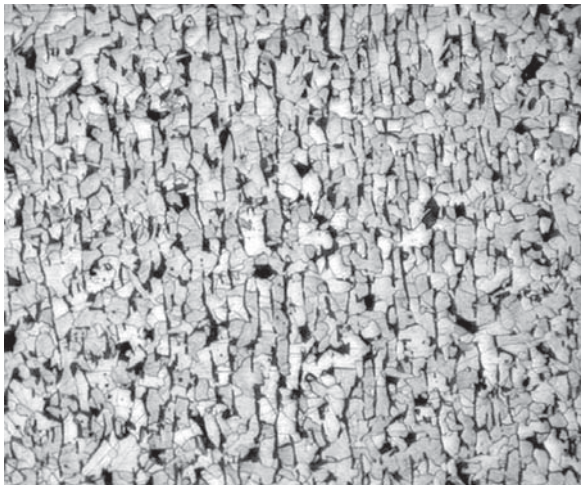

d) 2D/1R (1000X)

Figure C-2. Microstructure before and after one D/R cycle, specimen 1D/R-2.

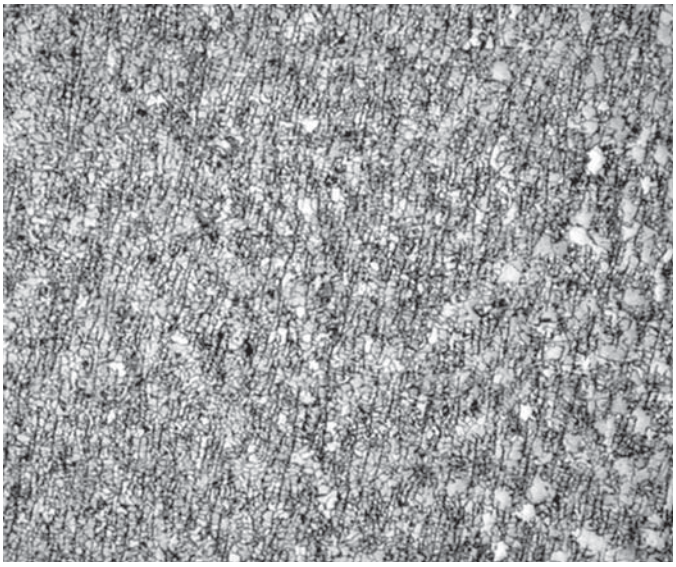

Figure C-3. Overheated specimen after one D/R cycle (1000X), 1D/R-2.

C.4.2 Two Damage/Repair Cycles

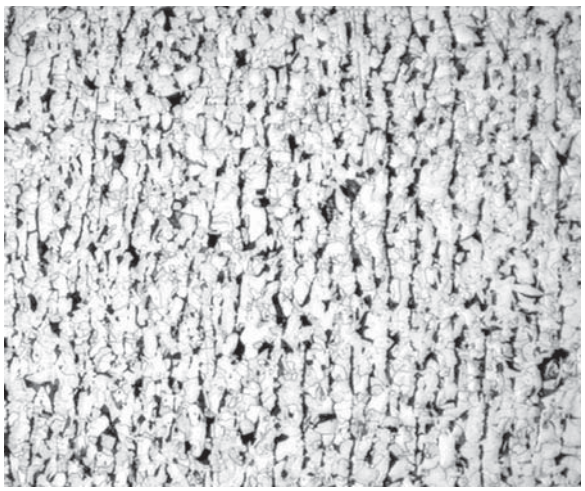

a) Original material (1000X)

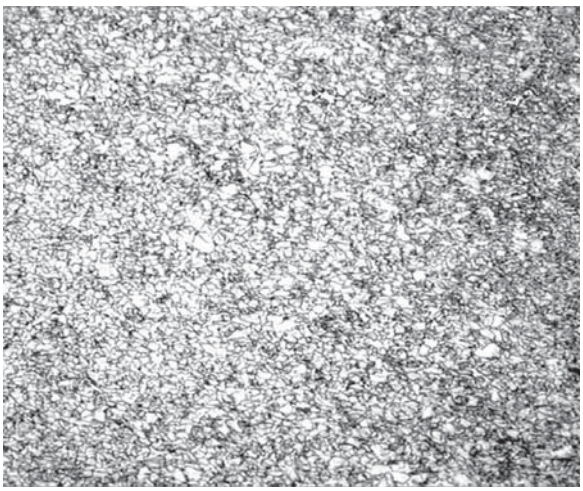

b) 2D/2R (1000X) - Overheated

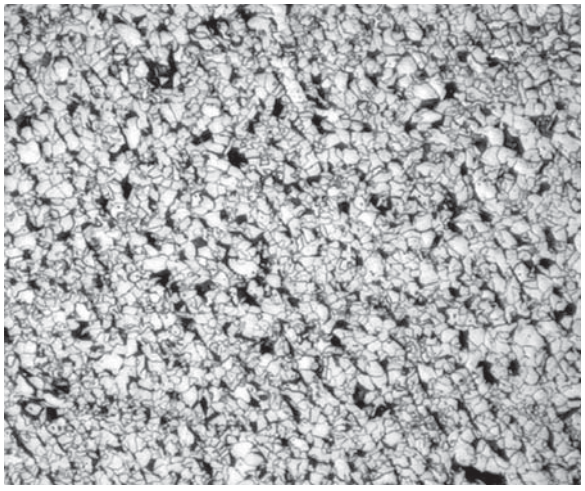

c) 2D/2R (1000X)

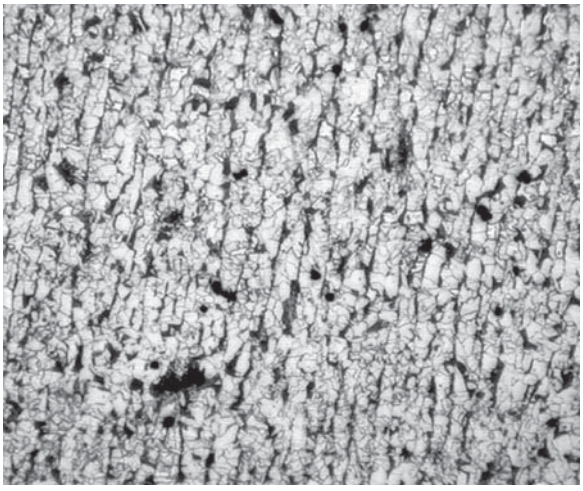

d) 2D/2R (1000X)

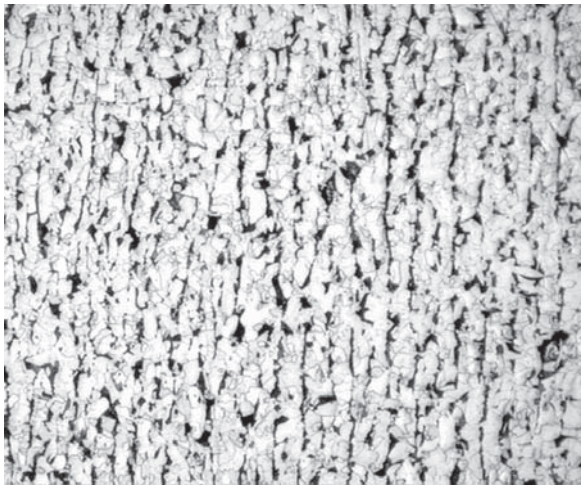

e) 2D/2R (1000X)

Figure C-4. Microstructure before and after two D/R cycles, specimen 2D/R-1.

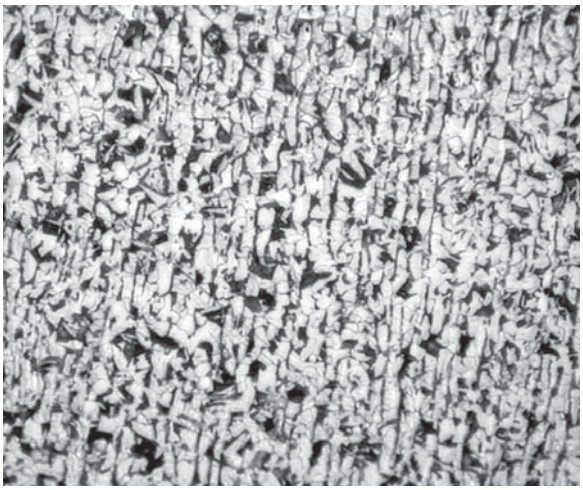

a) Original material (1000X)

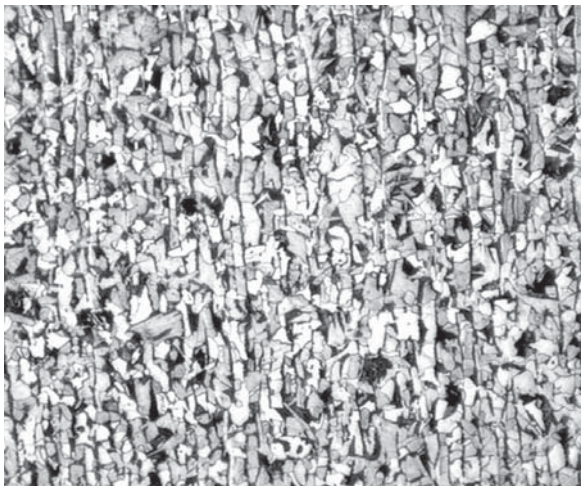

b) 2D/2R (1000X)

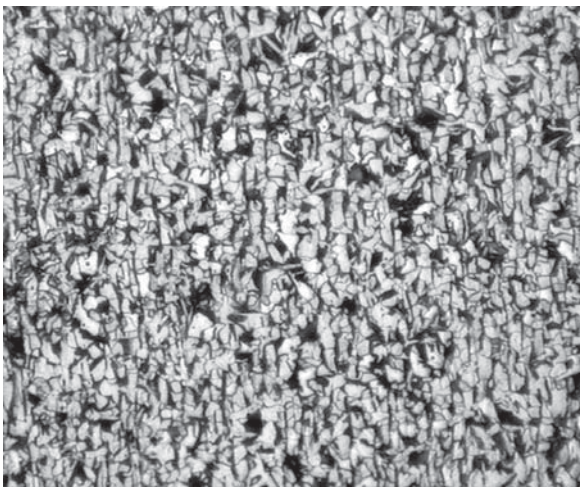

c) 2D/2R (1000X)

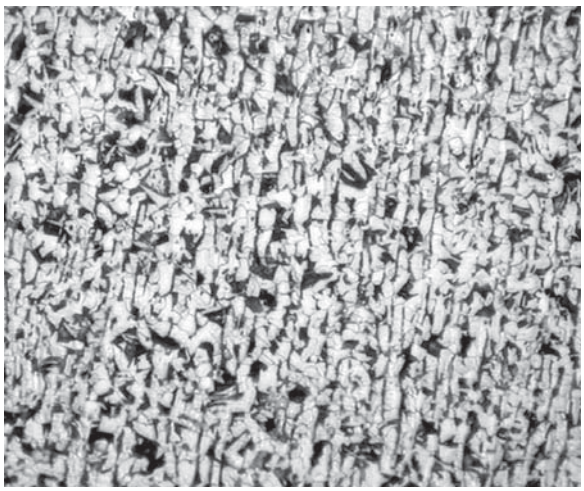

d) 2D/2R (1000X)

Figure C-5. Microstructure before and after two D/R cycles, specimen 2D/R-2.

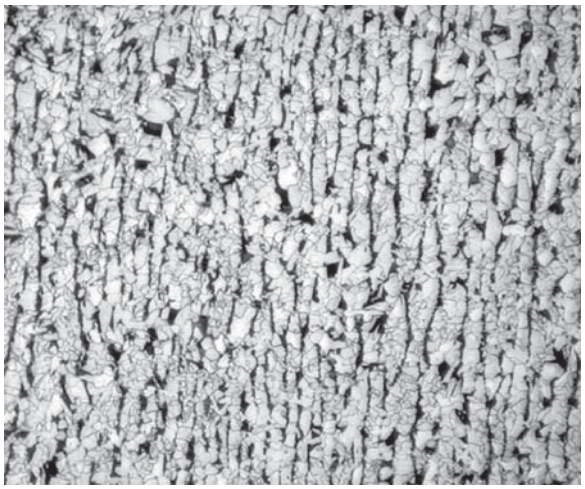

a) Original material (1000X)

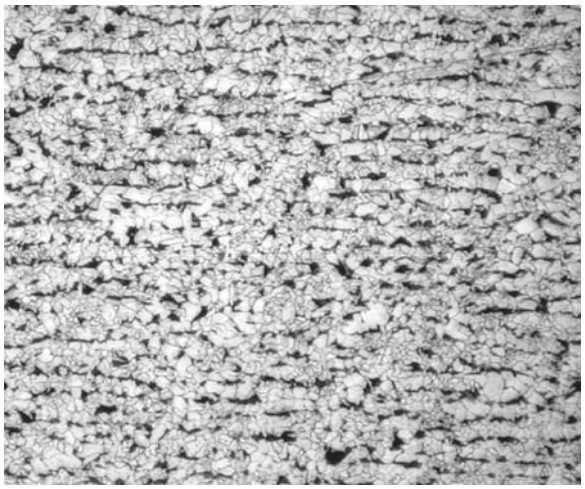

b) 2D/2R (1000X)

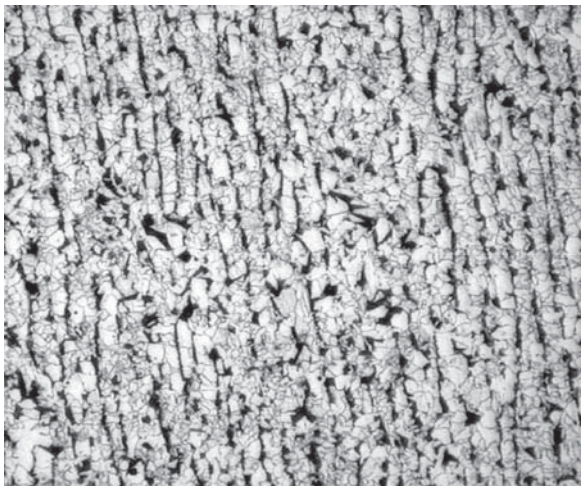

c) 2D/2R (1000X)

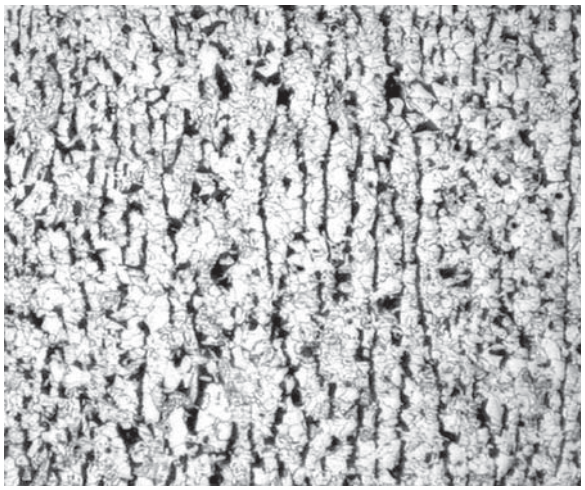

d) 2D/2R (1000X)

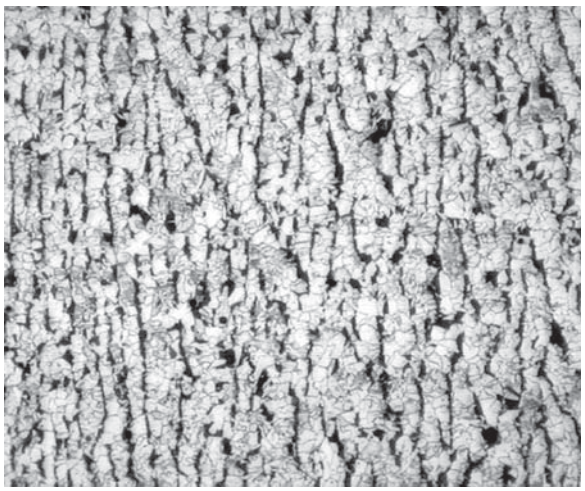

e) 2D/2R (1000X)

Figure C-6. Microstructure before and after two D/R cycles, specimen 2D/R-3.

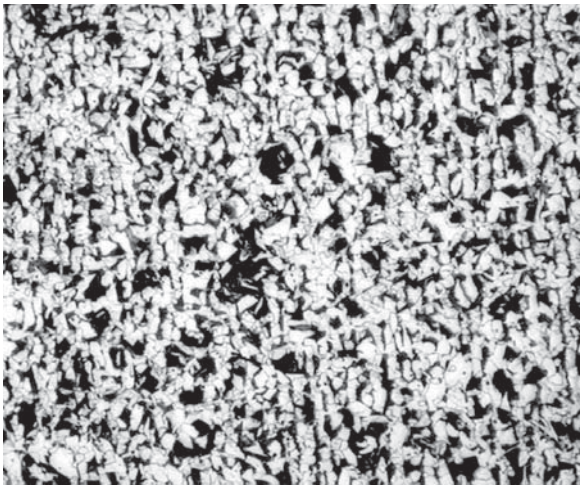

a) Original material (1000X)

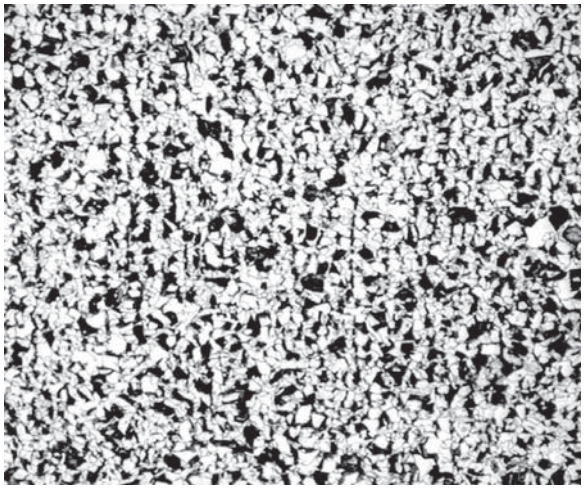

b) 2D/2R (1000X)

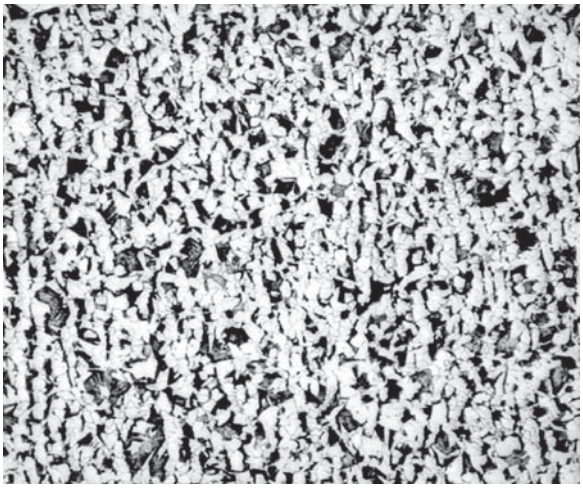

c) 2D/2R (1000X)

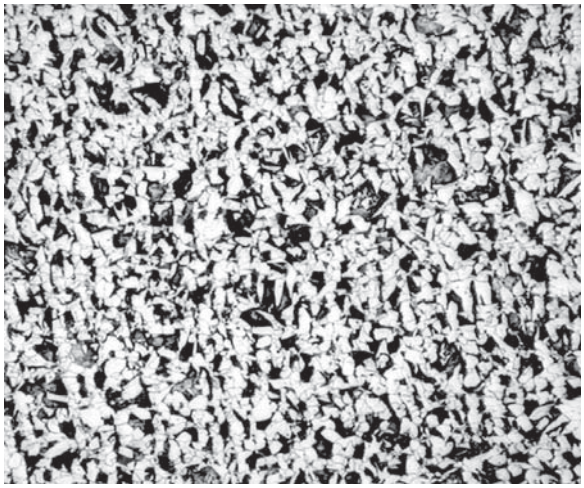

d) 2D/2R (1000X)

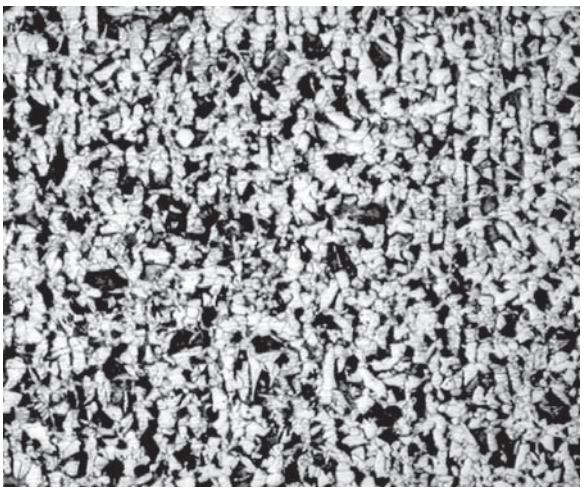

e) 2D/2R (1000X)

Figure C-7. Microstructure before and after two D/R cycles, specimen 2D/R-4.

C.4.3 Three Damage/Repair Cycles

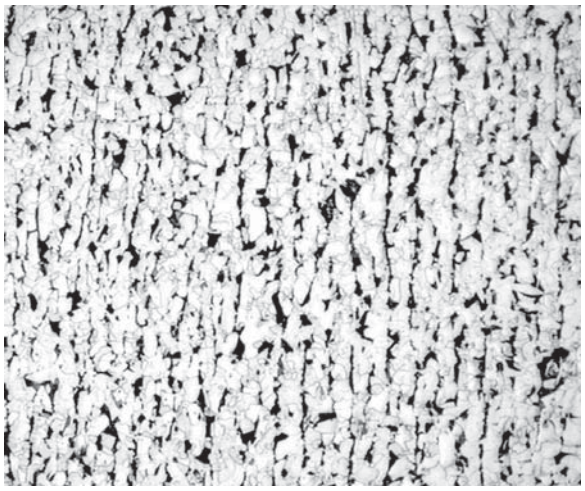

a) Original material (1000X)

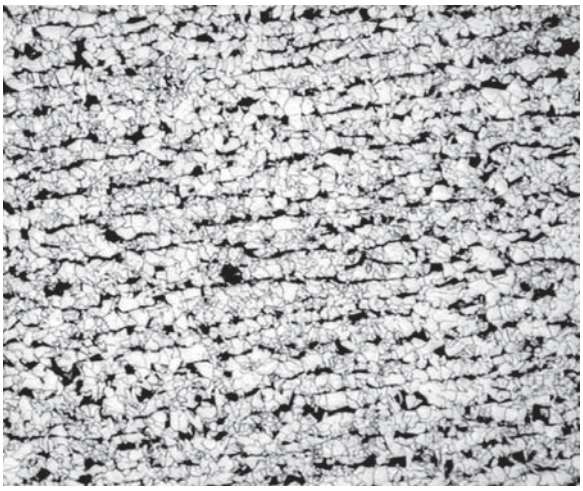

b) 3D/3R (1000X)

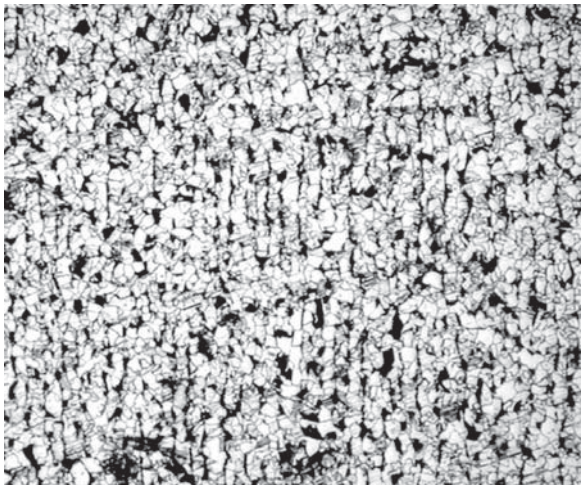

c) 3D/3R (1000X)

Figure C-8. Microstructure before and after three D/R cycles, specimen 3D/R-1.

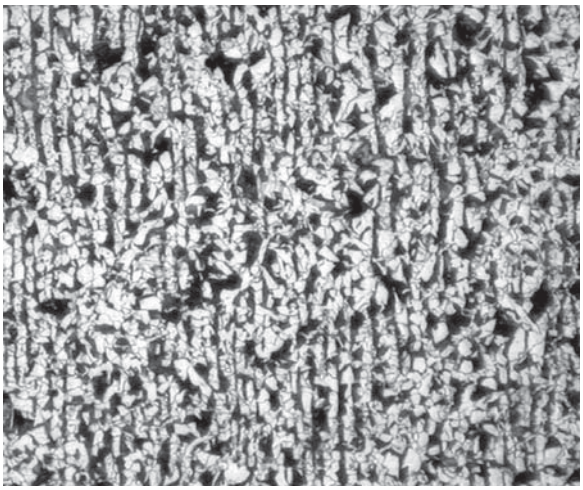

a) Original material (1000X)

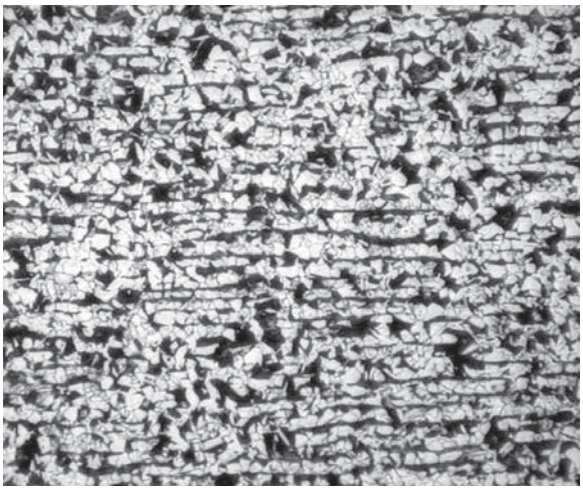

b) 3D/3R (1000X)

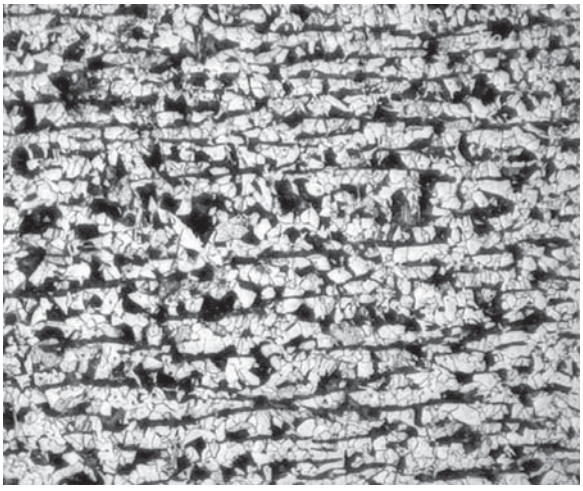

c) 3D/3R (1000X)

Figure C-9. Microstructure before and after three D/R cycles, specimen 3D/R-2.

APPENDIX D

Proposed Revisions to FHWA Manual

Based on the research conducted during NCHRP Project 10-63, the following revisions are proposed to FHWA Report No. FHWA-IF-99-004, "Heat-straightening Repair of Damage Steel Bridges—Manual of Practice and Technical Guide," dated October, 1998. Proposed revisions to Chapter 1, Chapter 3, and Chapter 4, and Chapter 9 follow. There are no proposed changes to the following chapters: Chapter 2, Chapters 5 through Chapters 8, and Chapters 10 through 14.

Proposed Revisions to Chapter 1

The following revision is proposed for Chapter 1.

Revision 1

Under the subheading "History of Heat-straightening," it is proposed to modify the fifth full sentence in the fourth paragraph on page 4.

Proposed Modifications

Well into the 1980's, the use of heat straightening was so little understood that one-half the States did not allow heat straightening repair of bridges (Shanafeltand Horn, 1984). At that time there were reasons why heat-straightening repair had not been widely accepted. First, the basic mechanism of heat-straightening was not well-understood in that the effects of both external restraints (jacking) and internal restraints (redundancy) were considered to be of minor concern rather than fundamental to the broad application of the process. Second, as a result of not identifying the importance of these parameters, there had been little documentation of the behavior of vee heated plates subjected to varying degrees of constraint and even less on rolled shapes. Third, while a fair amount of research indicated that most material properties are relatively unaffected by heat straightening, ~~two~~ some important aspects had been overlooked: the influence of strain aging on ductility; ~~and~~ residual stress distribution, and subsequent fatigue and fracture performance of repaired members. ~~Finally,~~ Fourth, the research information available was predicated almost entirely on laboratory studies of simple elements. Finally, the effects of multiple damage/repair cycles on the fatigue and fracture performance of large scale members was not studied explicitly. The reported field investigations were qualitative rather than quantitative and thus could not serve as a building block for validating heat straightening. Because of these voids in heat-straightening research, it was indeed true that the artesian practicing the trade was much more important than the engineer. Consequently, heat straightening repair was often not considered on engineered structures.

Proposed Revisions to Chapter 3

There are several proposed revisions to Chapter 3. In light of this, all of the text from Chapter 3 is reprinted below with the deleted and added text shown as strikethrough and underlined, respectively. The original figures, tables, and equations are not to be revised and are not included for brevity.

Chapter 3. Assessing, Planning, and Conducting Successful Repairs

As with other types of repair, a successful heat-straightening repair requires assessment, planning and design. Several procedures should be considered as part of the process. These aspects may include: determination of degree of damage, location of yield zones and regions of maximum strain, removing any nicks or gouges, limitations for heat-straightening repair, selection of heating patterns, and selection of jacking restraints. Each requires the exercise of engineering judgment. Outlined in this chapter are some key aspects of assessing, planning and designing a repair. One of the primary keys is maintaining coordination between the engineer, field supervisor or inspector, and the contractor conducting the repair.

Role of Engineer, Inspector and Contractor

The engineer is responsible for selecting the most appropriate repair technique for the specific damage. Alternatives must be evaluated and the most effective solution determined. The key considerations include: cost, constructability, adequate restoration of strength, longevity of repair, time to complete repair, aesthetics, and impact on traffic. These aspects constitute the concept we refer to as design. Although frequently overlooked, repairs should be designed in a similar manner to new structures. The typical process includes: selecting a trial repair scheme, conducting a structural analysis (which may require assumptions of certain geometric or material properties), sizing the parameters of the repair (or verifying the capacity after repair), possibly re-analyzing and redesigning, evaluating alternate repair or replacement schemes, and finally, providing complete details and specifications for the system selected. The engineer should also establish the acceptable levels of residual damage which may remain without adversely affecting the capacity (both strength and fatigue) of the member. Furthermore, the engineer must consider the consequence of brittle fracture, should it occur as a result of the repair process.

Heat-straightening repair is not the solution for every damage situation. The engineer's role is to make an assessment as to its specific applicability. Aspects to consider are: current condition of the rest of the structure and other anticipated repairs, degree of damage, presence of fractures, damage from earlier impacts, cause of damage and likelihood of repetitive damage occurring, accessibility, and the repair method's impact on material properties. Once the heat straightening alternative is selected, then the repair parameters such as traffic control, contractor access and work areas, permitted hours of work, typical heating patterns, maximum restraining forces and locations, and maximum heating temperature must be chosen. Finally, plans and specifications should be developed which generally define how the repair is to be accomplished.

Since most heat-straightening repairs are conducted by contractors, the field supervisor (or inspector), representing the bridge owner, has major responsibilities. The supervisor must insure that the repair is being conducted according to plans and specifications. Of particular importance is insuring that procedures are followed which are not detrimental to the steel.

The third member of the team is the contractor who actually executes the repair. The ultimate success of the project hinges on the skills and understanding for the project by the contractor's personnel. While others may have designed the repair plan, the details of execution lie with the contractor. Important considerations may include: (1) scaffolding arrangements; (2) selection of proper heating equipment; (3) making any preliminary repairs, such as grinding smooth any nicks and gouges prior to beginning the heat straightening repair; (4) implementing the restraint plan with appropriate jacks and come-alongs; (5) placing the heats in proper patterns and sequences; (6) analyzing the progress of the repair; and (7) adequacy of the repair. The contractor must be alert to the response of the structure and be prepared to suggest changes to expedite the process. In spite of our current knowledge and analytical capabilities, movements during heat straightening cannot always be predicted accurately.

The primary reasons for this difficulty are that: (1) damage patterns are often a complex mixture of the idealized cases and require experience to determine the details of the heating process; and (2) residual stresses and moments which may have been locked into the structure during the damage phase are sometimes difficult to predict and may prevent the expected movement. The contractor must be able to assess the reaction of the structure to the planned repair and suggest modifications if the structure is not performing properly. These modifications may range from changes in heating patterns and jacking arrangements to decisions on whether to remove secondary or bracing members during the repair.

Perhaps most important is that the engineer, the supervisor and the contractor maintain open and clear channels of communication. This interaction of the three key players in a heat-straightening repair will go a long ways toward insuring a successful project.

Keys to a Successful Repair

A successful repair requires the control and selection of certain specific parameters. The first key is the detailed inspection of the member in the as-damaged condition to identify any cracks, nicks, and gouges. The defects must be removed prior to beginning the actual heat straightening repair to minimize the potential for brittle fractures or crack extension during the actual repair. The second key is the selection of the heating patterns and sequences. The combination of vee, line and strip heats must be chosen to fit the damage patterns. Heat should only be applied in the vicinity of those regions in which yielding of the material has occurred. Typically, vee heats should be relatively narrow. A good rule of thumb is to limit the open end of the vee to 250 mm (10 in) for one inch thick plates. However, a smaller limit should be considered for progressively thinner plates. These limits will minimize distortion which might occur due to local buckling of the plate element.

The third key is to control the heating temperature and rate. Temperatures should be limited to 650°C (1200°F) for carbon and low alloy steels, 590°C (1100°F) for A514 and A709 (Grade 100 and 100W) quenched and tempered steels and 565°C (1050°F) for A709 (Grade 70W) quenched and tempered steel. Higher heats may adversely affect the material properties of the steel and lead to a weaker structure.

The fourth key is to control the restraining forces during repair. One of the most critical factors is the applied restraining force. Research has shown that the use of jacks to apply restraints can greatly shorten the number of heating cycles required. However, over-jacking can result in buckling or a brittle fracture during or shortly after heat straightening. To prevent such a sudden fracture as illustrated in fig. 3.1, jacking forces should always be limited. Recommended procedures to determining acceptable jacking forces are provided later in this manual. ~~The recommended procedure is to calculate the plastic moment capacity of the damaged member and limit the moment resulting from the combination of initial jacking forces and dead loads to one-half of this value.~~ Precautions should also be taken when applying restraining forces for different types of damage at one location (i.e., Category W and Category L). If practitioners do not take this precaution brittle fractures may occur. It is strongly recommended that jacks be gauged and calibrated with the maximum force limitation computed. Of course, the jacking forces should always be applied in the direction tending to straighten the beam. The execution of a heat-straightening repair that incorporates these keys must begin with the assessment of the damaged structure.

Steps in the Assessment Process

Many incidents resulting in damage to steel bridges produce an emergency situation to some degree. The first step in the rehabilitation process is to assess the degree of damage and the safety of the existing structure during a site investigation. The purpose of this section is to provide guidelines for damage assessment. These guidelines are in the form of steps required for a complete assessment. All aspects may not be required in each case. Judgment must be used when deciding if, and when, to eliminate a part of the process.

1. Initial Inspection and Evaluation for Safety and Stability

The purpose of the inspection is to protect the public and emergency service personnel. This inspection is often visual and conducted with special concern for safety. The major aspects of damage are recorded and documented with photographs and measurements. During this inspection, a preliminary list of repair options should be made. Particular attention should be paid to temporary needs such as shoring, traffic control, and other short-term considerations.

If heat-straightening is not chosen to be the repair method and/or it is anticipated that the damage will remain for any period of time, the impact area along with any welded details affected by the impact must be examined and treated. This work should be performed as early as possible and is recommended at the time of the initial inspection. Generally, treatment consists of grinding the impact area smooth of any surface nicks and/or gouges, removing any cracks revealed through inspection, and smoothing weld toes on nearby welded details that would see an increase in stress due to the localized damage or during the repair process. Micro cracks introduced during the impact may result in a severe brittle fracture during a subsequent impact, even if this does not occur at the same location.

A part of this evaluation may require a review of the design drawings and computations to determine the safety and stability of the bridge. Knowledge of the specific cause of damage may also influence the final decision on repair and should be investigated if possible. Typical damage causes are: (1) overheight or overwide vehicle impact; (2) overweight vehicles or overloads; (3) out-of-control vehicles or moving systems; (4) mishandling during construction; (5) fire; (6) blast; (7) earthquakes; (8) support or substructure movement; and (9) wind or water-borne debris.

2. Detailed Inspection for Specific Defects

The decision to conduct a heat-straightening repair depends on the type and degree of damage. Three aspects should be carefully checked: (1) signs of fracture; (2) degree of damage; and (3) material degradation.

Signs of Fracture. While some fractures are quite obvious, others may be too small to visually detect. However, it is important to determine if such cracks exist since they may propagate during the heat-straightening process. Specific attention should be placed at the impact area where severe compressive plastic deformation occurred. Micro cracks often form during the impact and inspection following the smoothing of the impact should ensure that such defects have been removed. Welded details within the vicinity of the impact area or at locations of plastic deformations caused by the impact should also be thoroughly inspected by either magnetic particle or ultrasonic methods. Any weld toe defects, such as shallow cracks or tears should be repaired by grinding. When in doubt, one of the following conventional methods can be utilized.

The use of a dye penetrant is effective in detecting cracks. The process involves first thoroughly cleaning the surface. Then a liquid dye is sprayed on the surface and permitted to stand, during which time the dye is drawn into surface discontinuities. Excess dye is then cleaned from the surface and a developing solution applied. The developer reacts with dye remaining in the cracks. The dye can be observed because of the color change.

Another procedure is to use magnetic particle inspection. A magnetic field is introduced by touching the metal with a yoke or prods. A flaw in the steel causes a disruption of the normal lines of magnetic flux. If the flaw is at or near the surface, lines of magnetic flux leak from the surface. Fine iron particles are attracted to the flux leakage and indicate the crack location.

A third procedure is ultrasonic testing by one of several techniques. These procedures typically involve the analysis of pulses passing through undamaged versus damaged material.

Finally, radiographic testing may be utilized to produce a visual image of any flaws in the material.

Degree of Damage. An evaluation of the degree of damage requires measurements to be taken. Two types of damage require measurements: (1) Overall bending or twisting of a member; and (2) localized bulges or sharp crimps. These measurements can be used to compute the maximum damage-induced strain or to determine the degree of damage. The usual procedure is to begin by measuring offsets from a taut line or straight-edge. A typical layout is shown in fig. 3.2. The idea is to use the unyielded adjacent regions as reference lines since their curvature is small in comparison to the plastic zones, or use the offsets in the damage zone to compute the degree of damage. For the first case, tangents from the straight portions define the angle or degree of damage between the tangents. If the offsets are taken in the elastic zone on either side of the damage as shown in fig. 3.2b, the degree of damage, ϕ_d, can be computed. Based on measurements taken at the site, degree of damage can be calculated as follows:

(Eq. 3.1)

where ϕ_d is the degree of damage or angle of permanent deformation at the plastic hinge and y_i is a measured offset as shown in fig. 3.2b. The length of damage, c_d, is defined by the chord connecting the tangents to the inelastically damaged region as shown in fig. 3.3. If ϕ_d and c_d are known, the radius of curvature can be computed as

(Eq. 3.2)

In some cases direct measurements of ϕ_d can be made. One procedure is to stretch two taut lines forming tangents on either side of the damage. By stretching the lines until they intersect, the degree of damage can be measured with a protractor. For small zones of damage, two straight edges can be used to produce the tangent intersections. Again, the angle of damage can be measured with a protractor. While this method may seem somewhat crude, a reasonable degree of accuracy can be obtained.

For the case the offsets are taken in the damage zone (see fig. 3.2a). The radius of curvature, R, can then be approximated as

(Eq. 3.3)

The degree of damage can then be calculated from:

(Eq. 3.4)

(Eq. 3.5)

It should be recognized that approximations are involved in using these equations. The assumption is made that the radius of curvature is constant over the entire length of the damage. However, the radius of curvature usually varies. If the damage curve is smooth, this assumption is fairly accurate. If the curve is irregular, the assumption becomes more approximate. For the more pronounced irregular curvatures, it is advisable to measure only the worst portion of the damaged region using the three point offset procedure and the calculation of radius of curvature from eq. 3.3. In general, the approaches described here give a good estimate of the radius of curvature and, consequently, strain. The use of these parameters in the design of repairs will be described in a later section.

Material Degradation. Certain aspects of material degradation will influence the decision to heat straighten. One area of concern relates to nicks, gouges and other abrupt discontinuities. Although not directly a material issue, such flaws located in the damage zone will be stress risers during the repair when jacking forces and heat are applied. If the material toughness has been decreased, these normally benign defects could lead to brittle fracture. It is recommended that such discontinuities be noted and ground to a smooth transition prior to heat straightening. This transition should be of at least a 1 to 10 slope. A second aspect relates to exposure to high temperature (such as a fire) when the damage occurred. As long as the temperature has not exceeded either the tempering temperature or the lower phase transition temperature, no permanent degradation would be expected to occur in the steel. However, if the damaged steel was exposed to higher temperatures, metallurgical tests should be performed to ensure material integrity before heat-straightening is applied. Tests that should be considered include: (1) a chemical analysis; (2) a grain size and microstructure analysis; (3) Brinell hardness tests; (4) Charpy notch toughness tests; and (5) tensile tests to determine yield, ultimate strength, and percent elongation.

Several visual signs may suggest exposure to high temperature including: melted mill scale, distortion, black discoloration of steel, and cracking and spalling of adjacent concrete. Tests can then be conducted at suspicious regions. For example, a significant increase in Brinell hardness, in comparison to undamaged areas of the same member, indicates potential heat damage. Or, for the Charpy V Notch test at 4.4° C (40 °F), a significant reduction in values over those from an undamaged specimen may indicate damage. The most definitive test is usually a micro structure comparison between damaged and undamaged pieces. Evidence of partial austenization and recrystallization into finer grain size indicates heating above the lower phase transition temperature.

Geometry of the Structure. Often the bridge configuration is available from design drawings and it is a good policy to confirm that the system does conform to these drawings. If drawings are not available, then enough measurements should be taken so that a structural analysis can be conducted if required.

Steps in the Planning and Design Process

Once the damage assessment is complete, the repair can be designed. The following steps may be required as part of this planning and design process:

- Analyze the degree of damage and maximum strains induced.
- Conduct a structural analysis of the system in its damaged configuration.
- Select applicable regions for heat-straightening repair.
- Select heating patterns and parameters.
- Develop a constraint plan and design the jacking restraint configuration.
- Estimate heating cycles required to straighten members.
- Prepare plans and specifications.

Each of these aspects are discussed in the following sections.

1. Analysis of Degree of Damage and Determination of the Maximum Strain due to Damage

Research data has shown that heat-straightening can be successful on steel with plastic strains up to 230 times the yield strain, ϵ_y, without drastically affecting the material properties of the steel. However, engineering judgment should be used for strain ratios past $150\epsilon_y$. ~~There is reason to believe that even larger strains can be repaired. However, since no research data exists beyond the $100\epsilon_y$~~ range, engineering judgment is required. In order to evaluate whether the damage exceeds this level, the maximum curvature should be measured as previously described. Shown in fig. 3.4 is a damaged beam of uniform curvature. The radius of the bend is defined as radius of curvature, R. Since strain is proportional to curvature and curvature can be computed from field measurements, it is often convenient to compare the radius of curvature to the yield curvature, R_y, expressed as

(Eq. 3.6)

where E = modulus of elasticity, F_y = yield stress, and y_y = the distance from the centroid to the extreme fiber of the element.

The radius of curvature is related to the strain by

(Eq. 3.7)

where R is the actual radius of curvature in the damaged region.

Since damage measurements are taken at discrete locations, the radius of curvature can be approximated from eq. 3.2 or 3.3. Once the smallest radius of curvature is determined in the damaged region, the maximum strain can be computed from eq. 3.7 and compared to the yield strain

(Eq. 3.8)

The ratio of maximum strain to yield strain, referred to as the strain ratio, μ, is used as one measure of the extent to which the steel has been damaged. From eqs. 3.7 and 3.8, the strain ratio is

(Eq. 3.9)

Since E is a constant for all steel grades (200,000 MPa or E = 29,000 ksi), μ can be obtained graphically in terms of the ratio R/y_{max} and F_y for various steel grades as shown in fig. 3.5. A similar approach can be used for localized bulges, buckling or crimps.

Heat-straightening repairs have been conducted for strains up to ~~$100\epsilon_y$~~ $230\epsilon_y$, or ~~$\mu = 100$~~ $\mu = 230$. Repairs may be successful at even greater strains. However, research studies have not included strains in excess of ~~$100\epsilon_y$~~ $230\epsilon_y$. Engineers should use judgment in straightening beyond this range. Also, fire damage involving high temperature may be an exception to this limit. If the distortion is due to fire, it is probable that material properties have been affected. Repair decisions should be based on metallurgical analysis and engineering judgment as well as strain limitations.

As a rule of thumb for single curvature bends with a plate depth about the axis of bending of up to 305 mm (12 in), if the degree of damage is less than 12°, it is not necessary to measure for maximum strain. The only exception would be if the region of damage were concentrated over an extremely short length resembling a sharp crimp as opposed to a plastic hinge type of bend.

Example 3.1

2. Conduct a Structural Analysis of the System

The strength of the damaged structure is usually evaluated by a structural analysis. This analysis serves two purposes: (1) to determine the capacity in its damaged configuration; and (2) to compute residual forces induced by the impact damage. The analysis can be based on the undeformed global geometry except when the displaced geometry of the frame or truss system (after damage) results in changes in internal forces by more than 20 percent. However, even if undeformed geometry is used in the analysis, the deformed geometry should be used when computing the member stresses. The allowable

stresses should be based on the original properties of the material. (The deformed geometry refers to global member deformations and not local severe bending as is sometimes present at the point of impact.)

When a member has a significant change in shape due to damage, the section properties should be modified when calculating stresses. While each specific application must be considered on an individual basis, some general guidelines can be developed. Assuming that no fractures have occurred, bending and compression members are the most critical to evaluate. Forces due to applied loads in tension members tend to straighten out-of-plane damage (and are thus self-correcting), while such forces in bending or compression members tend to magnify the damage.

Change in cross section shape. The primary variable in evaluating the stress level for a damaged bending member is the section modulus. Typically, the most serious strength reduction is due to deformations resulting from twisting or lateral distortion of the cross section. A good example is an impact on the bottom flange of a bridge girder by an over-height vehicle. Two ideal cases are evaluated here for two wide-flange sections. As shown in figs. 3.7 and 3.8, the damage is assumed to produce a rotation of the web about the juncture of the web and top flange. The bottom flange is modeled in two ways: either it remains parallel to the top flange, or it remains perpendicular to the web. Actual combinations of damage often fall between these two conditions. Plotted in fig. 3.7 and 3.8 are the variations in the selection modulus (for bending about the strong axis) associated with different levels of damage for two beams: a W24×76 and W10×39. The case of the bottom flange remaining perpendicular to the web is the more critical case for the comparison of section modulus values. As can be observed, the section modulus dips fairly rapidly with an increase in the cross section rotation. A 10° rotation results in a strength reduction within the range of 8–15 percent, depending on the section, while at 20°, strength reduction is between 18 and 29 percent. Although an engineer should evaluate the specific conditions and configuration of each case, a good general guideline is to repair the member if the section modulus is reduced by 10 percent. This level of damage typically corresponds to a rotation of approximately 10°. In reference to the field tests conducted on the W10×39 and W24×76 beams as described in Chapter 7, the damage induced was considered to be moderate. In both cases the flange remained almost perpendicular to the web. The calculated bending strength reduction for the W10×39 beam was calculated in the range of 25 percent. The reduction for the W24×76 beam was on the order of 9 percent.

P-Δ Effects. For compression members, the square of the minimum radius of gyration is the section property associated with the strength of the member. The effect of the two idealized cases of damage previously described is plotted in fig. 3.9 and 3.10. In this case, the configuration in which the bottom flange remains parallel to the top flange is the more critical. The curves are very similar for both wide-flange sections. The reduction in strength, as measured by the square of the radius of gyration, is not quite as large as the corresponding case for section modulus. The reduction is only about 5 percent for the 10° rotation and about 14 percent at 20° rotation. However, another aspect that must be considered when evaluating compression members is the strength reduction due to the P-delta effect. If a simply supported column has an initial midpoint deflection, y_o, due to impact damage, then the deflection (and bending moment) is amplified according to the amplification factor.

(Eq. 11.6)

where P is the axial load and P_{euler} is the Euler buckling load. This factor is taken into account in design codes by an adjustment in the safety factor for columns.

Consider the AISC code (1989), for example. The long column formula (eq. E2-2) is the classical Euler buckling formula, divided by a safety factor of 23/12. Conversely, the safety factor for tension members is given as 5/3. The reason for the higher safety factor for compression members is to account for the P-delta magnification effect. A plot of the amplification factor is given in fig. 3.11. As the load approaches the critical buckling load, the deflection (and consequently the moment) approaches infinity. Failure must therefore be defined as the point where the deflection (and consequently the moment) remains finite but becomes excessively large. The safety factor for column buckling was therefore increased by 0.25 above that used in tension members. As can be seen from fig. 3.11, this extra safety factor accounts for 0.08 of the total load ratio reduction to allowable values. In deciding upon this value, it was assumed that relatively small initial values of lateral deflections would exist due to lateral loads or fabrication imperfections, e.g., within the elastic range. When a compression member has larger permanent deformations well into the plastic or strain-hardening range due to damage, then the effective strength of the member is reduced by a larger factor than expressed by even the column safety factor.

In light of these considerations, even relatively small permanent deformations should be repaired for compression members unless additional bracing is added or a stability analysis is performed to justify that the strength reduction is small.

Residual forces. The analysis of residual forces in damaged systems requires a plastic analysis. To illustrate the procedure, a bridge girder laterally supported by diaphragms will be used. For lateral impact, such as might occur with an over-height vehicle, the girder acts as a continuous beam with the diaphragms as interior supports. If an impact load occurs, the lower flange has positive bending at the impact point and negative bending at the adjacent diaphragm supports. A lay-

out modeling this type of girder is shown in fig. 3.12. During impact, it is assumed that plastic hinges form at the impact point and at adjacent supports. These hinges form a mechanism from which the impact load can be computed. Using a plastic analysis, the load, P_u can be calculated and a moment diagram constructed, fig. 3.12b. The impact load is now applied in the reverse direction and an elastic analysis performed, fig. 3.12c. The superposition of these two diagrams (b and c) give the residual moments due to the impact which produces plastic deformation; fig. 3.12d. These resulting moments should be assessed in combination with other loadings such as the live and dead load on the bridge.

The effects of previous impacts, should they exist, must be considered in the evaluation. There have been a few examples in the field and in the laboratory where brittle fractures propagated from previously damaged areas not directly impacted during the more recent impact.

3. Select Regions Where Heat Straightening is Applicable

While the primary consideration for allowing heat-straightening repair is the degree of damage limitation, other criteria may also influence the decision. Of particular importance is the presence of fractures or previously heat-straightened members. A fracture may necessitate the replacement of part, or all, of a structural member. In some cases it may be feasible to heat-straighten the suspect region and then repair it in place by mechanical connectors. In other cases a portion of the member may be replaced while the remainder is repaired by heat straightening.

An example of combining heat-straightening with replacement is when one or more girders are impacted by an overheight vehicle. This type of accident often displaces the bottom flange. If the impact point is near diaphragms, the diaphragms are often severely damaged. An example is shown in fig. 3.13. It is usually much more economical to simply replace a diaphragm rather than taking a lengthy time to straighten it. The recommended procedure is to remove the diaphragm (especially if it would restrain desired movement of the member) heat-straighten the girder, and then replace the diaphragm with a new one.

In general, heat-straightening can be applied to a wide variety of structural members. However, some have cautioned about straightening fracture critical members (Shannafelt and Horn, 1984). Research has been conducted on the fatigue and fracture performance of steel bridge girders (NCHRP 10-63). Research has shown that a heat-straightening repair may be conducted up to three (3) times without adversely affecting the material properties or the fatigue performance of steel bridge members. However, the research recommended that the number of repair cycles be limited to two when impacts occurred at the same location. ~~Although there is no research data to support a ban on heat-straightening fracture critical members, practically no fatigue testing has been conducted.~~ If careful control of heating temperature (including the limits imposed by section 12.12 of the AASHTO/AWS D1.5 Bridge Welding Code) and jacking forces are maintained, and if notches and nicks are ground smooth, there is no reason to expect problems. It is recommended that additional care be used for fracture critical members to insure that the heat straightening is properly conducted.

4. Select Heating Patterns and Parameters

Typical Heating Patterns. The fundamental heating patterns have been described in Chapter 2. Since typical damage is often a combination of these fundamental damage types, a combination of heating patterns is often required. The key is to select the combination of patterns to fit the damage. When in doubt, a good policy is to address the attention to one of the basic heating patterns at a time. For example, remove the Category W damage prior to addressing the Category L damage. It should be noted that with proper combinations, several types of damage can be removed expeditiously. For example, suppose that a wide flange section is impacted such that the bending occurs about an axis at an arbitrary angle to the principal axes, i.e., bending occurs about both the strong and weak axis. The heating pattern, fig. 3.14, requires a vee heat on the web to restore the strong axis damage and vee heats on the flanges to restore the weak axis damage. The heats should be executed sequentially as numbered in fig. 3.14. Note that no strip heat is required on the web since a vee is used there. Restraining forces should be used to produce bending moments about both the strong and weak axis as indicated in fig. 3.14 tending to straighten the damage. Once the damage is corrected about one of the principal axes, the heating pattern should revert to one of the fundamental patterns until straightening is complete about the other principal axis.

As a second example, consider a wide flange beam with weak axis bending damage combined with a local bulge in one flange. The heating pattern is shown in fig.3.15. Vee heats are used on the top and bottom flanges along with a web strip heat similar to the standard weak axis pattern. However, partial depth vees are used on the flange with the bulge along with a series of line heats along bulge yield lines. Since a yield line is likely to occur at the lower web fillet, a line heat is also needed on the web. Restraining forces are used to create bending moments about the weak axis as shown in fig. 3.15. In addition, a jacking force should be applied on the local bulge as shown on the cross section in fig. 3.15. The sequence of heats is also indicated in the figure.

A third example is damage resulting from impact of a composite bridge girder which produces weak axis damage to the

bottom flange and twisting due to the restraint of the top flange. The heating pattern is shown in fig. 3.16 consisting of a bottom flange vee heat, a web strip heat and a line heat at the top fillet of the web. The heating sequence is shown in fig. 3.16 as well as the restraining moment required on the bottom flange.

A final example is the case of multiple plastic hinges formed about the weak axis such as might occur for a beam continuous over interior supports. The heating pattern is shown in fig. 3.17. Note the reversed direction of the vees to reflect the multiple curvature damage. The restraining moments must also reflect the reverse curvature nature of the damage as shown in the figure.

Vee Depth. In general the vee depth should be equal to the width of the plate being straightened. Partial depth vees provide no advantages in reducing shortening as some have speculated. The primary situation for half depth vees is in the repair of local damage.

Vee Angle. The angle of the vee is usually limited by practical considerations. It should be as large as practical for the specific application. If the open end of the vee is too wide, out-of-plane distortion often occurs. Likewise the vee area should be small enough to heat quickly so that differential cooling is limited. A good rule of thumb is to limit the open end of the vee to approximately one-third to one-half the plate width but not greater than 254 mm (10 in). These limits translate roughly to 20–30° vee angles. If the width of the open end of the vee, V, is selected, the vee angle is

(Eq. 3.10)

where W is th.e plate width.

Number of Simultaneous Vee Heats. Simultaneous vee heats may be performed with proper spacing. It is recommended that the vees be spaced at least one plate width, W, apart. Also, if multiple plastic hinges occur, each hinge may be heated simultaneously.

5. Develop a Constraint Plan

Since jacking forces can expedite repairs, it is recommended that such forces be utilized. Jacks should be located to produce their maximum effect in the zones of plastic deformation. It is recommended that jacks always be gauged and calibrated prior to use. Also, jacks must be properly secured so they will not fall out as pressure subsides during cooling. The loads applied to the structure should always be known and limiting values established. A jacking arrangement for a composite girder bridge is shown in fig. 3.18. Lateral forces are utilized on the lower flanges, fig. 3.18a, while jacks between flanges are used for local damage, fig. 3.18b.

For cases where residual moments are small, the jacking moment, M_j, should be limited to

(Eq. 3.11)

where M_p, is the plastic moment capacity of the member.

For cases where residual moments exist, the jacking moment should be limited to

(Eq. 3.12)

where M_r, is the residual moment and is positive when tending to straighten the member. Residual moments will be relieved during the first few heats. Rather than computing residual moments, an alternative is to use a jacking moment of only $\frac{1}{4}M_p$ during the first two cycles.

On occasion, a hairline fracture will occur or become visible during an intermediate cycle of heat-straightening repair. Instrumentation of Category L damage present in the flange has shown that horizontal forces used to remove Category W damage caused hairline fractures in the vicinity of the Category L damage regions (NCHRP 10-63). Although it was initially believed to be the vertical forces used to remove Category L damage, it was actually the horizontal forces being applied to the member. The presence of the Category L damage geometry produced secondary bending stresses when the horizontal forces used to remove the Category W damage are applied.

During the analysis of the member, the presence of the Category L damage must be considered when determining the restraining forces. To prevent this cracking either remove the Category L damage first prior to applying horizontal forces or reduce the horizontal force if both categories of damage are to be repaired simultaneously. A reasonable approach developed during NCHRP 10-63, is to reduce the horizontal force by 1% for every 1 increment of damage past the yield strain of the Category L damage. The approach proved successful in all cases when used. For example, a bulge in the flange due to the impact has a strain ratio of 65, thus the horizontal force determined without taking into consideration of the Category L damage must be reduced by 65%. For strain ratios over 100, the Category L damage must be removed or partially removed (geometry with a strain ratio less then 100) prior to applying horizontal force. As the Category L damage is removed, the horizontal forces may be increased up to 100% of the calculated once the Category L damage is completely removed. ~~The causes are believed to be: (1) excessive restraining forces being applied during the heating process; (2)~~

Another cause is believed to be repetitive repair of a redamaged element; and/or ~~(3)~~ the growth of micro cracks initiated during the induction of damage. As the presence of Category L damage ~~item (1)~~ is the primary cause, restraining forces

should always be specified at safe limits and should be monitored during actual repair. As for multiple repairs, the ~~For item (2) the repair of previously heat straightened~~ material should be limited to only two damage/repair cycles.

One problem associated with the computation of jacking forces is that for indeterminate members, the bracing, diaphragms or other attachments may be difficult to model. In addition, it is sometimes necessary to make an estimate in the field as to the magnitude of jacking forces. The jacking force limit can be approximated by measuring the deflection when the force is applied. Since end support restraint conditions will fall between the two ideal cases of simple and fixed supports, the deflection can be calculated by estimating the degree of restraint. The deflection that produces a maximum stress equal to 50 percent of yield for 248 MPa (36 ksi) yield strength steel on a center point loaded member can be expressed as:

(1) For 248 MPa (36 ksi) steel
  (a) Simple supports

(Eq. 3.13)

  (b) For fixed supports

(Eq. 3.14)

(2) For 345 MPa (50 ksi) steel
  (a) Simple supports

(Eq. 3.15)

  (b) For fixed supports

(Eq. 3.16)

where l is the clear span length and y_{max} is the distance from the centroid of the steel section to the extreme fiber. A safe jacking force should produce a midpoint deflection within the range of these two values, depending on the level of end restraints.

Example 3.2

6. Estimate the Heats Required to Straighten the Members

The estimate of number of heats provides a time line for the project. Comparing the estimated movement with the actual movement as it progresses also indicates whether the heating is being properly done. The number of heats, n, can be completed as

(Eq. 3.17)

where ϕ_p is the predicted plastic rotation per heat and ϕ_d is the degree of damage. Formulas for the plastic rotation associated width various structural shapes and damage conditions are provided in the Part II of this manual.

7. Repair Plans and Specifications

The final step is to prepare plans and specifications for the project. These plans will be the supervisor's guide as well as the contractor's directive. Suggested specifications are given in Chapter 12.

Example 3.3

Supervisor's Responsibilities

Preparation of the area to be repaired. It has been shown that small nicks and gouges produced during the impact can propagate and lead to brittle fractures during the repair process. In addition, small defects and hairline cracks can develop at weld toes as the repair proceeds. Thus, the supervisor must ensure that all nicks and gouges be ground smooth and weld toes be ground smooth to reduce the stress concentration at the toe prior to beginning the repair process.

Monitoring the temperature. Excessive temperatures may cause surface damage or lead to increased brittleness. Temperature can be monitored in several ways. One of the most accurate is to use temperature-sensing crayons. These crayons melt at a specified temperature and are available in increments as small as 14°C (25°F) (fig. 3.20). By using two crayons that bracket the desired heating temperature, accurate control can be maintained. The crayons will burn if exposed directly to the flame of the torch. Therefore, the torch must be momentarily removed (one or two seconds) so that the crayons may be struck on the surface. An alternative is to strike the crayon on the backside at the point being heated.

Another temperature monitoring method is to use a contact pyrometer (fig. 3.21). This device is basically a thermocouple connected to a readout device. It can be used in a matter similar to a temperature crayon by placing it on the surface. Because the pyrometer relies on full contact with a smooth surface, the readings vary with position and pressure, typically underestimating the actual temperature. It is recommended that the pyrometer be calibrated with temperature crayons prior to using.

Infrared devices are also available. These devices record the temperature and provide a digital readout.

To complement the crayons, pyrometer, or infrared devices, visually observe the color of the steel at the torch tip. Under ordinary daylight conditions, a halo will form on the steel around the torch tip, fig. 3.22. At approximately 650°C (1200°F) this halo will have a satiny silver color in daylight or

bright lighting. The observation of color is particularly useful for the technician using the torch to maintain a constant temperature. However, this is the least accurate method of monitoring temperature and is approximate at best.

Controlling restraining forces. Another concern for the heat-straightening supervisor is the control of restraining forces. Typically hydraulic or mechanical jacks are used to apply restraining forces (see fig. 3.23 as an example) and should be calibrated so that the force being exerted can be determined. The maximum allowable force should be computed as part of the design process and specified in contract documents.

Approving Heating Patterns. The supervisor should approve the heating patterns and torch paths used. The general patterns can be set as part of the design of the repair. However, as heating progresses there may be a need to modify the patterns. In addition, the supervisor should continuously inspect, using the appropriate techniques, for the development of cracks at susceptible locations. The supervisor should understand the principles for using various patterns and approve modifications on site as required.

Checking Tolerances. A significant concern is the tolerance for the completed repair. The contract documents should specify the allowable tolerances and the supervisor should verify that these limits either have been met or where (and why) exceptions were accepted. Research has been conducted in NCHRP Project 10-63 on the acceptable tolerances of a completed repair. The presence of Category L damage in the flange can cause secondary stresses which my increase the in-service stress at that location. This is of importance if remaining damage is near a welded detail, especially more severe fatigue categories (such as D, E, and E′). In an attempt to estimate the effect of residual damage, an analytical solution was developed based on the results of a finite element parametric study conducted as a pilot study as part of NCHRP 10-63. The resulting empirical equation, shown below, is useful for determining the acceptable tolerance of a repair. The development of the equation is present in the NCHRP report summarizing that work.

$$SAF = \left(\frac{(1.35\ln(H) + 4.25)t_f^{-.06} - 1.2}{-\ln(40H^{0.43})} \right) \ln(L) + (1.35\ln(H) + 4.25)t_f^{-.06} + 0.1H(b_f - 10)$$

where, the height of the residual damage, H, inches, the length of the residual damage, L, inches, flange thickness, t_f, inches, and flange width, b_f, inches.

While tolerance levels similar to that of new construction may be used, often a looser tolerance level may be used to reduce the number of heat cycles required, especially in restricted areas and to minimize the cost of the repair. This decision should be made as part of the design process.

The above items relate specifically to heat straightening. The supervisor should also exercise normal control of the job site, as with any construction project, including monitoring of safety procedures.

Common Mistakes to Avoid

Because heat straightening has evolved as an art form, many practitioners have developed some skills. Most of these craftsmen have worked in steel fabrication or erection and many are experienced welders. They know methods to remove distortion in steel. However, many of their techniques are not heat straightening. The most common mistakes are:

Mistake No. 1: Heating the Steel Until it is Cherry Red

Such an approach is dangerous because the steel may pass through both the lower critical and the upper critical temperatures. The heating/cooling cycle may not result in a reversible molecular change. The heat-straightened steel may have brittle characteristics and not be suitable for bridge applications. Use temperature crayons to verify the heating temperature.

Mistake No. 2: Excessive Restraining Force Before Heating or Jacking the Girder Straight While it is Hot

Over-jacking can lead to a sudden brittle fracture. It may also result in micro cracks not readily visible which will weaken the structure. All jacks should be gauged and the forces limited to safe levels well below the material yield stress.

Mistake No. 3: Heating Too Large an Area

Some feel that the more surface area heated the better. However, the principle of heat-straightening is to allow differential heating followed by contraction during cooling to move the steel. Heat-straightening is most effective when small regions are heated. Narrow vee, strip or line heats, with unheated metal in between minimizes overall expansion yet allows contraction cooling to take place. In fact, heating too much area may prevent heat-straightening.

Mistake No. 4: Heating Outside the Yield Zones

The goal of heat straightening is to gradually restore the yield zones to their original configurations. By limiting heat to only the vicinity of these areas, the damage mechanism is reversible. Heating in nonyielded regions often results in a misaligned structure.

Mistake No. 5: Using Inefficient or Improper Heating Patterns

Certain heating patterns have been shown to be particularly effective: vee heats on major axis plate element bending, line heats for minor axis bending, and strip heats on stiffening elements. An understanding of the role of each heating pattern is essential to effective heat straightening.

Mistake No. 6: Not Conducting a Proper Inspection and Surface Preparation Prior to Initiating the Heat Straightening Repair

To minimize the likelihood of the development of fractures initiating from nicks and gouges as well as cracks developing at weld toes as the repair process proceeds, it is critical to fully inspect the damaged location and grind smooth any surface defects, such as nicks and gouges produced by the impact. In addition, weld toes should be ground smooth to minimize the likelihood of the development of hairline cracks at these locations.

Checking Procedures for Supervisors

Remember that the goal is not just to straighten the damage, but to straighten it safely. There are a number of checks that should be made by the supervisor as the repair progresses.

1. Review and approve all heating patterns prior to initiating the repair.
2. Ensure all surface nicks and gouges have been ground smooth whether or not a heat-straightening repair will be performed.
3. Periodically check the jack gauges to insure that excessive force is not being used.
4. Periodically monitor the temperature using temperature sensing crayons, a contact pyrometer, or other sensing device.
5. Periodically check to ensure no cracks are growing.
6. Constantly observe the color of the steel at the torch tip. In normal daylight lighting, the steel should have a satiny silver halo at the tip. At night or in heavy shadows, a slight dull red glow may be visible.
7. Establish reference points from which to measure movements. A taut line is useful although it must be moved aside during heating. In smaller regions a straight edge may be used. Sometimes it is convenient to measure from a fixed part of the adjacent structure which will not move during the straightening process.
8. Always be sensitive to safety issues since the work is usually performed with at least some vehicle lanes open. Insure that jacks and other equipment are secured from falling.
9. Final approval should be based on meeting the specified tolerances.

Key Points to Remember

- The engineer's role is to design the repair.
- The field supervisor monitors the repair process to insure it meets plans and specifications.
- The contractor implements the design.
- Communication is essential between engineer, supervisor and contractor.
- Keys to a successful repair include:
  - Selection of appropriate heating patterns and sequences.
  - Controlling the heating temperatures and rates.
  - Using suitable restraining forces.
- Damage assessment includes:
  - Initial inspection and evaluation for safety and stability.
  - Detailed inspection for specific defects such as signs of fracture and material degradation.
  - Taking measurements to characterize damage.
  - Determining the cause of damage.
  - Determining the presence of cracks, tears or other problems not amenable to heat-straightening repair.
  - Grinding/smoothing any surface nicks and gouges whether or not a heat-straightening repair will be performed.
- Steps in the planning and design process include:
  - Analysis of degree of damage and determination of maximum strain due to damage.
  - Conducting a structural analysis of the system.
  - Selecting regions where heat-straightening is applicable.
  - Selecting heating patterns and parameters.
  - Developing a constraint plan.
  - Developing repair plans and specifications.
- Supervisor's responsibilities include:
  - Monitoring the heating temperature.
  - Monitoring restraining forces.
  - Approving heating patterns.
  - Checking Tolerances.
  - Continued use of NDT to verify quality of the repair or to verify no cracks are initiating or propagating. This may need to be done throughout the repair process.
- While some rational limitations exist when considering the heat-straightening option, engineering judgment is an essential ingredient for a successful repair.

Proposed Revisions to Chapter 4

There are several proposed revisions to Chapter 4. In light of this, all of the text from Chapter 4 is reprinted below with the deleted and added text shown as strikethrough and underlined, respectively. The original figures, tables, and equations are not to be revised and are not included for brevity.

Chapter 4 Effects of Heating on the Material Properties of Steel

Introduction

The potential for detrimental effects from heating damaged steel has limited the implementation of heat straightening. However, with an understanding of the properties of steel, heat straightening can be safely conducted. Heating steel reduces the yield stress as well as the elastic modulus but the coefficient of thermal expansion increases with temperature. The behavior of these parameters complicates attempts to understand the response of steel to heat straightening. In addition to these short-term effects, heat can result in long-term consequences which may be detrimental.

The large majority of steels used for bridge construction in the United States are either carbon, low alloy steel, or those steels designated as 'HPS' according to ASTM A709. At ambient temperature, these steels have three major constituents: ferrite, cementite and pearlite. The iron-carbon equilibrium diagram shown in fig. 4.1 illustrates the relationship of these components. Ferrite consists of iron molecules with no carbon attached, cementite is an iron-carbon molecule, (Fe&); and pearlite is a mixture of cementite (12 percent) and ferrite (88 percent). A low carbon steel has less than 0.8 percent carbon, too little carbon to develop a 100 percent pearlite compound, resulting in pearlite plus free ferrite molecules. High carbon steels (carbon content between 0.8 and 2.0 percent) have more carbon than required to form pearlite, resulting in a steel with additional cementite. Low carbon steels tend to be softer and more ductile because these are characteristics of ferrite. Cementite is hard and brittle thus high carbon steels are harder and less ductile.

Temperatures greater than about 700C (1300F) begin to produce a phase change in steel. This temperature is often called the lower critical (or lower phase transition) temperature. The body centered cubic molecular structure begins to assume a face centered cubic form. With this structure, a larger percentage of carbon will be carried in solution. When steel cools below the lower critical temperature, it attempts to return to its body centered structure. Since this change requires a specified time frame, rapid cooling may not permit the complete molecular change to occur. Under these circumstances, a hard, strong and brittle phase called martensite occurs. The steel in this form may have reduced ductility and be more sensitive to brittle fracture under repeated loads.

The upper critical (or upper phase transition) temperature is the level at which the molecular change in structure is complete. At this temperature (around 8 15 925°C or 1500–1700°F for most steels, depending on carbon content) the steel assumes the form of a uniform solid solution called austenite. It is at temperatures between the lower and upper critical that a wide range of mill hot rolling and working can occur. As long as the temperature is lowered slowly in a controlled manner from these levels, the steel assumes its original molecular configuration and properties. This temperature control is more difficult to maintain at a fabrication shop or in the field Residual Stresses in Heat-straightened when conducting heat straightening repairs.

Consequently, if the temperature during heat straightening is not kept below the lower critical temperature, undesirable properties may be produced during cooling. It is this concern that has limited the application of heat straightening in many cases. A related issue is the question of residual stresses. When heated steel cools, the surfaces having the most exposure to the cooling environment contract more rapidly. This unequal contraction produces the residual stresses found in most steel shapes and it is important to understand how heat straightening affects these residual stress patterns. The purpose of this chapter is to first provide data on the residual stress patterns of heat-straightened steel, and second, to provide a summary of how heat straightening affects material properties.

Residual Stresses in Heat-straightened Plates

Although residual stresses are often mentioned in literature on heat straightening, there has been little documented research in this area. Past research was conducted in the context of heat curving (not heat straightening), and thus is somewhat limited in its applicability to heat straightening. Some of the most notable research was conducted at the University of Washington (Roeder 1985), where a finite element model was developed to predict the local behavior of a plate element subjected to a vee heat. Residual stresses were estimated using the model and experimental strains were also measured. An example of Roeder's results are shown in fig. 4.2.

Experimental research was conducted (Brockenbrough 1970b) to back up earlier theoretical residual stress studies (Brockenbrough 1970a) on heat-curved plate girders subjected to line heats. These stresses, determined by the "sectioning method," were reasonably consistent with the theoretical values. Similar theoretical methods were used on vee-heated plate elements (Nicholls and Weerth 1972) and on wide flange beams (Horton 1973). However, the results were not supported by any experimental data.

Significant residual stresses occur in most structural steel members. Such stresses usually result from differential shrinkage during cooling in the manufacture of both rolled and welded built-up shapes. However, the cutting and punching process during fabrication may also produce residual stresses. Residual stresses are quite high and values may reach 50 percent of yield for some rolled shapes and approach yield for some welded built-up members. With one exception, residual stresses have been neglected in code requirements governing steel design. The reasons for neglecting residual stresses relate

to two characteristics: (1) The ductility of steel allows for a moderating redistribution of residual stresses when a member is subjected to large loads, and (2) since residual stresses are self-equilibrating, large compressive stresses at one location on a cross section are balanced by tensile stresses at another location. As a consequence, the stresses at a specific cross section produced by applied loads is additive to the residual stresses at some points and are subtractive at others. The result is that the ultimate strength of a member is usually not affected by residual stresses. The exception is compression members in which high residual stresses may reduce the buckling strength. American design codes account for residual stresses in compression members by assuming an average residual stress value of 50 percent of the yield stress. This assumption may lead to somewhat conservative designs for rolled shapes (which have smaller residual stresses) and slightly less conservative designs for welded built-up shapes (which have larger residual stresses). European codes have adopted the multiple column curve approach in which different formulas are used depending, on the magnitude of residual stresses. For these codes the level of residual stress affects the design capacity.

Avent, Robinson, et. al. (1993) have conducted research to provide insight as to whether heat straightening produces some negative effects due to residual stresses. The study included: both plates and rolled shapes; variations in vee angle, vee depth and level of external restraining forces; and degree of initial damage. Residual stress patterns were determined by using the "sectioning method," a well-established, but destructive procedure. After taking initial distance measurements between two fixed points on the steel, a narrow strip containing these points is cut out (by milling to avoid heating the steel). The distance is measured again and the change reflects the magnitude of residual stresses in that strip. Practical considerations limit strips to approximately % in width and changes in length are quite small over the gauge lengths required; typically 4 in. These considerations limit the accuracy of the process. However, the results provide a reasonable assessment of residual stress patterns after heat straightening. For all residual stress values given in this chapter, a positive sign denotes tension and negative denotes compression stresses.

An unheated plate (Plate UH) was tested for residual stresses to provide the basis for determining changes resulting from vee heats. Stresses found in each strip are plotted in fig. 4.3. The values are fairly low and the shape compares reasonably well with standard residual stress assumption and previous experimental measurement (Avent and Wells 1982). A series of $100 \times 6 \times 610$ mm ($4 \times */4 \times 24$ in) long, initially straight A36 steel plates were vee heated four times each. The heating parameters are shown in table 4.1, Residual stresses were measured across the vee heated zone for each plate with the 102 mm (4 in) gauge length centered on the vee for each strip. A distinction can be made by classifying "small vee angles" as those being less than or equal to 60″ and "large vee angles" as those greater than 60′. These two categories have significantly different magnitudes of residual stresses, especially at the edges. The averages of all plates within each category are shown in fig. 4.4. The smaller vees exhibited considerably higher compressive stresses at the edges.

The residual stress patterns in all of the plates were similar in shape to Roeder's theoretical distribution (fig. 4.2), where normalized values were used. An evaluation of the individual results indicates that most vee heat parameters had little effect on residual stresses. The exception was that the largest vee angle cases (82″) had maximum stresses of 40–60 percent less than those with smaller vee angles. However, for vee angles from 20–60°, the residual stress variation was small. Similarly, neither the jacking ratios nor depth ratios significantly influenced residual stresses. In all cases, the distribution of residual stresses was symmetrical. Thus, with the exception of vee angle, it appears that the heating/cooling cycle is the primary factor influencing residual stresses. Since the entire cross section was elevated to the same temperature, the residual stress distribution tended to be symmetrical. In comparison to the unheated plate, the maximum stresses were found to be over 100 percent larger. For vees in the 20–60″ range, the maximum compression residual stresses were on the order of 172 MPa (25 ksi).

A second series of $100 \times 6 \times 610$ mm ($4 \times ′/4 \times 24$ in) long plates were initially damaged and then heat straightened. The parameters are shown in table 4.2. After straightening, average residual stresses were determined by the sectioning method for three different regions on the damaged plated: Regions A, B, and C (see fig. 4.5). Typically, eight strips were cut from each plate. The plates were classified in groups of small degree of damage (6″) and large degree of damage (12 to 24″) where degree of damage, (pd, is defined as shown in fig. 3.3. These two groups experienced slightly different residual stress patterns. The small degree of damage classification exhibited a maximum strain ratio (eq. 3.9) of approximately 30 times yield strain and the larger degree of damage cases 80 to 100 times yield strain. The residual stress distributions for both cases are shown in figs. 4.6 and 4.7.

Since all of these plates had significant damage, a large number of heats (25 100) were required to straighten them. It appears that the repetitive heating tended to reduce the residual stresses in comparison to the undamaged heated plates. All but one of the five plates exhibited the parabolic distribution predicted by Roeder (1985). The exception (plate II) had compression stresses at the center as well as the edges. As a result the average values for the two plates with the 6″ damage did not follow the expected pattern. For all cases the maximum compressive stresses at the edges ranged between 83–179 MPa (12–26 ksi) and, the tensile stresses ranged between 55–83 MPa (8–12 ksi). The stresses were computed using the commonly

assumed value of 200,000 MPa (29,000 ksi) for the steel's modulus of elasticity (E). It should be noted that a few of the gage holes were destroyed in the stripping process, thus rendering the strips unreadable. Based on the measured residual stresses,' a theoretical model can be developed by assuming the distribution to be parabolic. With a maximum tensile stress of 69 MPa (10 ksi) and a maximum compressive stress of 138 MPa (20 ksi), the residual stresses can be approximated by

(Eq. 4.1)

Residual Stresses in Rolled Shapes

Residual stress patterns have been experimentally determined for some representative samples of angles, channels and wide flange sections. The geometry of the shapes prevented measurements with the extensometer on both sides of certain strips. However, the continuity and consistency of the values indicate that by just measuring one side, sufficient accuracy was obtained. The residual stress values for angles are shown in fig. 4.8–4.11. The strip number locations are shown in the figures along with the location of the vee and strip heats.

In the two originally undamaged angles (figs. 4.8 and 4.9), the residual stress patterns were quite similar. Somewhat higher compressive stresses were found at the edges in Fig 4.9. The only difference between these two specimens was the vee angle used (20″ and 45″, respectively). For these two cases the apex of the vee was located at the toe of one leg and a strip heat was used on the opposite leg.

The residual stresses for a 4×4~114 angle that was damaged and then heat straightened is shown in fig. 4.10. An interesting fact is that the damaged angle specimen exhibited the same pattern of residual stresses as the undamaged angles although the damaged angle had somewhat higher values. For this case, the apex of the vee was located at the heel of one leg and a strip heat was not required on the opposite leg. It is apparent that the heating/cooling process in the angles results in quite high (around 280 MPa or 40 ksi) compressive stresses near the toes, regardless of the location of the vee apex, relative to the stiffening element. For each of these cases the residual stresses were large compressive values at edges and comers and somewhat smaller tensile forces over the central portion of each cross section element.

The residual stress pattern for an unequal leg angle is shown in fig. 4.11. The angle was damaged and straightened with vee heats on the long leg. Since the apex of the vee was at the heel, no strip heat was required on the stiffening leg. Here the pattern varied from the equal leg angles, although the maximum values were of similar magnitude (approximately equal to the yield stress).

Of primary importance is the observation that residual stresses in heat straightened angles are quite high and approach yield stress at some points. While the distribution of these stresses may vary, the magnitudes are similar to that of welded built-up shapes.

The residual stresses for a category S heating pattern on an originally undamaged C 6×8.2 channel are shown in fig. 4.12. The pattern is not as well defined as for angles. However, significant residual stresses were found with the magnitudes approaching the yield stress.

Residual stresses were also experimentally determined in the heated region of W 6×9 wide flange beams using the sectioning method. In all of the beams, eight strips were cut from each flange, and six strips were cut from the web (see figs. 4.13 and 4.14). The shape of the extensometer used to measure the gage lengths prohibited obtaining stresses in the web within about 1.5 inches from either of the flanges, thus limiting stress reading to six strips.

An unheated specimen (Beam UH) was tested for residual stress (fig.4.15), to compare with the heated specimens. These stresses closely matched a plot of the residual stresses in a roller straightened W6×20 shape shown in the Structural Stability Research Council's "Guide to Stability Design Criteria for Metal Structures" (1976). Roller straightening (or rotorking) is a common mill practice for straightening small wide flange shapes to meet sweep and camber tolerances. The process redistributes and greatly reduces the initial residual stresses in the flanges (a characteristic evident in Beam UH, where these stresses are quite low).

Eight undamaged W 6×9 wide flange beams were heated using the standard patterns (five Category S and three Category W). Four heats were conducted for each beam. The heating parameters are shown in table 4.3. Plots of the residual stress patterns are shown in figs. 4.16–4.23. From the residual stress patterns in the heated undamaged beams, the following observations are made:

- The residual stresses are greatly increased when vee heats are applied to undamaged beams. The maximum values equal yield for Category S and approximately one-half yield for Category W heats.
- The patterns were significantly different in the Category S and Category W heated specimens.
- Jacking ratio and depth ratio were again found to not significantly change the stress patterns, when all other parameters were held constant.
- By classifying the 20- and 30-degree vee angles as small and the 45 degree vee angles as large, there were significant pattern differences in the two classifications in the Category S specimens (no significant difference in Category W specimens).

Four W 6×9 wide flange beams were bent about their weak axis (Category W) and repaired using the standard patterns.

All beams were repaired with % depth, 45″ vees and a jacking ratio of 50 percent.

A unique part of these tests was that all beams except the first were re-damaged and repaired several times. Residual stresses were obtained after the last repair cycle for each beam. In each case the degree of damage was approximately 7O which required about 20 heats to complete the repair. Residual stress measurements were made on beams after 1,2, 4, and 8 damage/repair cycles. Measurements were taken at the center of damage. Shown in fig. 4.24 are the average residual stresses in the flanges of the specimens for the different categories and locations (the shortening of the beams prevented the measurement of residual stresses in the webs, except for the single damage/repair cycle). The stresses were fairly consistent in the beams with one and two damage/repair cycles and fairly consistent in those with four and eight damage/repair cycles. This behavior indicates that the number of damage cycles has some effect on the residual stress distribution. Values are shown, using an assumed modulus of elasticity of 200,000 MPa (29,000 ksi).

It is interesting to note that the residual stress patterns in all of these beams were exactly opposite in nature to that of the undamaged beams which had tension in the flanges and compression in the web. For the damage/repair cases, the large number of vee heats tended to shorten the flanges more than the strip heats shortened the web. Thus the flanges had tension stresses while the web had compression stresses. The web compression was obvious by severe web buckling which occurred after a number of damage/repair cycles (A correction factor was applied to account for curvature when computing the residual stress of each strip). Actual repairs would have required this local buckling to be heat straightened.

Residual stresses were measured for a single W 6x9 beam with Category S damage which was repaired using the standard pattern. The residual stress patterns are shown in fig. 4.25. Both flanges were in compression while the web was in tension. The maximum compressive stresses in the flanges approached yield while those in the web were somewhat less. A comparison of the residual stresses for the undamaged and damaged beams showed a reasonably good correlation for Category S.

The large residual stresses created during heat straightening have several implications. First, if the member is a compression element, the high residual stresses are similar to welded built-up members. Since U.S. codes use a single column curve concept, these members are all treated the same and no capacity reduction would be assumed. However, if multiple column curves are used (typical of many European countries), then heat straightened columns would fall in a lower strength curve after heating due to residual stresses. Consequently, there would be some loss of design strength. Second, high tensile residual stresses reduce the effectiveness of jacking forces by effectively canceling out the compressive stresses in areas with externally applied force which causes compressive stresses. Movement could be reduced or even reversed, if the jacking force moment does not compensate for the residual stresses.

Basic Material Properties From Laboratory Tests

Thermal Expansion.—One of the most fundamental aspects of heat straightening is the thermal expansion characteristics of steel. The coefficient of thermal expansion is a measure of the rate of strain per degree temperature. Between 65650°C (250–1,200°F) this coefficient varies directly with temperature such that the rate of expansion increases as temperature increases (Blodgett, 1972; Ditman, 1961; Nichols and Weerth, 1972; Roeder, 1985). A plot showing the variation of the coefficient of thermal expansion for low carbon steels is shown in fig. 4.26 (Roeder, 1985). Most curves of this type do not exceed a temperature of 650–760°C (1200–1400°F) because some research has indicted that the thermal expansion may become irregular over the range of temperatures between 700–870°C (1300–1600°F). This region is referred to as the phase transformation zone and the behavior is attributed to molecular change which might have detrimental effects on the steel properties. However, Roeder has shown that for vee heats the thermal expansion continues to increase in a well-behaved manner up to 870°C (1600°F) for carbon steels, although at this temperature, surface damage such as pitting becomes evident.

Modulus of Elasticity.—Between 30–650°C (86–1200°F), the Modulus of elasticity decreases with increasing temperature. At 650°C (1200°F) the Modulus of steel typically decreases to one-half of its Modulus at room temperature. This relationship is shown in fig. 4.27 where E, is the modulus at an ambient temperature of 21°C (70°F) which is 200,000 MPa (29,000 ksi) and T is in degrees Fahrenheit. Two investigators (Nicholls and Weerth, 1972 and Horton, 1973) have reported the results of measuring the Modulus of elasticity after the heat straightening. No appreciable change in the Modulus of elasticity was found after completing the heat straightening process and allowing the material to cool to ambient temperature.

Yield Stress.—Two aspects are important in relating the yield stress to the heat straightening process. The first is the variation in the yield stress during the heating process. The second is the permanent effect heat straightening has on yield stress after the steel has cooled. A plot of the yield stress versus temperature (Roeder, 1985) is shown in fig. 4.27 for carbon steel where T is the temperature in degrees Fahrenheit and F, is the nominal yield stress at 21°C (70°F). It can be seen that the yield stress may be on the order of 40 percent its original value when the temperature reaches the 650°C (1200°F) associated

with heat straightening. This characteristic has the positive effect of enabling plastic deformation to occur at relatively low stresses during the straightening process. However, it may produce a negative effect in that the area being heated is temporarily weakened.

Of long-range interest is the effect on the yield strength after cooling has taken place. A number of researchers have measured the yield stress after the heating/cooling cycle to determine the modified characteristics. For the carbon steel tests representing over 25 specimens from various investigators (see table 10.1), the yield stress increases an average of 10 percent after heat straightening. Six specimens of high strength, low alloy steel showed a 2 percent increase in yield stress while eight specimens of heat-treated, high strength carbon steel showed an average increase in yield stress of 7 percent. The only steel that showed a decrease in yield stress was the quenched and tempered steel where the average of 12 specimens produced a 6 percent decrease in yield stress. This data indicated that the long term effects of the heat straightening process have a small but generally positive effect on the yield stress. In addition, the tested specimens were heated for various lengths of time, cooled both by air and by quenching with a mist, and were subjected to various superimposed loads and residual stresses. None of theses variables had significant effect on the yield stress with the possible exception of the quenched and tempered steel. In the case of quenching, the yield stress was, on the average, unchanged from the original yield.

Ductility After Heat Straightening.—Ductility has often been measured as the elongation over a two inch gage length expressed as a percentage. Test data (see table 10.1) shows that there is typically a 10–20 percent decrease in ductility after the steel has experienced a cycle of heat straightening. This range is the percent reduction and should not be construed as the actual reduction. The average decreases are: carbon steels, 8 percent; High strength, low alloy steels 18 percent; quenched and tempered steels, 14 percent; and quenched and tempered constructional alloy steels, 11 percent. While these changes in ductility characteristics are significant, the magnitude of the reduction is in an acceptable range.

Notch Toughness.—The Charpy V-notch test is widely used as a guide to the toughness of steels in structures susceptible to brittle fracture. A small rectangular bar with a specified V-shaped notch at its mid-length is simply supported at its ends as a beam and fractured by a blow from a swinging pendulum. The amount of energy required to fracture the specimen is calculated from the height to which the pendulum rises after breaking the specimen. The data is taken at a range of temperatures and a plot of energy versus temperature (on the abscissa) is generated. The resulting curve is S-shaped with an upper limit asymptote of constant energy absorption as the temperatures increase above a certain upper critical temperature and a lower limit asymptote as the temperature goes below the lower critical temperature. These limits are referred to as the upper and lower shelf. Tests (see table 10.1) have shown that there is no significant change in the upper shelf energy absorption before and after the heat straightening process for any grade of steel.

A second measure of the notch toughness can also be obtained from the Charpy tests. The temperature at which 50 percent of the upper shelf energy was absorbed, T_{50}, is measured and the difference between the original T_{50} and the T_{50}, after a completion of a heat straightening cycle is checked. Positive differences represent a decrease in notch toughness due to heat straightening while negative numbers represent an increase. Researchers (table 10.1) have found a considerable variation within a given steel grade. However, the average values indicate that only the quenched and tempered, low alloy steels have a significant positive shift (180C or 32°F).

Another measure of notch toughness is the fracture transition temperature. This temperature is the one in which the percentage of shear fracture is 50 percent of the cross section. Pattee, et. al. (1969) used this criterion in evaluating several grades of steel that had been heat straightened. The Drop Weight Tear test was used instead of the similar Charpy test. The fracture transition temperature changes were modest for all cases except the A517-A steel where there was a significant positive shift indicating a fracture sensitivity.

Shanafelt and Horn (1984) have recommended that fracture critical members (non-redundant tension members or components) not be repaired by heat straightening unless the member is fully strengthened by the addition of cover or splice material. No technical data was presented to back up this recommendation. The data presented here suggest that such restrictions are overly conservative with perhaps the only exception being the high strength quenched and tempered steels. The reductions in notch toughness are relatively modest otherwise.

The research findings of NCHRP Project 10-63, which focused on the fatigue and fracture performance of heat straightened girders, have confirmed that generally there is no decrease on fatigue life of the detail for up to three damage/repair cycles, when no significant defects remain in the members after the repair. However, ensuring that no significant defects remain is difficult to guarantee and often required completely repairing the original weld, which effectively erased the original damage and repair. Hence, in some cases, the fatigue tests were essentially tests of repair welds. The NCHRP study also examined the influence of multiple damage/repair cycles on the CVN energy of the steel. The findings were similar to others studies [Varma et al] which have shown that considerable scatter can be expected in the CVN data. Generally, a decrease in CVN values were observed as the number of damage repair cycles increased.

Prior to the work conducted by Connor, et al as part of NCHRP 10-63, one series of fatigue tests on flame straightened members were found in the literature (The shortening . . . , 1946). In this case three eye bars of A-7 steel were heat shortened and then fatigue cycled. When compared to similar specimens which had not been heated, the fatigue strength at both 500,000 and l,000,000 cycles were similar. Although data is sparse, there is no indication that carbon steels will have a shortened fatigue life after heat straightening.

Rockwell Hardness.—A few investigators have conducted Rockwell hardness tests on heat straightened specimens. Patee, et al. (1969, 1970) indicated that the hardness test may be a better measure of material properties than tensile tests because the hardness test measures such a small area. Harrison (1952) also conducted hardness tests. Both of these researchers found that the hardness values did not change appreciably before and after heat straightening.

Mechanical Properties of Heat-Straightened Plates

Most testing for the basic mechanical properties of heat-straightened plates have been conducted on undamaged plates. These tests were typically conducted on undamaged plates which had been vee heated only 3 or 4 times. Researchers concluded from these tests that: (1) little change occurred in modulus of elasticity, (2) slight increases were found in yield and ultimate tensile stress, and (3) lo-25 percent reduction in ductility was observed. Of more significance are the properties of damaged plates (or rolled shapes) after experiencing the large number of heats required to fully straighten the member. To investigate this behavior, material properties tests were conducted on damaged plates in which a large number of heats had been applied. Tensile tests were conducted on coupons taken from the residual stress strips described previously. Yield strength, tensile strength, percent elongation, percent reduction area; and modulus of elasticity were determined for plates P-9 through P-14. For each plate, coupons were taken from the heated area at the apex (strip 1 or 2), middle (strip 4 or 5), and open end (strip 7 or 8) of the vee. Also, a strip from an unheated region of the same plate (strip UH) was tested for comparison purposes.

Yield Stress and Tensile Strength.—The results of the coupon tests are shown in table 4.4. Some coupons exhibited significant increases in yield stresses over that of the unheated material (most notably at the top of the vee). The average increase for eight coupons at the vee apex was 17 percent. This value is nearly twice the increase found for the undamaged plates discussed in the previous section. It is obvious that the large number of repetitive heats provided a degree of heat treatment not reflected in a small number of heats on undamaged plates. The maximum tensile strength values were more consistent, having variations of less than 4 percent except for plate No. 14, which had a 10 percent increase. The net effect of heat straightening is to narrow the gap between yield stress and maximum tensile strength.

Modulus of Elasticity.—Based on limited data, it has been assumed that single vee heats on mild steel did not affect the modulus of elasticity. However, the results shown in table 4.4 indicate considerable variation in modulus of elasticity. Variations for a given plate ranged from 11–77 percent. The average values for plates P-9 and P-14 increased 11 percent and 30 percent, respectively. However, the average values for the other four plates decreased in the range of 13–31 percent. This evidence indicates that heat straightening tends to reduce the modulus of elasticity in the heated regions.

Ductility.—The percent elongation significantly decreased for all strips tested. This result is consistent with previous tests on undamaged vee heated plates. The elongation of the unheated strips ranged from 41–46 percent while the average for each of the heated plates ranged from 32–37 percent. Thus the elongation of heat-straightened plates tended to decrease by nearly one-third but all still met or exceeded material specification requirements.

An important observation is that the changes in material properties resulting from the damaging and straightening processes were very similar for each plate, in spite of the differences in degree of damage, jacking ratio, vee depth and the number of heats applied. It appears that these parameters do not significantly affect material properties.

An independent sample t-test was conducted for each property in table 4.4 to attach a statistical significance to the effects of one damage/straightening cycle on these properties. This test is an excellent method to determine the confidence level for predicting changes from some process or event, even with a small number of samples. Table 4.5 shows the confidence levels of one damage/repair cycle causing an increase (or decrease) in the particular material properties of a steel plate specimen. A high level of confidence exists that yield strength will increase, and that percent elongation will decrease (at all positions within the heated region). However, the confidence level of increased tensile stress and decreased reduction of area are low since values under 95 to 97.5 percent are often rejected in hypothesis testing (Hicks 1982).

Considering only the high confidence levels for yield stress increase and ductility reduction, the respective percentages of these properties (for each specimen) in relation to those in the unheated specimens and the ASTM standards are listed in table 4.6. For yield stress, the ASTM standard minimum value is 248 MPa (36 ksi), and the standard for minimum percent elongation is 34 percent for a 50 mm (2 in) gauge length. It

should be noted that the highest values for yield stress (414 MPa or 60.1 ksi) was obtained in strip #2 of plate P-14. This was the only plate with a depth ratio of 0.75 for which tensile tests were conducted. Because this strip #2 is in a region that has undergone compressive deformation but has not been directly heated, it is suspected to retain more strain hardening effects than if it were contained within the vee heated area (as other strip #Z's are for full-depth vees). The minor re-stretching effect in the upper portions of this plate (addressed by Roeder, 1985) may have caused cyclic hardening not experienced if the material was heated. This specimen alone (among the plates) experienced a significant increase in tensile strength over the unheated specimen for that plate (10 percent). It should also be noted that similarly elevated yield and tensile strengths were experienced (near the vee apex) after the first damage cycle in the study of repetitively damaged wide flange beams, described in the next section where a depth ratio of 0.75 was also used.

Mechanical Properties of Heat-Straightened Wide Flange Beams

Tensile tests were conducted on strips taken from four W 6×9 beams damaged by bending about their minor axis (Category W). The residual stresses for these beams were discussed earlier and the results shown in fig. 4.24. In each case 45″, ¾ depth vees and a 50 percent jacking ratio were used. The standard Category W pattern of vee heats on both flanges and a strip heat on the web was employed. In addition to evaluating material properties, the purpose of these tests was to determine the effects of repetitive cycles of damage and repair. Consequently, Beam B-l was damaged and repaired once, while Beams B-2 to B-4 were damaged and repaired twice, four times and eight times, respectively. In each case the degree of damage was in the range of 6–8″ and required about 20 heat cycles to repair. After the last damage/repair cycle for each beam, one of the flanges was sectioned and tensile tests conducted on strips near the apex, center and open end of the vee. The resulting properties are given in table 4.7 where UH indicates an unheated strip (see fig.4.14 for strip numbers). Yield Stress.—A significant increase in yield stress and tensile strength occurred near the apex of the vee and it was progressively larger in proportion to the number of damage/repair cycles. A plot of the variation is given in fig.4.28. The yield stresses at other locations increased in the range of 9–21 percent and averaged a 13 percent increase (similar to the damaged plate results). The data confirms that the apex of the vee is the most sensitive zone. Repetitive damage and repair cycles result in large increases in yield stress, especially after two or more cycles. Tensile strength followed a similar pattern as shown in table 4.7 and fig. 4.29. However, the tensile strength at the apex increased at only half the rate of the yield stress as shown in table 4.8. This narrowing of the normal gap between yield stress and tensile strength suggests that heat straightening should be limited to no more than 2 damage/repair cycles.

Modulus of Elasticity.—The modulus of elasticity averaged 8–23 percent lower for members with one or two damage/repair cycles. However an increase was observed for the beam with four cycles. In general, the level of variation was similar to that of damaged plates.

Ductility.—The elongation after one or two damage/repair cycles (31–32 percent) followed the trend of plates with about a one-third reduction. However, for four or eight cycles the elongation is proportionally reduced as shown in fig. 4.30 and table 4.8. The data reinforces the conclusion of limiting the number of damage/repair cycles to no more than two.

Mechanical Properties from Heat Straightened Girders

Studies of mechanical properties for field straightened girders are rare. However, one such study was conducted by Putherickal, (1992). The Iowa Department of Transportation has allowed heat straightening of bridge girders for a number of years. One such girder (W 30 × 108) was removed from service several years after repair for reasons unrelated to the original heat straightening repair. Identical tests were conducted on a segment in the heat straightened zone and from an unheated segment.

A micro structure comparison between the heated and unheated specimens showed clear signs of re-crystallization in the heat straightened area. The heated piece was partly austenitized and re-crystallized into finer grains. This evidence indicates that the steel was heated above the lower critical temperature.

A summary of the mechanical properties measured is given in table 4.9. Both yield and tensile strength increased significantly but the increases were not proportional. Elongation decreased significantly and the Brinell hardness indicates that material became harder, indicating that the material was overheated. The Charpy V notch values in the unheated regions were poor. However, the values in the heated regions were even worse. All the data suggest that the material in the over-heated zone became more brittle. The need for careful control of material temperature during heating is reinforced by this field data.

This example illustrates that even though it is not advisable to overheat steel during heat straightening, it does not necessarily mean that the member should be scrapped if accidentally overheated. Rather, engineering judgment is required to determine the safety of the member based on data presented in this manual.

Member Shortening

The subject of member shortening due to heat straightening has been mentioned in the literature but little research has been conducted. One researcher stated that using smaller vee depth ratios should result in less member shortening, given any particular damage situation (Moberg 1979). However, it could be argued that less shortening would occur when using full-depth vee heats, since the top fibers have been heated and are subjected to a tensile stress. In fact, the amount of shortening in a member can be quite significant, regardless of the vee depth used. Fig. 4.31 shows the basic concept of the shortening phenomenon. If the plate is damaged about its strong axis with a midpoint loading as shown, the top edge of the plate experiences compressive yielding (shortening) and the bottom edge of the plate experiences tensile yielding (stretching). As the plate is subjected to the heat straightening process, the top edge experiences some "re-stretching" in the longitudinal direction (as evidenced by Roeder's strain distribution). However, these positive strains are small in comparison to the simultaneous shortening of the bottom edge of the plate. To quantify the amount of shortening experienced for a given amount of damage, measurements were made on some of the deformed plates. Cold bending will usually result in an increase in the centerline length of a member. To eliminate this factor, the initial lengths were measured before damage was induced and final measurements taken after heat straightening was completed. Regardless of initial and final lengths, all of the shortening occurs only within the damaged region (meaning shortening should not be expressed as a percentage of total length, but simply as a length itself).

A plot of shortening vs. degree of damage is shown in fig. 4.32 for $6 \times 100 \times 610$mm ($\% \times 4 \times 24$ in) plates bent about their strong axis. The shortening varies quite directly with degree of damage, up to a certain point (somewhere between 18 and 24 degrees), for the specimens studied. Shortening appears to be a function of plate width (since strain will vary with plate width for a given angle of damage). The shortening is also affected by the degree of damage itself, but does not vary with vee depth ratio, at least in the 0.75 to 1.00 range. The amount of shortening in the full depth vees of Plate P-14 was about the same as for deformed beams P-9 and P-11 in which the same amount of damage was experienced and %-depth vees were used. All of the specimens with % depth vees followed the same trend of shortening exhibited by those heated with full-depth vees. A formula for estimating shortening is:

(Eq. 4.2)

Four beams (W6×9's) were also investigated for shortening in the study. Each beam was damaged repeatedly about its weak axis to an angle of about seven degrees (approximately the same as the least damaged of the deformed plates). Each incident of damage was repaired using 45 degree vees with a depth ratio of 0.75 and a load ratio of 0.5. The number of damage/repair cycles varied for each of the beams but each repair cycle consisted of approximately 20 heat cycles. Each time a beam was damaged and straightened, a net shortening of about 2.5 mm (0.10 in) occurred in the heated region. These values agreed well with the plate shortening equation. It therefore appears that eq.4.2 can be applied to wide flange beams as well as plates.

Redistribution of Material

As a result of shortening, the heated portions of the deformed plate elements thickened (or upset) upon straightening. This fact becomes especially important in influencing future damage (if any) of the plate element. After the residual stress strips were cut from each plate element, thicknesses were measured at various locations along each strip. Thicknesses at five points on each of the eight strips were measured to 0.025 mm (0.001 in) accuracy.

Thickening was greatest for the plates damaged to the largest degrees. For example, in Plate P-10, which was the specimen with the greatest amount of damage (23.62″), the thicknesses (measured for each strip) along the center of damage averaged 16.6 mm (0.655 in). When compared to the average thickness of the plate before damage (12.3 mm or 0.485 in), the thickening resulted in a 32 percent increase in cross-sectional area. At points further away from the center of damage, thickening is less pronounced, but nevertheless, some thickening occurs within the entire yield zone. While a thicker cross-section results in a stronger member at that location, little structural significance should be placed on the thickening experienced.

For the damaged wide flange beams, thickening also occurred in the heated region. After straightening the first time, the thickening caused a spreading of the yield zone in each subsequent re-damage. The thickening resulted in a smoother distribution of curvature (due to thinner portions further from the centerline tending to yield first), although the total angle of damage was kept as consistent as possible for each bend. Due to the larger yield zone, the heat locations were spread over a greater length. The number of heats required to straighten each bend remained fairly consistent, just more widely distributed.

Impact of Heat Straightening on Mechanical Properties of Steel

Clearly, research data indicates that heat straightening does affect mechanical properties of steel. Early researchers used undamaged steel and a small number of heats to conclude

that property changes were minimal. However, tests on damaged and heat-straightened plates and beams indicate that some property changes may be of significance. Yield stress may increase by as much as 20 percent in some cases, especially in the vicinity of the apex of vee heats. Tensile strength also increases but at only one-half the rate of yield stress. The ductility as measured by percent elongation may decrease by one-third and the modulus of elasticity may decrease by over 25 percent in some heated regions.

The importance of increased yield stress and tensile strength and decreased ductility in the specimens lies in the areas of stress concentrations and fatigue. Stress concentrations often occur around discontinuities in structural members such as holes, fillets, welded stiffeners, and notches (Barsom and Rolfe, 1987). Structural designers rely on the ductility of the material to redistribute the load around a mild stress concentration, such as a drilled hole, within specification-imposed limits for fatigue. However, a decrease in ductility may reduce inelastic stress redistribution, thus the higher stresses remain concentrated.

Fatigue life is the total number of cycles (load fluctuations) required at a certain stress range ~~level~~ to cause the initiation and propagation of cracks to a critical size. The "fatigue limit" is the maximum stress range at which an infinite number of cycles can theoretically be applied without initiating and propagating a crack. Cycles at ~~of~~ stress ranges above the "fatigue limit" lead to a lower fatigue life for any given material and configuration and the presence of notches, holes, welds, and other stress concentrations lowers the fatigue limit.

~~Studies have shown that the fatigue-crack initiation threshold in various steels is related to the yield strength as well as tensile strength (Barsom and Rolfe 1987). This threshold basically establishes a maximum stress for a given configuration geometry at which an infinite number of cycles can be applied without crack initiation. Equations basing the threshold on both tensile strength and yield stress have been formulated and agree well with each other for most structural steels (where the ratios of tensile strength to yield stress are fairly consistent). However, the tensile strength to yield stress ratio may be altered in heat-straightened members. In general, the fatigue-crack initiation threshold increases with tensile as well as yield strength, but tensile strength increases in the heat straightened plates were relatively small, when compared to ductility losses. Thus, improvement of the fatigue-crack initiation threshold, based solely on tensile strength, could possibly be more than offset by increased stress due to the reduced stress redistribution permitted by the ductility loss. Some reduction in the fatigue limit might occur as a result.~~

Studies have confirmed that fatigue strength of welded and bolted structures is independent of the strength of the steel. This is because the small benefits associated with higher strengths steels are by far overshadowed by the negative effects on fatigue life introduced by welding and bolting. For example, the defects and residual stresses present in every welded detail will dominate the fatigue strength far more than the influence of yield strength.

Like ductility, fracture toughness (a value proportional to the energy consumed during plastic deformation) may decrease as a material's yield strength changes during heat straightening. The ability of a particular flaw or stress riser to cause crack initiation or even catastrophic damage depends on the fracture toughness of the material. Because the subject of stress concentrations and brittle fracture depends of specific conditions, it is difficult to make recommendations without detailed analyses of the particular situations. In general, heat-straightening areas that will sustain high stress concentrations in service should be avoided when possible and only done after a sufficient analysis by a qualified engineer. However, since varying degrees of damage seem to have similar material properties after heat straightening, degree of damage alone should not be the deciding factor on whether or not a member should be straightened. ~~Therefore, the suggestion to use damage strain as made by Shanafelt and Horn (1984) to limit heat straightening in high fatigue areas (where strain hardening was the basis) are considered only as precautionary limits with little scientific rationale. Further study should be conducted to determine if heat straightening should be allowed for any degree of damage in areas with fatigue-sensitive details or very high cycles of fatigue loadings.~~

Since the effects of heat straightening on material properties do not relate to the degree of damage of plates and beams (at least past the initial strain hardening point), Shanafelt and Horn's suggested limit of five percent nominal strain in tension members (41.67 times yield strain, if assumed yield strain is 0.0012) has no basis. Recall that this constitutes a fairly small angle of damage in a plate element bent about its weak axis, especially with a large plate width. Research has shown that a strain of at least 100 times yield strain (ϵ_y) can be heat straightened with little difference in material properties from that of repairs with much smaller strains. Thus, except for severe fatigue sensitive areas, material properties should not be the primary determining factor when contemplating the use of heat straightening.

The data presented here provides guidance as to how many times a girder can be damaged and heat straightened in the same zone. Changes in all the material properties become more evident with the increasing number of damage/repair cycles. These changes are particularly significant at the region associated with the apex of the vee. After two damage/repair cycles, the property changes are still relatively modest. But after four damage cycles, the increase in yield and tensile strength, and the loss in ductility were sharper. Since the variation in yield is larger, the gap between yield and tensile strength decreases as the damage/repair cycles increase. As shown in table 4.7 the ratio of

yield-to-tensile strength is around 68 percent for unheated specimens. That ratio increases to 78 percent after one damage/repair cycle and to 88 percent after 8 cycles. This behavior combined with the ductility decreasing with each damage/repair cycle, results in an increasingly brittle material. This data illustrates why over-jacking during repairs may fracture the beam after a number of damage/repair cycles in the same zone.

As mentioned previously, the point at which loss in ductility becomes dangerous is case-specific. However, the extreme losses encountered in the repetitively damaged beams show that there is probably a limit to the number of times that any given member should be repaired. Material property changes were usually small after two cycles. Thus, whatever is safe to straighten once could usually be safely straightened twice under the same conditions. The changes become significantly greater after 4 and 8 damage/repair cycles, respectively. These findings are further substantiated by the fact that during one study of full-scale simulated bridge girders, one girder exhibited brittle behavior by cracking during a heat in its third damage/repair cycle. Based on this research evidence, re-damaged members at the same location should not be subjected to heat straightening more than twice, even for strains well under 100 ϵ_y.

Proposed Revisions to Chapter 9

The following revision is proposed for Chapter 9.

Chapter 9. Heat-Straightening Repair of Localized Damage

Damage in steel members can be broadly classified as global and local damage. Different methods are required for the heat-straightening repair of these types of damage. Global damage is the overall deformation of the damaged section with respect to its supports. Local damage is characterized by plastic strain occurring only in the region of impact. It includes small bulges, bends or crimps in single elements of the cross section. The two most frequently encountered patterns can be categorized for convenience as flange bulges and web buckles as shown in fig. 9.1. Flange bulges are associated with local damage to un-stiffened cross section elements such as a flange of a girder. Web buckles are associated with local damage to stiffened cross section elements such as the web of a girder. All are classified as Category L damage. However, two sub-classifications will be used: Category L/U for local damage to un-stiffened elements, and Category L/S for damage to stiffened elements.

The focus of past heat-straightening research has been on various aspects of repairing global damage. However, it is a rare situation when localized damage doesn't occur concurrently with global damage. Yet, little published information has been available on how to repair local damage by heat straightening. As a result, localized damage is often repaired improperly by cold mechanical straightening and hot mechanical straightening, as well as heat straightening.

In cold mechanical straightening, the steel is restored to its original shape by applying external loads in excess of the plastic capacity of the section while the steel is still at ambient temperature. In hot mechanical straightening, the steel is heated to very high temperatures (often greater than 927°C or 1700°F) causing a severe reduction in yield strength and plastic capacity. The steel is then straightened by external forces. The forces used are smaller than those used in cold mechanical straightening but are still in excess of the yield capacity of the heated steel. Both methods involve straightening of the steel by mechanical means. As a result, these techniques may involve strain hardening which results in a loss of ductility and increased brittleness. The safe alternative is heat straightening. Described in this chapter are methodologies for repairing localized damage using heat straightening.

Local damage patterns display two main characteristics: large plastic strains (usually tensile) in the damaged zone, and bending of plate elements about their weak axis. If the local damage is to be repaired, shortening must be induced in the damaged area equal to the elongation caused when the element was damaged. In addition, the distortion along the yield lines must be removed as part of the repair process. Studies on global damage repair have shown that vee heated regions shorten significantly during cooling and that line heats can be used to induce bending about the yield lines. Thus a combination of line and vee heats can be used to repair localized damage.

Localized damage near a transverse stiffener requires special attention during the repair. During laboratory test repairs, cracks were observed to form at the flange-stiffener weld connection and subsequently extend into the flange. To avoid this cracking, the whole stiffener or the portion of the stiffener near the flange being repaired should be removed prior to heat-straightening. Upon completion of the repair, the stiffener may be replaced or reconnected to the flange if required.

It has been discovered that the restraining force used to remove sweep (global damage) from a beam can lead to hairline cracking in the localized damage areas. Although this does not affect the restraining force used for the localized damage, the calculated strain ratio of the localized damage is used in determining the reduction in restraining force used to remove the global damage. Finite element studies and laboratory testing indicated that the applied restraining forces may produce large tensile stresses adjacent to the localized damage which can lead to hairline fractures and possibly brittle pop-in frac-

tures. Reducing the horizontal restraining force (used to remove sweep) one percent for each unit of strain ratio, as determined for the localized damage, appears to prevent brittle fractures during the repair process.

An acceptable tolerance of a completed repair of localized damage has also been investigated. The presence of Category L damage in the flange can cause secondary stresses which my increase the in-service stress at that location. This is of importance if remaining damage is near a welded detail, especially more severe fatigue categories (such as D, E, and E'). In an attempt to estimate the effect of residual damage, an analytical solution was developed based on the results of a finite element parametric study. An empirical equation is located in Chapter 3 for determining the acceptable tolerance of a repair.

Abbreviations and acronyms used without definitions in TRB publications:

AAAE	American Association of Airport Executives
AASHO	American Association of State Highway Officials
AASHTO	American Association of State Highway and Transportation Officials
ACI–NA	Airports Council International–North America
ACRP	Airport Cooperative Research Program
ADA	Americans with Disabilities Act
APTA	American Public Transportation Association
ASCE	American Society of Civil Engineers
ASME	American Society of Mechanical Engineers
ASTM	American Society for Testing and Materials
ATA	Air Transport Association
ATA	American Trucking Associations
CTAA	Community Transportation Association of America
CTBSSP	Commercial Truck and Bus Safety Synthesis Program
DHS	Department of Homeland Security
DOE	Department of Energy
EPA	Environmental Protection Agency
FAA	Federal Aviation Administration
FHWA	Federal Highway Administration
FMCSA	Federal Motor Carrier Safety Administration
FRA	Federal Railroad Administration
FTA	Federal Transit Administration
IEEE	Institute of Electrical and Electronics Engineers
ISTEA	Intermodal Surface Transportation Efficiency Act of 1991
ITE	Institute of Transportation Engineers
NASA	National Aeronautics and Space Administration
NASAO	National Association of State Aviation Officials
NCFRP	National Cooperative Freight Research Program
NCHRP	National Cooperative Highway Research Program
NHTSA	National Highway Traffic Safety Administration
NTSB	National Transportation Safety Board
SAE	Society of Automotive Engineers
SAFETEA-LU	Safe, Accountable, Flexible, Efficient Transportation Equity Act: A Legacy for Users (2005)
TCRP	Transit Cooperative Research Program
TEA-21	Transportation Equity Act for the 21st Century (1998)
TRB	Transportation Research Board
TSA	Transportation Security Administration
U.S.DOT	United States Department of Transportation